CLIMATE ASSESSMENT

A DECADAL REVIEW
1981–1990

U.S. DEPARTMENT OF COMMERCE
National Weather Service
National Meteorological Center
Climate Analysis Center

CLIMATE ASSESSMENT

A DECADAL REVIEW
1981–1990

EDITORS: M. S. Halpert
C. F. Ropelewski

TECHNICAL ASSISTANCE:
J. D. Kopman

U. S. DEPARTMENT OF COMMERCE
NATIONAL OCEANIC AND ATMOSPHERIC ADMINISTRATION
NATIONAL WEATHER SERVICE
NATIONAL METEOROLOGICAL CENTER

TABLE OF CONTENTS

	Page
LIST OF FIGURES	ii
CONTRIBUTORS	v
PREFACE	vii
EXECUTIVE SUMMARY	1
INTRODUCTION	3
SURFACE TEMPERATURE	
Global	4
Regional	23
PRECIPITATION	
Global	29
Regional	41
CRYOSPHERE	
Snow and Ice	49
TROPOSPHERIC ANALYSIS	
Tropospheric Temperatures	53
700 mb Heights	56
Teleconnections	62
Atmospheric Blocking	68
Ozone	70
MAJOR CLIMATE EVENTS	
Southern Oscillation	71
Warm and Cold Regions	80
Global Climate Anomalies	82
ACKNOWLEDGMENTS	85
REFERENCES	87
APPENDIX	
Northern Hemisphere DJF and JJA temperature and precipitation percentiles	89

List of Figures

Page

Figure 1. NH surface temperature anomalies (1981-1990)..... 5

Figure 2. SH surface temperature anomalies (1981-1990)..... 6

Figure 3. Global surface temperature index time series..... 7

Figure 4. NH and SH surface temperature index time series..... 8

Figure 5. NH surface temperature anomalies (1981-1985)..... 10

Figure 6. NH surface temperature anomalies (1986-1990)..... 10

Figure 7. SH surface temperature anomalies (1981-1985)..... 11

Figure 8. SH surface temperature anomalies (1986-1990)..... 11

Figure 9. NH and SH seasonal temperature anomalies (MAM)..... 13

Figure 10. NH and SH seasonal temperature anomalies (JJA)..... 14

Figure 11. NH and SH seasonal temperature anomalies (SON)..... 15

Figure 12. NH and SH seasonal temperature anomalies (DJF)..... 16

Figure 13. NH December - May surface temperature anomalies (1981-1990)..... 18

Figure 14. NH June - November surface temperature anomalies (1981-1990)..... 18

Figure 15. SH December - May surface temperature anomalies (1981-1990)..... 19

Figure 16. SH June - November surface temperature anomalies (1981-1990)..... 19

Figure 17. Global seasonal surface temperature index time series.. 20

Figure 18. NH seasonal surface temperature index time series..... 21

Figure 19. SH seasonal surface temperature index time series..... 22

Figure 20. Annual US temperature expressed as decadal means and in a time series 25

Figure 21. Seasonal US temperature expressed as decadal means..... 26

Figure 22. Specified US surface temperature anomaly errors..... 27

Figure 23. Soviet Union surface temperature anomalies..... 28

Figure 24. NH annual precipitation percentiles (1981-1990)..... 31

Page

Figure 25. NH precipitation percentiles (DJF, MAM 1981-1990)..... 32

Figure 26. NH precipitation percentiles (JJA, SON 1981-1990)..... 33

Figure 27. SH precipitation percentiles (DJF, MAM 1981-1990)..... 36

Figure 28. SH precipitation percentiles (JJA, SON 1981-1990)..... 37

Figure 29. Annual global precipitation index time series..... 39

Figure 30. Seasonal global precipitation indices..... 40

Figure 31. Precipitation index time series for southeastern US; midwestern US; western US; and Europe..... 42

Figure 32. Precipitation index time series for western Sahel; northern Australia; India; and southeastern Asia..... 43

Figure 33. October-March total precipitation western US..... 45

Figure 34. Percent area of the contiguous US experiencing severe to extreme long-term wet conditions..... 46

Figure 35. Percent area of the contiguous US experiencing severe to extreme long-term drought..... 47

Figure 36. Annual total number of hurricanes and tropical storms in the North Atlantic Ocean..... 48

Figure 37. Time series of Eurasian snow cover area and Eurasian temperature anomalies for spring and summer..... 50

Figure 38. Time series of the Arctic sea ice area anomalies for the northern winter and summer and of the Antarctic sea ice area anomalies for the southern winter and summer.. 51

Figure 39. Time series of global lower tropospheric temperature anomalies derived from satellite data..... 54

Figure 40. Time series of global tropospheric (850-300 mb) temperature anomaly derived from radiosonde data..... 55

Figure 41. Average 700 mb geopotential height anomalies (1981-1990)..... 57

Figure 42. Average 700 mb geopotential height anomalies (DJF, 1981-1990)..... 58

Figure 43. Average 700 mb geopotential height anomalies (JJA, 1981-1990)..... 59

Figure 44. Average 700 mb geopotential height anomalies (MAM, 1981-1990)..... 60

Page

Figure 45. Average 700 mb geopotential height anomalies (SON, 1981-1990)..... 61

Figure 46. Smoothed time series of the PNA index..... 63

Figure 47. Smoothed (95-day running mean) time series of the West Pacific, the West Atlantic, the East Atlantic, and the Eurasian indices..... 65

Figure 48. Smoothed (365-day running mean) time series of the West Pacific, the West Atlantic, the East Atlantic, and the Eurasian indices..... 66

Figure 49. Time series of the 250 mb zonal mean wind anomaly (1979 to 1990)..... 67

Figure 50. Time series of a circumpolar vortex mass index..... 68

Figure 51. Time-longitude cross section of a blocking index..... 69

Figure 52. Time series of total ozone..... 70

Figure 53. Sea surface temperature anomaly patterns for DJF 1982-83, JJA 1987, and JJA 1988..... 73

Figure 54. Time series of the Tahiti minus Darwin SOI..... 74

Figure 55. Time series of anomalous OLR in the central equatorial Pacific..... 74

Figure 56. Anomalous 500 mb temperature for JJA 1988, SON 1988, DJF 1988-1989, and MAM 1989..... 75

Figure 57. Anomalous 500 mb temperature for JJA 1982, SON 1982, DJF 1982-1983, and MAM 1983..... 76

Figure 58. Time-latitude section of zonally averaged 500 mb temperature anomalies..... 77

Figure 59. Time-latitude section of average 500 mb temperature anomalies over the longitude band 120°W-180..... 78

Figure 60. Time-latitude section of 200 mb zonally averaged zonal wind anomalies..... 79

Figure 61. Locations of regions experiencing warmer and colder than normal temperatures during the decade of the 1980's for DJF, MAM, JJA, and SON..... 81

Figure 62. Major global climate anomalies 84

CONTRIBUTORS

Air Resources Laboratory/ERL/NOAA

J. K. Angell

Climate Analysis Center/NMC/NWS/NOAA

G. D. Bell
M. Chelliah
D. R. Garrett
M. E Gelman
M. S. Halpert
J. D Kopman
V. E. Kousky
A. J. Miller
D. Miskus
R. M. Nagatani
E. A. O'Lenic
C. F. Ropelewski
P. Sabol
H. M. van den Dool

Climatic Research Unit, University of East Anglia, (UK)

P. D. Jones

Hadley Centre for Climate Prediction and Research, (UK)

D. E. Parker

Institute for Global Climate and Ecology (USSR)

G. V. Gruza
E. Ya. Rankova
E. A. Semenyuk
G. A. Nestorova
L. V. Korovkina
M. Yu. Bardin

Johnson Research Center, University of Alabama in Huntsville

J. R. Christy

NASA Marshall Space Flight Center

R. W. Spencer

National Climate Data Center NESDIS/NOAA

T. R. Karl
R. R. Heim Jr.

State Hydrologic Institute, Leningrad (USSR)

V. Ya. Vinnikov

World Data Center – B, Obninsk (USSR)

V. N. Razuvayev

PREFACE

The publication of this annual Climate Assessment is the second time we have attempted to summarize contemporary climate data and statistics on the state of the global climate system. This year, at the end of the decade, we have focused on global observations from an historical perspective.

A summary of this type is motivated by an international concern for potential global warming and possible consequences which may occur. Although a comprehensive study has recently been completed by the Intergovernmental Panel on Climate Change (IPCC), this report has been written to stay abreast of new results and to display new analyses which more clearly define contemporary climate anomalies. Therefore, this assessment is also a contribution to a new project for the World Meteorological Organization (WMO) on the Early Detection of Climate Change.

The purpose of this report is to provide a technical resource which can be used to address questions concerning the possibility of changes to the global climate system. Depending on how the question is asked, these analyses can contribute to an assessment of the current state of the climate system. However, not all observational evidence supports the global change hypothesis. Furthermore, during this past decade there have been some outstanding climate events: a record El Niño/Southern Oscillation (ENSO) event in the Pacific, record monthly warm surface temperatures in the Northern Hemisphere, and severe droughts in several regions.

We admit that we are not able to provide a complete analysis of all pertinent variables. The assessment of global cloud cover, the analysis of ocean circulation, or a measure of the vitality of the surface vegetative cover is beyond the present scope of this report. We have also omitted important topics on climate impacts of the national economy. In succeeding years, however, we hope to build on this year's accomplishments to develop an improved and more sensitive climate assessment.

I would also like to emphasize the collaborative nature of this report. It is derived from NOAA contributions from the National Environmental Satellite, Data, and Information Service (NESDIS), the Office of Oceanic and Atmospheric Research (OAR) and the National Weather Service (NWS). However, we have included some special contributions from universities in the U.S., and important results from several laboratories in the U.K. and U.S.S.R. I would like to thank all the contributors for their cooperation and willingness to share new results. Special recognition should also go to the co-editors, Michael S. Halpert and Chester F. Ropelewski, for bringing the project to completion. Partial support for this project came from the Climate Perspectives Project of the NOAA Office of Climate and Global Change.

No single report of this kind can hope to be complete and comprehensive. Nevertheless, our goal is to provide a coherent description of the climate of the 1980s using key climate parameters as soon as they become available.

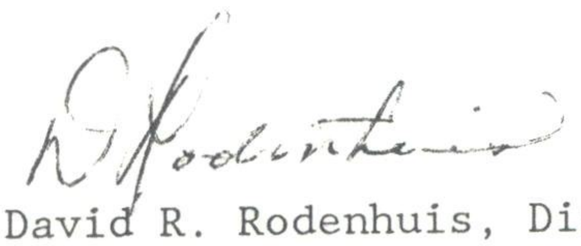

David R. Rodenhuis, Director
Climate Analysis Center

EXECUTIVE SUMMARY

Based on surface temperature estimates for the 1980's, this climate assessment agrees with other related studies that this decade is the warmest in the record. Moreover, the following characteristics of surface temperature during the decade are now also clear. These include:

- The Northern Hemisphere dominates the record.
- The 1986 to 1990 period is clearly warmer than the first half of the decade and the temperature anomaly patterns are similar for each 5-year period.
- Temperature anomalies in the first half of the year (December through May) in both hemispheres dominate the annual anomaly patterns.
- The Southern Oscillation has a clear effect on the interannual variability of the global temperature, but it does not explain all of the observed patterns and variations.

Still to be resolved are the small but important difference between satellite and radiosonde estimates of the global tropospheric temperatures. These differences may point to inadequacies of the radiosonde network or in the algorithms for converting satellite data to temperature.

A preliminary examination of the Northern Hemisphere tropospheric circulation patterns suggest:

- There have been small, but significant, systematic shifts in the hemispheric circulation patterns during the 1980's.
- Components of the circulation changes during the 1980's are consistent with the observed surface temperature and precipitation anomaly patterns.

Precipitation has traditionally been harder to characterize than surface temperature. However, the analysis presented here suggests:

- The summer monsoon rainfall amounts for western Africa, southeastern Asia and northern Australia have decreased over the past decade or longer.
- The summer monsoon rainfall over the Indian sub-continent had very large year-to-year variations in the past decade, but no clear decadal trend is evident.
- The global precipitation analysis suggests that mid-latitude precipitation may have increased during the past decade while tropical monsoon precipitation decreased.

Thus, while several temperature and precipitation records were set during the 1980's, it is still not clear whether these are simply large excursions of the climate system or whether these variations signal trends towards a clearly different climate.

Investigation of interannual variability has confirmed that the large swings in the Southern Oscillation were associated with some of the largest global scale year-to-year variability of the 20th century. In particular, during the decade of the 1980's, the Southern Oscillation experienced its strongest warm episode of the century (1982/83) and its strongest cold episode in 50 years (1988). These were associated with:

- Record droughts in India, Australia and the western Pacific, and record rainfall in western South America during the 1982-83 warm episode.

- Record rainfall in India and Australia during the 1988 cold episode.

- Large temperature anomalies in the global tropics and in northwestern North America.

- Variations in the global scale tropospheric and surface temperature and precipitation patterns.

The cryospheric component of the climate system has only been measured consistently for less than twenty years. Analyses of these data suggest:

- Record Northern Hemispheric surface temperatures in spring of 1990 may be related to snow cover deficiencies over Eurasia.

- Sea ice area shows no clear trends during the decade.

While our understanding and analyses of all of the climate variations that occurred in the 1980's is far from complete, certain aspects of the variability can be listed. We hope that a description of these climate system characteristics of the past decade serves as a piece to the "large puzzle" that must be solved.

INTRODUCTION

The purpose of this review is to identify the principle features of the global climate during the decade of the 1980's. Temperature, precipitation, and circulation anomalies are derived and, for the most part, compared to the past 40 years.

Several previous studies have examined surface temperature and precipitation records spanning much longer periods of time. The temperature studies have two features in common, a) they all require corrections to the early data, and b) they all suggest that surface temperatures during the recent decade are several tenths of a degree (0.3°C to 0.6°C) higher than a century ago (IPCC, 1990). To a large extent the interpretation of these longer time series depends upon a willingness to accept the validity of various corrections and assumptions applied to data prior to the mid-1940's.

We eliminate much of this problem by confining the bulk of the analysis to the past 40 years. In effect, this report accepts the vast body of previous work based on long-term surface data and concentrates instead on the question "What, if anything, makes the climate of the 1980's unique?". This review attempts to tie variations in the surface climate with those in the atmospheric circulation and other components of the climate system.

SURFACE TEMPERATURE

GLOBAL

Surface temperatures for the decade of the 1980's averaged above normal over most areas of the globe. Temperature anomalies averaged for the whole decade (**Fig. 1**) show that almost all areas of the Northern Hemisphere experienced positive anomalies. Only Greenland and Baffin Island experienced mean negative anomalies less than -0.5°C. The largest positive anomalies were found over the central and eastern Soviet Union and over Alaska and western Canada. Northern Hemisphere sea surface temperature (SST) anomalies were generally small and positive, except in an area in the North Pacific and another area in the North Atlantic around Greenland. The Southern Hemisphere was also dominated by above normal temperatures (**Fig. 2**), except for an area in central South America. SST anomalies in all three southern ocean basins averaged above normal, with a fairly substantial area in the east Pacific averaging greater than 0.5°C above normal. This latter feature is most likely a reflection of the very large SST anomalies associated with the El Niño/Southern Oscillation (ENSO) event of 1982-1983.

Time series of the estimated global land anomaly during the 1980's (**Fig. 3**) shows that all median temperature anomalies were positive with the exception of the slight negative value for 1985. Median temperature anomalies in the latter half of the 1980's were clearly above those earlier in the record. The median value for 1990, 0.5°C, was larger than any other median value in this time series. Thus, approximately half of the 2° latitude by 2° longitude land areas in this analysis had average temperature anomalies of 0.5°C or greater. 1990 is also particularly striking because the median anomaly is equal to or greater than the 70th percentile of all other years with the exceptions of 1953, 1981, 1987, and 1989. The 1990 values are also notable because only slightly more than 10% of the world's land areas experienced negative annual temperature anomalies (one would expect approximately 50% for near normal conditions). Extreme temperature anomalies for both 1981 and 1987 were comparable to 1990 in showing 10% or more of the land areas with 1°C or greater positive temperature anomalies.

Other warm periods appear in this time series, notably 1957 to 1961, but in the early record only 1953 shows annual values comparable to those of the 1980's. The effects of the El Niño/Southern Oscillation on these calendar year annual temperatures is not clear, (Halpert and Ropelewski, 1991) but there is a tendency for larger positive (negative) median values to be associated with the years following warm (cold) episodes.

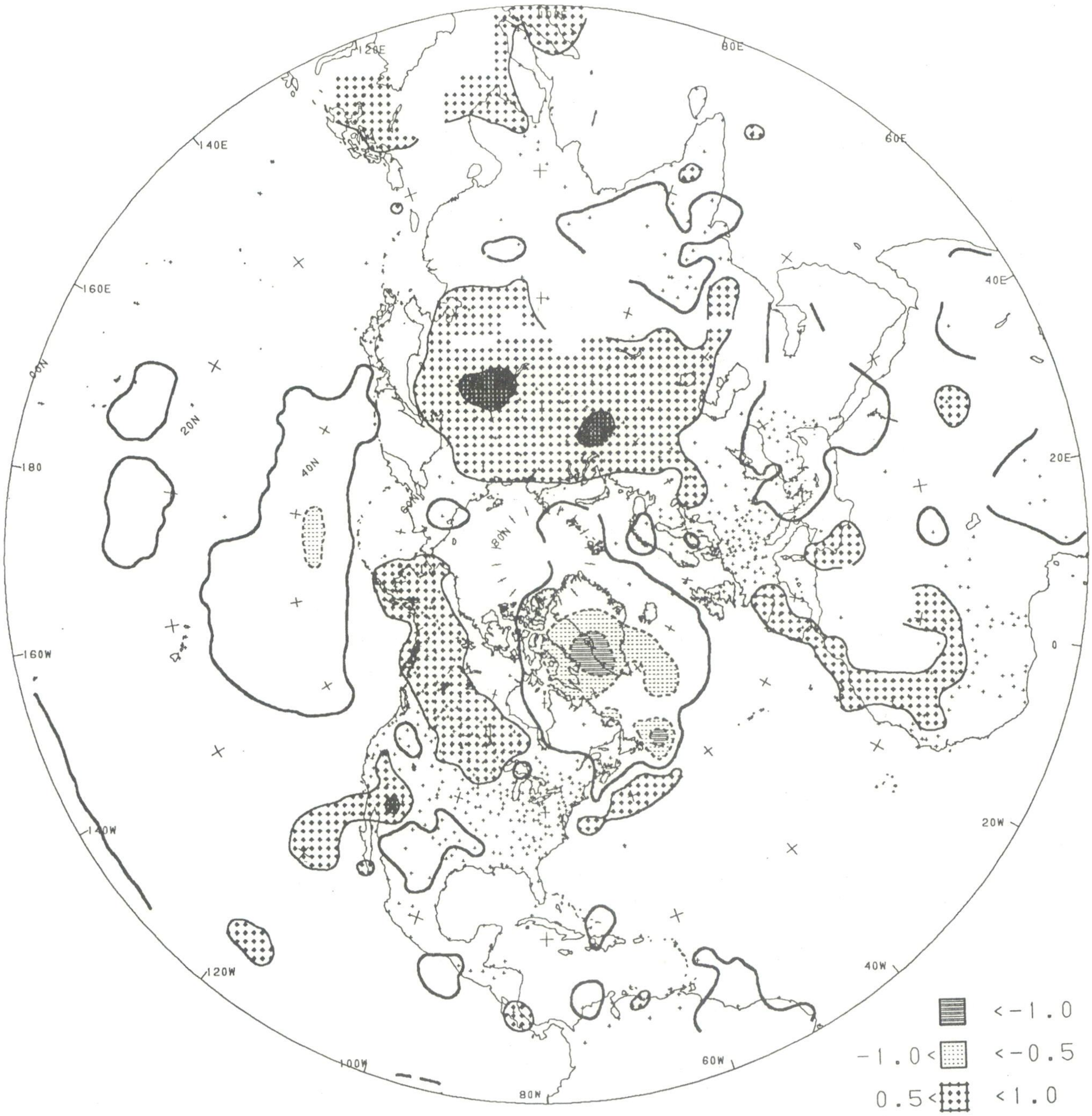

Fig. 1. Northern Hemisphere surface temperature anomaly for the period 1981-1990. Analysis based on station data over land and sea surface temperature (SST) over the water. Anomalies for station data are from the 1951-1980 base period, while SST anomalies are computed as departures from the COADS/ICE climatology (Reynolds, 1988). Small plus signs indicate locations of data over land. Contour interval is 0.5°C, with negative anomalies dashed.

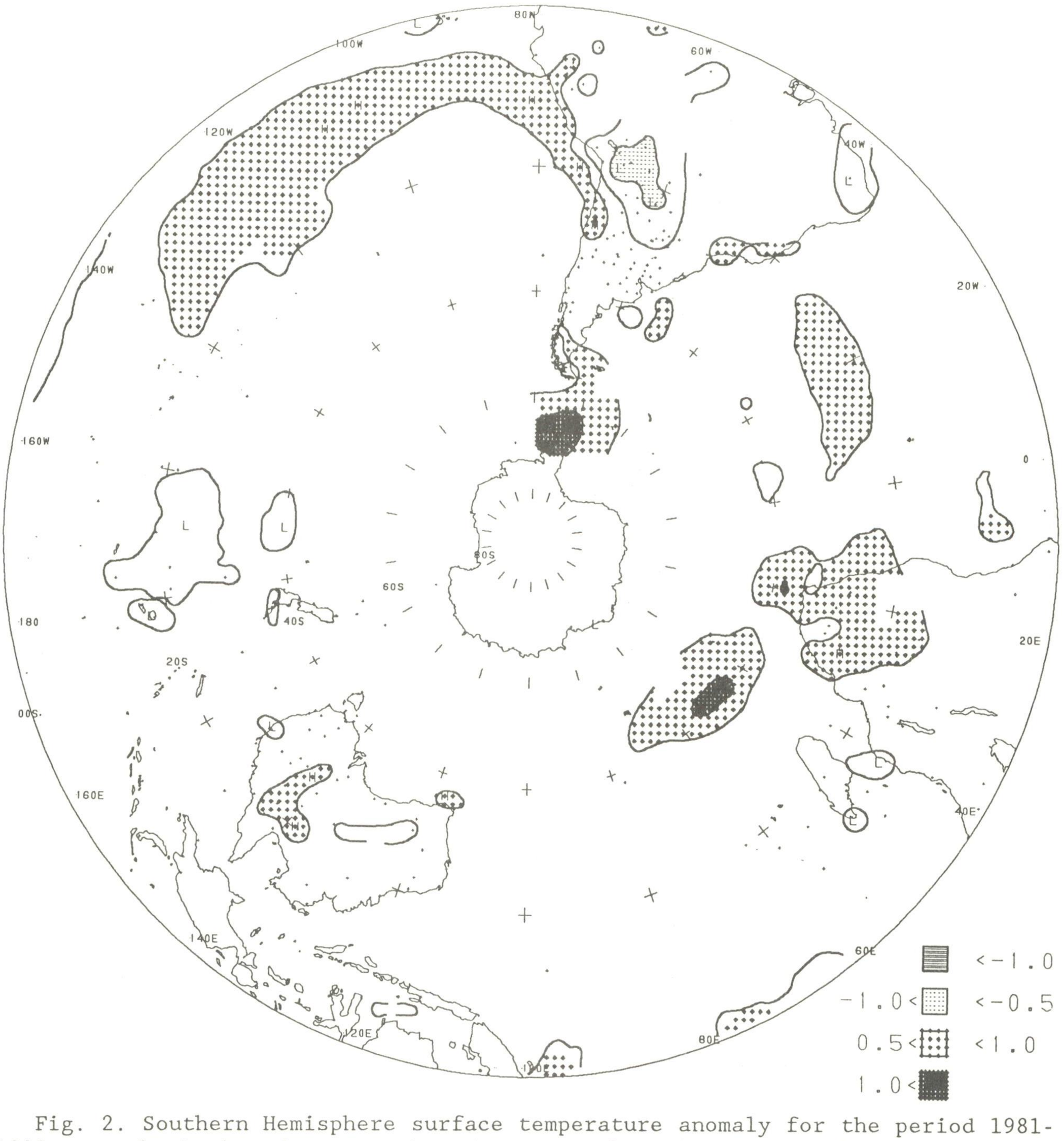

Fig. 2. Southern Hemisphere surface temperature anomaly for the period 1981-1990. Analysis based on station data over land and sea surface temperature (SST) over the water. Anomalies for station data are from the 1951-1980 base period, while SST anomalies are computed as departures from the COADS/ICE climatology (Reynolds, 1988). Small plus signs indicate locations of data over land. Contour interval is 0.5°C, with negative anomalies dashed.

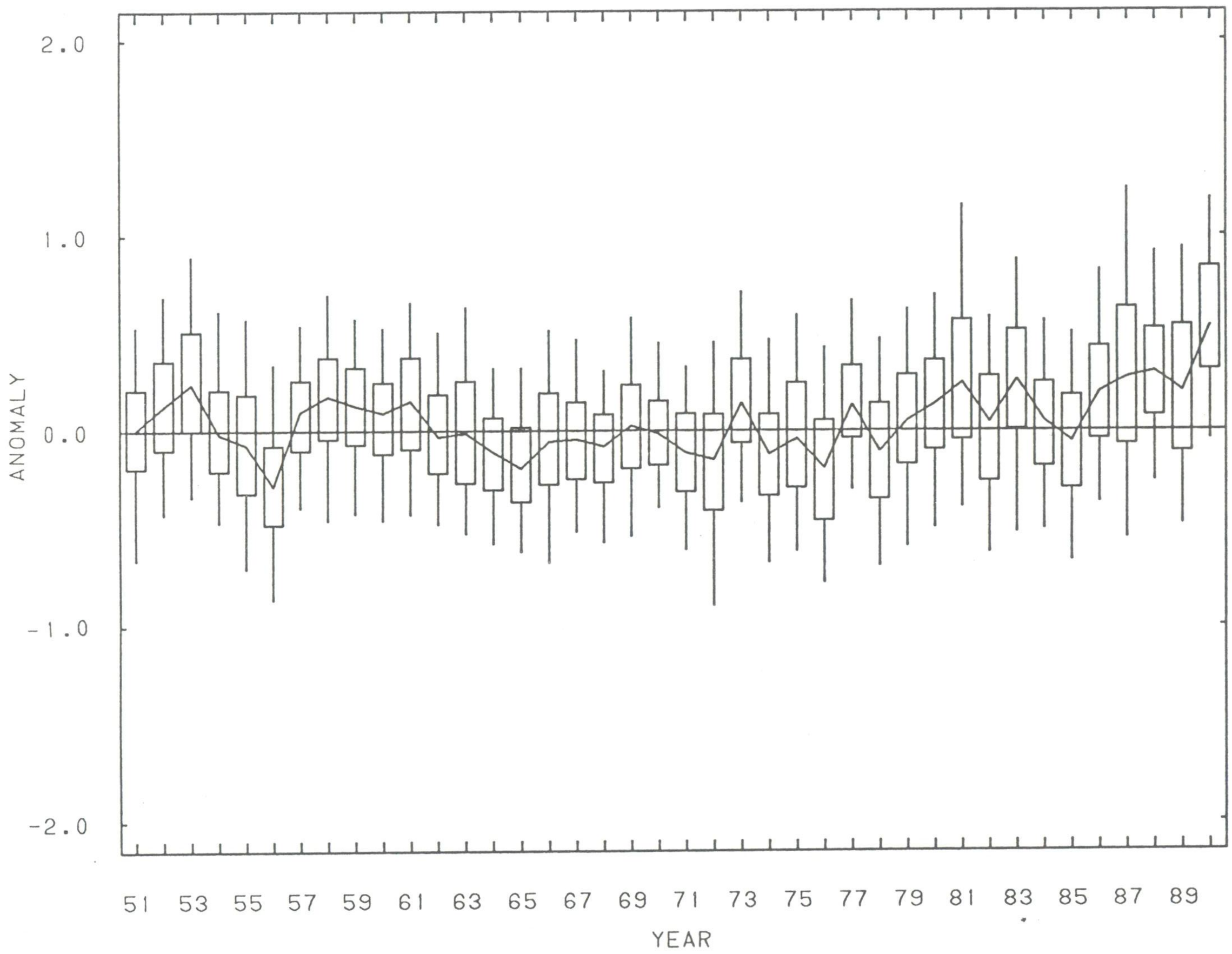

Fig. 3. Global surface temperature index based on the average annual temperature anomalies in 2^{o} latitude by 2^{o} longitude areas over land. The solid line represents the 50%, or median, temperature anomaly for each year. Each "box" delineates the temperature anomalies at the 70th and 30th percentiles while the "whiskers" (lines) delineate the 90th and 10th percentile values. The anomalies are with respect to the 1951 to 1980 base period.

The Northern Hemisphere time series (**Fig. 4a**) is almost identical to the global series since most of the land area, as well as most of the surface data, are located in the Northern Hemisphere. It is somewhat surprising, however, that the overall character of the Southern Hemisphere temperature time series (**Fig. 4b**) is very similar to the Northern Hemisphere series. Both hemispheres show the 1980's to be warmer than earlier decades. One difference is that the Southern Hemisphere median temperatures for 1980 and 1988 are both larger than those for 1990. The Southern Hemisphere also shows closer relationships to the Southern Oscillation, with each of the warm episode years showing positive median temperature anomalies (except for 1965) and each of the cold episode years showing below median anomalies (except for 1988). The two coldest years in the Southern Hemisphere series, 1956 and 1975, are associated with cold Southern Oscillation episodes.

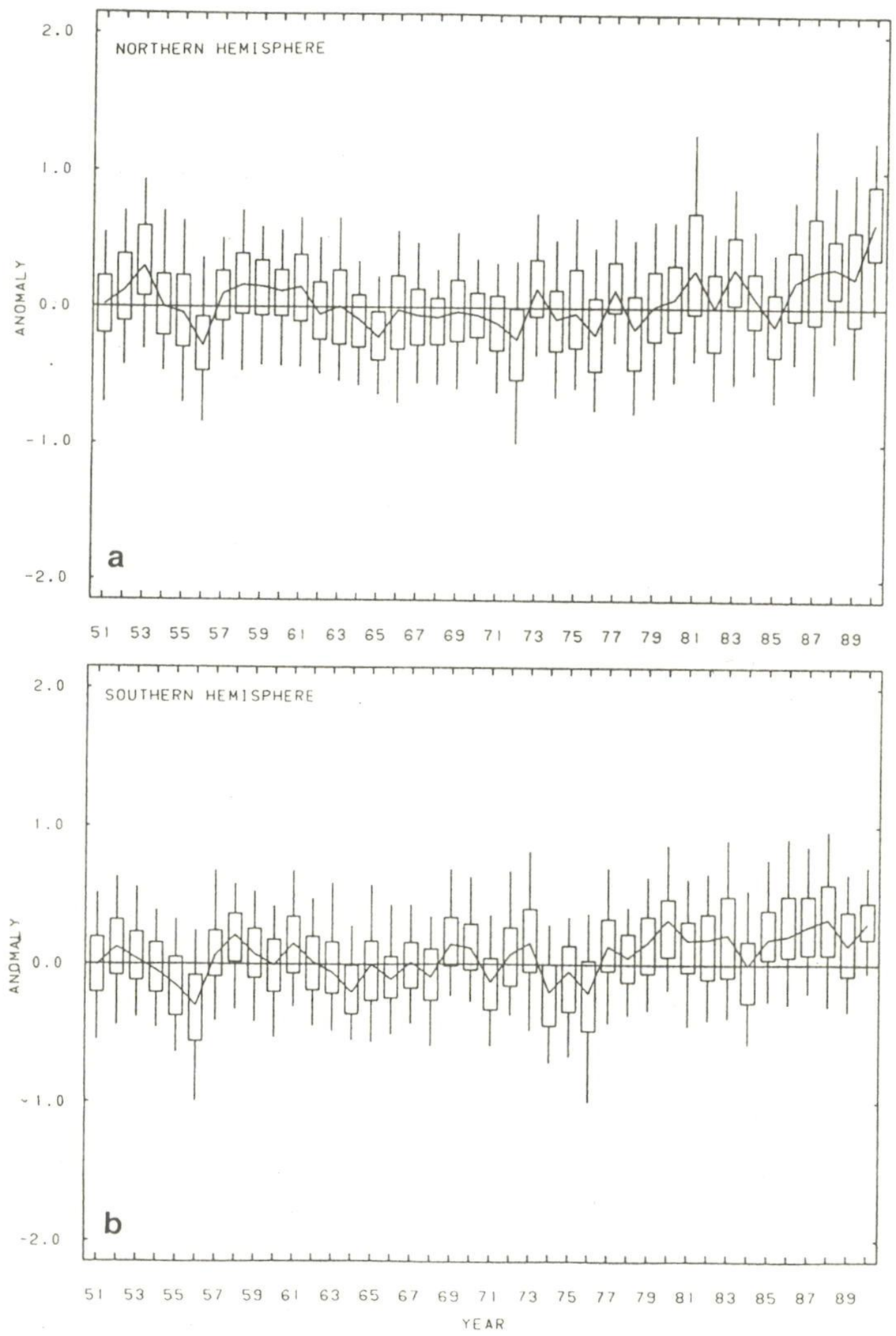

Fig 4. A) Northern Hemisphere and B) Southern Hemisphere surface temperature index based on the average annual temperature anomalies in 2^{o} latitude by 2^{o} longitude areas over land. The solid line represents the 50%, or median, temperature anomaly for each year. Each "box" delineates the temperature anomalies at the 70th and 30th percentiles while the "whiskers" (lines) delineate the 90th and 10th percentile values. The anomalies are with respect to the 1951 to 1980 base period.

The following global temperature estimates were obtained from the State Hydrological Institute, Leningrad, USSR. These are consistent with time series of median temperatures (**Fig. 3**) and similar estimates received from the Climatic Research Unit, University of East Anglia.

Mean annual surface air temperature for the greater part of the Earth (90 N - 60 S) as departures from an average for the 1951-1975 period (^{o}C)

	0	1	2	3	4	5	6	7	8	9
1880		-0.31	-0.27	-0.31	-0.60	-0.40	-0.40	-0.52	-0.21	-0.08
1890	-0.36	-0.41	-0.39	-0.42	-0.36	-0.26	-0.15	-0.06	-0.35	-0.21
1900	0.06	-0.08	-0.17	-0.31	-0.42	-0.22	-0.14	-0.38	-0.33	-0.23
1910	-0.24	-0.28	-0.18	-0.20	-0.02	0.03	-0.17	-0.43	-0.34	-0.17
1920	-0.10	-0.09	-0.14	-0.18	-0.13	-0.08	0.15	0.03	0.05	-0.16
1930	0.04	0.12	0.07	-0.14	0.06	-0.02	0.04	0.16	0.13	0.01
1940	0.15	0.15	0.16	0.02	0.16	0.06	0.05	0.16	0.07	0.02
1950	-0.07	0.07	0.09	0.18	-0.02	-0.10	-0.19	0.07	0.17	0.12
1960	0.07	0.10	0.08	0.05	-0.25	-0.16	-0.06	-0.03	-0.12	0.04
1970	0.03	-0.15	-0.07	0.19	-0.09	-0.02	-0.16	0.18	0.10	0.21
1980	0.27	0.37	0.14	0.35	0.08	0.07	0.21	0.38	0.36	0.27
1990	0.52									

These estimates are based on data from 301 and 265 land meteorological stations in the Northern and Southern Hemispheres, respectively. The description of analysis method and sources of this data are given in Vinnikov et, al., 1990. The statistically optimum method for spatial averaging, used in the analysis, provides a sufficiently accurate spatial averaging procedure when using data from a limited number of stations, smaller than used by other research groups. Updating was done at the State Hydrological Institute, Leningrad, USSR, by using the facilities of WDC-B, Obninsk, USSR and CAC/NOAA Washington D.C., USA .

The data show that the last decade was much warmer than any other during the period of instrumental meteorological observations based on land stations in the Northern and Southern Hemisphere.

An examination of the two halves of the decade in the Northern Hemisphere (**Figs. 5 and 6**) reveals that average temperature anomalies were somewhat larger during the latter half of the decade over Asia and North America. Specifically, temperatures averaged about 0.5^{o}C warmer over Siberia and northwestern North America. Elsewhere, anomalies were fairly consistent during both periods, although the negative anomalies in Greenland were larger during the first half of the decade. In the Southern Hemisphere (**Figs. 7 and 8**), temperature anomalies over land were more consistent between the two halves of the decade, except over northern Australia, where anomalies were more than 0.5^{o}C warmer during the latter half of the decade. SST anomalies in the South Atlantic and in the southern Indian Ocean were significantly larger during the 1986-1990 period with smaller anomalies occurring over the eastern Pacific.

1981 – 1985

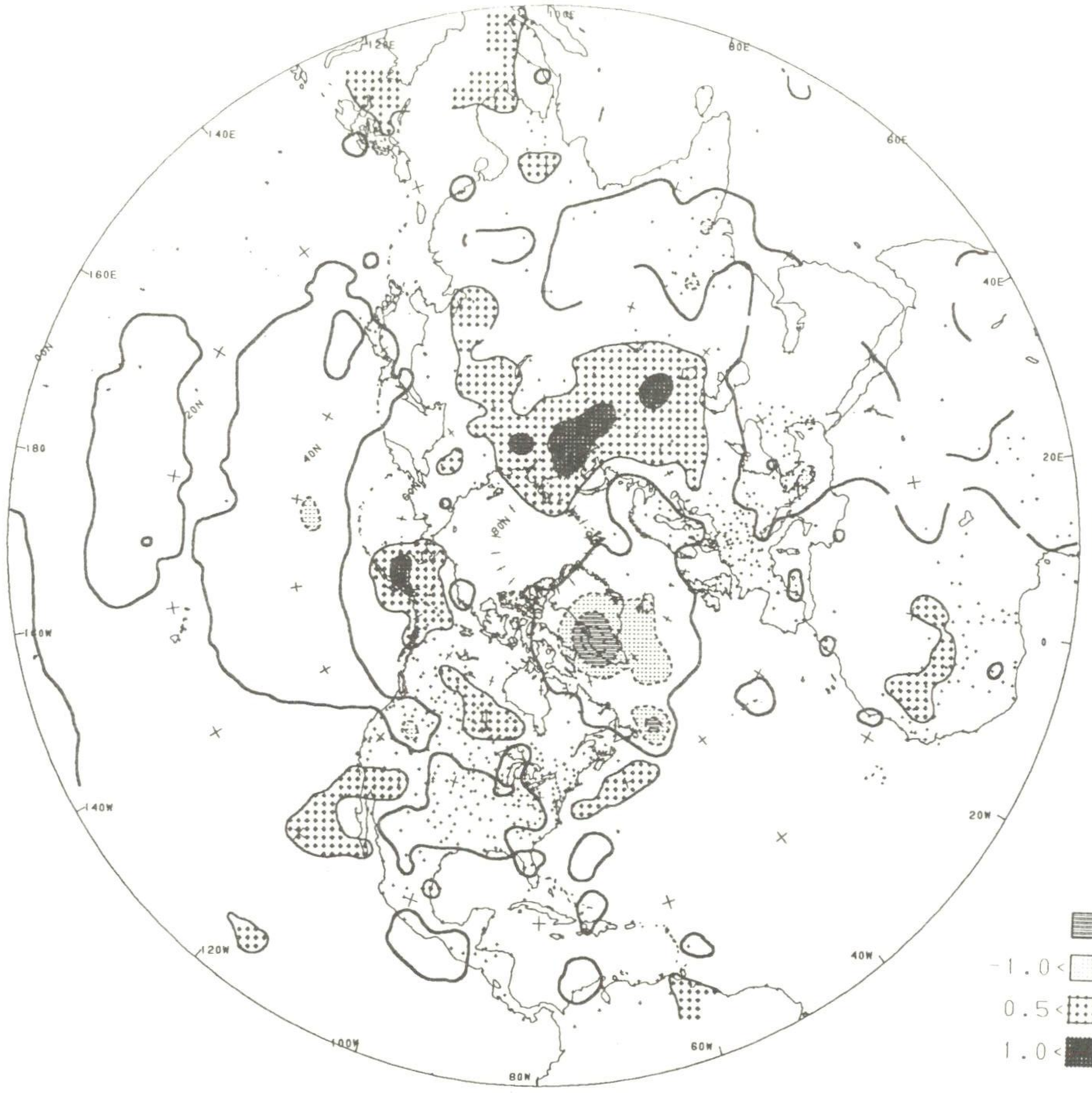

Fig. 5. N. Hemisphere surface temperature anomaly for the period 1981-85. Analysis based on station data over land and sea surface temperature (SST) over the water. Anomalies for station data are from the 1951-80 base period, while SST anomalies are computed as departures from the COADS/ICE climatology (Reynolds, 1988). Contour interval is 0.5°C.

1986 – 1990

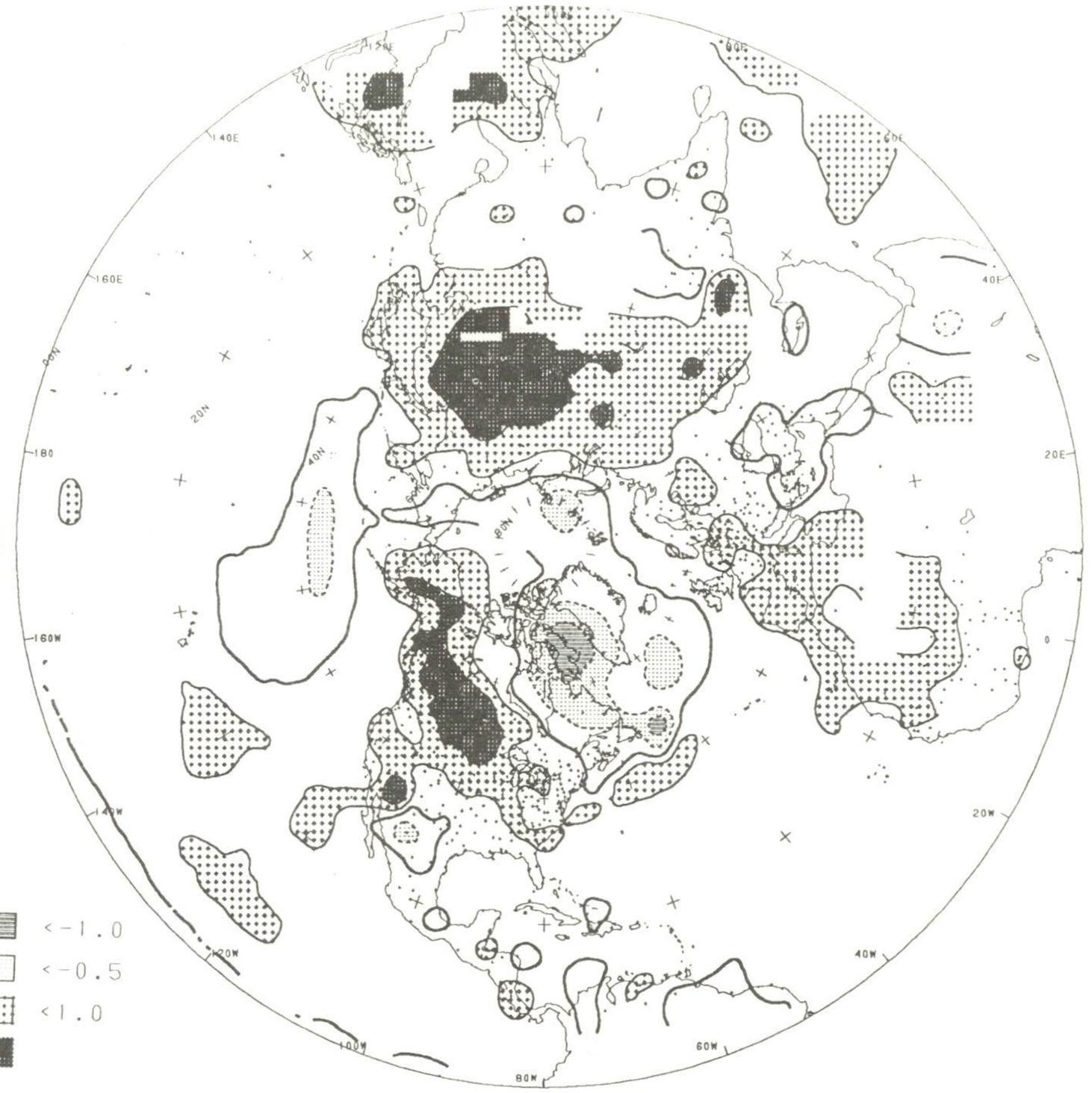

Fig. 6. N. Hemisphere surface temperature anomaly for the period 1986-90. Analysis based on station data over land and sea surface temperature (SST) over the water. Anomalies for station data are from the 1951-80 base period, while SST anomalies are computed as departures from the COADS/ICE climatology (Reynolds, 1988). Contour interval is 0.5°C.

1981 – 1985

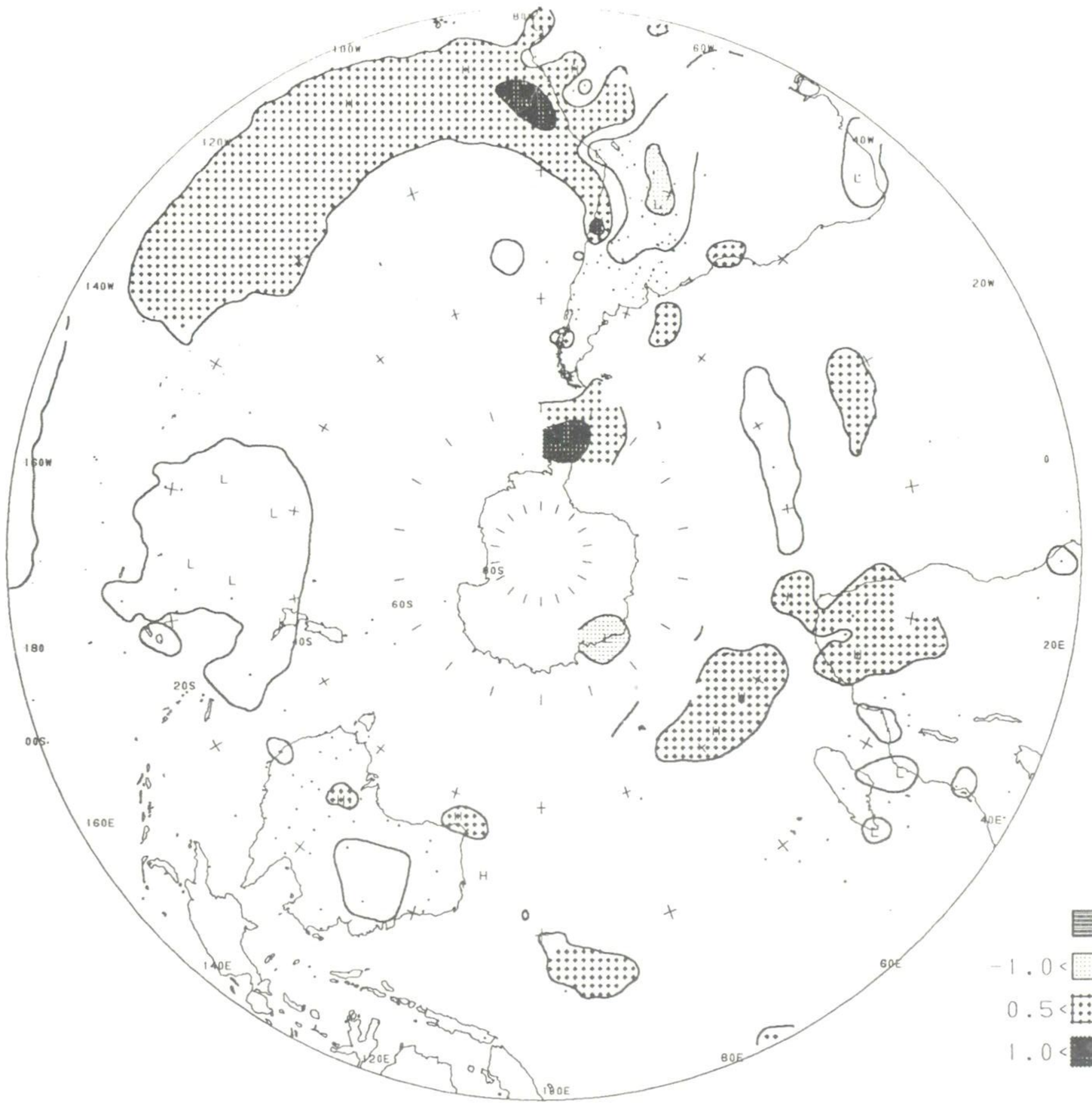

Fig. 7. S. Hemisphere surface temperature anomaly for the period 1981-85. Analysis based on station data over land and sea surface temperature (SST) over the water. Anomalies for station data are from the 1951-80 base period, while SST anomalies are computed as departures from the COADS/ICE climatology (Reynolds, 1988). Contour interval is 0.5°C.

1986 – 1990

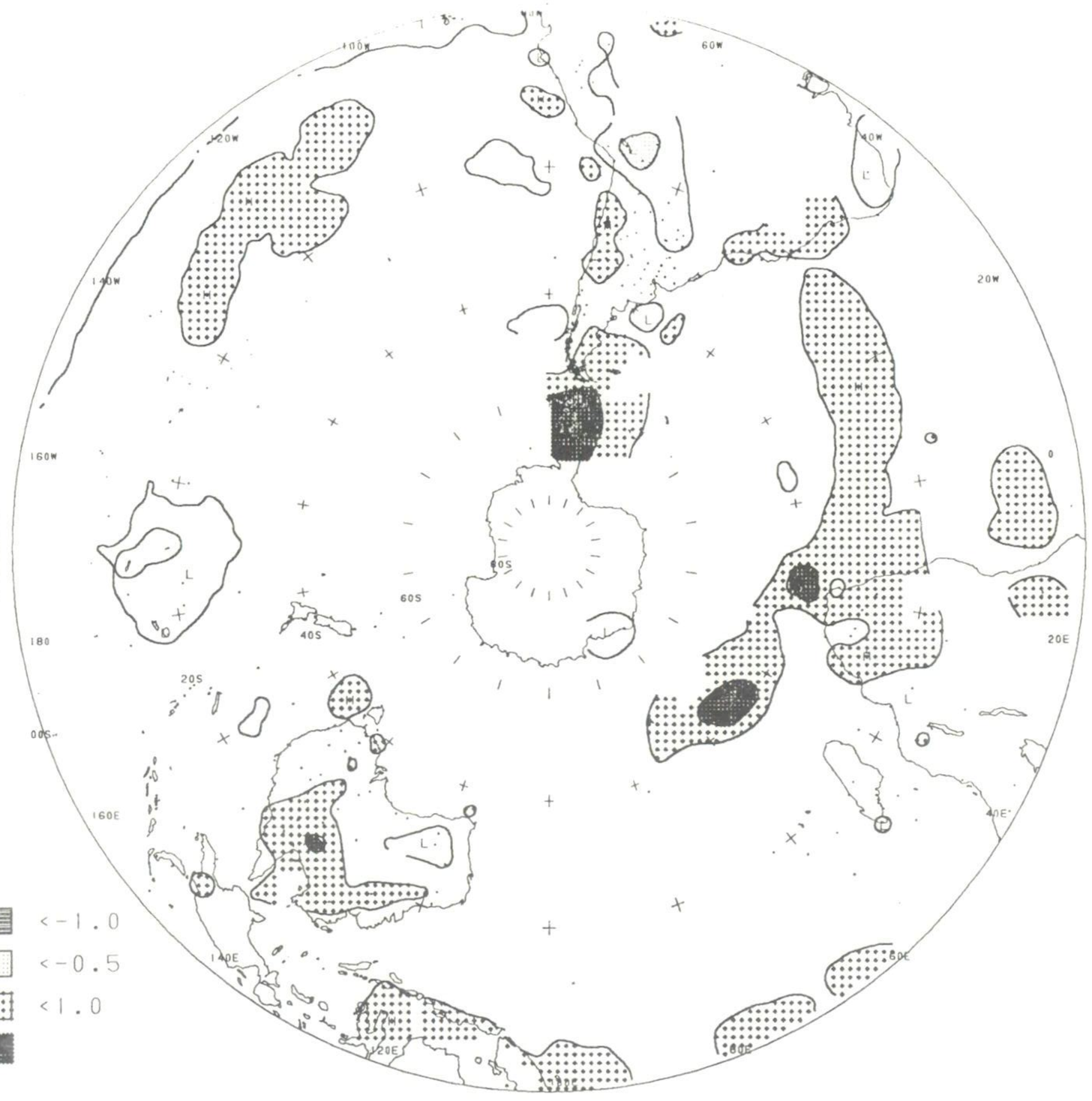

Fig. 8. S. Hemisphere surface temperature anomaly for the period 1986-90. Analysis based on station data over land and sea surface temperature (SST) over the water. Anomalies for station data are from the 1951-80 base period, while SST anomalies are computed as departures from the COADS/ICE climatology (Reynolds, 1988). Contour interval is 0.5°C.

Although most areas of the globe experienced above normal average temperatures for the decade, the anomalies were inconsistent from season to season. **Figures 9-12** show the temperature anomalies for the two hemispheres by traditional seasons. Over the Northern Hemisphere (**Figs. 9a-12a**), the separation of anomalies into seasons shows that much of the decadal warmth resulted from above normal temperatures during the DJF and MAM seasons, with that warmth concentrated over northern and central Asia and over northwestern North America. During the JJA season, anomalies were smaller over North America and negative over large parts of Asia. The temperature anomalies were positive over Siberia during the SON season, but were less than -1.0°C below normal over Alaska and western Canada. Over western Africa, temperatures were above normal during the MAM, JJA, and SON seasons. The DJF season, however, averaged below normal during the decade. Temperature departures were generally small during all seasons in the Southern Hemisphere (**Figs. 9b-12b**), except for over the Antarctic peninsula, where large positive anomalies occurred during the MAM and JJA seasons.

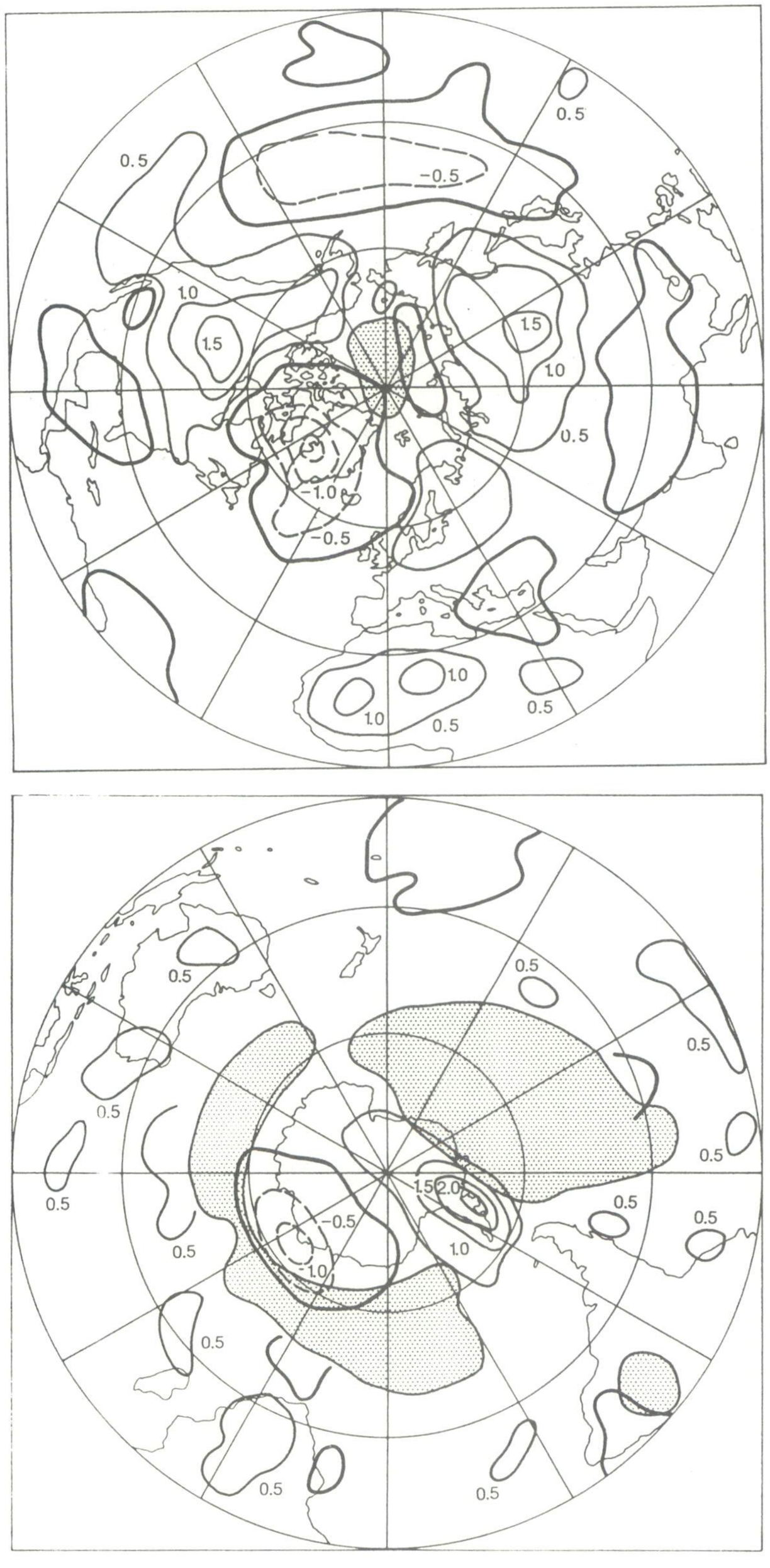

Figure 9. MAM seasonal temperature anomalies for the a) Northern and b) Southern Hemisphere from the 1950-1979 base period. Contour interval is 0.5°C, with negative anomalies dashed. Shaded areas indicate regions with insufficient data to perform analysis. Figure courtesy of the Climate Research Unit, University of East Anglia and the Hadley Centre, UKMO.

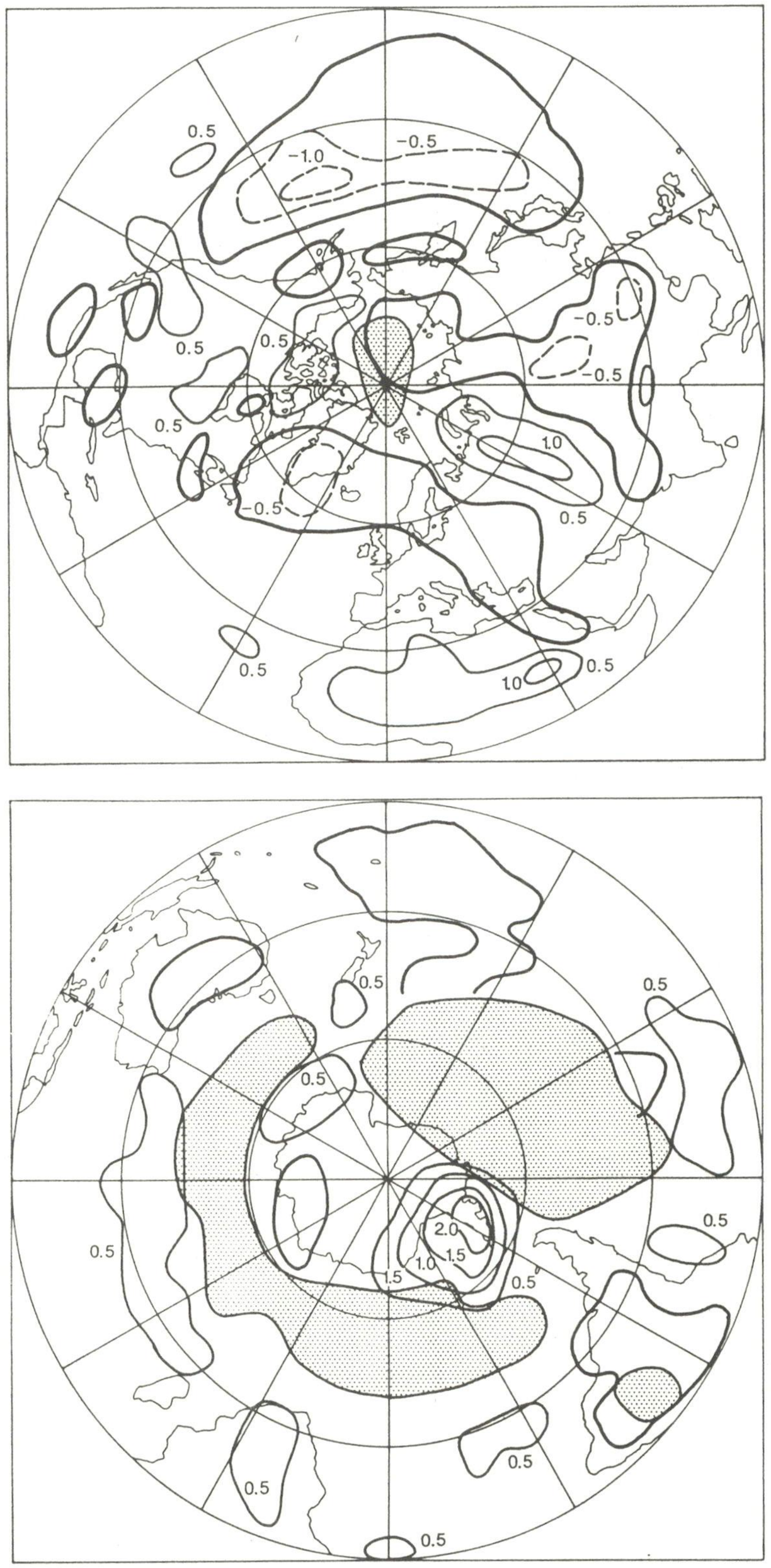

Figure 10. JJA seasonal temperature anomalies for the a) Northern and b) Southern Hemisphere from the 1950-1979 base period. Contour interval is 0.5°C, with negative anomalies dashed. Shaded areas indicate regions with insufficient data to perform analysis. Figure courtesy of the Climate Research Unit, University of East Anglia and the Hadley Centre, UKMO.

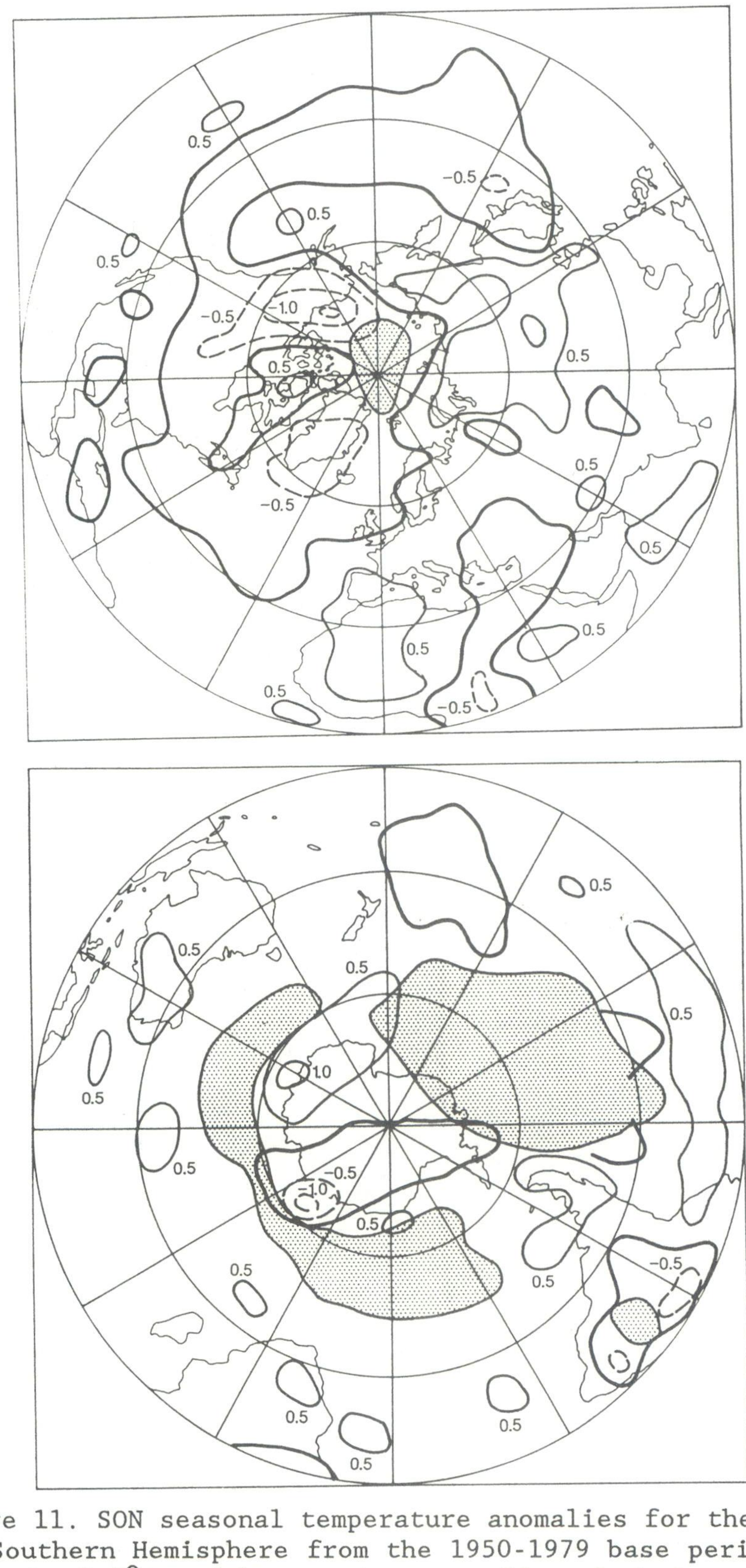

Figure 11. SON seasonal temperature anomalies for the a) Northern and b) Southern Hemisphere from the 1950-1979 base period. Contour interval is 0.5°C, with negative anomalies dashed. Shaded areas indicate regions with insufficient data to perform analysis. Figure courtesy of the Climate Research Unit, University of East Anglia and the Hadley Centre, UKMO.

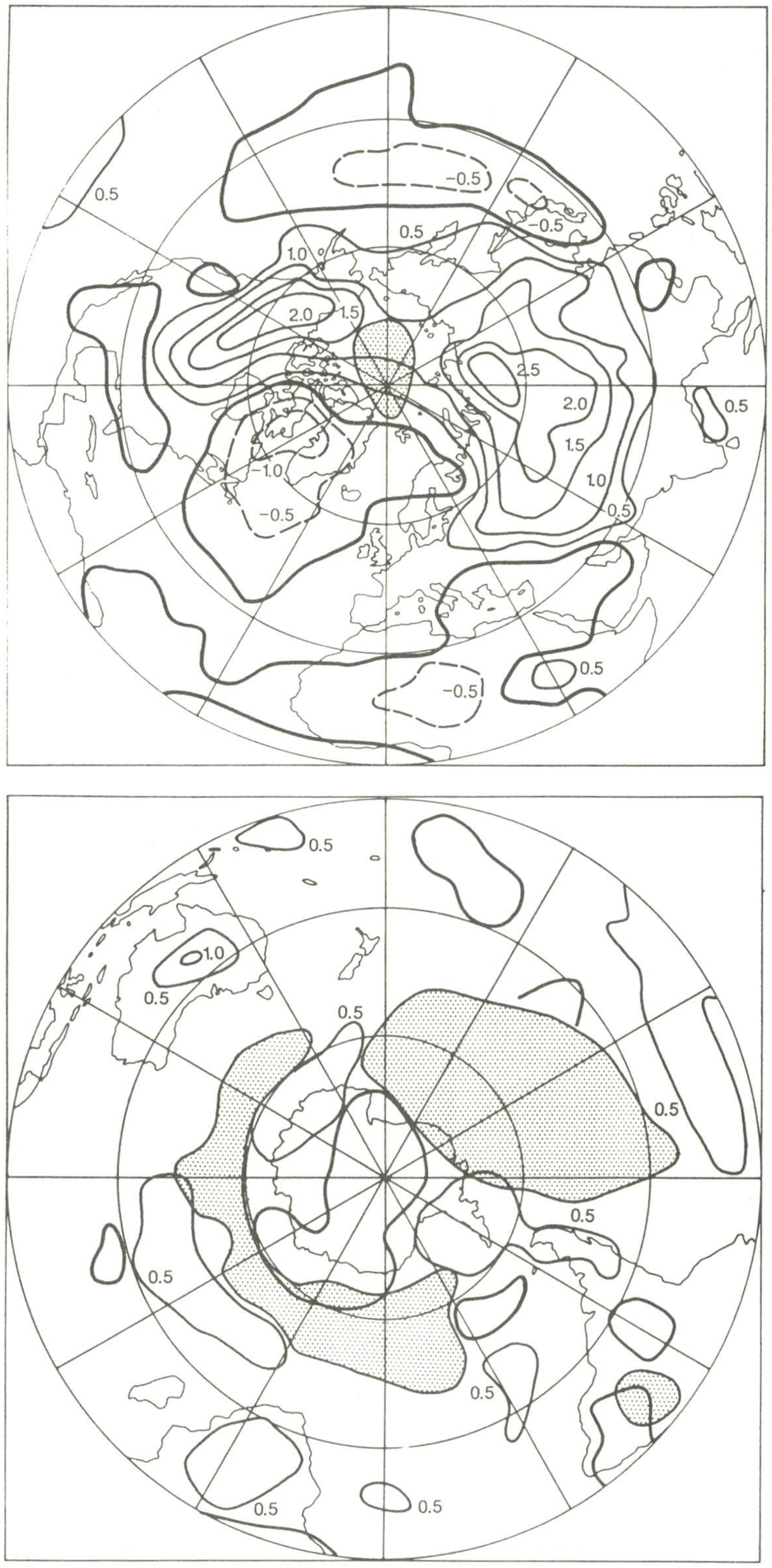

Figure 12. DJF seasonal temperature anomalies for the a) Northern and b) Southern Hemisphere from the 1950-1979 base period. Contour interval is 0.5°C, with negative anomalies dashed. Shaded areas indicate regions with insufficient data to perform analysis. Figure courtesy of the Climate Research Unit, University of East Anglia and the Hadley Centre, UKMO.

The large differences in temperature anomalies between the first and second half of the year can be seen in **Figs. 13 and 14**. The December - May period (**Fig. 13**) had average temperatures greater than 1.5°C above normal covering a large area over Alaska and western Canada. Another large area with positive anomalies exceeding 1.0°C was found over Siberia. Large negative anomalies were found over Greenland. During the June - November period (**Fig. 14**), anomalies over Alaska and western Canada were negative, albeit small. This shift implies a reduction in the amplitude of the annual cycle over this region. In the Southern Hemisphere, the largest differences between the December - May (**Fig. 15**) and the June - November period (**Fig. 16**) occurred over South America, where negative anomalies larger the -1.0°C during the June - November were replaced by much smaller negative anomalies during December - May. Temperature anomalies over Australia and southern Africa, as well as hemispheric SST anomalies, were similar during both periods.

The global seasonal time series (**Fig. 17**) suggest that the character of the annual temperature anomalies is determined, to a large extent, by the anomalies in the DJF and MAM seasons. This agrees with the analysis shown in **Figs. 13 and 14**. The median anomalies tend to be smaller in magnitude during JJA and SON. The lengths of the 10th and 90th percentile lines (whiskers) clearly indicate that the largest spatial variability occurs in northern winter (DJF) and the least in northern summer (JJA).

The Northern Hemisphere median time series (**Fig. 18**) clearly shows higher amplitude variations than the global plots during DJF. However, the differences between the global and Northern Hemisphere time series are much less in the remaining seasons.

The magnitudes of the Southern Hemisphere anomalies (**Fig. 19**) are smaller than those in the Northern Hemisphere for each season. The southern winter (JJA) and spring (SON) seasons do not appear to dominate the annual temperature curves as the analogous seasons do in the Northern Hemisphere. With the exception of the JJA season of 1984, all of the Southern Hemisphere seasonal median temperatures are positive during each season of the 1980's.

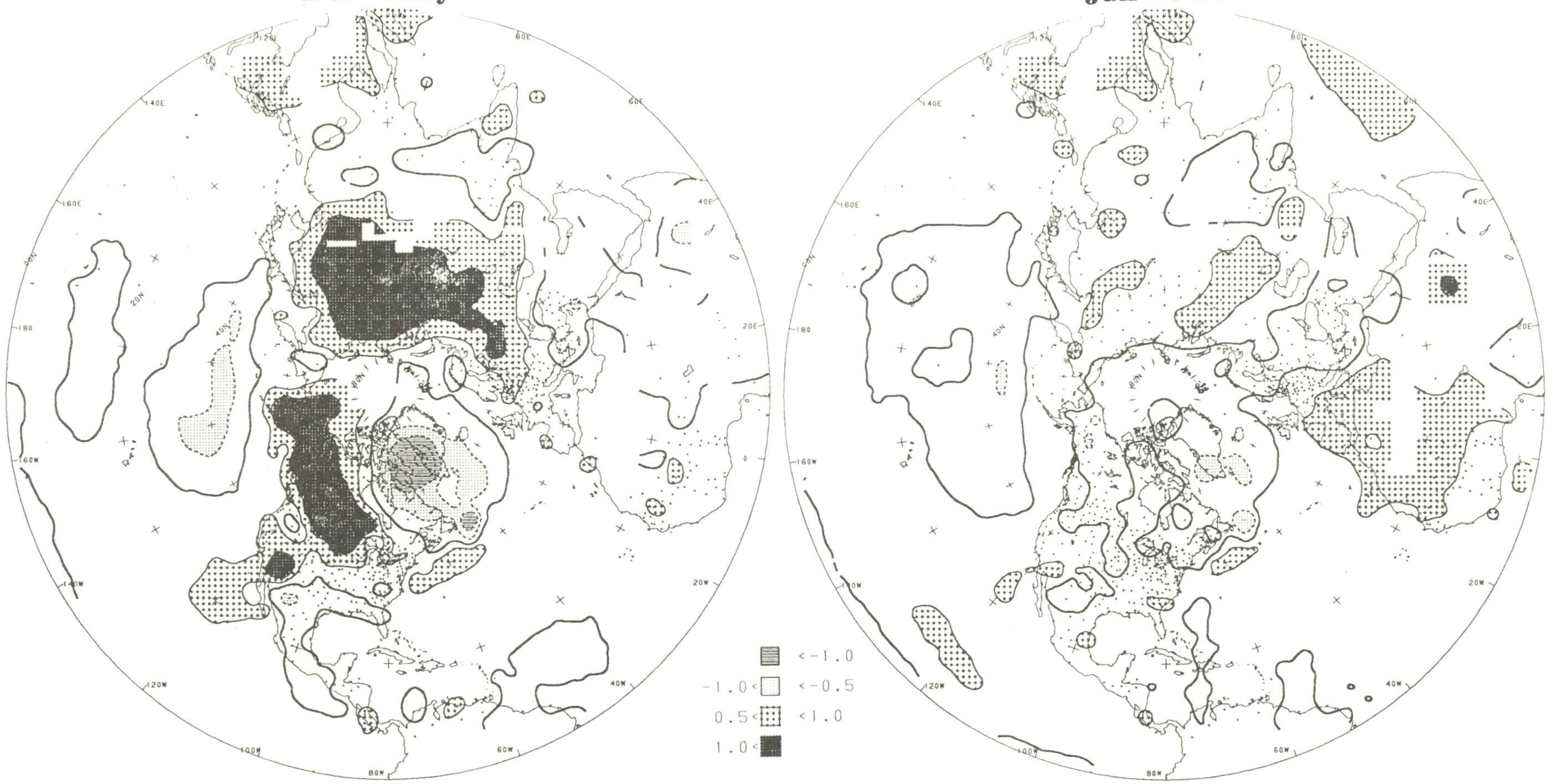

Fig. 13. N. Hemisphere December - May surface temperature anomaly for the period 1981-90. Analysis based on station data over land and sea surface temperature (SST) over the water. Anomalies for station data are from the 1951-80 base period, while SST anomalies are computed as departures from the COADS/ICE climatology (Reynolds, 1988). Contour interval is 0.5°C.

Fig. 14. N. Hemisphere June - November surface temperature anomaly for the period 1981-90. Analysis based on station data over land and sea surface temperature (SST) over the water. Anomalies for station data are from the 1951-80 base period, while SST anomalies are computed as departures from the COADS/ICE climatology (Reynolds, 1988). Contour interval is 0.5°C.

Dec – May

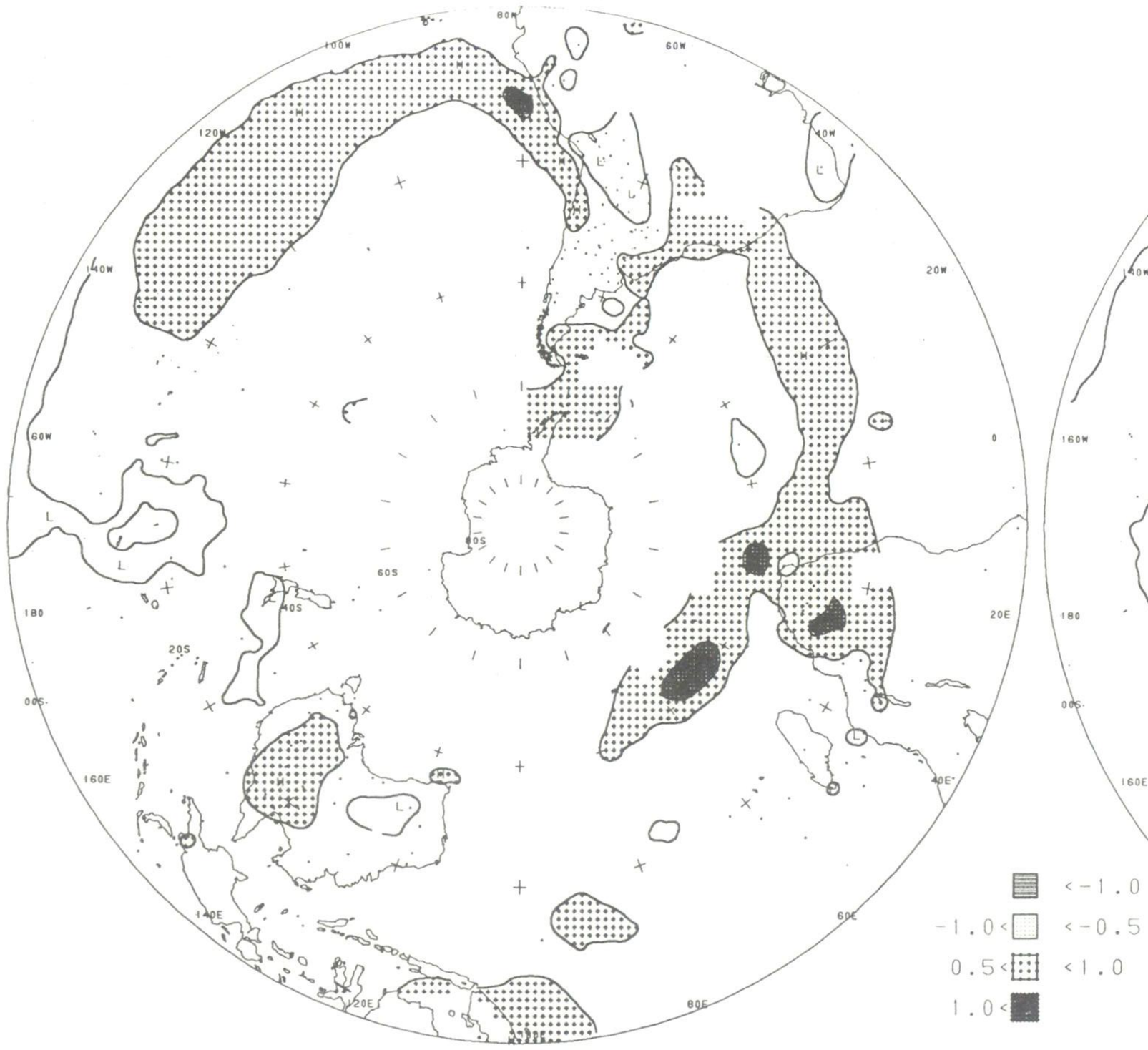

Fig. 15. S. Hemisphere December - May surface temperature anomaly for the period 1981-90. Analysis based on station data over land and sea surface temperature (SST) over the water. Anomalies for station data are from the 1951-80 base period, while SST anomalies are computed as departures from the COADS/ICE climatology (Reynolds, 1988). Contour interval is 0.5°C.

Jun – Nov

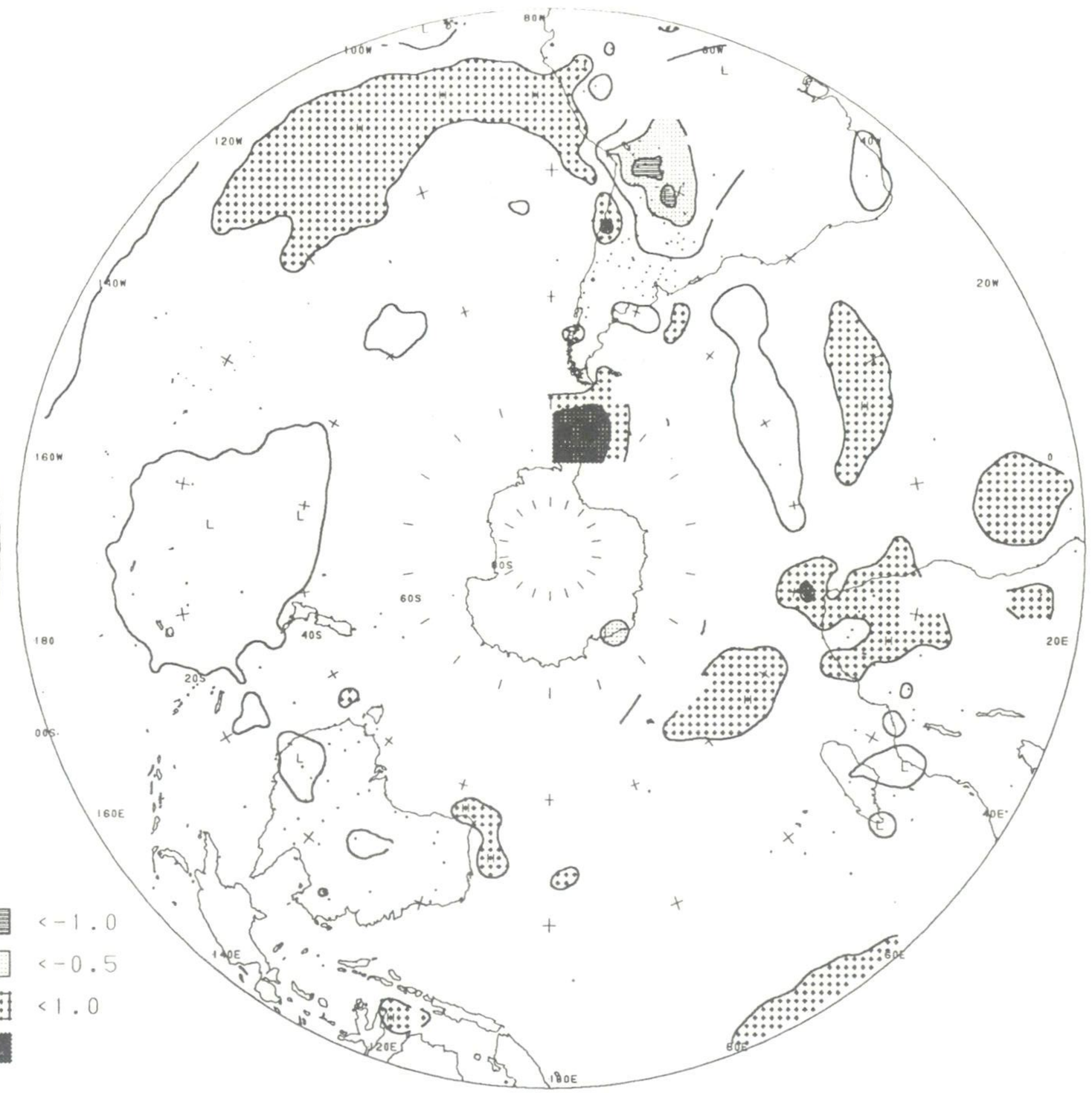

Fig. 16. S. Hemisphere June - November surface temperature anomaly for the period 1981-90. Analysis based on station data over land and sea surface temperature (SST) over the water. Anomalies for station data are from the 1951-80 base period, while SST anomalies are computed as departures from the COADS/ICE climatology (Reynolds, 1988). Contour interval is 0.5°C.

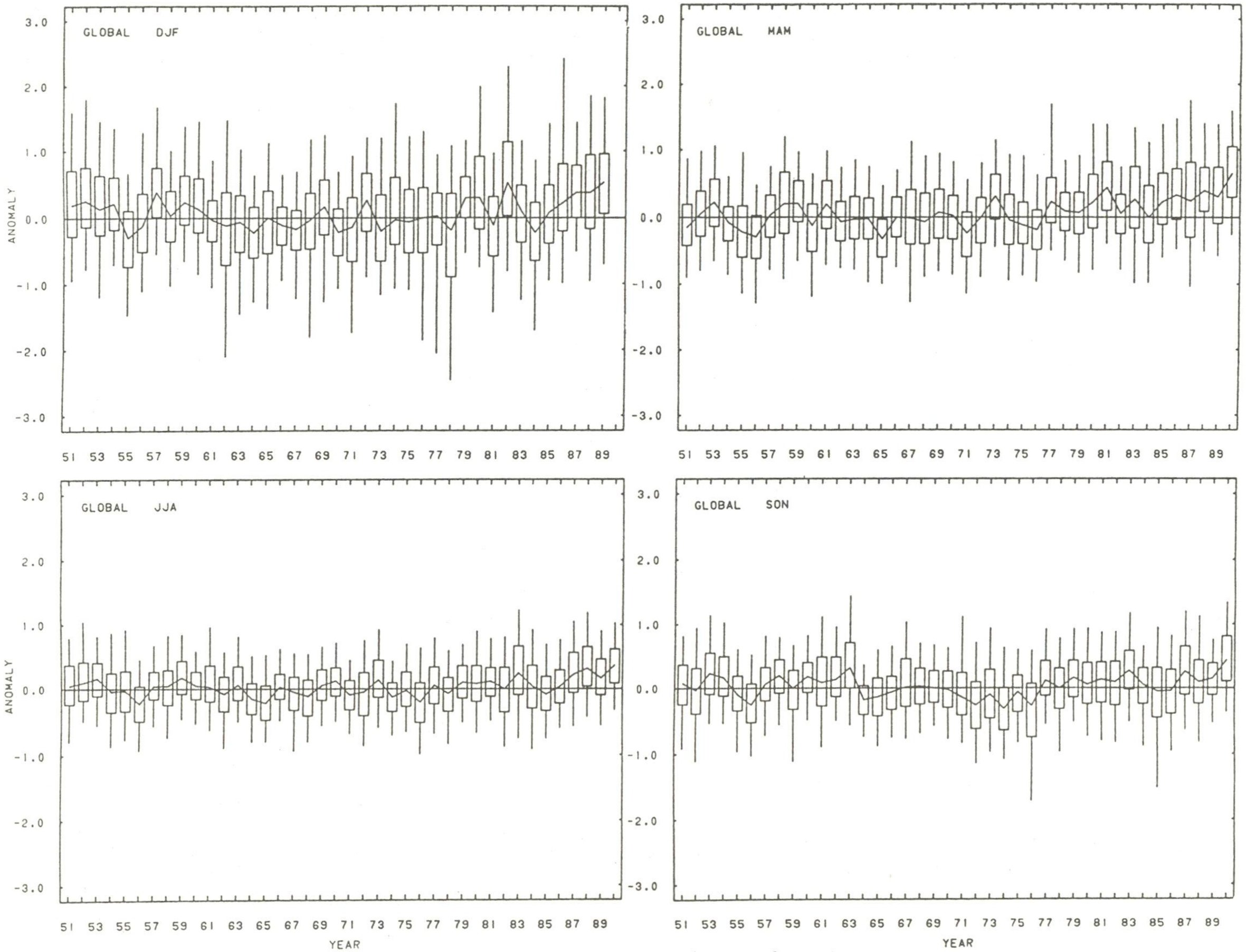

Fig. 17 Global seasonal surface temperature index based on the average temperature anomalies in 2^{o} latitude by 2^{o} longitude areas over land. The solid line in each panel represents the 50%, or median, temperature anomaly for each year. Each "box" delineates the temperature anomalies at the 70th and 30th percentiles while the "whiskers" (lines) delineate the 90th and 10th percentile values. The anomalies are taken with respect to the 1951 to 1980 base period.

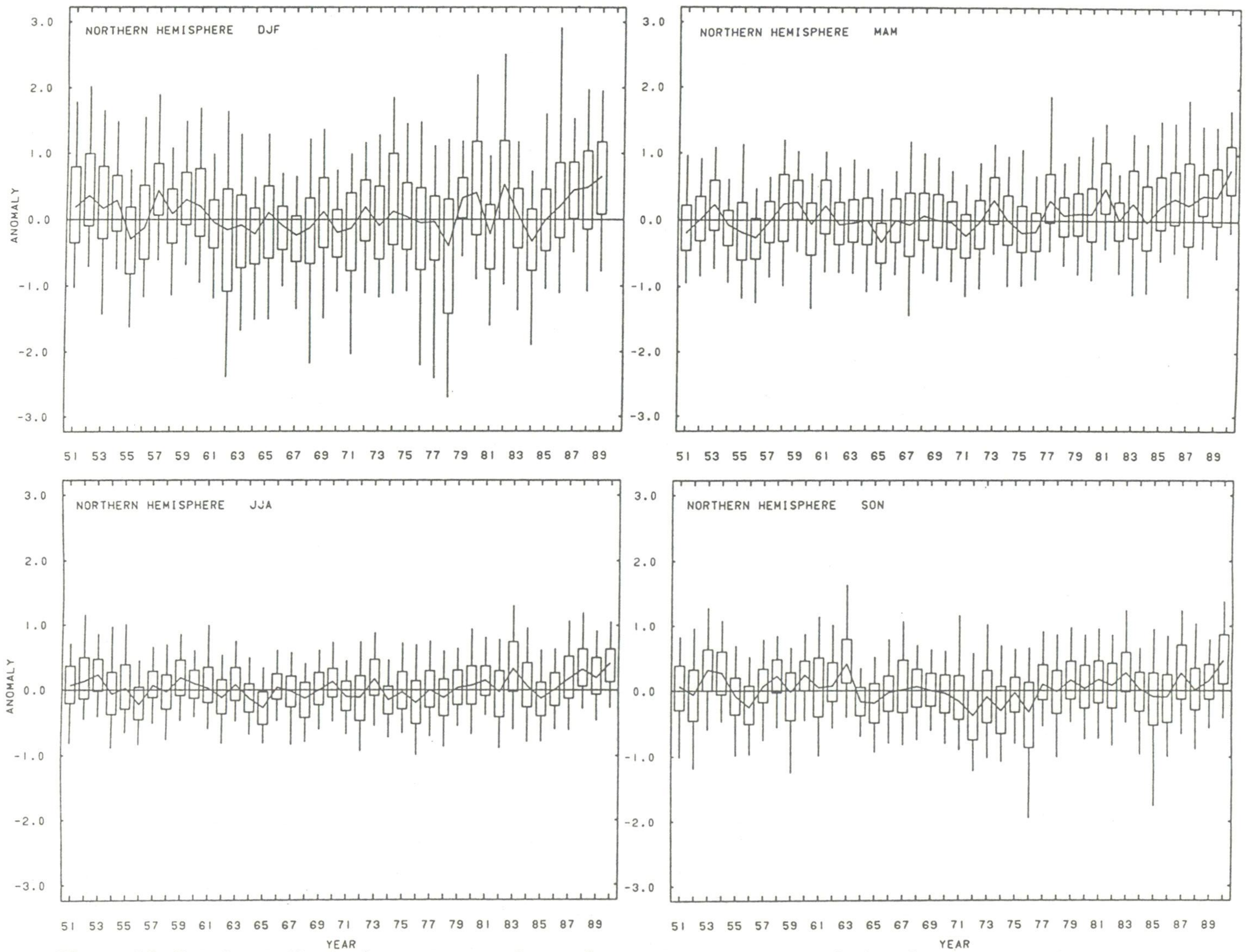

Fig. 18 Northern Hemisphere seasonal surface temperature index based on the average temperature anomalies in 2^{o} latitude by 2^{o} longitude areas over land. The solid line in each panel represents the 50%, or median, temperature anomaly for each year. Each "box" delineates the temperature anomalies at the 70th and 30th percentiles while the "whiskers" (lines) delineate the 90th and 10th percentile values. The anomalies are with respect to the 1951 to 1980 base period.

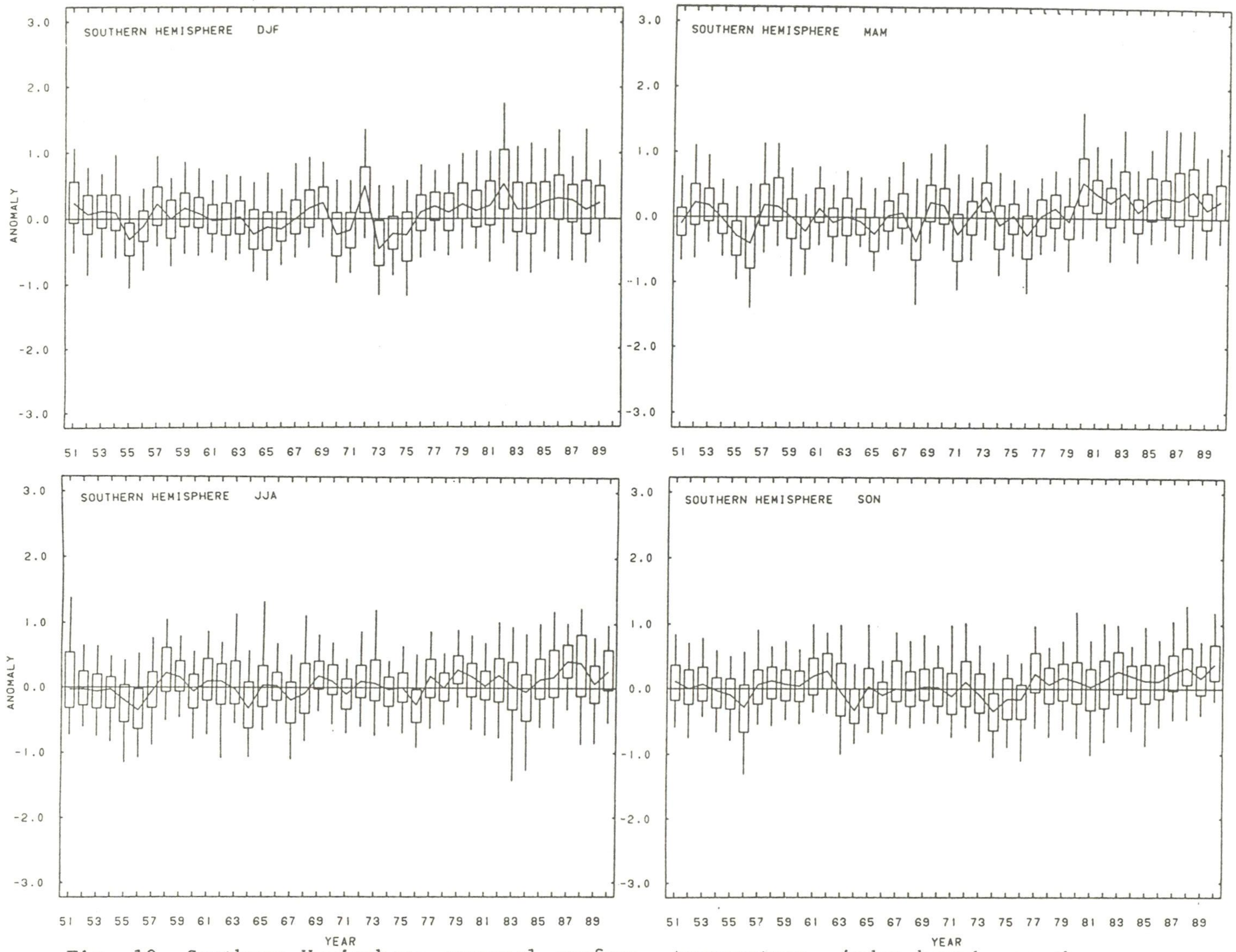

Fig 19. Southern Hemisphere seasonal surface temperature index based on the average temperature anomalies in 2^{o} latitude by 2^{o} longitude areas over land. The solid line in each panel represents the 50%, or median, temperature anomaly for each year. Each "box" delineates the temperature anomalies at the 70th and 30th percentiles while the "whiskers" (lines) delineate the 90th and 10th percentile values. The anomalies are with respect to the 1951 to 1980 base period.

REGIONAL

In the United States, the decade of the 1980's ranks as the second warmest of the century, behind the 1930's and just ahead of the 1950's (**Fig. 20a**). **Figure 20b** shows the time series of the United States annual mean temperature from 1901 through 1990. Although the decade as a whole averaged well above normal, half of the years experienced mean temperatures below the long-term mean. However, the warmth during 1981, 1986, 1987, and 1990, which all averaged greater than than 1.0°C above normal, resulted in a much warmer than average decade.

The distribution of temperature anomalies by seasons during the 20th century for the United States is shown in **Fig. 21**. The bar graph depicting mean spring temperatures (**Fig. 21b**) shows that spring temperatures during the 1980's were by far the highest of the 20th century and accounted for the majority of the above normal temperatures found in the United States during the decade. Winter temperatures (**Fig. 21a**), while averaging higher than the previous two decades, were still lower than the four prior decades. Summer temperatures (**Fig. 21c**) ranked third highest of the century while fall temperatures (**Fig. 21d**) ranked third lowest.

Global surface temperature observations have shown an increase during the latter half of the 1980s (**Fig. 3**). This trend is also found in U. S. surface temperatures (**Fig. 20b**). However, there appears to be no counterpart in the lower troposphere (1000-400 mb) according to higher spatial resolution satellite observations (**Fig. 39**) (Spencer, et al., 1990). Assuming that the satellite data are correct, this implies that the upper air circulation has been relatively unaffected by systematic surface warming.

A technique developed by Klein (1983) for computing contemporaneous surface temperature anomalies from the upper-air height anomaly pattern may be useful in diagnosing the surface warming, since those <u>specified</u> anomalies would tend to underestimate the actual observed anomalies. Thus, higher surface temperatures, for a given circulation, would appear as a negative error of the objectively specified temperatures.

The Klein specification technique is used to specify surface temperatures from prognostic 700 mb height anomaly patterns. Here we apply the method to <u>observed</u> 700mb height anomalies.

The equations developed in this technique are of the form,

$$Y_i = c_j*X_j+c_k*X_k+c_l*X_l+\ldots \quad , \qquad (1)$$

where Y_i = specified surface temperature at station i,
C_m = coefficient for grid-point m,
X_m = 700 mb height anomaly at grid-point m.

The coefficients developed by this technique incorporate information about the surface temperature-versus-height relationship in the dependent datasets during the training period, 1948-1981 in this case. The training datasets used as input for computing the coefficients are simultaneous monthly mean 700 mb height anomalies at 133 grid-points over North America and surrounding oceans (the predictors) and anomalies of monthly mean

surface temperature at 109 stations over the continental United States (the predictands) from 1948-81. The predictors are chosen in a stepwise fashion so that the first predictor explains the largest fraction of the variance of the training dataset, the second explains the next largest fraction, exclusive of that explained by the first, etc.

The procedure used in the current study is to apply the equations described above to a set of observed monthly mean 700 mb height anomalies for 1981 to 1990. Surface temperature anomalies computed from this dataset by means of the equations (specified temperatures) are then compared with observed temperature anomalies at 109 stations for the same period. The specified surface temperature anomaly errors, averaged over the continental United States, are shown in **Fig. 22**. The time series plotted is the result of a 13-point (12-month) running mean. Thus, the series begins with July 1981 and ends with June 1990.

The time series of specified surface temperature anomaly errors shows a sharp rise from negative values in 1981 (specified less than observed) to mainly positive values in 1982. Specified temperature anomalies over-estimate actual surface temperature anomalies from late 1983 through much of 1985. Since mid-1987, specified anomalies have been consistently less than observed anomalies over the United States, by as much as $0.5^{o}C$. Furthermore, there is a clear trend for decreasing values of the error of specified anomalies beginning in mid-1984 and continuing through mid-1990.

This trend is precisely the type that would occur if, for a given circulation pattern, the average surface temperature during the latter period was higher than in the 1951-80 period. The specified anomalies, while appropriate, in the mean, for the period of the dependent data set (1948-81), were increasingly underestimating the temperature in the latter era. It is also consistent with the observed trend in surface temperature for the United States (**Fig. 20b**).

Surface temperature analyses (obtained from the World Data Center-B, Obninsk) over the Soviet Union were also significantly above normal during the 1981-1990 period. All of the Soviet Union during the decade of the 1980's experienced positive temperature anomalies (**Fig. 23**) , with anomalies greater than $1^{o}C$ found over western Siberia. The areal extent of positive temperature anomalies during the three earlier decades was smaller, although there is a trend toward increasing amounts of area with positive temperature anomalies with time.

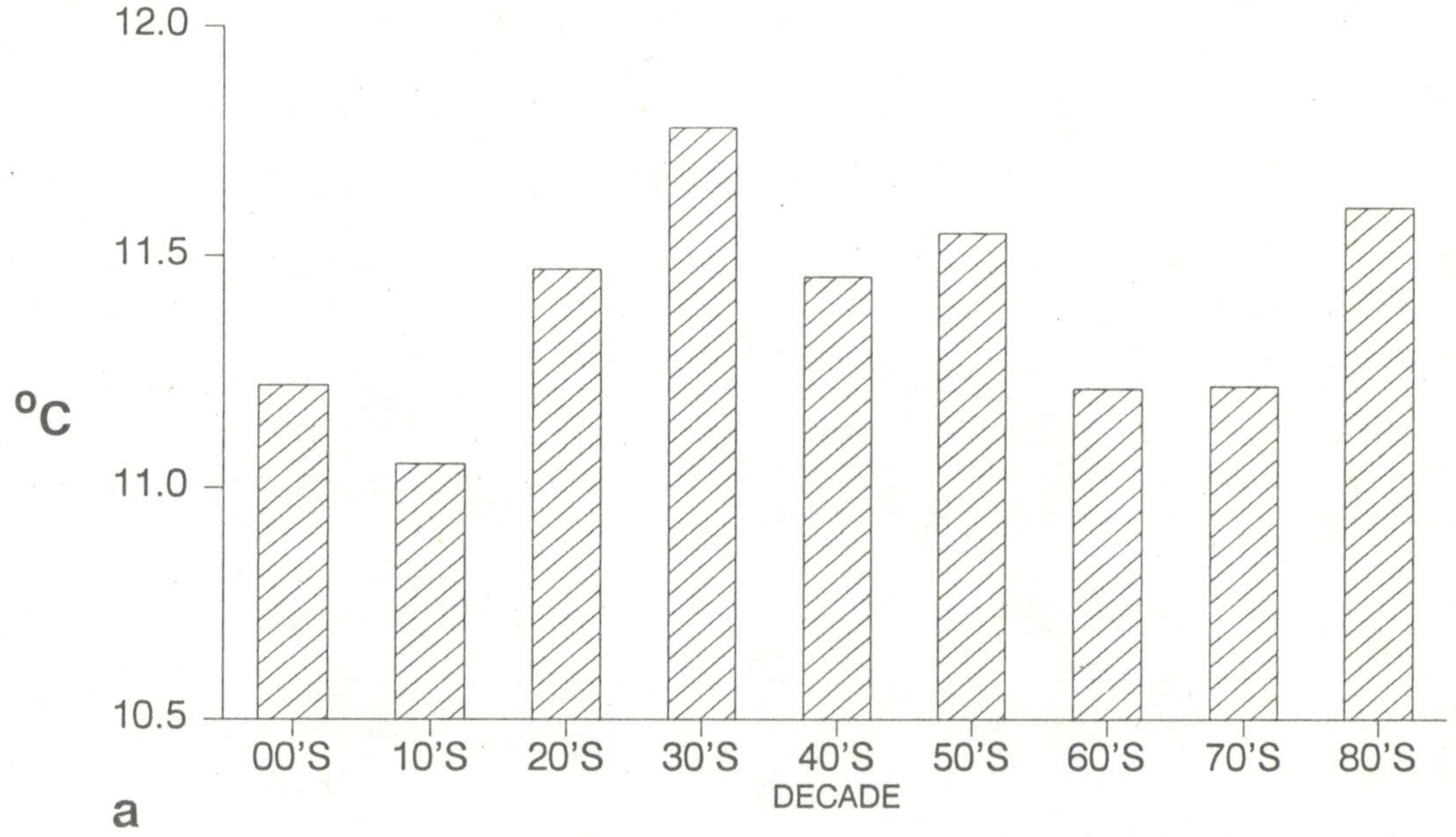

National Climatic Data Center, NOAA

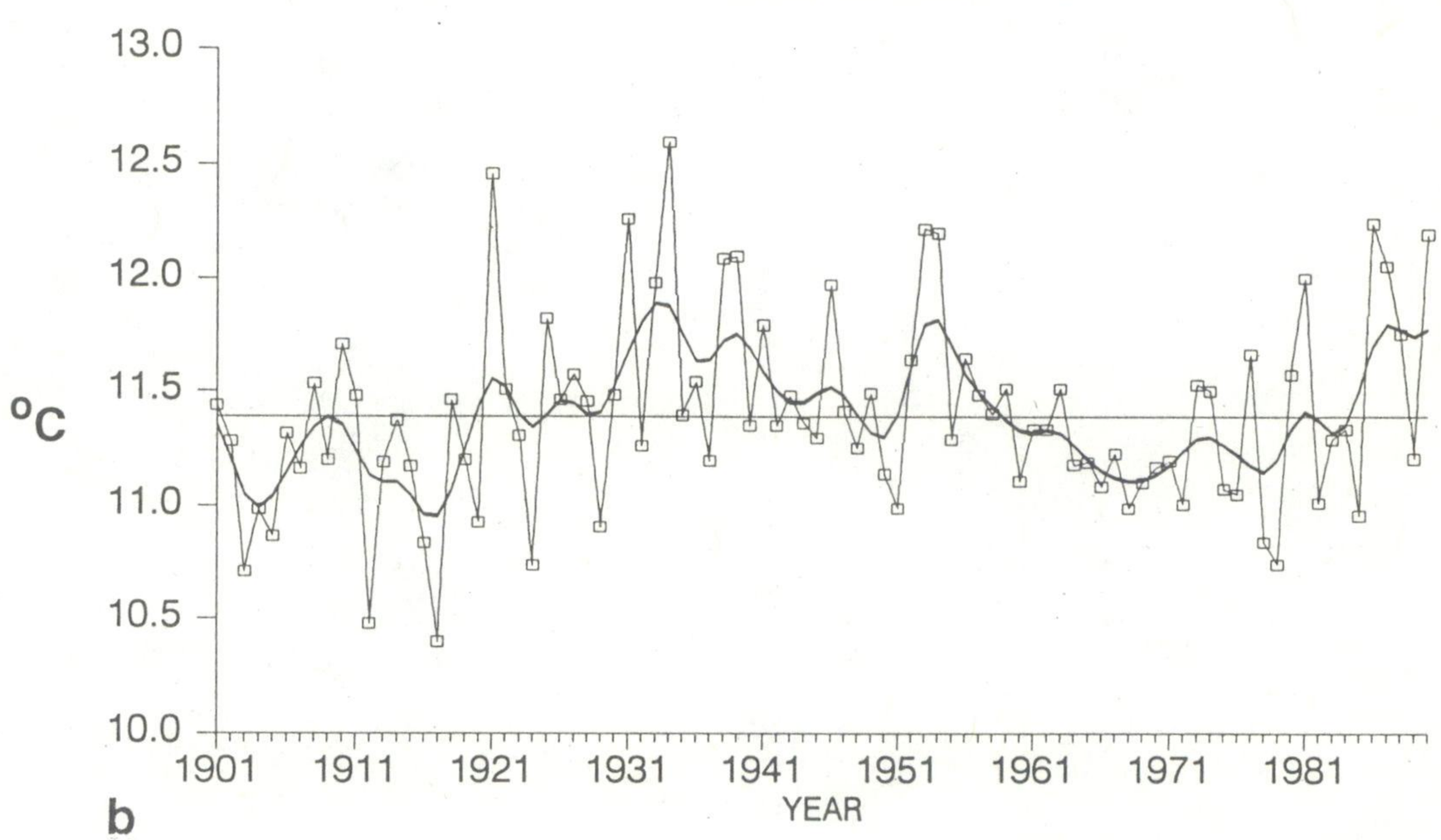

National Climatic Data Center, NOAA

Figure 20. U. S. national annual temperature expressed as a) decadal means for the decades 1901-10 through 1981-90, and as b) a corresponding annual time series line graph with a filtered curve for 1901-1990. The ten annual values within each decade were averaged to determine a decadal mean value for the decade.

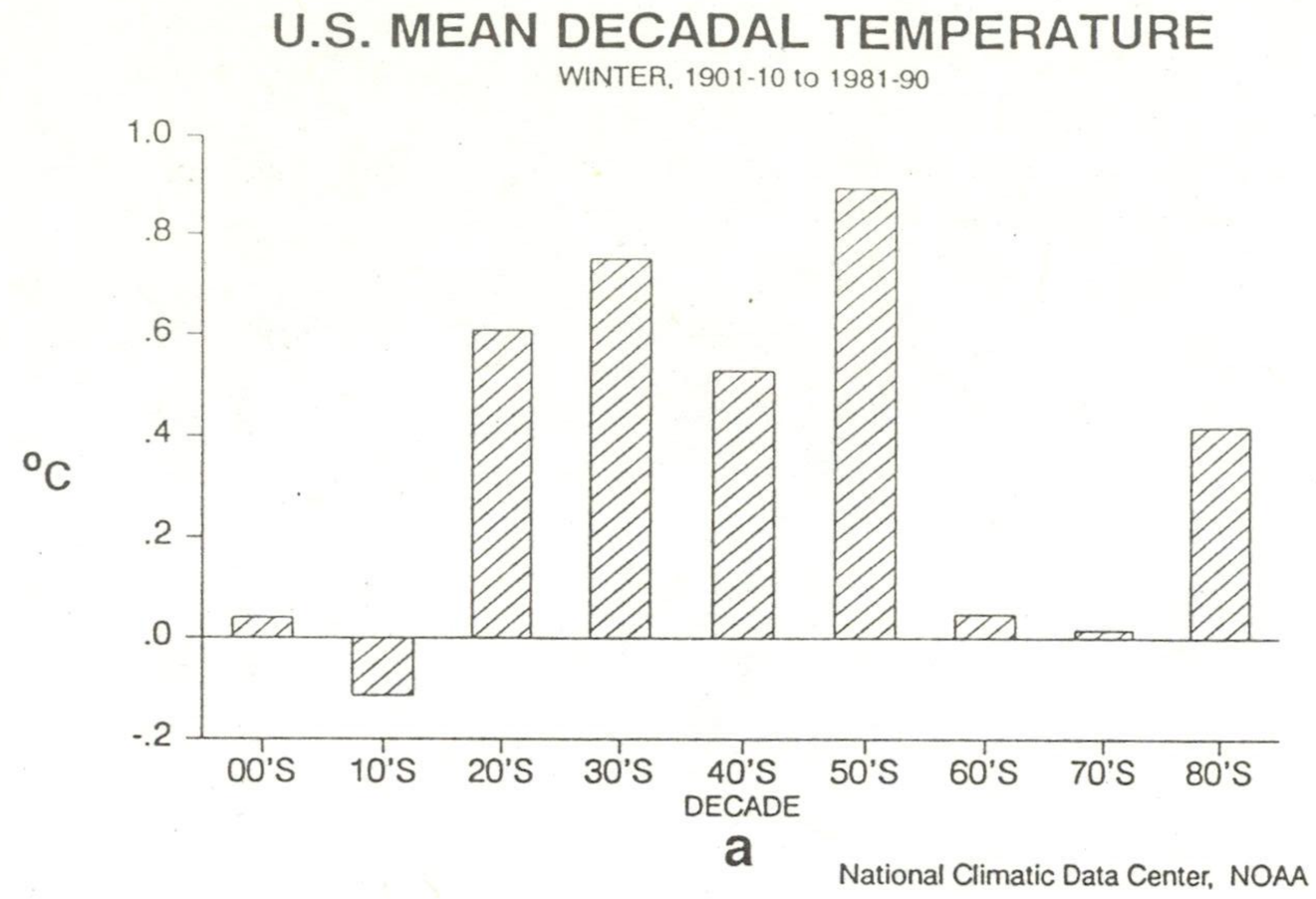

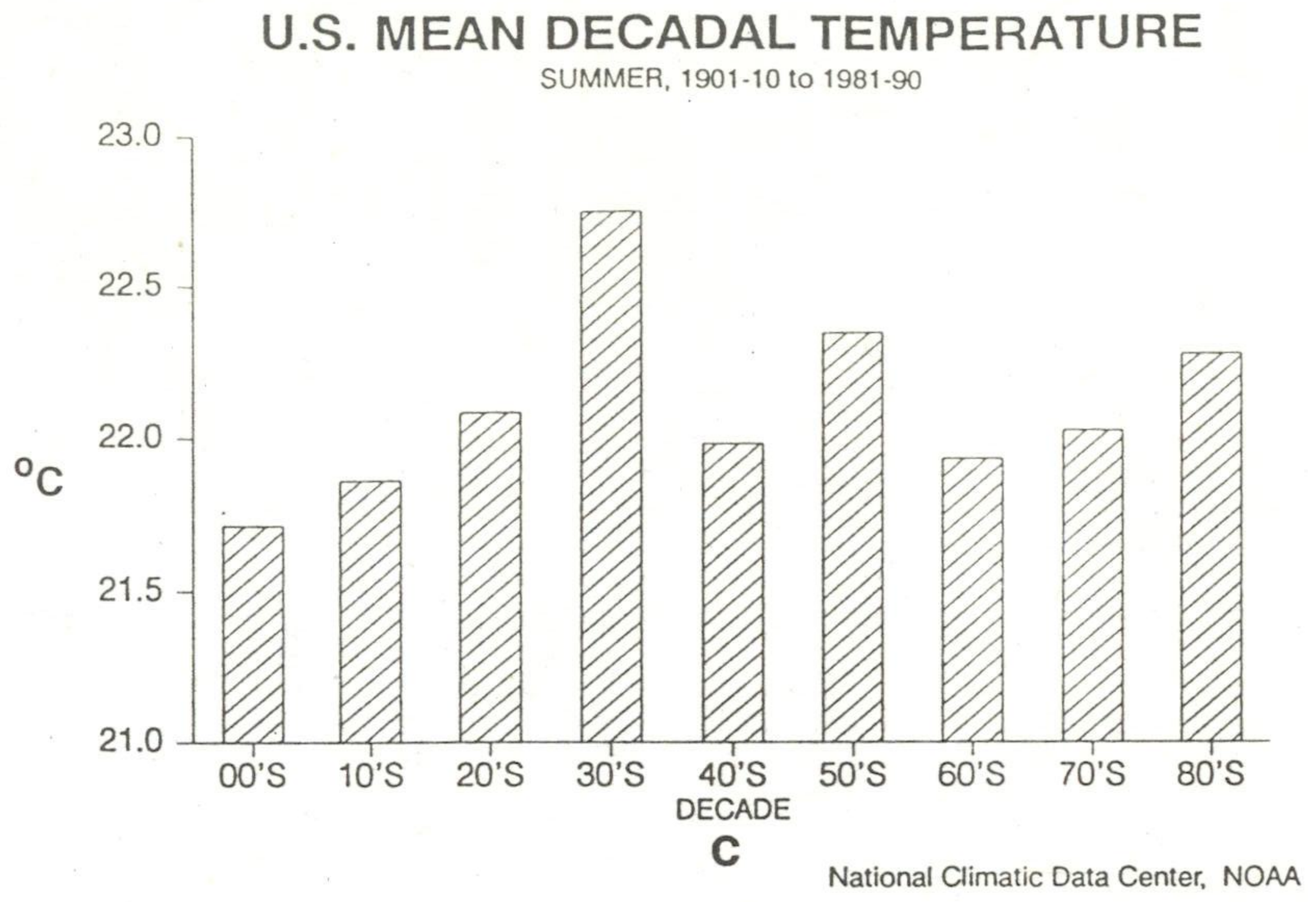

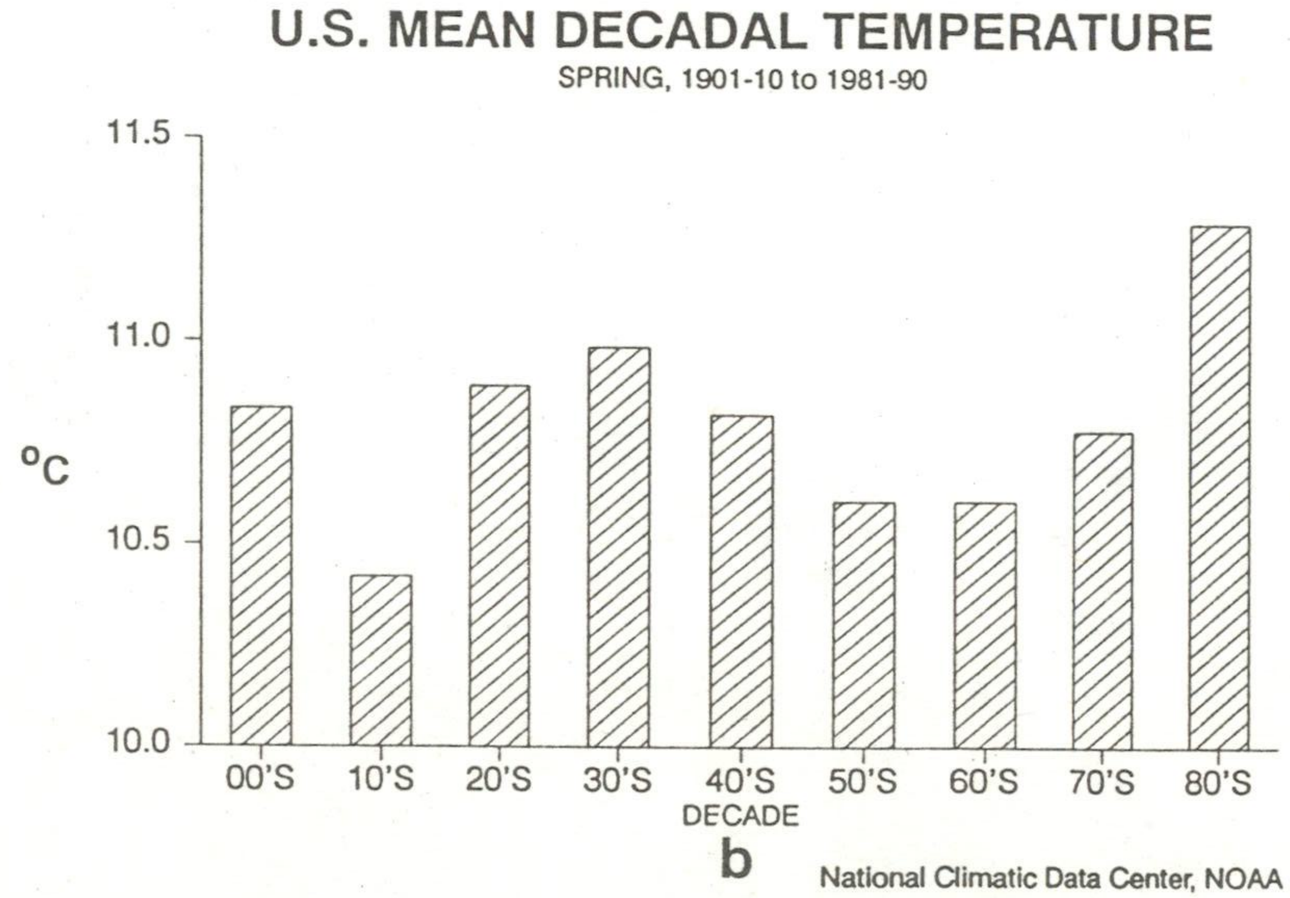

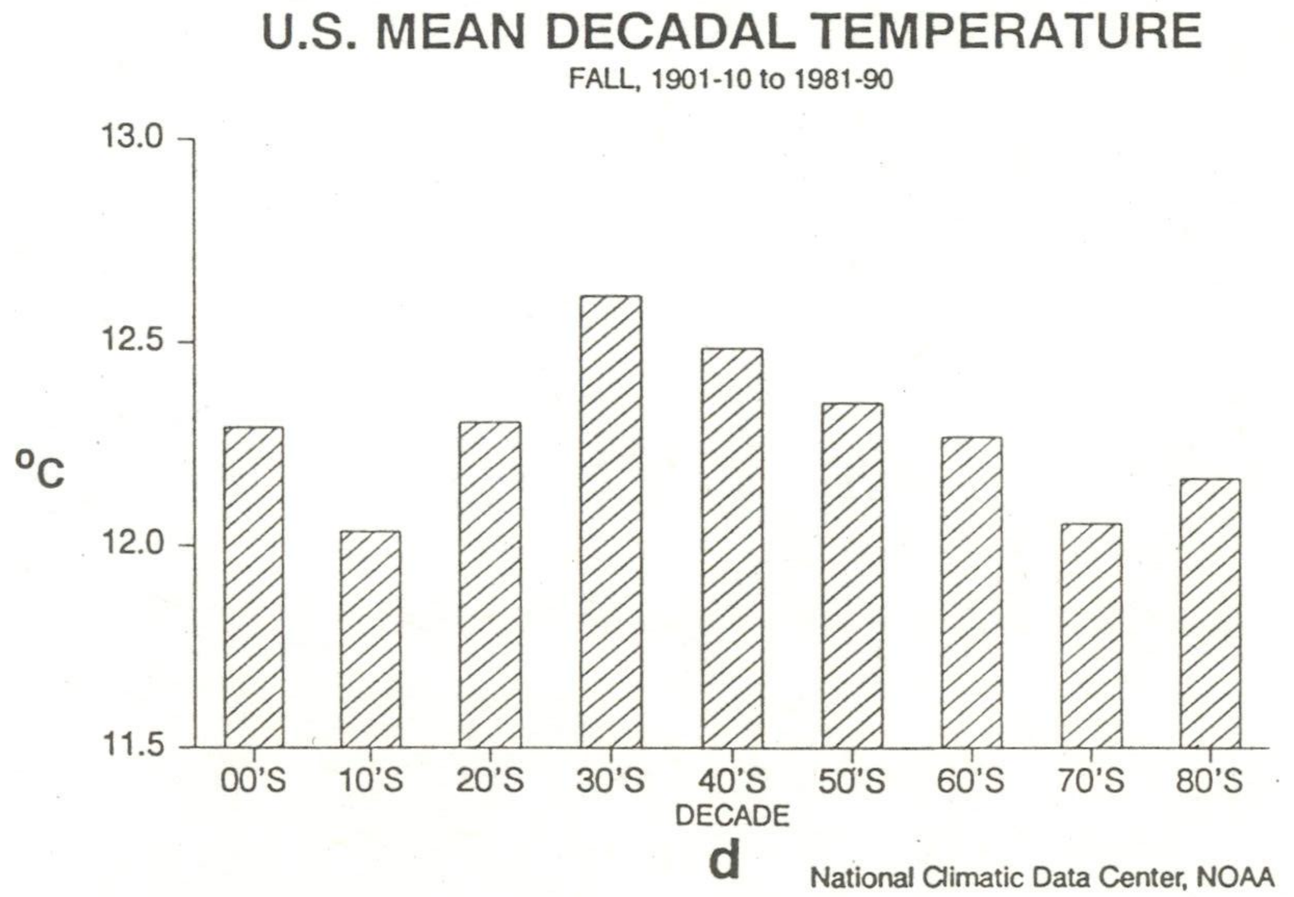

Figure 21. U. S. national seasonal temperature expressed as decadal means for the decades 1901-10 through 1981-90 for a) winter, b) spring, c) summer and d) fall. The ten seasonal values within each decade were averaged to determine a decadal mean value for the decade.

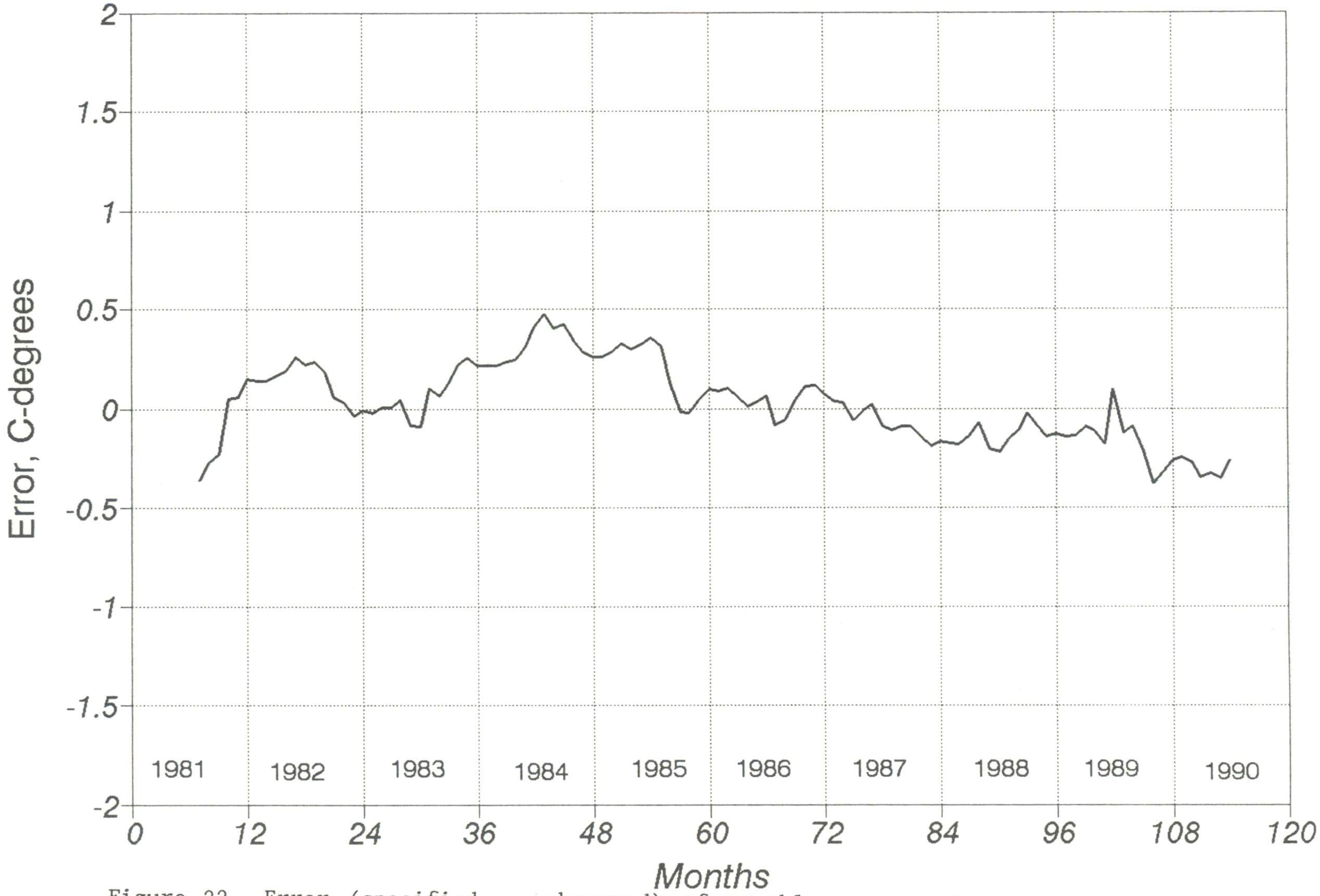

Figure 22. Error (specified - observed) of monthly mean surface temperature anomalies computed from observed 700mb heights using specification equations. Each point corresponds to an average of the errors for a given month of error values at 109 stations over the continental U.S.. Values plotted are the result of a 12-month running mean. Plot begins in July 1981 and ends in June 1990.

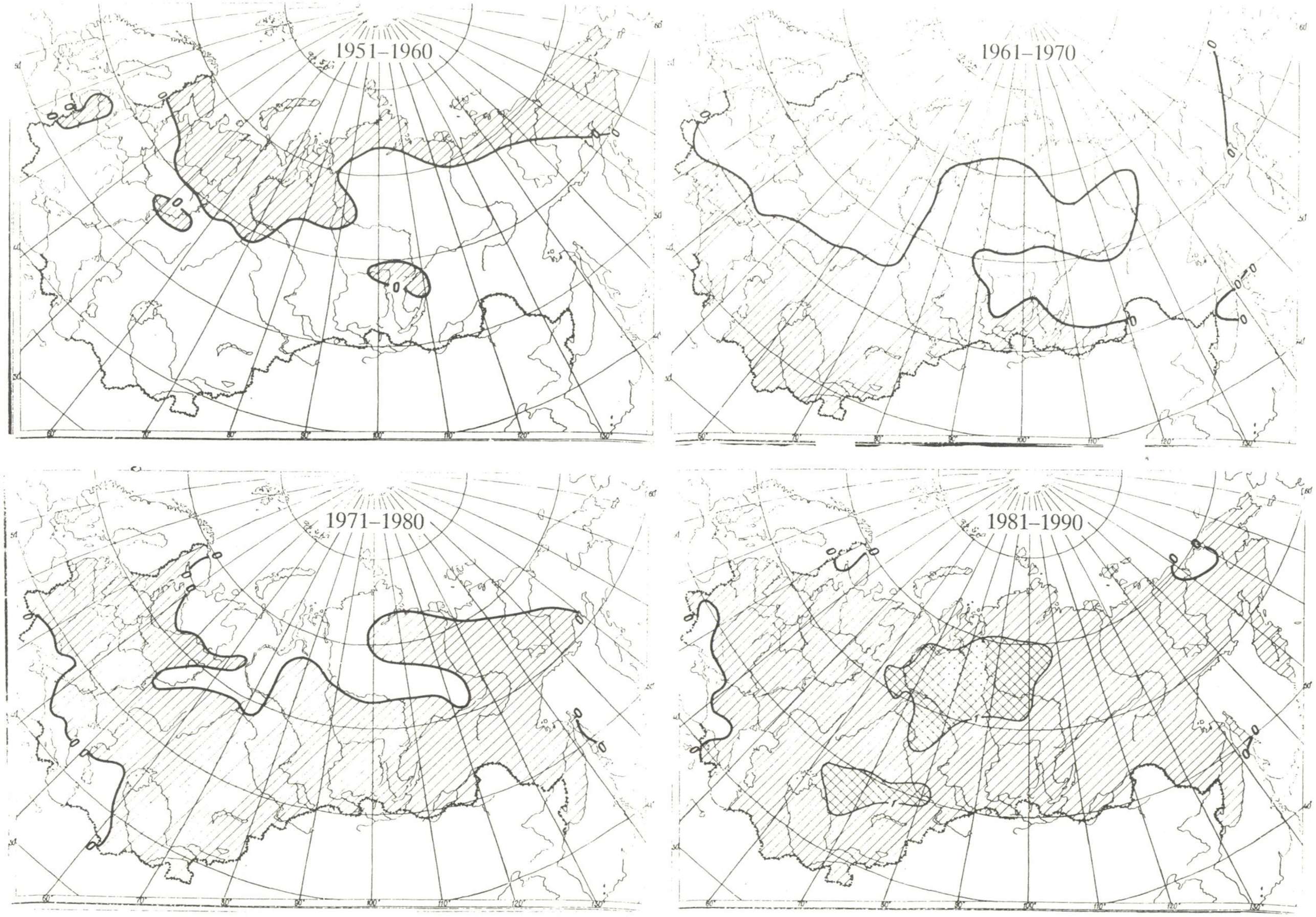

Fig. 23. Soviet Union surface temperature anomalies for the decades 1951-60, 1961-70, 1971-80, 1981-90. Hatched areas indicate positive anomalies less than 1°C, cross-hatched areas are anomalies greater than 1°C and unshaded areas indicate negative anomalies. Anomalies are from the 1951-1980 base period.

Figure courtesy of the World Data Center-B, Obninsk, USSR.

PRECIPITATION

GLOBAL

Global precipitation is more difficult to characterize than temperature. In part, this is because precipitation has a very large spatial structure. In addition, large regions of the globe experience a pronounced annual cycle of precipitation, with the majority, if not all, of the precipitation falling over part of the year, and very little, or none, falling during the remainder of the year. There is also an apparent tendency for many areas to fail to observe or report precipitation during the heart of the dry season.

A map of the annual precipitation for the decade (**Fig. 24**), indicates that it was wet over much of North America and northern Europe, while southern Europe and extreme eastern and southeastern Asia tended to be dry. The large areas with no analyses attest to the lack of complete annual data at a substantial number of stations. There were not enough data to support annual analyses over northern South America, most of Africa and large portions of Asia.

In general, the seasonal precipitation analyses for the decade (**Figs. 25 and 26**) are based on more data than the annual summary. In addition, because of the inherent seasonality in precipitation, these analyses provide the basis for a more meaningful interpretation of precipitation anomalies during the decade.

The December through February season decadal percentiles (**Fig. 25a**) shows relatively dry areas for northern North America and northeastern Asia. The North American dry area is roughly coincident to the areas showing positive temperature anomalies on the annual (**Fig. 1**), and winter seasonal (**Fig. 12**), analyses. This suggests relationships between winter snowfall and temperature in the region. Analysis of snow cover suggests relationships are strongest in the spring season over Eurasia (Fig. 37a). The Eurasian precipitation percentile patterns are not particularly well related to the surface temperature patterns during winter. Above median winter precipitation characterized the decade in northern Europe while drier than median conditions were evident in southern Europe.

The spring (March through May) precipitation analysis (**Fig. 25b**) shows a tendency for a continuation of above median precipitation over Northern Europe and below median to the south. The low amounts of winter and spring precipitation in southern Europe and northern Africa suggests that the median annual precipitation (**Fig. 24**) reflects a failure of the normal seasonal rains in the Mediterranean region. In North America, above median spring precipitation is evident in an area stretching from the Great Basin southward into Mexico. Dry spring conditions for the decade appear in the southeastern United States. Other dry areas in eastern Asia suggest less than median precipitation during its normal dry season.

The summer (June through August) precipitation analysis, **Fig. 26a**, shows the drought conditions in the Sahel regions of western Africa. Decadal summer rainfall in the Sahel was below the 30th percentile over

a wide area. Generally speaking, precipitation of less than the 30th percentile for one given rainy season represents drought conditions. The low percentiles in the Sahel over a ten year period signify catastrophic shifts in the decadal precipitation pattern. This is consistent with the summer decadal 700 mb height anomalies (**Fig. 43**) which suggest that significant changes occurred in circulation over northern Africa. The analysis also suggests that the area of precipitation deficiency extended well southward of the Sahel and into coastal regions of western Africa.

Below median summer precipitation for the decade is also evident in the area from northeastern China through Southeast Asia (**Fig. 26a**). Thus, of the major summer monsoon precipitation regions in the Northern Hemisphere, only India shows no significant decadal anomaly. However, the time series of precipitation for India (**Fig. 32c**) shows that the decade was characterized by large interannual variability.

The decadal dry conditions in Southeast Asia and the Sahel extended into the September through November season (**Fig. 26b**). This suggests that normal monsoon conditions were not, in general, alleviated by late season rains in these regions during the 1980's. Large portions of North America, including much of the United States, experienced above median fall precipitation during the decade. An exception to this overall wet pattern is over the eastern seaboard of the United States, with "normal" conditions in an area from New England extending through the Middle Atlantic area and dry conditions in extreme southern Florida.

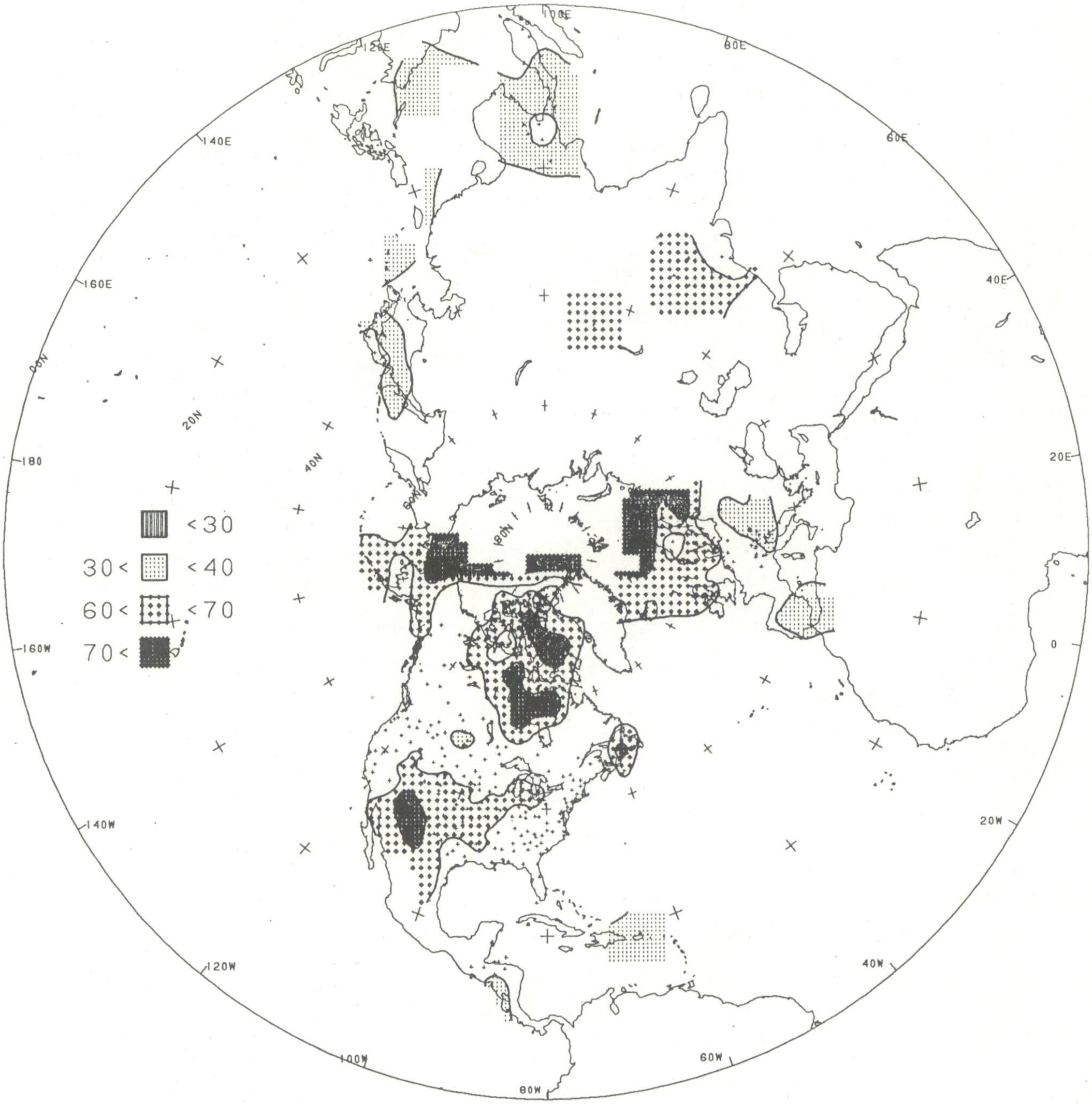

Fig. 24. Northern Hemisphere annual precipitation percentiles for the 1981-1990 period based on a Gamma distribution fit to the 1951-1980 base period. Station locations are denoted by small "+"; analysis not done in areas with insufficient data.

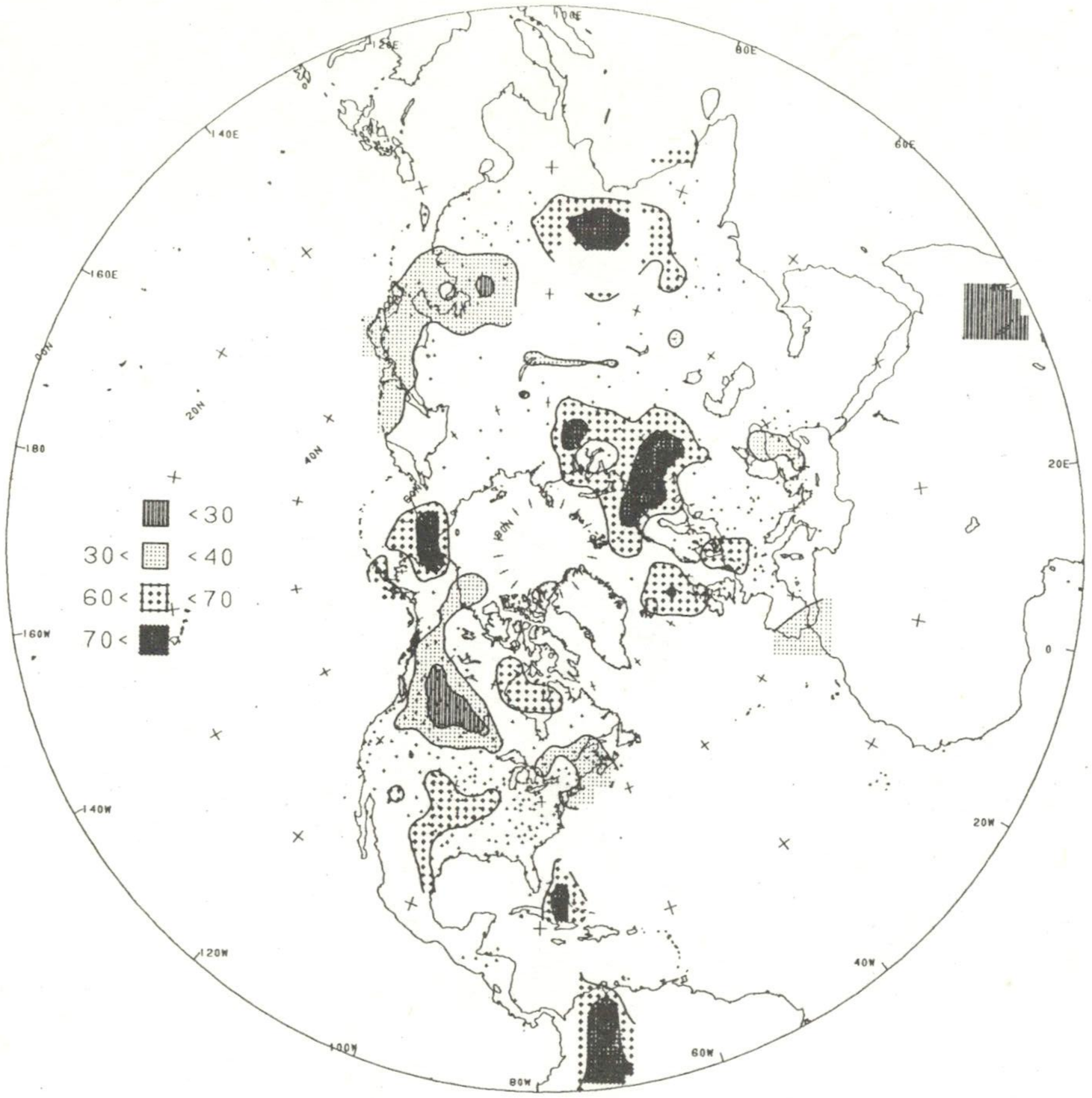

a

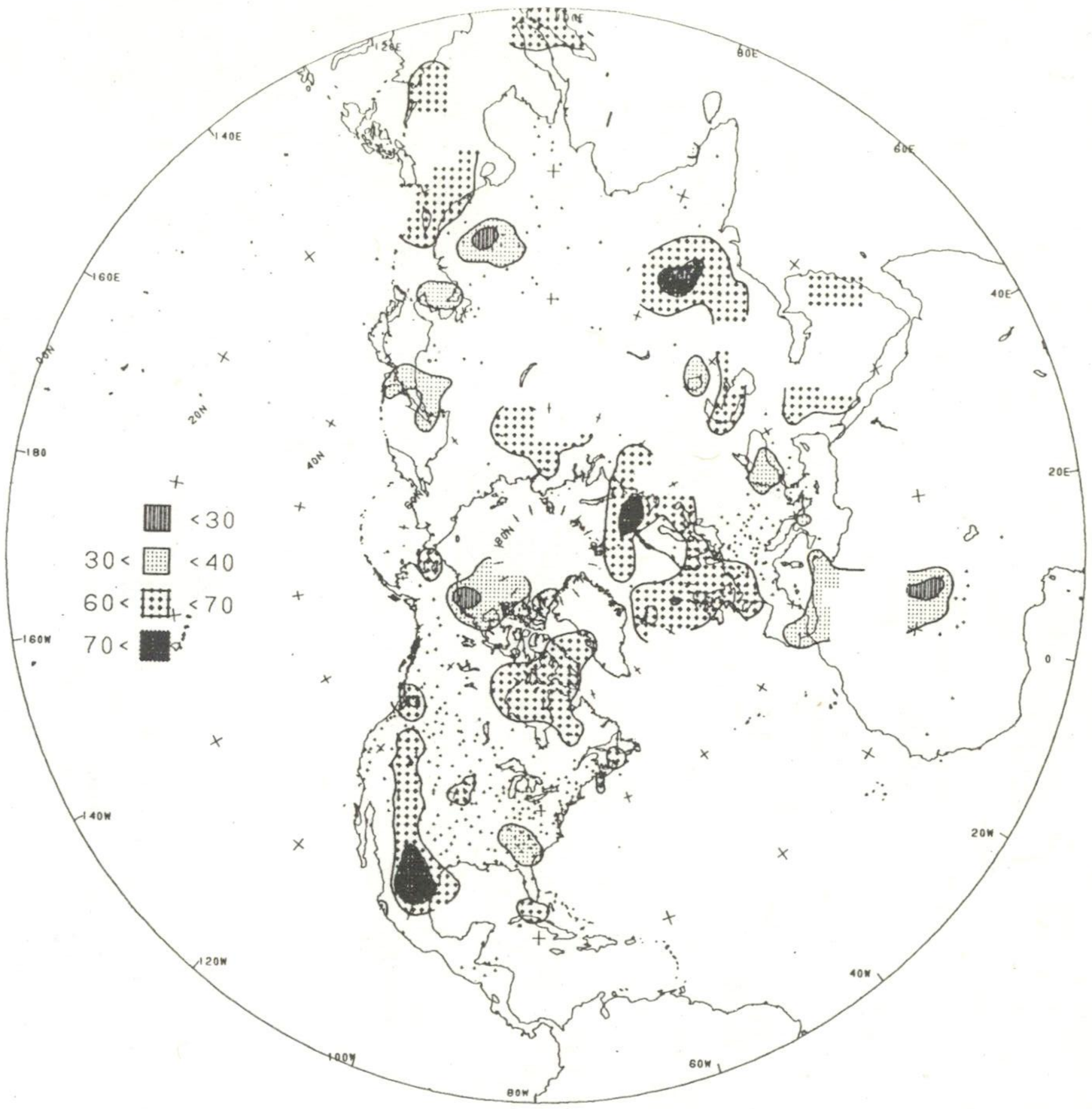

b

Fig. 25. Northern Hemisphere precipitation percentiles for a) DJF and for b) MAM for the 1981-1990 period based on a Gamma distribution fit to the 1951-1980 base period. Station locations are denoted by small "+"; analysis not done in areas with insufficient data.

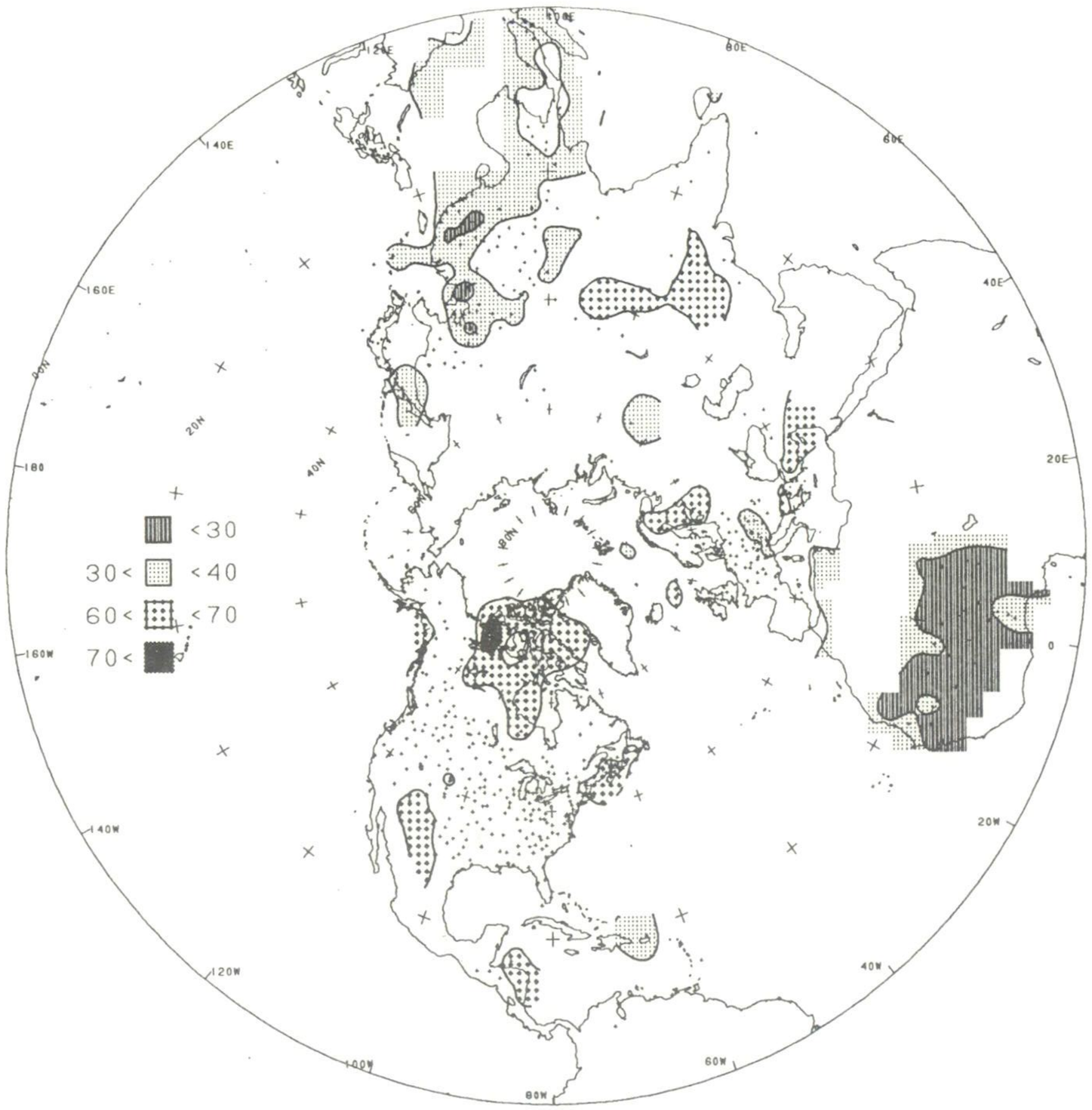

a

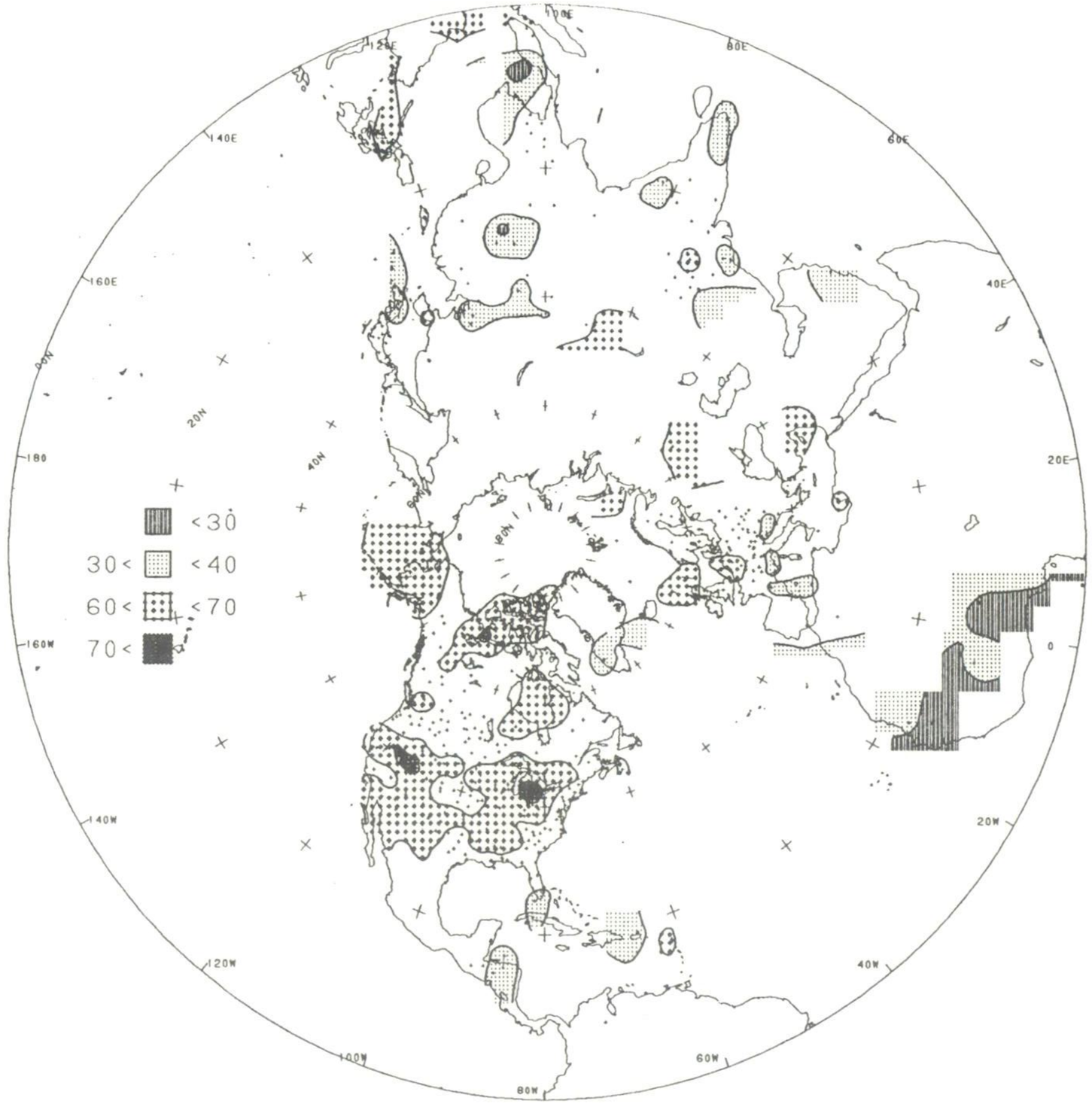

b

Fig. 26. Northern Hemisphere precipitation percentiles for a) JJA and for b) SON for the 1981-1990 period based on a Gamma distribution fit to the 1951-1980 base period. Station locations are denoted by small "+"; analysis not done in areas with insufficient data.

It is even more difficult to characterize precipitation over the Southern Hemisphere than in the Northern Hemisphere since the land area and number of surface reporting stations are relatively small. Nonetheless, seasonal precipitation anomaly maps for the decade (Figs. 27 and 28) provide some measure of the large scale precipitation anomalies during the 1980's.

During the Southern Hemisphere summer (December through February), dry anomalies dominate Australia as well as the higher latitudes of Africa and South America (**Fig 27a**). Drier than normal conditions are also indicated on several of the islands equatorward of Australia. In the Pacific and Australia, these drier than normal conditions can be at least partially attributed to the El-Niño/Southern Oscillation (ENSO) episodes of 1982/83 and 1986/87 (Ropelewski and Halpert, 1987). Apparently the "big wet" associated with the 1988 cold Southern Oscillation episode was not sufficient to balance the ENSO related anomalously dry periods. Likewise, the extremely wet conditions over far western South America reflect the almost unprecedented precipitation associated with the 1982/83 ENSO.

Anomalously dry conditions dominated the Southern Hemisphere fall (March through May) over most areas except for southern South America, **Fig 27b**. While the extreme dry fall conditions over southeastern Africa might, in part, be attributed to the ENSO events, the remainder of the precipitation anomalies can't be easily explained in relation to the Southern Oscillation.

In contrast to precipitation in the other seasons, southern winter (June through August) over the decade was characterized by above median rainfall over many land areas of the hemisphere (**Fig. 28a**). The above median precipitation values over northern Australia can be attributed to a few episodic events during this otherwise almost rainless season in that part of the continent.

The dry springtime (September through November) conditions in southern Australia and above median precipitation in western South American (**Fig. 28b**) over the decade may be another manifestation of the two ENSO episodes which occurred during this decade.

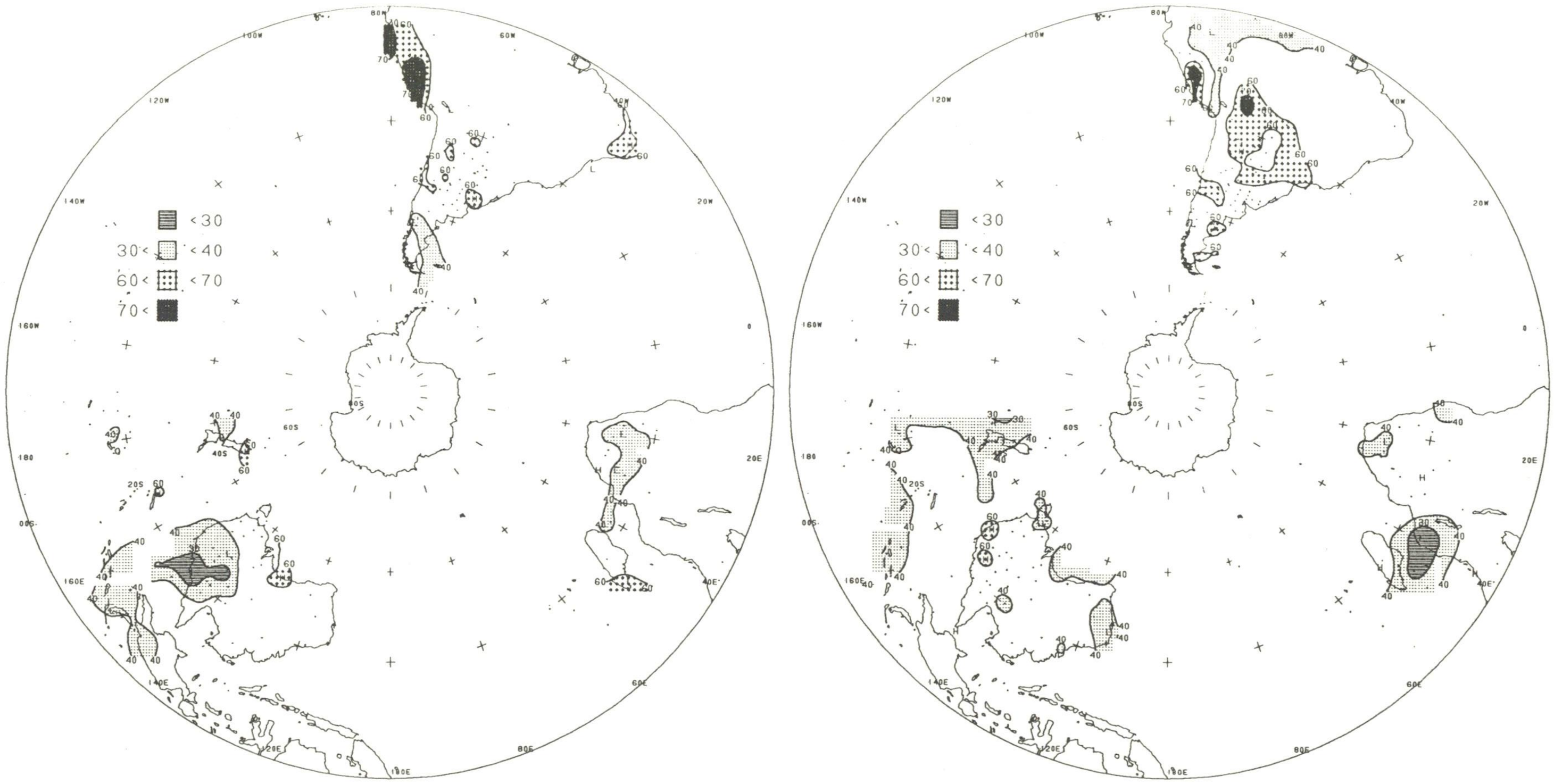

Fig. 27. Southern Hemisphere precipitation percentiles for a) DJF and for b) MAM for the 1981-1990 period based on a Gamma distribution fit to the 1951-1980 base period. Station locations are denoted by small "+"; analysis not done in areas with insufficient data.

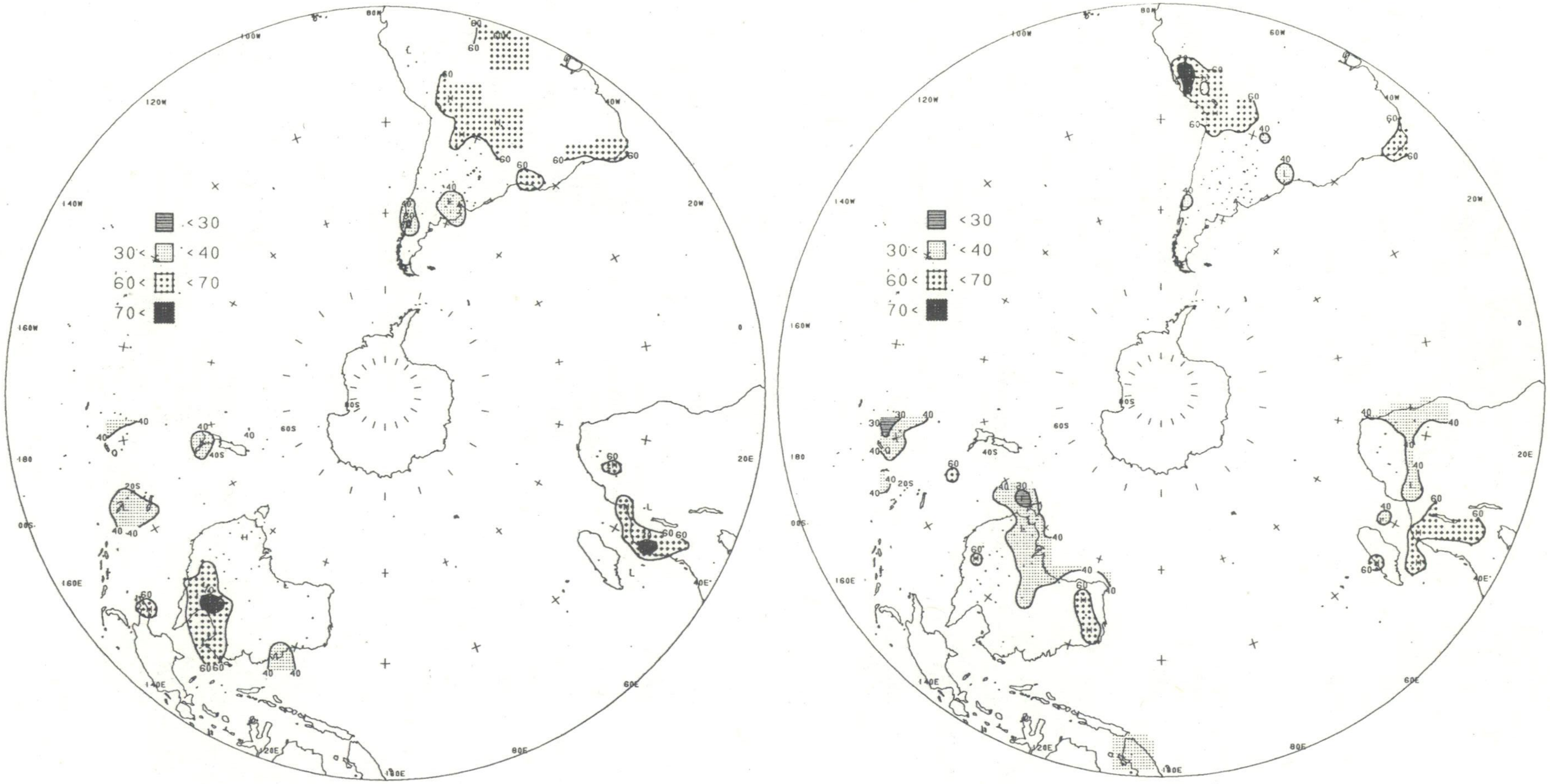

Fig. 28. Southern Hemisphere precipitation percentiles for a) JJA and for b) SON for the 1981-1990 period based on a Gamma distribution fit to the 1951-1980 base period. Station locations are denoted by small "+"; analysis not done in areas with insufficient data.

It is far from obvious how to correctly characterize the temporal evolution of precipitation on a global scale. In **Fig. 29**, we attempt to capture annual global precipitation variability through the use a of non-parametric statistical index. In this index, precipitation at each station over the past 40 years is ranked and then transformed into a percentile rank. Average percentile ranks are formed for each 2^{o} latitude by 2^{o} longitude grid square. The statistics (median, 10, 30, 70, and 90th percentiles) of these values for all grids (area weighted) are computed for each year and plotted as a time series.

The median values of the global annual precipitation index for the 1980's suggest that this decade was, perhaps, more variable than earlier decades in the record. The wettest year on record by this measure was 1983, in which precipitation for half of the areas (median) ranked in the 75 percentile or greater. Furthermore, 10 percent of the areas experienced their wettest year in the 40 year record. Conversely, 1988 was one of the driest years in the record, with the lowest median index value in the series. These extremes may have been related to the strong warm Southern Oscillation episode of 1982/83, on the one hand, and the 1988 cold Southern Oscillation episode on the other.

The ten percentile values (lower whiskers) for the annual precipitation index time series (**Fig. 29**) suggest that most of the extreme dry periods occurred during the 1950's and early 1960's. This interesting result, given the observed decrease in African and southern Asian monsoon precipitation during the 1980's (**Fig. 32**), suggests that precipitation may be on the increase in other regions.

None of the seasonal precipitation indices for the globe show any strong systematic changes in global precipitation (**Fig. 30**). Only the Northern Hemisphere fall season (September through November) suggests that the early and mid-1980's were clearly wetter and the 1950's drier than the other decades. These global scale seasonal indices also show no clear association with the Southern Oscillation. Thus, these indices may suggest no organized secular changes in the seasonal global precipitation over the past 40 years. On the other hand, the indices may be interpreted as showing that the observational network and data base are not adequate to measure small changes in global scale precipitation over the period.

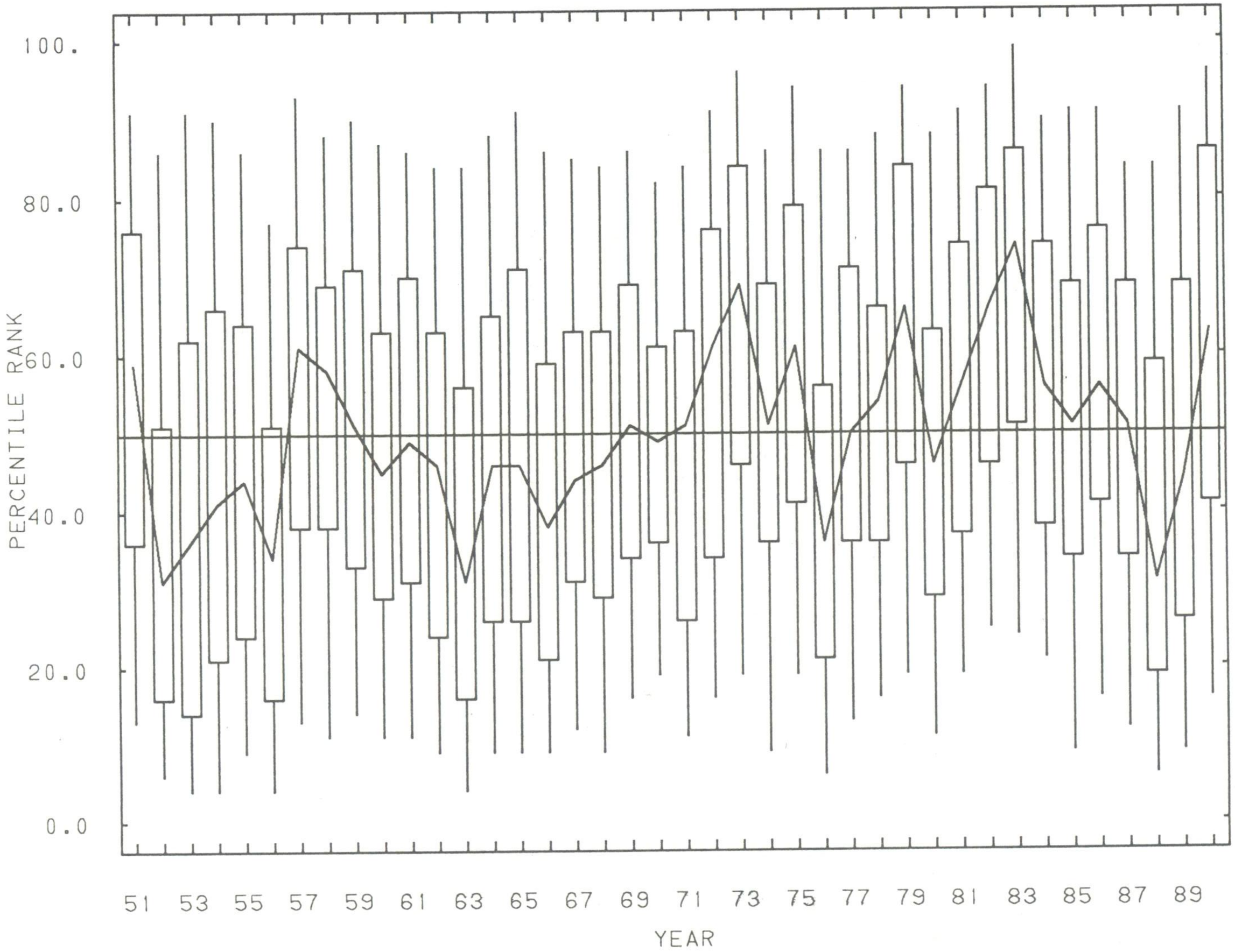

Fig. 29. Time series of the annual global precipitation index. The solid line gives the median value of the percentile rank for precipitation. The index is based on station precipitation in 2^{o} latitude by 2^{o} longitude grids. The median value of this index gives the percentile rank observed in half of the observational grid. The lower (upper) vertical lines, or whiskers, for each year gives the 10th (90th) percentile. The lower (upper) shoulder of the boxes for each year gives the 30th (70th) percentile.

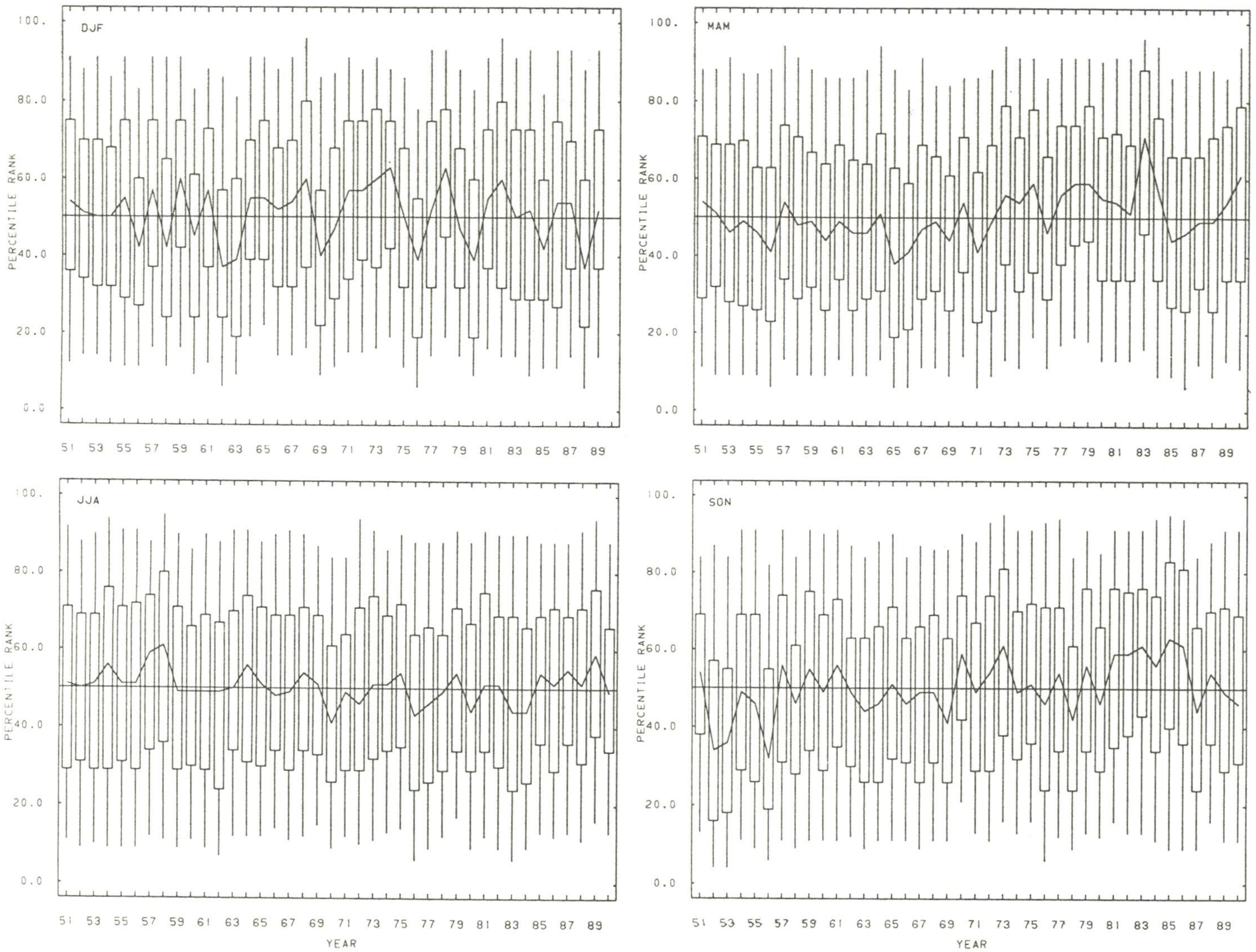

Fig. 30. Time series of the seasonal global precipitation indices, for Winter (DJF), Spring (MAM), Summer (JJA), and Fall (SON). The solid line gives the median value of the percentile rank for precipitation. The index is based on station precipitation in 2^{o} latitude by 2^{o} longitude grids. The median value of this index gives the percentile rank observed in half of the observational grid. The lower (upper) vertical lines, or whiskers, for each year gives the 10th (90th) percentile. The lower (upper) shoulder of the boxes for each year gives the 30th (70th) percentile.

REGIONAL

Indices of precipitation for regions of the United States and Europe (**Fig. 31**) suggest that mid-latitude precipitation during the 1980's was generally characterized by large interannual variability. Nonetheless, wet conditions appear to have dominated the mid-western United States over the past decade (**Fig. 31b**), while the western states experienced dry conditions over the last four years of the decade (**Fig. 31c**). Dry conditions were also experienced in the southeastern United States over the four year period 1985 to 1988.

Abnormally dry conditions in the Sahel continued and intensified throughout the decade of the 1980's (**Fig. 32a**). An index based on data for 20 stations distributed throughout the western Sahel (Lamb, 1982) is used to monitor rainfall for the June through September period. Rainfall during these four months accounts for over 90% of the regions yearly precipitation. Rainfall decreased during the early part of the decade, with the driest seasons occurring during 1983 and 1984. Towards the end of the decade, seasonal precipitation totals increased. 1988 and 1989 marked the first time since the 1960s that the Sahel had received near normal rainfall in two consecutive years. Precipitation for the decade, however, ended on a poor note as amounts were well below normal during 1990.

Similar precipitation indices for two other monsoon regions, northern Australia (**Fig. 32b**) and southeastern Asia (**Fig. 32d**) also show dry conditions for most of the decade. The northern Australia time series for its summer monsoon period (November through April) shows positive precipitation index values only for 1981, 1982 and 1989. It is curious to note that during the 1980's, both the Sahel region and southeastern Asia (**Fig. 32d**) consistently showed strong negative precipitation index values while the Indian summer monsoon showed much more year to year variability (**Fig. 32c**). In fact, according to this index, India suffered one of its worst droughts, associated with the 1986/87 ENSO, followed by one of its wettest years, associated with the 1988 cold Southern Oscillation episode. This suggests that the Indian summer monsoon is more closely related to interannual variability in the climate system while the two flanking monsoon areas appear to be responding more to longer term secular climate changes.

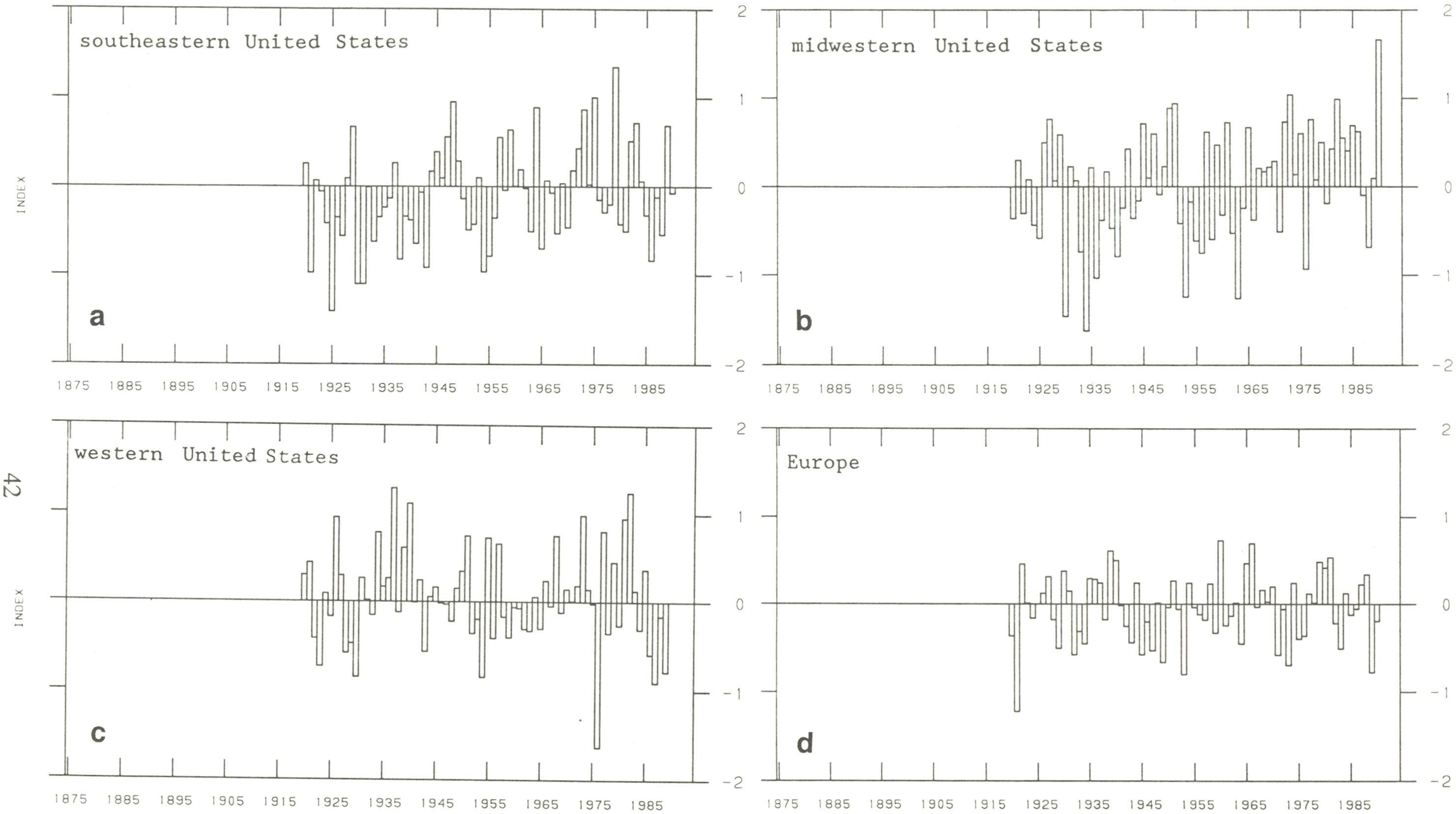

Fig. 31. Precipitation index (average gamma percentiles of station precipitation within the regions) time series for a) southeastern United States, calendar year; b) midwestern United States, calendar year; c) western United States, October - March; and d) Europe, calendar year.

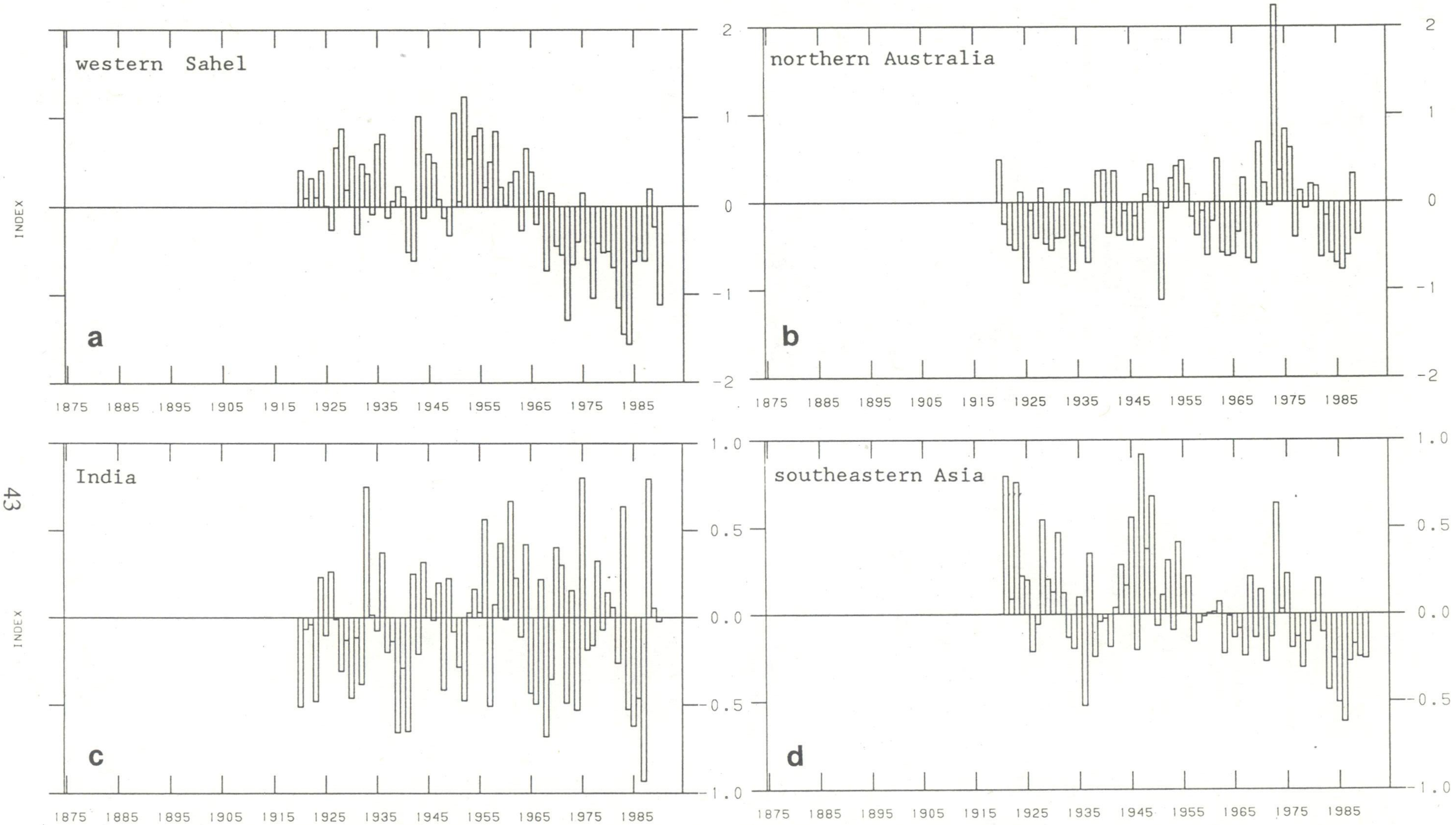

Fig. 32. Precipitation index (average gamma percentiles of station precipitation within the regions) time series for a) western Sahel, June - September; b) northern Australia, November - April; c) India, June - September; and d) southeastern Asia, April - September.

Dry conditions have affected the west coast of the United States during their last four rainy seasons (**Fig. 33**). Although none of the individual years during this period were as severe as the very dry years of 1976 and 1977, the cumulative effect of the last four October through March periods has resulted in unprecedented water shortages.

The Palmer Drought Severity Index (PDSI) gives an indication of prolonged periods of abnormal dryness or wetness. **Figures 34 and 35** show the percent area in the contiguous United States that experienced severe and extreme wet and dry conditions, respectively. As might be expected, the time series are out of phase, so that when large areas of the country are very dry, small areas experience very wet conditions. During the 1980s, the United States experienced two periods when more than 25% of the country had severe and extreme PDSIs. Neither of these drought episodes affected as much of the country as the droughts of the 1930s and the 1950s. However, the wet spell in the middle of the decade (**Fig. 34**) was the largest of the 20th century. This is consistent with the precipitation anomaly analysis for the decade (Fig. 24), which shows excess precipitation in the central United States over the decade.

The number of hurricanes and tropical storms during the 1980's (Fig. 36) was near the long-term mean. However, two of the most devastating North Atlantic hurricanes on record occurred in the late 1980's. Hurricane Gilbert was one of the strongest hurricanes in history and caused over $5 billion damage throughout the Caribbean, Mexico, and Texas in September 1988. During September 1989, Hurricane Hugo caused over $5 billion worth of damage in the southeastern United States.

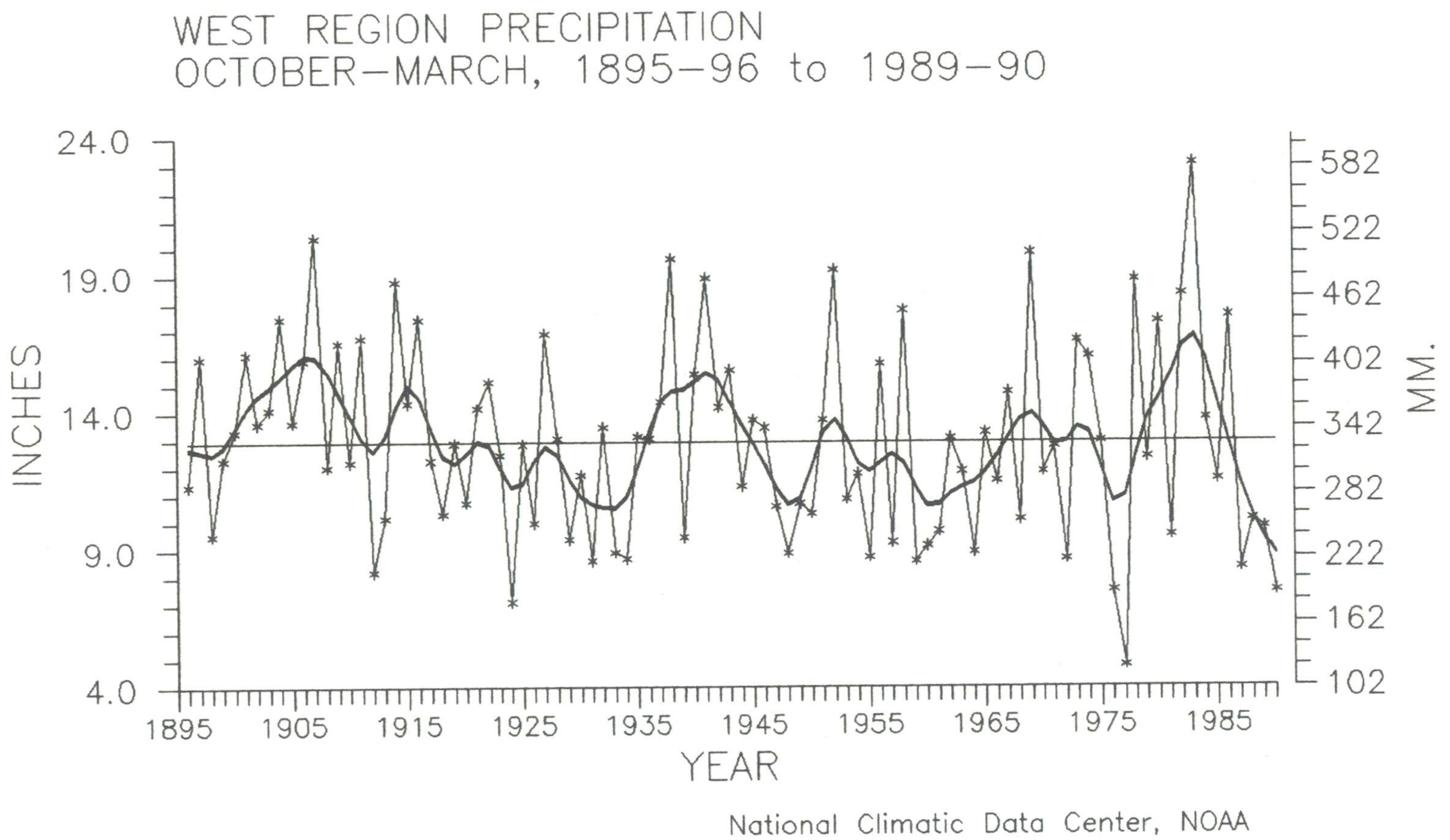

Figure 33. October-March total precipitation for the West region of the United States from 1895-96 through 1989-90. Asterisks are actual values; binomially filtered values are indicated by the solid line.

CONTIGUOUS UNITED STATES
SEVERE AND EXTREME WET SPELL

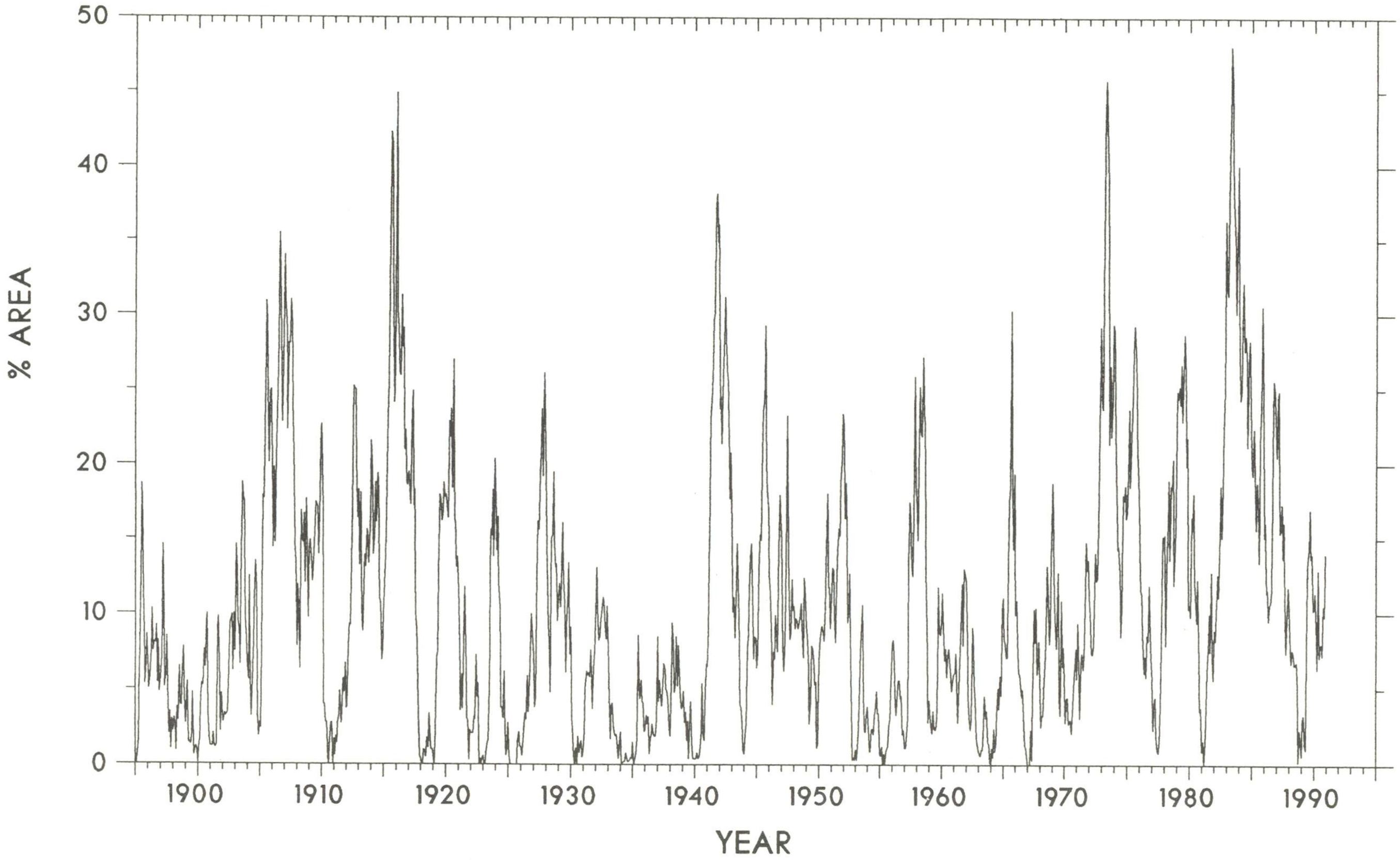

NATIONAL CLIMATIC DATA CENTER, NOAA

THROUGH 12/1990

Figure 34. Percent area of the contiguous United States experiencing severe to extreme long-term wet conditions, as measured by the Palmer Drought Severity Index, for January 1895 through December 1990.

CONTIGUOUS UNITED STATES
SEVERE AND EXTREME DROUGHT

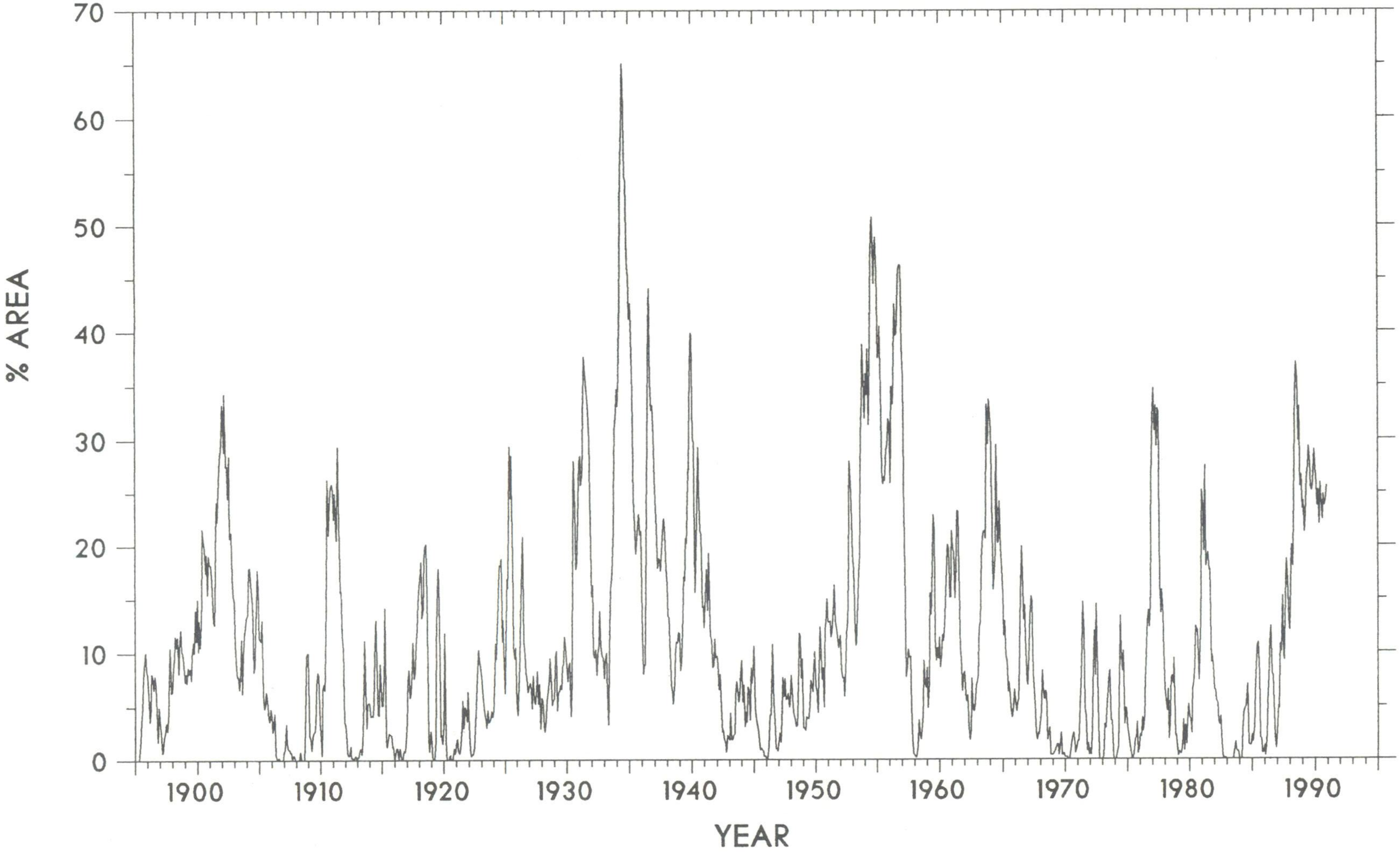

Figure 35. Percent area of the contiguous United States experiencing severe to extreme long-term drought, as measured by the Palmer Drought Severity Index, for January 1895 through December 1990.

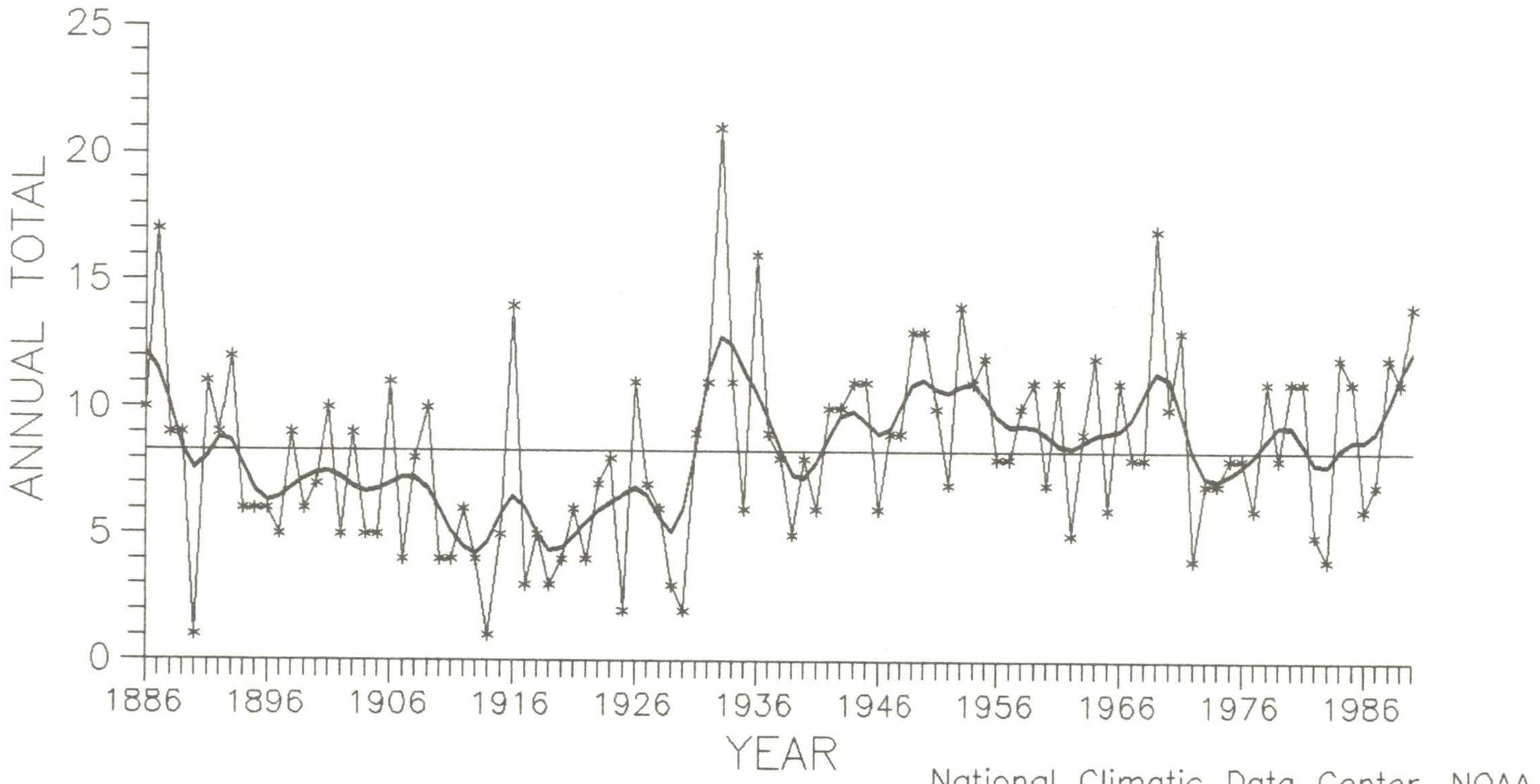

Figure 36. Annual total number of hurricanes and tropical storms in the North Atlantic Ocean from 1886 through 1990. Asterisks are actual values; binomially filtered values are indicated by the solid line.

CRYOSPHERE

SNOW AND ICE

The warmer than average temperatures in the Northern Hemisphere during the 1980's may be linked in part to the variations in snow coverage. Snow cover area has been monitored by satellites since 1966 and consistently on a global scale since 1973. Time series of Eurasian snow cover and temperature anomalies provide some evidence for the hypothesis that the two are related (**Fig. 37**). This time series plot suggests that during the spring and, to a lesser extent summer, snow cover area and temperature anomalies are inversely related. Since positive "global" temperature anomalies are strongly influenced by the Northern Hemisphere spring temperatures in Eurasia (**Fig. 1**), the extreme temperature anomaly of spring 1990 may have been, in part, related to the reduced snow cover area during spring and summer. No strong relationships between snow cover area and surface temperature anomaly were evident in the time series for the fall and winter seasons.

The time series of anomalous areal extent of Arctic sea ice for the summer and winter seasons (**Fig. 38a**) show no clear relationships to the global or Northern Hemisphere surface temperature. Even though the warmest year in the modern record, 1990, was also the year with the minimum in summer (August - September) Arctic sea ice, other low Arctic sea ice summers were associated with near zero or slightly negative temperature anomalies. No systematic trends are apparent in the Arctic sea ice time series for either season.

The time series of both the Antarctic summer and winter anomalous sea ice areas (**Fig. 38b**) show little evidence of long term trends or relationships to the Southern Hemisphere temperature anomalies. Sea ice anomalies appear to be systematically larger early in the record compared to the recent decade. The large negative winter anomalies in the late 1970's are associated with the evolution of a persistent polynya, or large ice-free area within the Weddell Sea. The polynyas are thought to be associated with low frequency fluctuations in the deep ocean circulation.

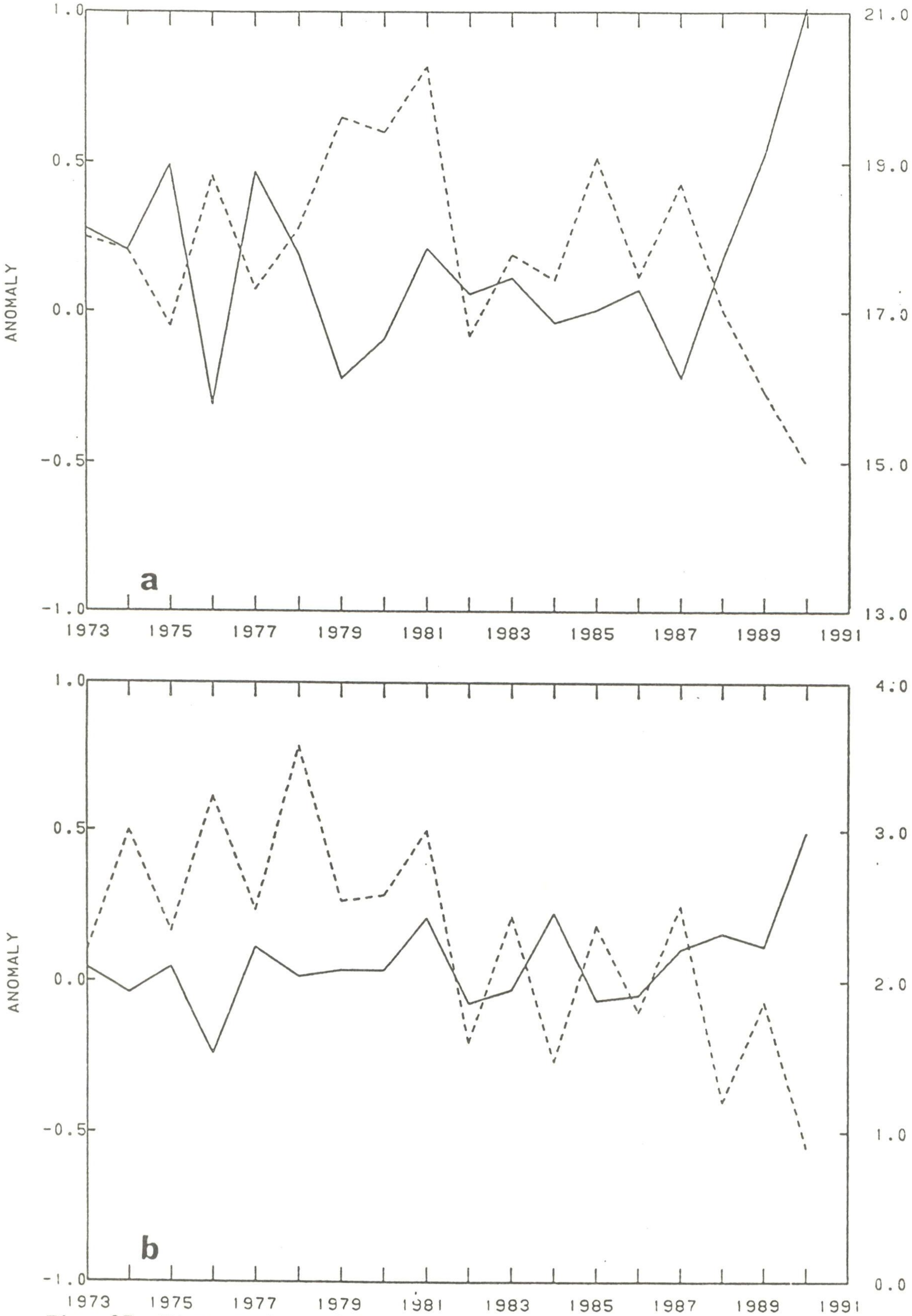

Fig. 37. Time series of Eurasian snow cover area derived from satellite data (dashed) and Eurasian temperature anomaly (solid) derived from an analysis of surface weather stations for a) spring, and b) summer. The left hand scale gives the temperature anomaly in degrees Celsius while the right hand scale gives the snow cover area in 10^5 km^6.

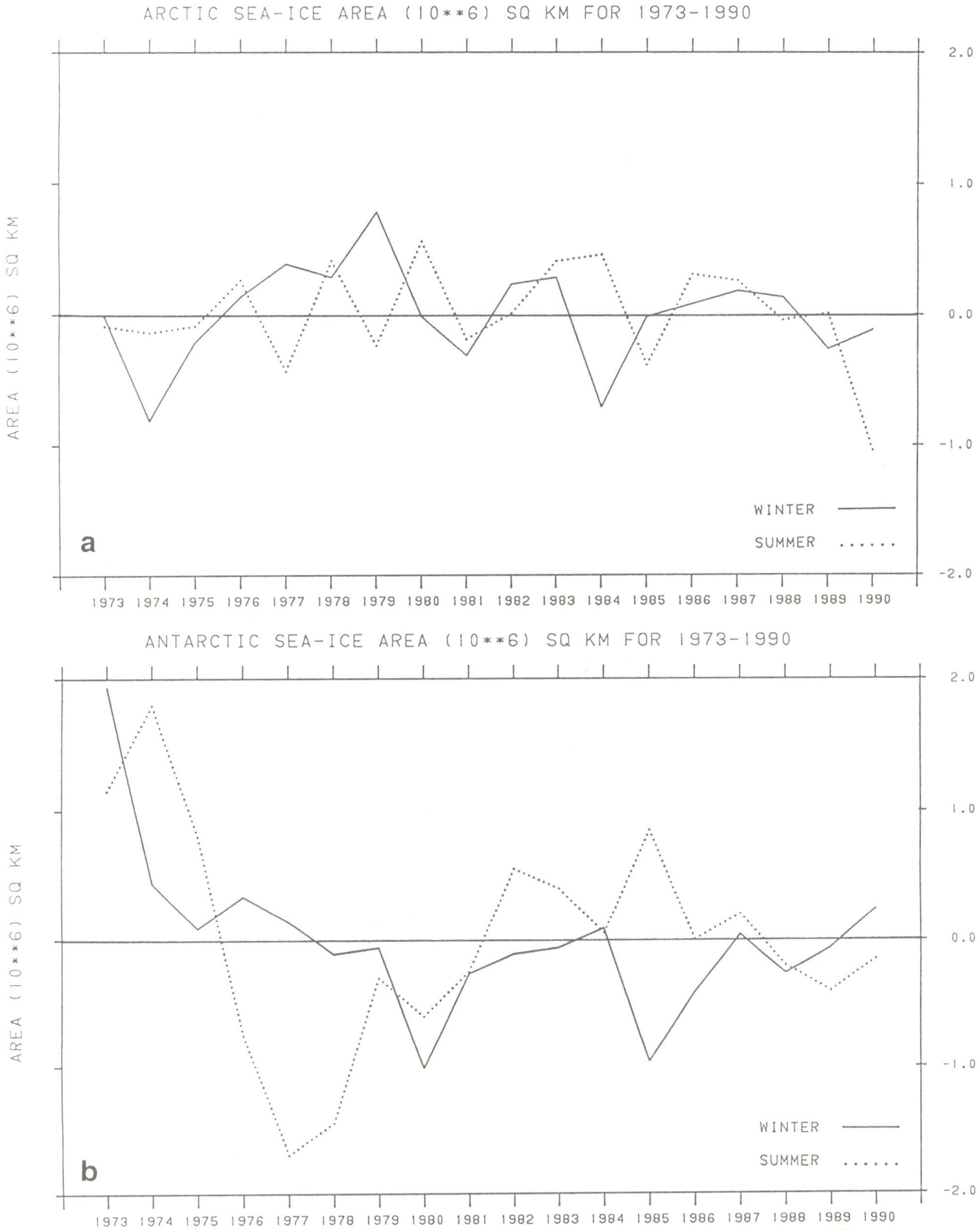

Fig. 38. a) Time series of the Arctic sea ice area anomalies for the northern winter (solid line), average of January and February, and summer (dashed line), average of August and September. b) Time series of the Antarctic sea ice area anomalies for the southern winter (dashed line), average of August and September, and summer (solid line), average of January and February. Sea ice areas are derived from analyzed charts based on satellite data.

TROPOSPHERIC ANALYSIS

TROPOSPHERIC TEMPERATURES

The time series of the global lower tropospheric (1000-400 mb) temperature anomalies derived from Microwave Sounding Unit (MSU) satellite observations (**Fig. 39**) show considerable interannual variability but little evidence of strong temperature trends over the 1979 to 1990 period. As pointed out by Spencer and Christy (1990), there are significant differences in the character of the "global temperature" time series derived from the MSU and various time series based on surface station data. In particular, virtually all surface based analyses indicate that March 1990 (Table 1) was the warmest month and 1990 the warmest year on record. The MSU data, however, indicate that December 1987 was the warmest month and that 1987 and 1988 both had anomalies comparable or greater than those of 1990. The reasons for these differences are the subject of continuing active research.

The time series of tropospheric mean temperature derived from radiosonde data (**Fig. 40**) more closely resembles the surface temperature record than the MSU temperature estimates. In this time series, 1990 appears to be the warmest year in the 33 year record (1958 to 1990) by a small margin. Angell (1990) attributes the large positive temperature anomalies of 1982, and 1987/88 to ENSO.

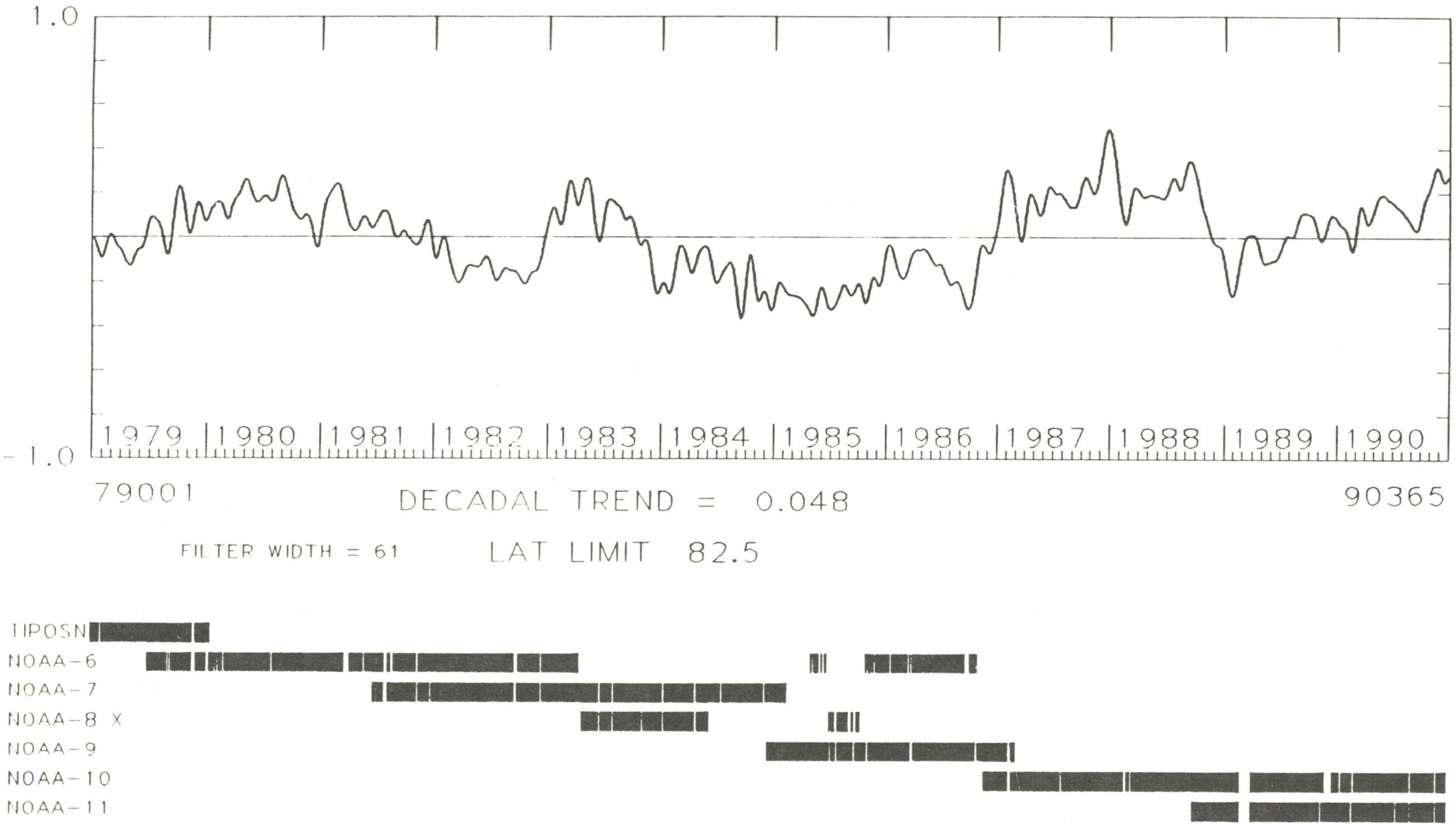

Fig. 39. Time series of global lower tropospheric temperature anomalies derived from satellite Microwave Sounding Unit (MSU) observations, (Spencer et al., 1990). The bars below the time series indicate the operational observational periods of various NOAA satellites over the 12 year period.

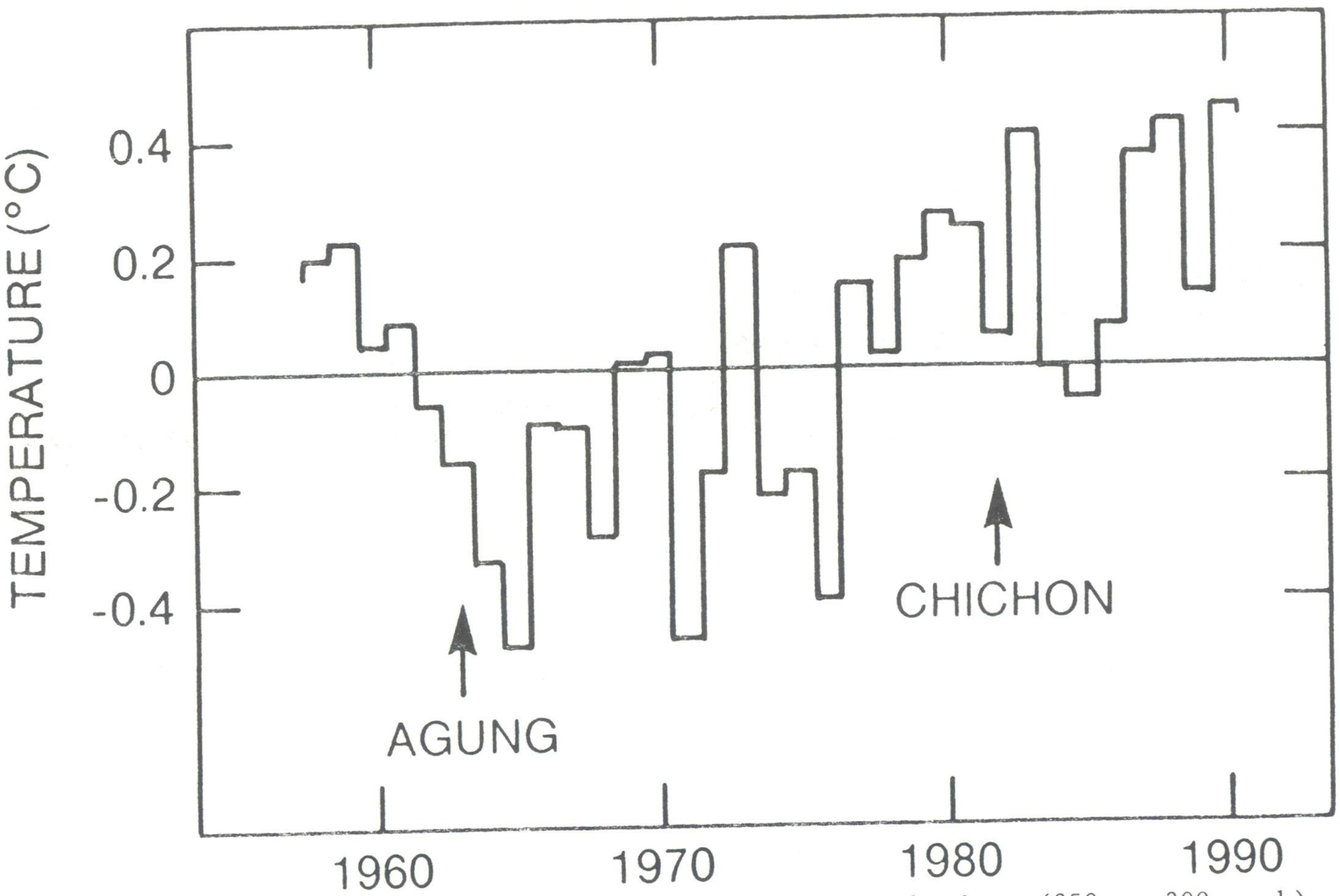

Fig. 40. Time series of global tropospheric (850 -300 mb) temperature anomaly derived from radiosonde data, after Angell (1990).

700 MB HEIGHTS

The Northern Hemispheric circulation decadal mean at 700 mb during the 1980's is compared to the 1951-1980 base period in **Fig. 41**. Shading depicts regions that are locally significant at the 95 and 99% level based on a 2-sided t-test for 38 degrees of freedom (Panofsky and Brier, 1968). The 700 mb data consist of the monthly, seasonal and annual mean geopotential heights derived from the twice-daily Northern Hemisphere 700 mb height National Meteorological Center (NMC) analyses for the period 1951 through 1990. The data are originally on a 541 point grid converted to a more uniform equal area grid of 358 points (Barnston and Livezey, 1987). The data set has been corrected to remove a positive height bias, evident in summer during the early and middle 1950's over the Caribbean and North Africa (Barnston and Livezey, 1987).

In the decade of the 1980's, the largest 700 mb height anomalies occurred during the winter (DJF) season, as the Aleutian and Icelandic lows were more than 30 meters deeper (**Fig. 42**) than the mean. These and other centers of negative height anomalies are regions of higher natural variability and are not statistically significant. This is found to be true for the other seasons and in the annual mean as well.

In general, the major centers of positive height anomaly centers in the middle and higher latitude regions of the Northern Hemisphere are locally significant at the 95% level (**Figs. 41 to 45**). Among these regions, for the annual mean conditions (**Fig. 41**), is one extending from northwest Canada across the northeastern United States into the Atlantic ocean. Another region is centered over the Mediterranean Sea and extends over western Europe. A small center near 55°N,105°E corresponds to the maximum in observed surface temperature anomalies (Fig. 1). Other height anomalies are consistent with the hemispheric temperatures observed during the decade. The above normal heights found during the winter (**Fig. 42**) and the spring (**Fig. 44**) seasons over northwestern North America and eastern Asia are also consistent with the much above normal temperatures observed during those seasons (**Figs. 12 and 9**, respectively). Positive height anomalies also appear over the regions of northern Africa and southern Europe, which have been experiencing relatively dry conditions (Figs. 24, 25 and 26) over the decade. However, significant height anomalies in the subtropical oceans should be considered with caution in light of "data quality and availability" in these regions and the changes in the data assimilation procedures over the course of the 40-year period.

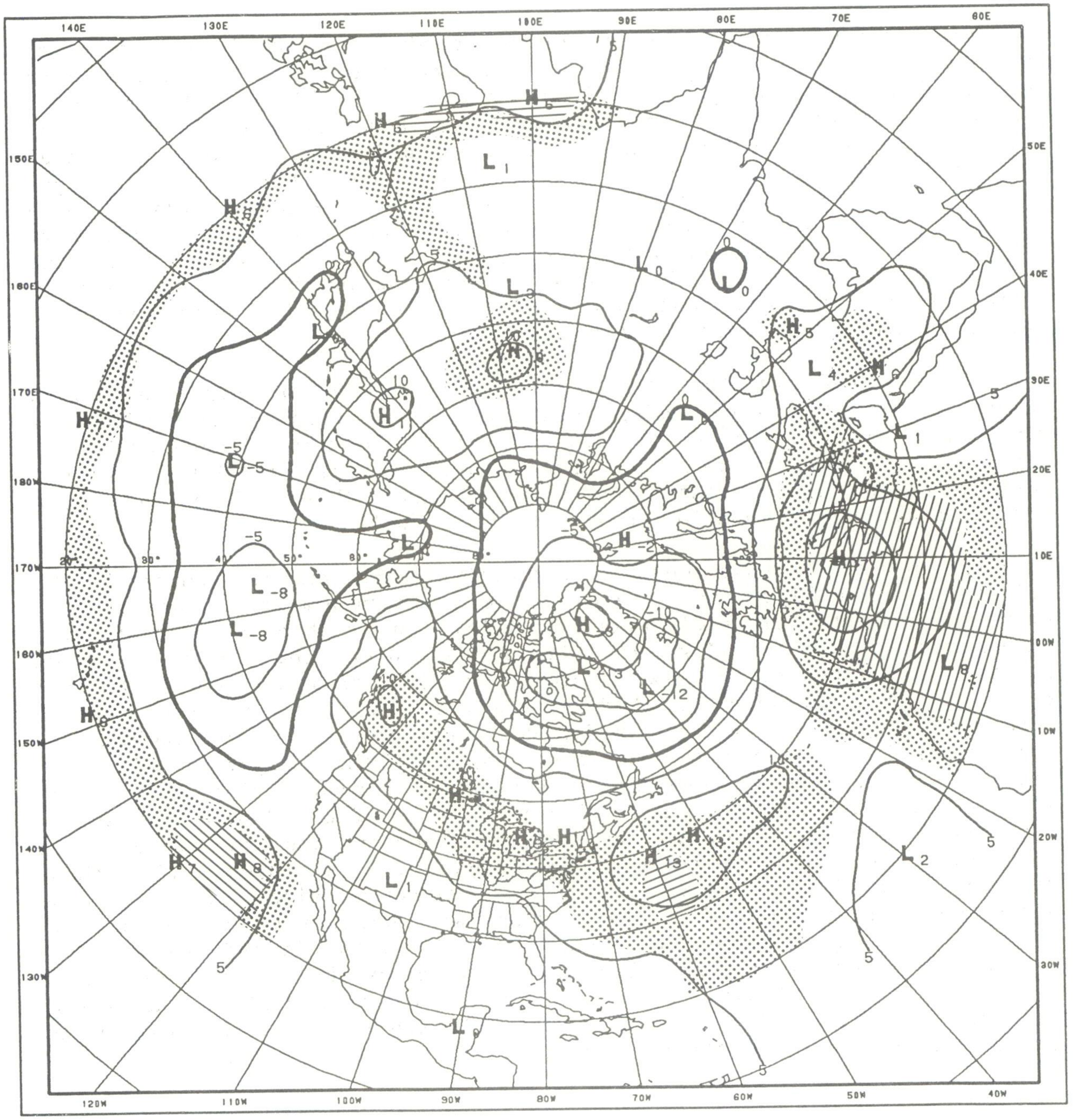

Fig. 41. 700 mb geopotential height anomalies for the decade of the 1980's. Anomalies are computed from the 1951-1980 base period. The contour interval is 5 meters. Dotted (shaded) areas indicate regions that are locally significant at the 95% (99%) level based on a 2-sided t-test.

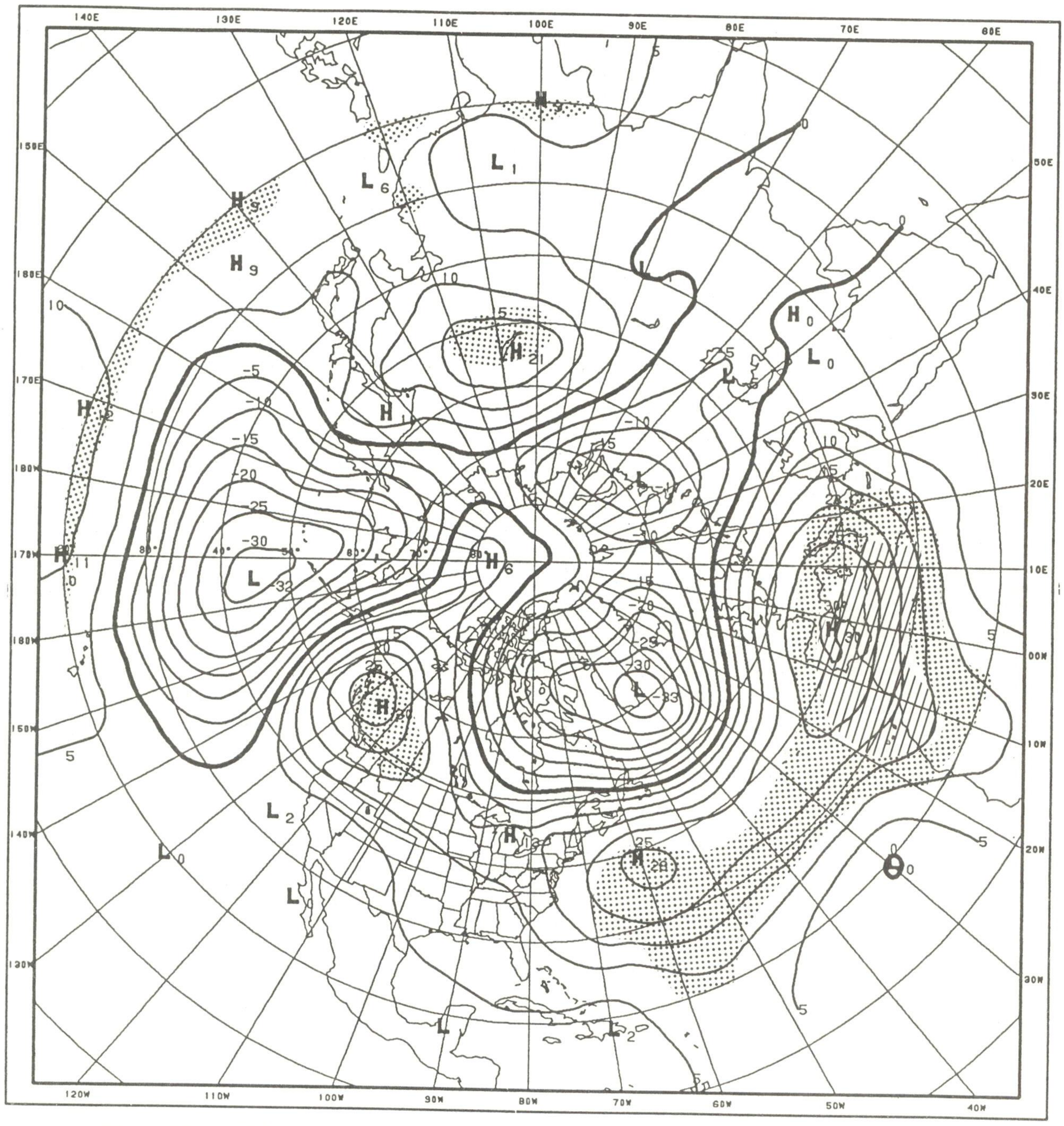

Fig. 42. 700 mb geopotential height anomalies for the decade of the 1980's for the DJF season. Anomalies are computed from the 1951-1980 base period. The contour interval is 5 meters. Dotted (shaded) areas indicate regions that are locally significant at the 95% (99%) level based on a 2-sided t-test.

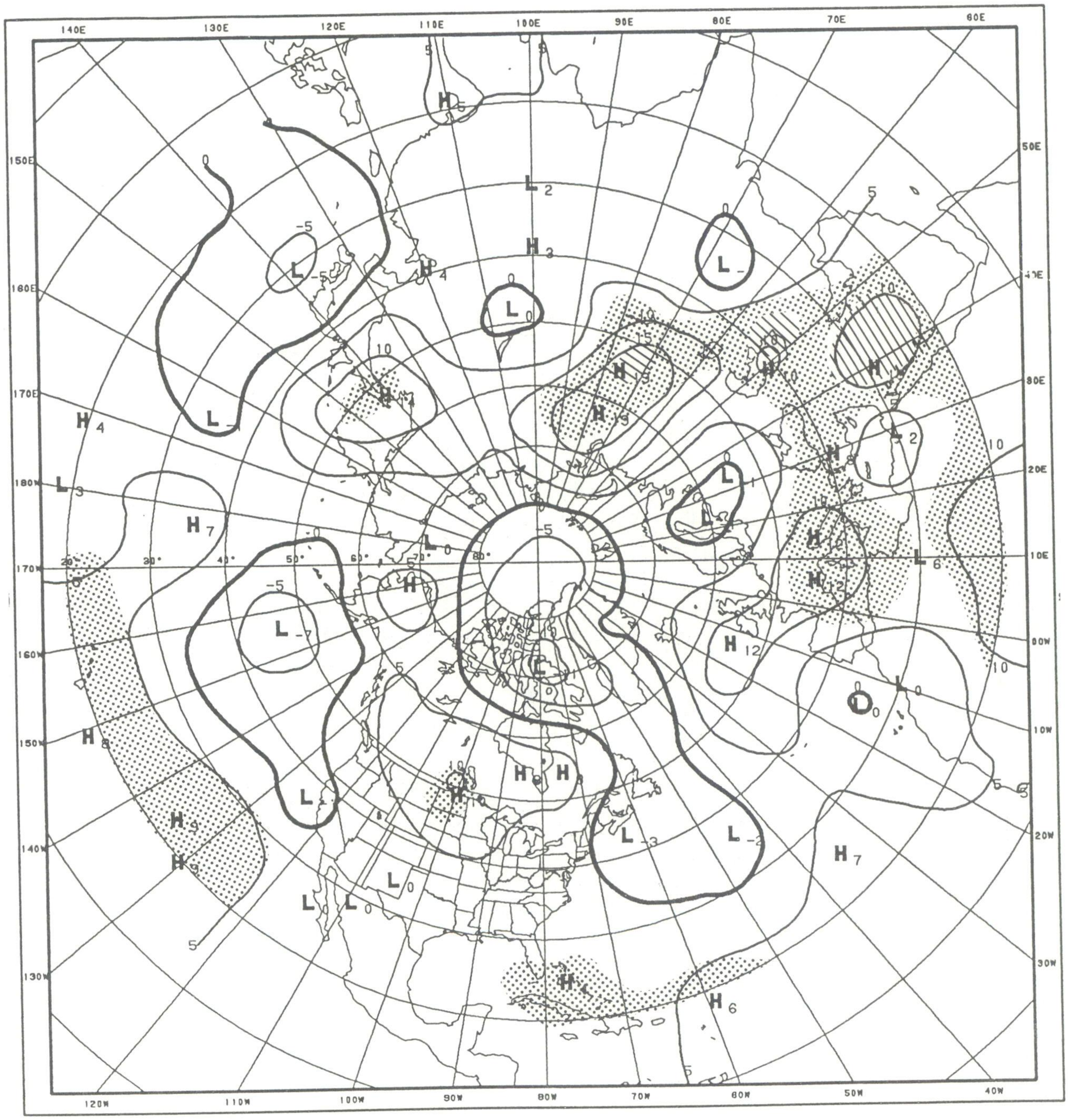

Fig. 43. 700 mb geopotential height anomalies for the decade of the 1980's for the JJA season. Anomalies are computed from the 1951-1980 base period. The contour interval is 5 meters. Dotted (shaded) areas indicate regions that are locally significant at the 95% (99%) level based on a 2-sided t-test.

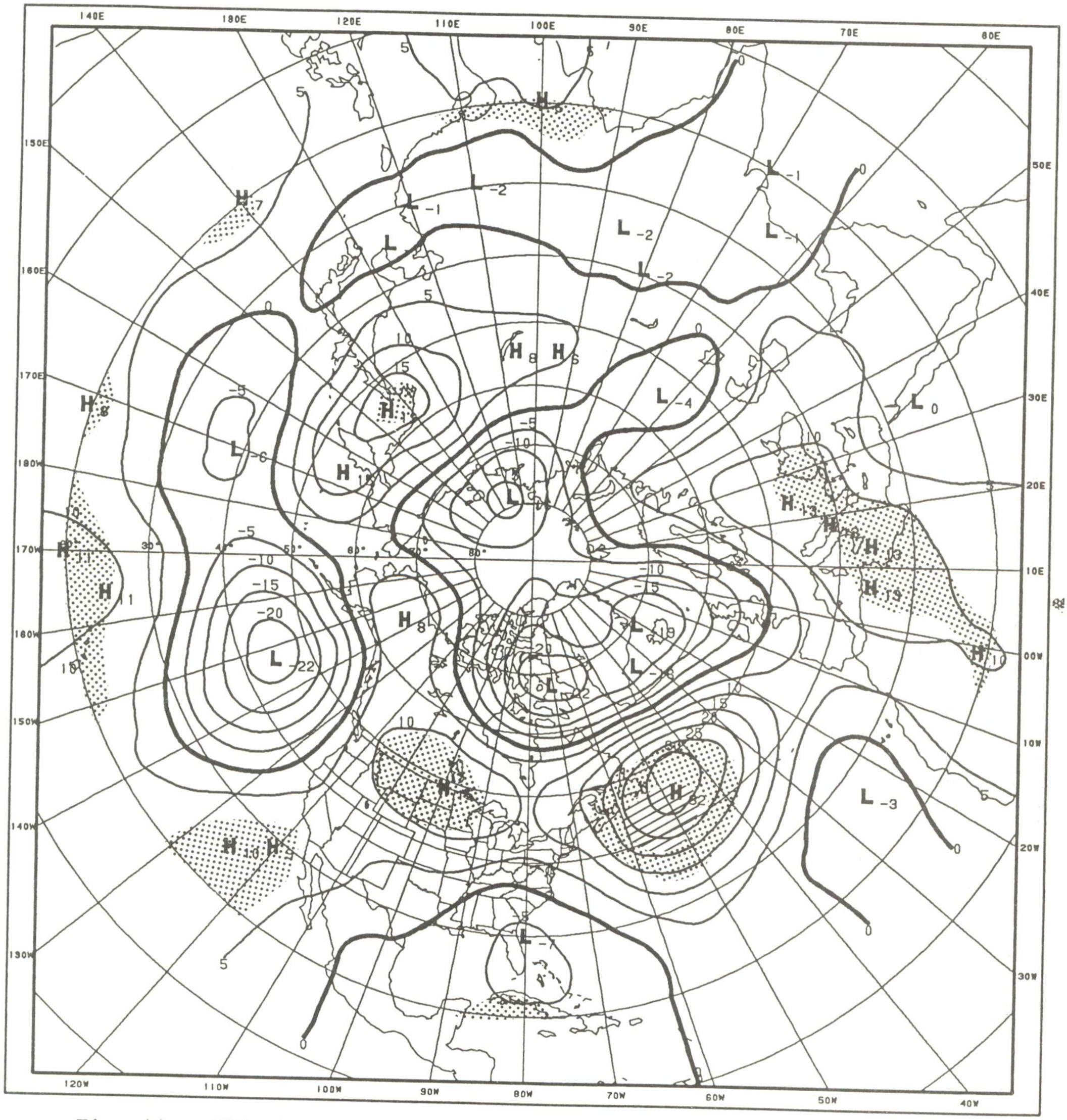

Fig. 44. 700 mb geopotential height anomalies for the decade of the 1980's for the MAM season. Anomalies are computed from the 1951-1980 base period. The contour interval is 5 meters. Dotted (shaded) areas indicate regions that are locally significant at the 95% (99%) level based on a 2-sided t-test.

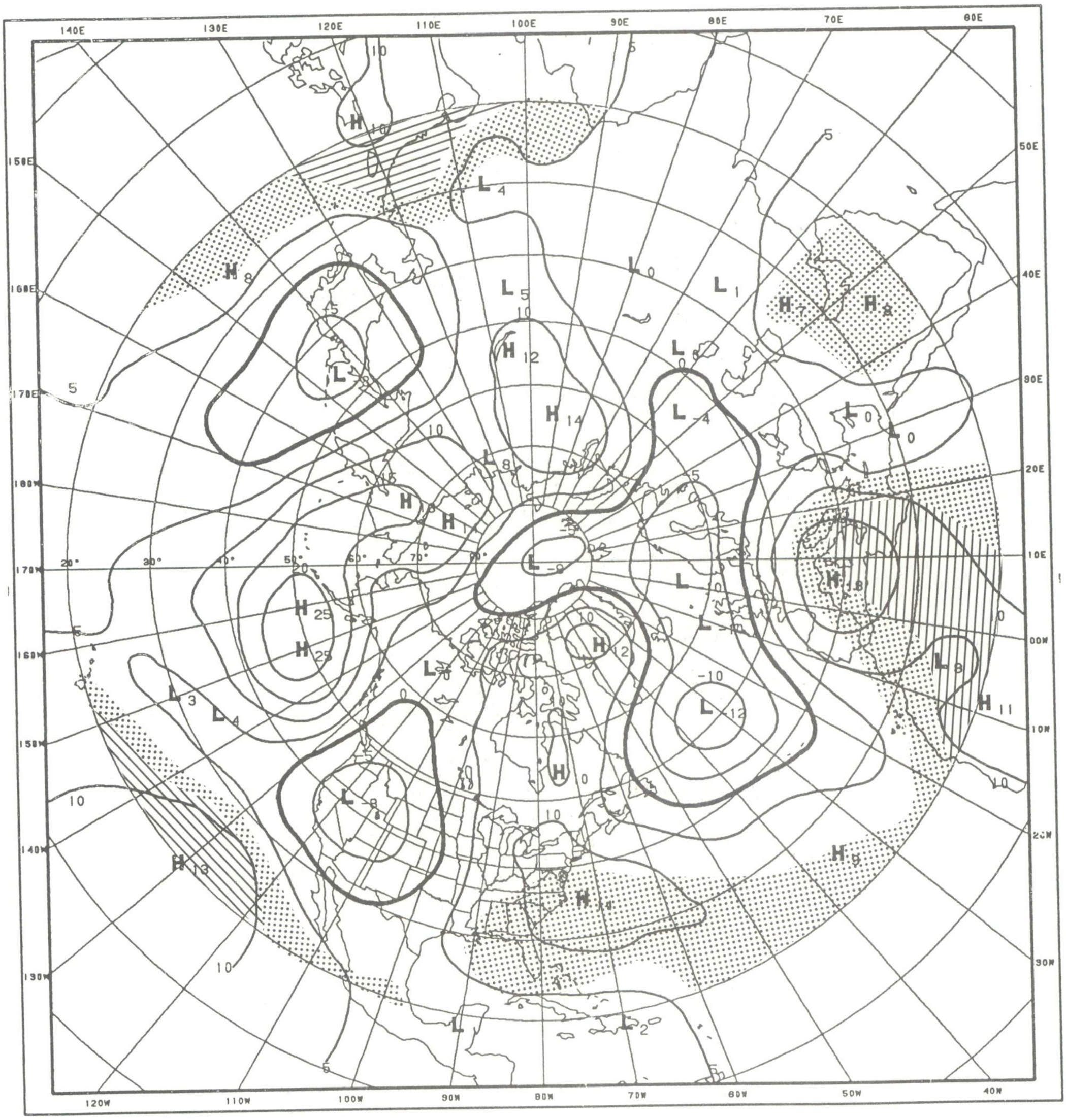

Fig. 45. 700 mb geopotential height anomalies for the decade of the 1980's for the SON season. Anomalies are computed from the 1951-1980 base period. The contour interval is 5 meters. Dotted (shaded) areas indicate regions that are locally significant at the 95% (99%) level based on a 2-sided t-test.

TELECONNECTIONS

Variability of the geopotential height field in the Northern Hemisphere extratropics is dominated by weather systems having periods of 10 days or longer (Blackmon, 1976). These low-frequency fluctuations tend to occur over distant geographic regions, and are often organized into distinct spatial patterns or teleconnections (Wallace and Gutzler, 1981). Five primary teleconnection patterns have been found in the Northern Hemisphere extratropical middle troposphere, and are most prominent in seasonally averaged data (Blackmon et. al. (1984). Interannual variability of the teleconnection patterns can be examined using a 365-day averaging interval. Standardized 700 mb indices describing the seasonal and interannual evolution of the five teleconnection patterns for the period 1964-1990 are shown in **Figs. 46-48**.

The Pacific/North American (PNA) pattern is the most robust of the extratropical teleconnection patterns (Blackmon et. al., 1984). Both the intra-annual and interannual behavior of the PNA pattern are strongly influenced by the El Niño/Southern Oscillation (ENSO) cycle (Horel and Wallace, 1981). The positive phase of the PNA pattern is characterized by positive height anomalies over the east-central Pacific and western North America, and by negative height anomalies over the northeast Pacific and the southeast United States; a negative pattern index indicates anomalies in the opposite sense.

Time series of 95-day and 365-day running mean PNA index values are shown in **Figs. 46a and 46b**, respectively. Together, these two time series illustrate a high-amplitude, high-frequency intra-annual pattern superimposed upon a low-amplitude, low-frequency interannual pattern. There is a clear tendency for the largest absolute values of the 95-day averaged time series to be most pronounced during those winters in which the SOI is significantly non-zero. The winter pattern then dissipates during spring, but becomes re-established the following winter despite the return to near-zero SOI values. The time series (**Fig. 46b**) suggests that during the 1980's, the positive phase of the PNA pattern dominated. This is consistent with the 700 mb height anomaly patterns (Figs. 41-45).

The West Pacific (WP) pattern reflects major meridional shifts in the position of the western North Pacific jet stream. This pattern is characterized by a north-south dipole of height anomalies having anti-nodes centered over the west-central North Pacific and the Kamchatka Peninsula. The time series of 95-day and 365 day running mean WP index values are shown in **Figs. 47a and 48a**, respectively. The positive phase of the WP pattern reflects positive height anomalies throughout the western North Pacific and the Aleutians, and negative height anomalies throughout the west-central North Pacific; a negative pattern phase indicates anomalies in the opposite sense.

As with all of the teleconnection indices, there exists a clear tendency for persistence of a particular phase of the WP pattern, followed by a sharp transition to the opposite phase of the pattern. Two major positive and negative phases of the WP pattern occurred during the 1980's (**Fig. 48a**). Prolonged positive phases occurred between 1984 and 1986, and between 1988 and 1990. Prolonged negative phases occurred between 1981 and 1982, and between 1986 and 1987.

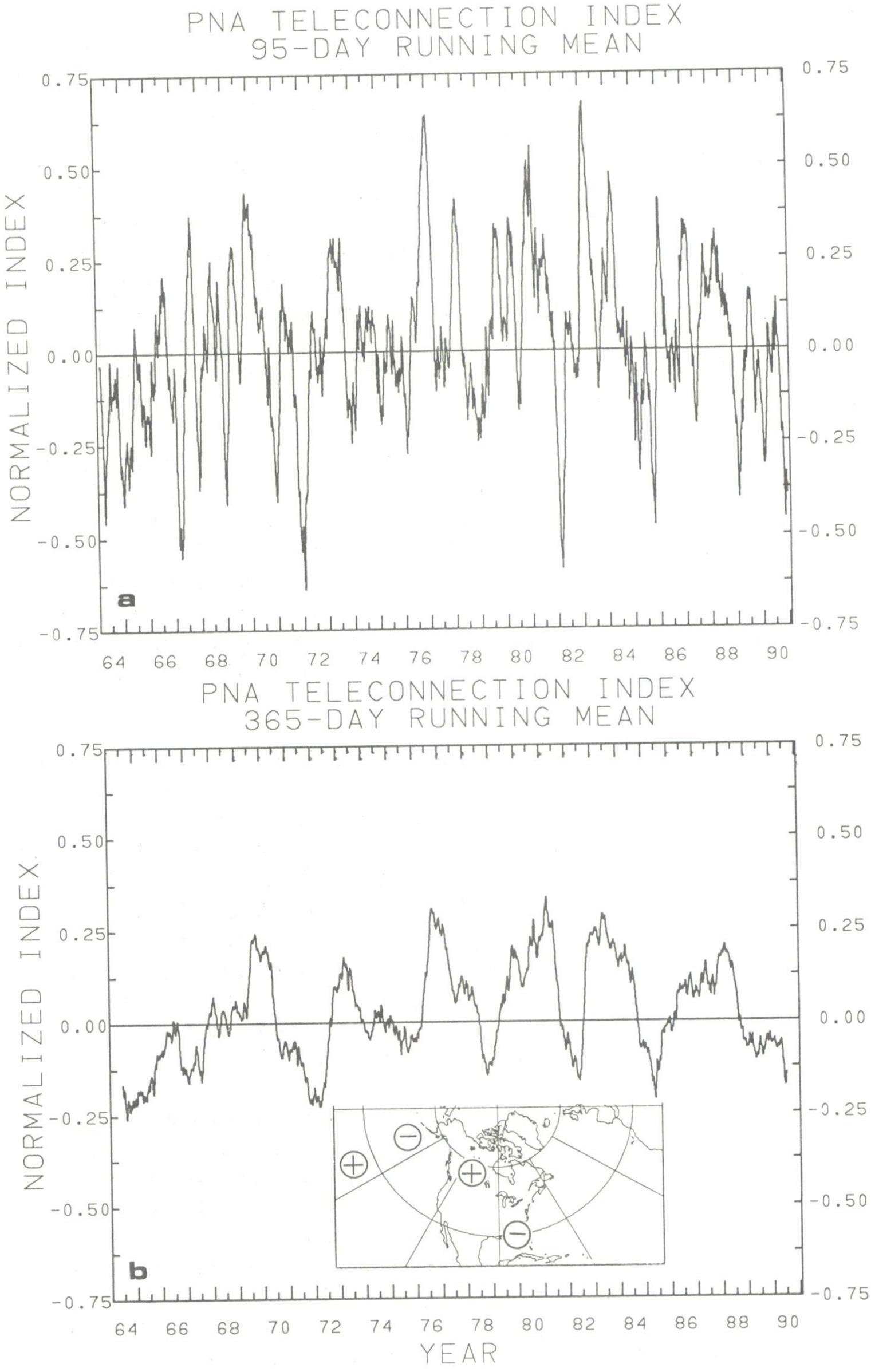

Fig. 46. Time series of the (a) 95-day running mean and (b) the 365-day running mean values of the standardized 700 mb teleconnection pattern indices for the Pacific/North American (PNA) pattern. Running means are determined from daily 700 mb height data for the period August 1964 through December 1990. Indices are normalized using 27-year (1964-1990) daily mean and standard deviation values. Large (small) tick marks along horizontal axes indicate 1 January (1 July) of a given year. Inset illustrates positive phase of the teleconnection pattern index, with height anomalies over centers of action indicated by (+) and (-) signs.

The West Atlantic (WA) pattern is structurally similar to the WP pattern, and reflects major meridional shifts in the position of the western North Atlantic jet stream. The time series of 95-day and 365 day running mean WA index values are shown in **Figs. 47b and 48b**, respectively. The positive phase of the WA pattern reflects positive height anomalies throughout the northwestern and north-central North Atlantic, and negative height anomalies throughout the central North Atlantic; a negative index value indicates anomalies in the opposite sense. The index was positive throughout the late 1960's and the late 1970's, and negative throughout the early 1970's and throughout most of the 1980's, except for brief interruptions during the 1982-83 and the 1986-87 ENSO events.

The East Atlantic (EA) teleconnection pattern reflects a wavelike structure with three centers of action. The pattern encompasses a meridional dipole of height anomalies over the eastern North Atlantic, and a zonal "wave" of height anomalies extending eastward from the northeast North Atlantic to the southwest Soviet Union. The time series of 95-day and 365 day running mean EA index values are shown in **Figs. 47c and 48c**, respectively. A positive phase of the EA pattern reflects anomalously high 500 mb heights over the North Atlantic and low heights over the subtropical Atlantic and eastern Europe; a negative index value indicates anomalies in the opposite sense. Interannual variability of the EA and WA patterns is positively correlated prior to 1988. Weaker interannual variability of the EA pattern was generally noted during the 1980's, however, while strong interannual variability existed over the western and central Atlantic.

The Eurasian (EU) teleconnection pattern also reflects a wavelike structure with three centers of action. The pattern extends eastward from northern Europe to the central Soviet Union and the western North Pacific, and reflects generally high teleconnectivity over the Eurasian Continent. The time series of 95-day and 365 day running mean EU index values are shown in **Figs. 47d and 48d**, respectively. A positive EU pattern is characterized by negative height anomalies over northern Europe, positive height anomalies over the west-central Soviet Union, and negative height anomalies over the western North Pacific; a negative index value indicates anomalies in the opposite sense. Large interannual variability of the EU pattern is observed throughout the 1970's, with negative values tending to dominate during the decade. Notably less interannual variability is observed throughout the 1980's. The mean height anomalies for the decade (**Fig. 41**) suggest a weak negative EU pattern.

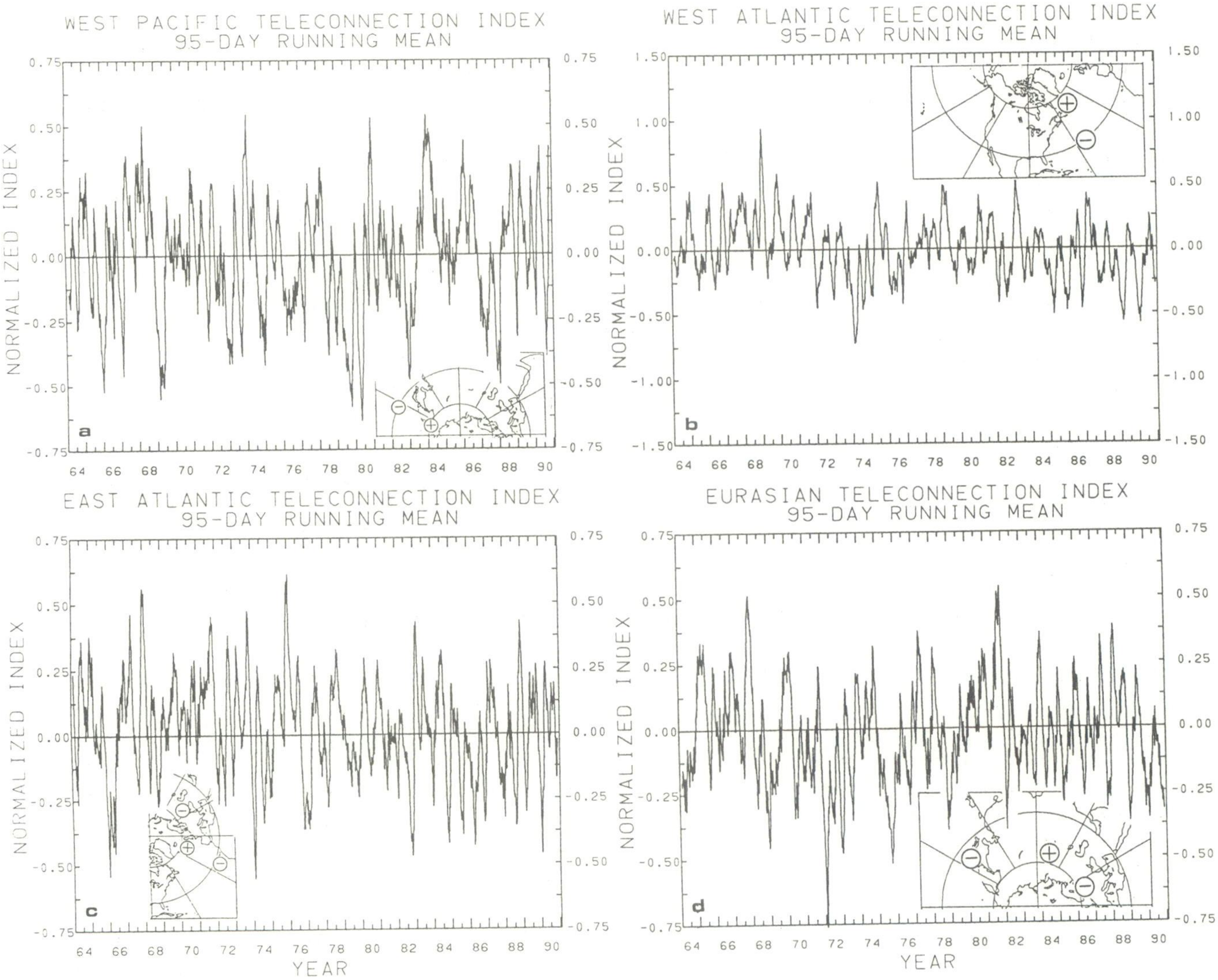

Fig. 47. Time series of the 95-day running mean values of the standardized 700 mb teleconnection pattern indices for: (a) the West Pacific (WP) pattern, (b) the West Atlantic (WA) pattern, (c) the East Atlantic (EA) pattern, and (d) the Eurasian (EU) pattern. Running means are determined from daily 700 mb height data for the period August 1964 through December 1990. Indices are normalized using 27-year (1964-1990) daily mean and standard deviation values. Large (small) tick marks along horizontal axes indicate 1 January (1 July) of a given year. Inset illustrates positive phase of the teleconnection pattern index, with height anomalies over centers of action indicated by (+) and (-) signs.

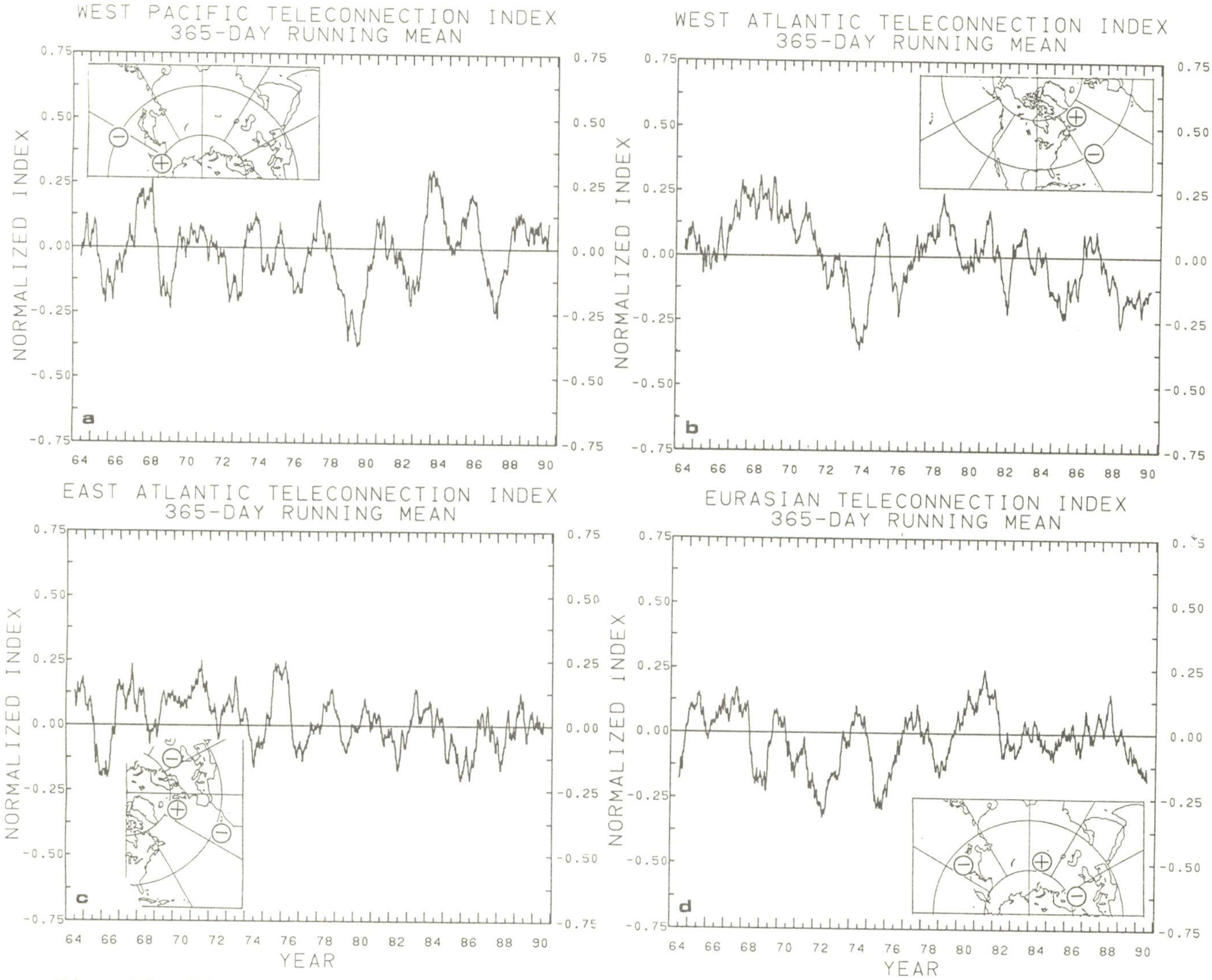

Fig. 48. Time series of the 365-day running mean values of the standardized 700 mb teleconnection pattern indices for: (a) the West Pacific (WP) pattern, (b) the West Atlantic (WA) pattern, (c) the East Atlantic (EA) pattern, and (d) the Eurasian (EU) pattern. Running means are determined from daily 700 mb height data for the period August 1964 through December 1990. Indices are normalized using 27-year (1964-1990) daily mean and standard deviation values. Large (small) tick marks along horizontal axes indicate 1 January (1 July) of a given year. Inset illustrates positive phase of the teleconnection pattern index, with height anomalies over centers of action indicated by (+) and (-) signs.

The interannual behavior of the zonally averaged jet streams in the Northern Hemisphere (**Fig. 49a**) and Southern Hemisphere (**Fig. 49b**) is strongly influenced by sea surface temperature anomalies in the equatorial Pacific. Specifically, large equatorward shifts in the zonally averaged jet stream positions are apparent during the 1982-1983 and 1986-1987 ENSO events. The large poleward contraction of the jets in mid-1988 may be associated with the 1988 cold SO episode. During the 1988-89 period, large negative SST anomalies characterized the equatorial Pacific. The Southern Hemisphere jet appeared to have strengthened during this period, but relaxed in 1990. The Northern Hemisphere high latitude jet remained strong through the end of the decade. These interannual variations in the zonal mean jet stream position are thought to influence the background circulation upon which higher frequency weather systems evolve (Simmons et. al., 1983).

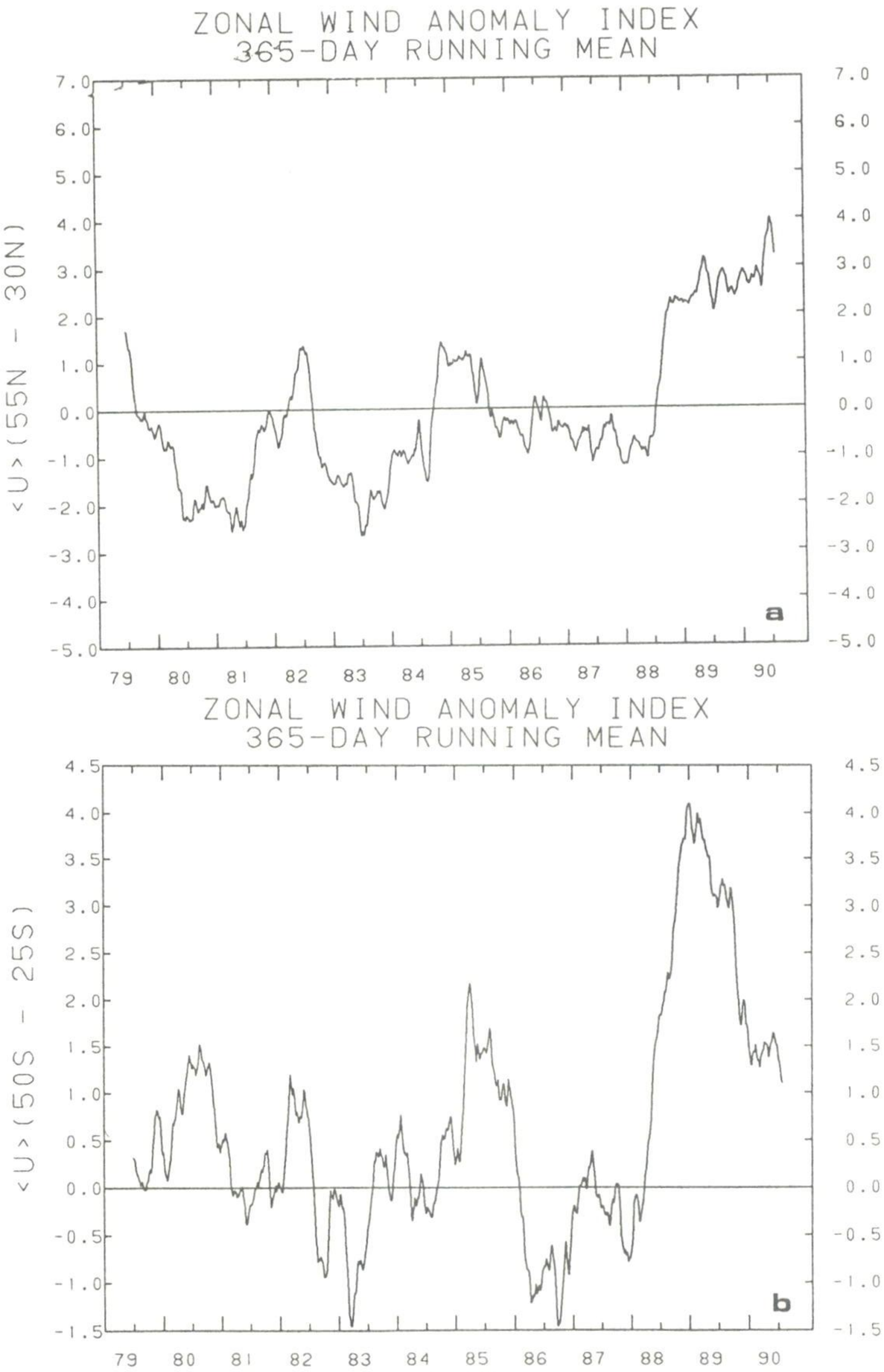

Fig. 49. The u-component of the 250 mb zonal mean wind anomaly averaged over 10^{o} latitude bands (<u>) for the period 1979 to 1990. The time series show 365-day running mean values of: (a) the difference between <u> centered at 55^{o}N and <u> centered at 35^{o}N [<u>(55^{o}N - 30^{o}N)]; and (b) the difference between <u> centered at 55^{o}S and <u> centered at 25^{o}S [<u>(55^{o}S - 25^{o}S)]. Large (small) tick marks along horizontal axes indicate 1 January (1 July) of a given year.

ATMOSPHERIC BLOCKING

An index of the extent and strength of the circumpolar 500 mb vortex (**Fig. 50**) indicates an expanded and/or deepened circumpolar low over the Northern Hemisphere during the mid-1980's. This suggests that the polar front tended to extend equatorward of it's normal position during the 1984 through 1986 period. No long term secular trends are evident in this index.

Blocking patterns are more pronounced during the winter season and are usually found between 40°W and 30°E, 40°E and 100°E and 170°E and 120°W. **Figure 51a** shows a time-longitude cross section of a wintertime blocking index in a latitudinal band from 30°-70°N between 1951 and 1990. Occurrences of extended periods of blocking during the winters throughout the 1980's is similar to earlier periods, although there appears to be less short term blocking in the 1980's between 10°E and 40°E. There is a suggestion that Atlantic sector blocking shifted eastward during the period.

In the summer (**Fig. 51b**), episodes of blocking are usually of shorter duration than during winter over Europe and the USSR, but major blocking regimes over the eastern Pacific are more common. During the decade of the 1980's, the majority of major blocking episodes over the Pacific-North American sector appear to have shifted westward during the early part of the decade. The last few years, however, has seen a shift of blocking episodes back to the position found during the earlier decades.

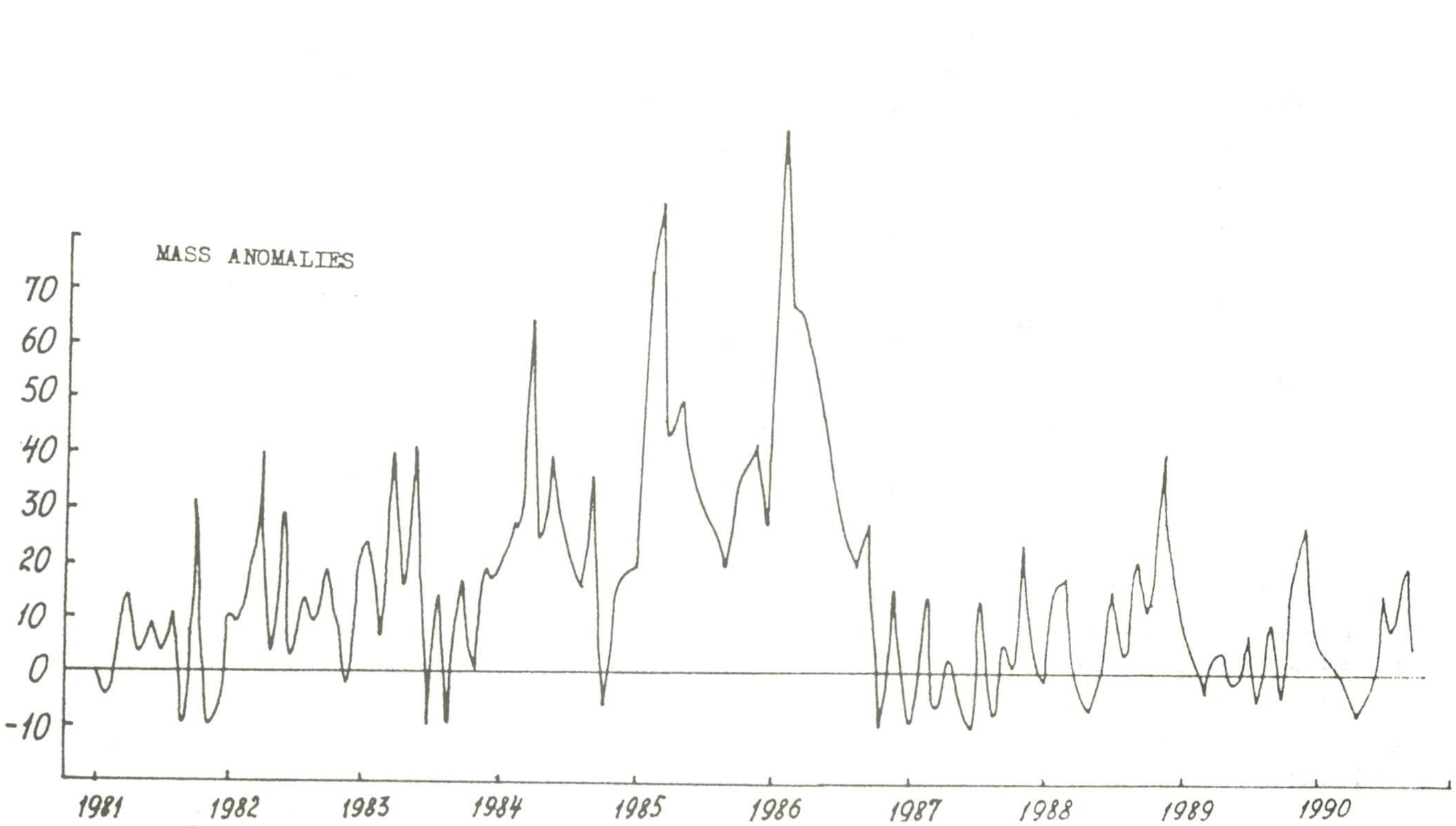

Fig. 50. Time series of a circumpolar vortex mass index. Values are anomalies with respect to the 1951 to 1980 base period. Positive anomalies suggest deeper and/or expanded circumpolar vortex.

Figure courtesy of the Institute for Global Climate and Ecology (USSR).

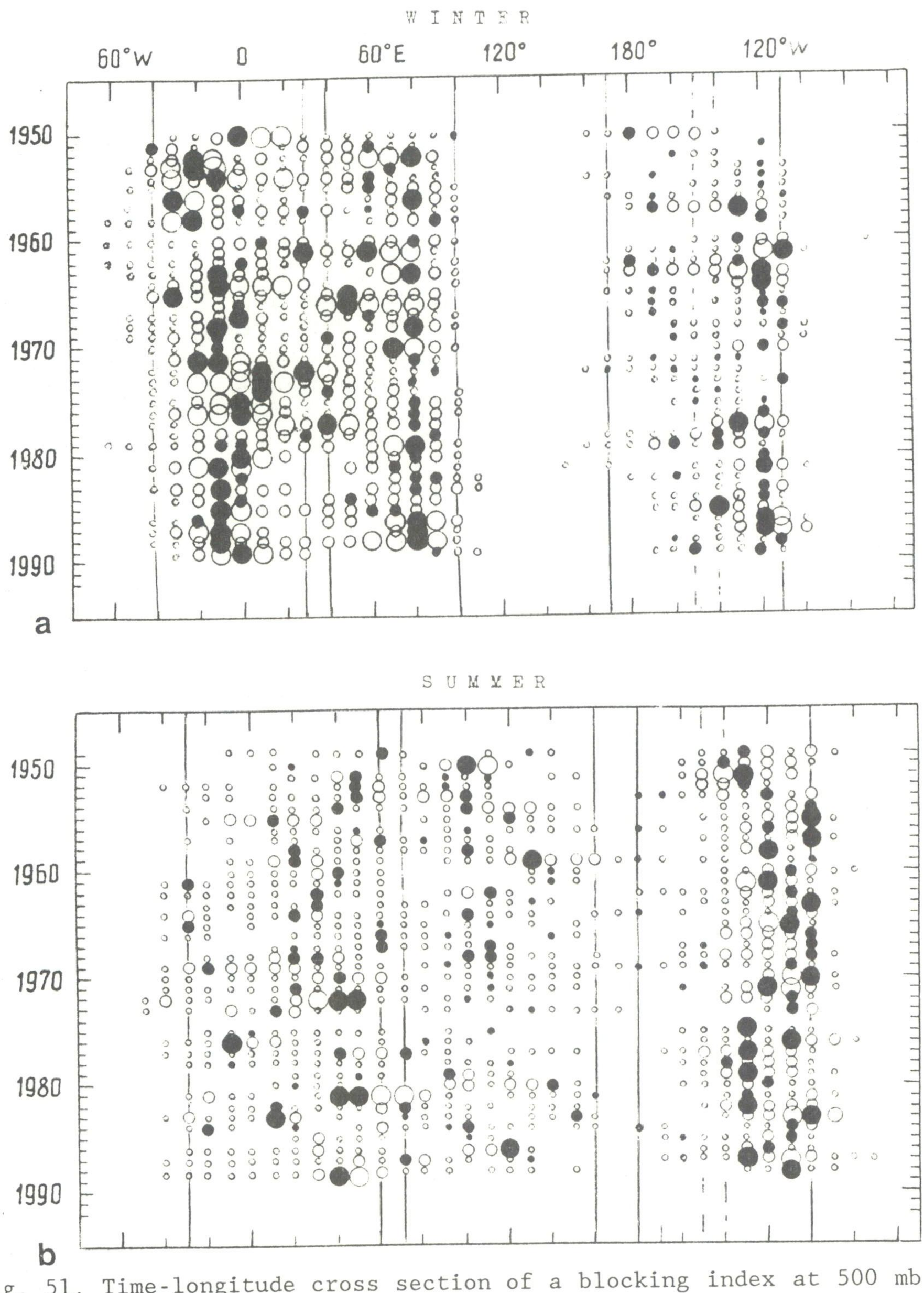

Fig. 51. Time-longitude cross section of a blocking index at 500 mb for the latitudinal band from 30°N - 70°N for a) winter and b) summer. Blackened circles show the centers of maximum total seasonal duration. Smallest circles are for durations between 20 and 40 days, medium circles are for 41 - 60 days, and largest are for > 60 days.

Figure courtesy of the Institute for Global Climate and Ecology (USSR).

OZONE

Monthly averaged SBUV data from the NASA Nimbus 7 satellite, beginning in November 1978 and extending to September 1986, have been combined with SBUV/2 data from the NOAA-9 satellite from March 1985 to October 1988 and adjusted to ground-based data. **Figure 52** shows the decadal time series from both satellites.

For total ozone, data from both instruments have been combined and adjusted to the Dobson network. The satellite data are integrated from 60N to 60S and the time series is then fitted with an autoregressive time series model which includes a trend, an annual and semi-annual cycle, an F10.7 solar flux term, and the QBO cycle. The calculated trend, within a 95 percent confidence interval, shows a decrease in the total ozone in this time period of -2.45 (±.62) percent/decade.

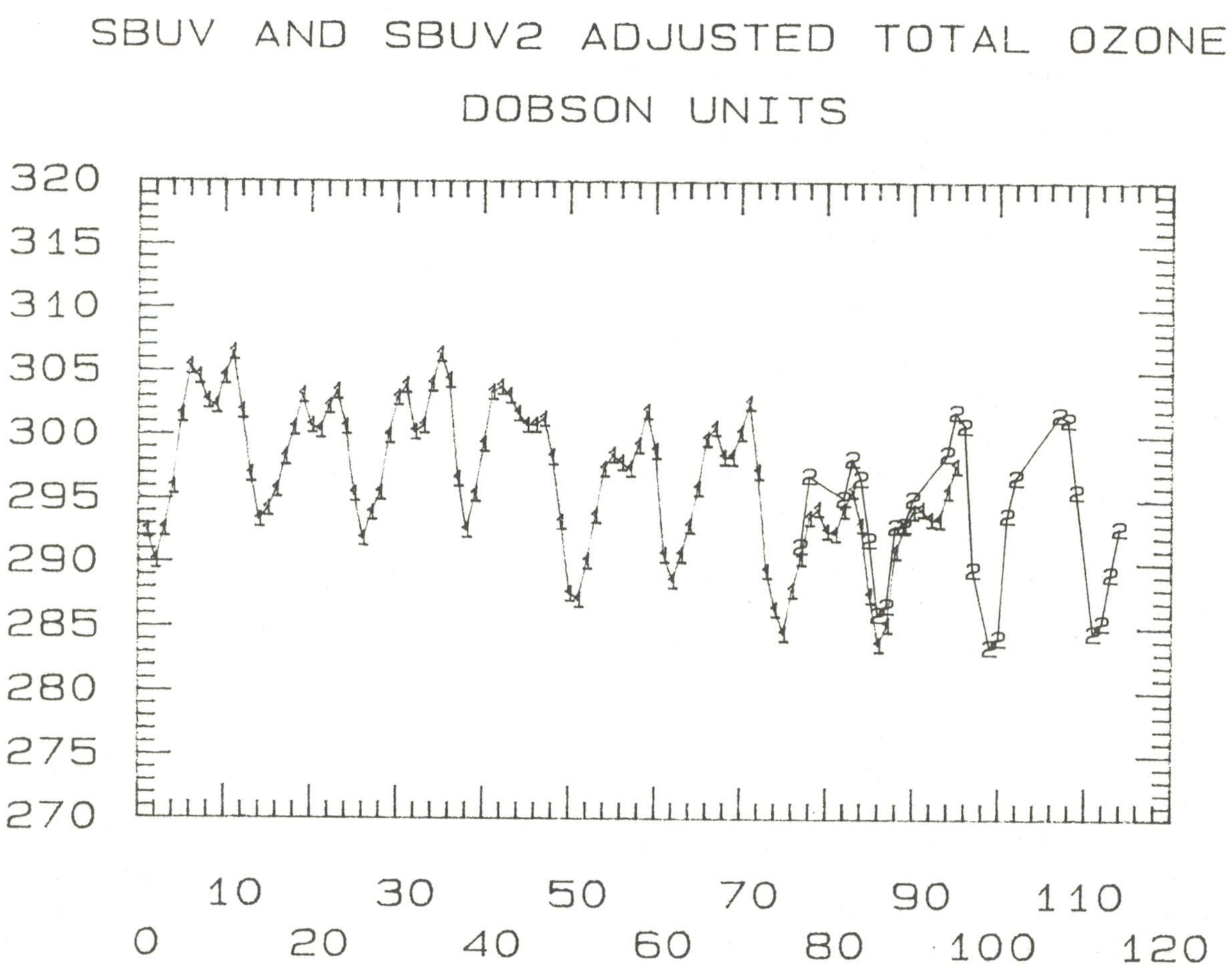

Fig. 52. Time series of monthly averaged total ozone in Dobson units from November 1978 through October 1988. The 1s are data from Nimbus 7, while the 2s are data from NOAA 9. The overlap period extends from March 1985 to September 1986.

MAJOR CLIMATE EVENTS

SOUTHERN OSCILLATION

The decade of the 80's featured one of the strongest tropical Pacific warm (El Niño/Southern Oscillation - ENSO) episodes (1982-83) of the last century, one of the strongest cold episodes (1988-89) during the last 50 years and a strong central Pacific warm episode (1986-87). **Figures 53 and 54** show the sea surface temperature anomaly patterns at the height of these extremes in the Southern Oscillation and the time series of the Tahiti-Darwin Southern Oscillation Index, respectively. These three major episodes were accompanied by global circulation and precipitation anomalies, which in some cases reached extreme proportions.

During warm (cold) episodes, atmospheric convection as indicated by the OLR index (**Fig. 55**) becomes enhanced (weakened) over the anomalously warm (cool) water in the central equatorial Pacific. This abnormal convection serves to anomalously heat (cool) the tropical troposphere, thus providing an enhanced (weakened) equator to pole thermal gradient and enhanced (weakened) subtropical upper-tropospheric jet streams, especially in the winter hemisphere. The heating (cooling) of the troposphere is initially found in the vicinity of the enhanced (weakened) convection, but it gradually spreads throughout the tropics (**Figs. 56 and 57**). The largest temperature anomalies are generally observed in the vicinity of the anomalous convective activity.

The zonally averaged 500 mb temperature (**Fig. 58**) is used as an index of the tropospheric heating and cooling associated with variations in the intensity of tropical convective activity. Positive anomalies (zonally averaged, exceeding $1^{o}C$, and locally exceeding $2^{o}C$, **Figs. 58 and 57**, respectively) were observed in the tropics during the two ENSO episodes of 1982-83 and 1986-87. However, it is apparent from **Figs. 56 and 58** that the cold episode of 1988-89 also had a remarkable impact on mid-tropospheric temperatures, with zonally averaged anomalies less than $-1.4^{o}C$ (locally less than $-2.5^{o}C$) in the tropical belt.

During periods of anomalously warm or cold conditions in the tropical mid-troposphere there is a tendency for the mid-latitudes to experience opposite temperature anomalies. Thus, during warm (cold) episodes when the tropical mid-troposphere is anomalously warm (cold) the mid-latitude mid-troposphere is anomalously cold (warm). This tendency, which is evident in the zonally averaged 500 mb temperature anomalies, is even more striking if the averages are computed for the central and eastern Pacific sector ($120^{o}W$-180, **Fig. 59**) instead of over all longitudes. It is evident that the cold episode of 1988-89 affected the tropical and extratropical mid-tropospheric temperature anomalies from early 1988 until early 1990 (a period of about two years). During that period, the mid-latitudes in both hemispheres were dominated by anomalously warm conditions, especially in the Pacific sector, which were accentuated in the Northern Hemisphere during the northern winter season.

Consistent with the above changes in the pattern of mid-tropospheric temperature anomalies, subtropical upper tropospheric westerlies are stronger than normal during warm episodes and weaker than normal during cold episodes (**Fig. 60**). Both the cooler than normal period 1984-85 and the cold episode of 1988-89 featured upper tropospheric easterly anomalies (weaker than normal westerlies) in the subtropics and lower mid-latitudes of both hemispheres. During the warm episodes of 1982-83 and 1986-87, stronger than normal westerlies were observed in the subtropics of both hemispheres.

These changes in the intensity of the subtropical jet streams and in the pattern of mid-tropospheric temperature anomalies are associated with variations in the global pattern of precipitation anomalies. The patterns of anomalous precipitation that are associated with both warm or cold extremes of the Southern Oscillation have been documented by Ropelewski and Halpert (1987, 1989). They show that subtropical regions of North and South America experience above (below) normal rainfall during warm (cold) episodes; periods when the subtropical jet streams are stronger (weaker) than normal. Also, rainfall tends to be less than normal, during warm episodes, over portions of India and Australia as convective activity shifts eastward over the anomalously warm water in the central equatorial Pacific. Conversely, during cold episodes both the Australian and Indian monsoons are enhanced and rainfall tends to be above normal. These conditions were observed during the 1980's associated with the three extremes in the Southern Oscillation cited above.

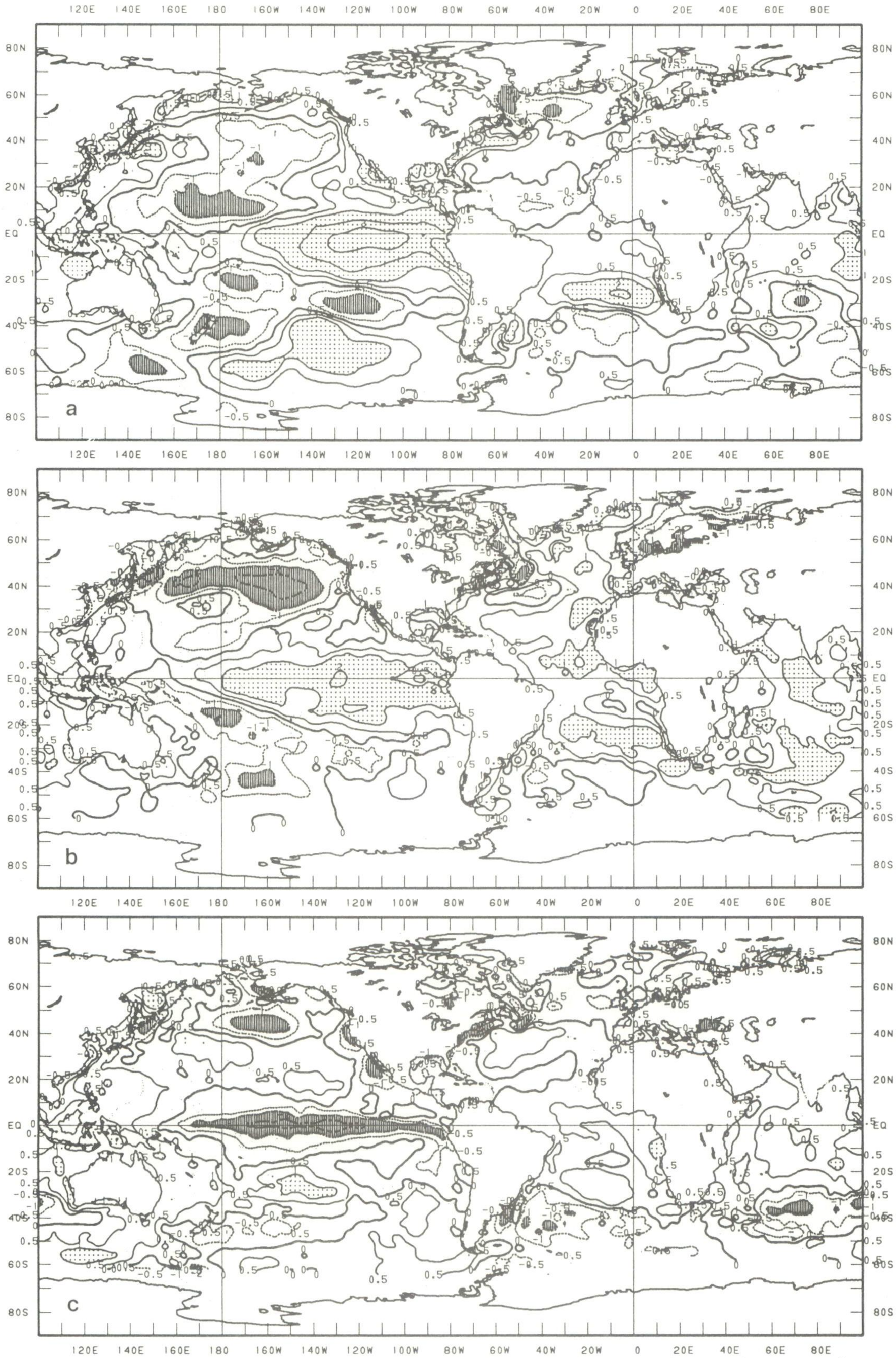

Fig. 53. Sea surface temperature anomaly patterns for a) December 1982-February 1983, b) June-August 1987, and c) September-November 1988. Contour interval is 1°C, with additional contours drawn for +0.5°C. Anomalies less than -1°C are shaded and greater than 1°C are stippled. Anomalies are computed as departures from the COADS/ICE climatology.

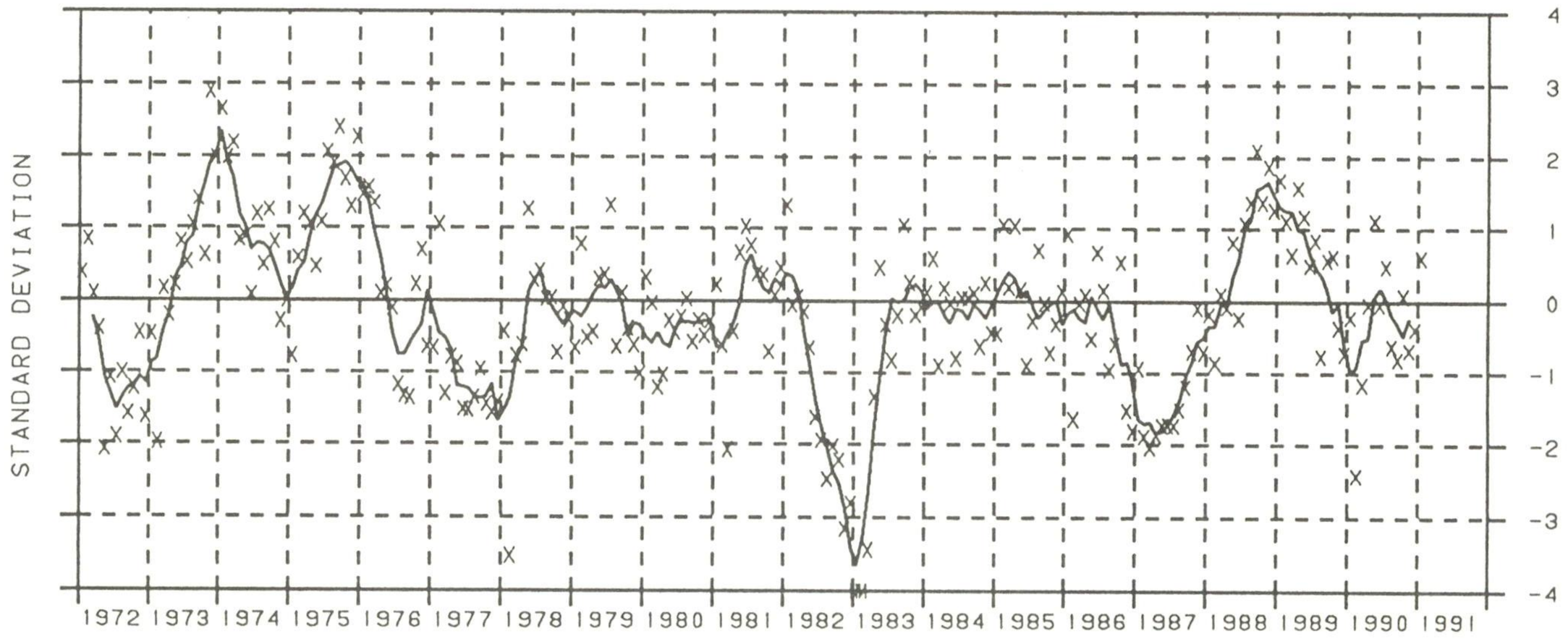

Fig. 54. Five-month running mean of the difference between the standardized sea level pressure anomalies at Tahiti and Darwin (Tahiti-Darwin). Values are standardized by the mean annual standard deviation. Crosses are individual monthly means.

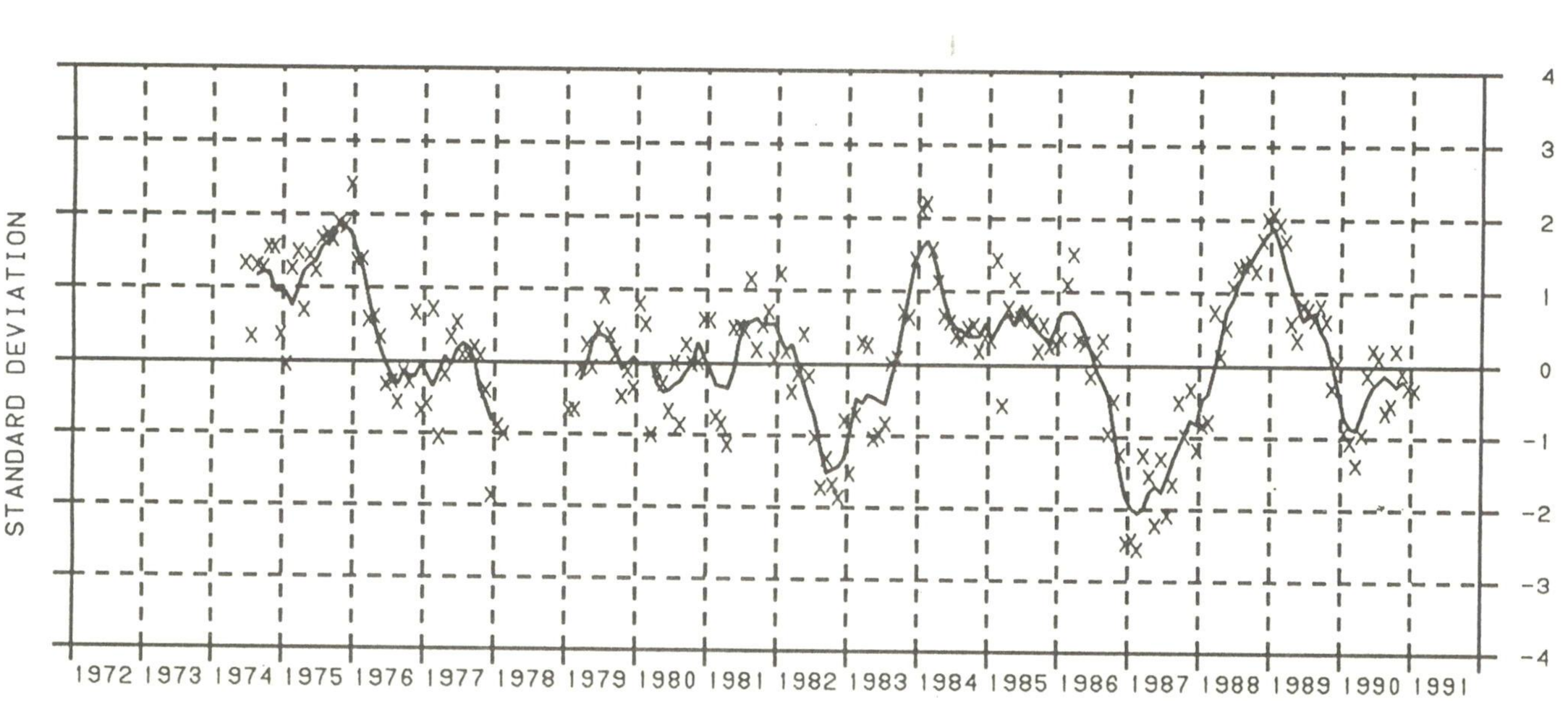

Fig. 55. Five-month running mean of the standardized monthly anomaly in outgoing longwave radiation over the area $5^{o}N$-$5^{o}S$, $160^{o}E$-$160^{o}W$.

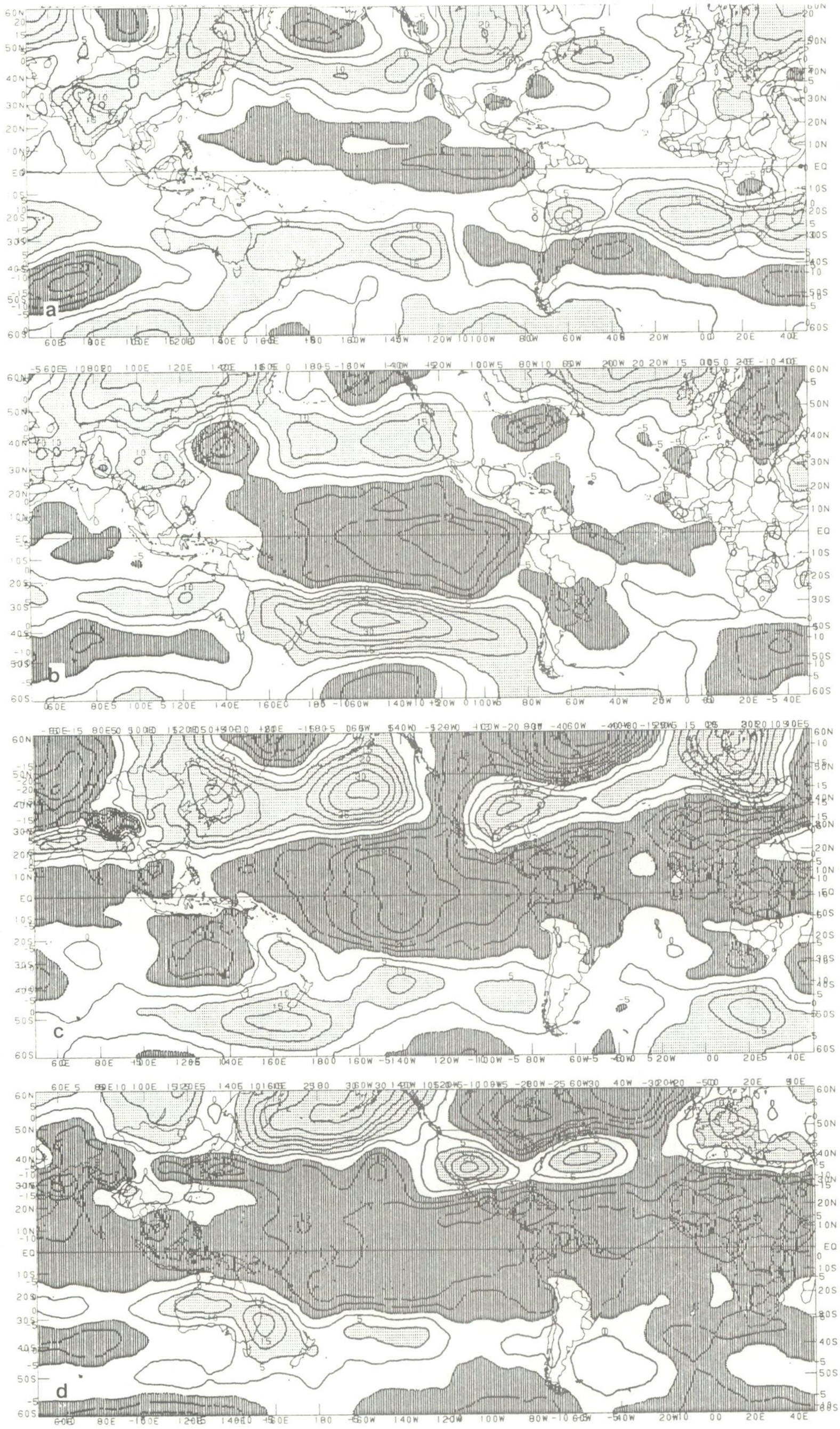

Fig. 56. Anomalous 500 mb temperature for a) June-August 1988, b) September-November 1988, c) December 1988-February 1989, and d) March-May 1989. Contour interval is 0.5°C. (Contour values have been multiplied by 10.) Dark (light) shading indicates anomalies less (greater) than -0.5°C (+0.5°C).

Fig. 57. Anomalous 500 mb temperature for a) June-August 1982, b) September-November 1982, c) December 1982-February 1983, and d) March-May 1983. Contour interval is 0.5°C. (Contour values have been multiplied by 10.) Dark (light) shading indicates anomalies less (greater) than -0.5°C (+0.5°C).

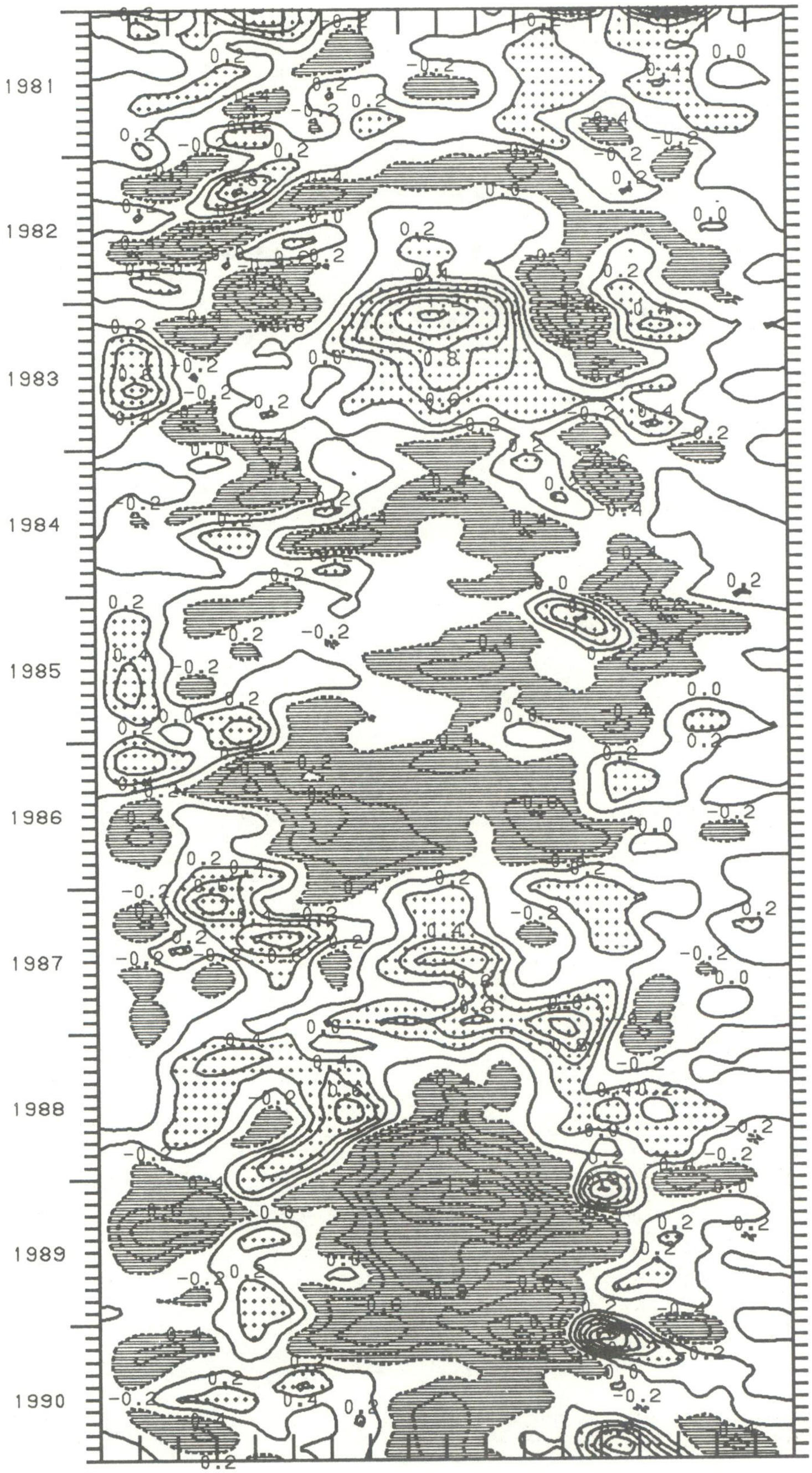

Fig. 58. Time-latitude section of zonally averaged 500 mb temperature anomalies. Contour interval is 0.2°C. Anomalies are computed with respect to the 1979-1988 monthly means.

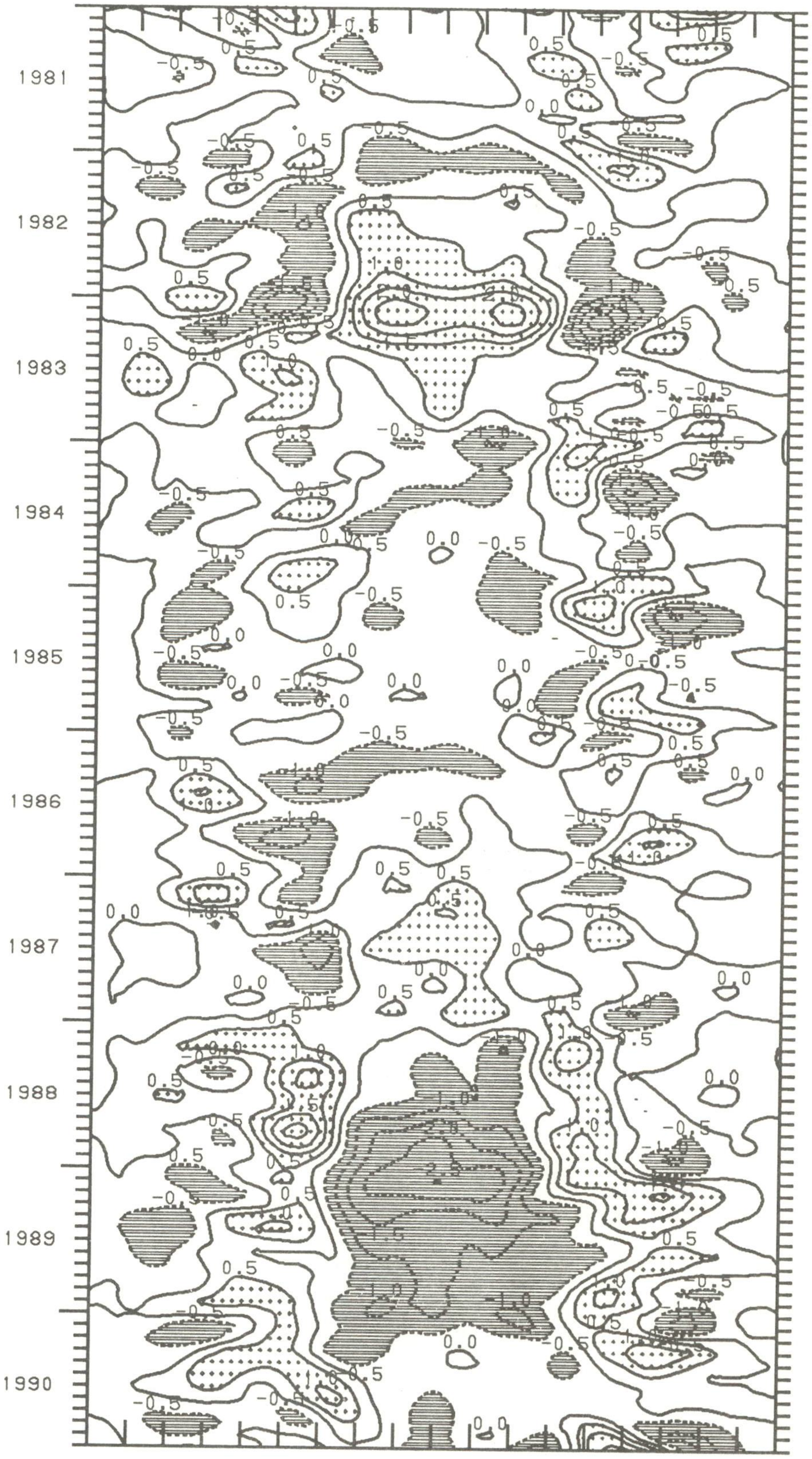

Fig. 59. Time-latitude section of average 500 mb temperature anomalies over the longitude band 120°W-180. Contour interval is 0.5°C, Anomalies are computed with respect to the 1979-1988 monthly means.

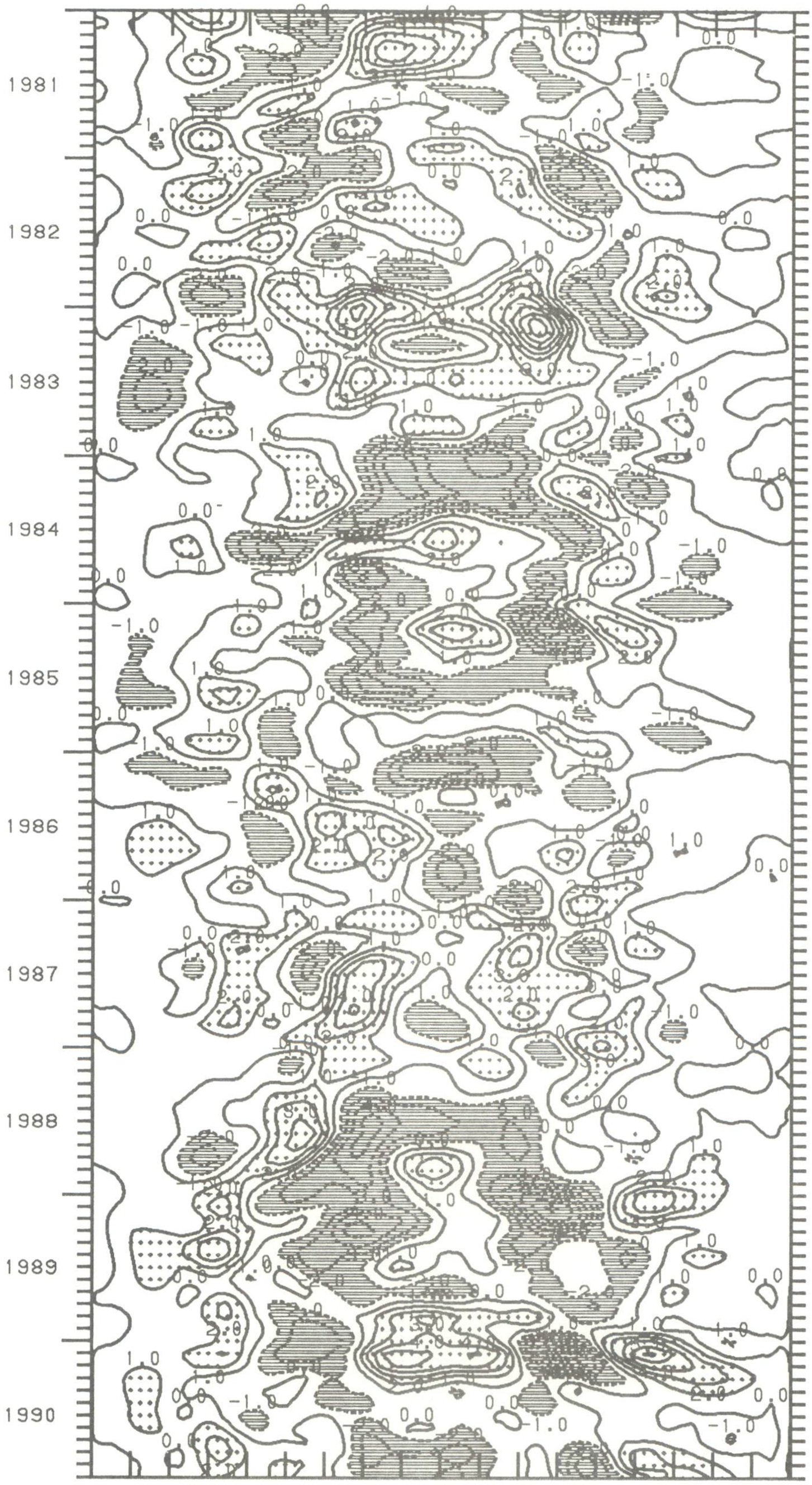

Fig. 60. Time-latitude section of 200 mb zonally averaged zonal wind anomalies. Contour interval is 1 ms^{-1}. Anomalies are computed with respect to the 1979-1988 monthly means.

WARM AND COLD REGIONS

During the decade of the 1980's, the most extensive regions (covering more than twenty million sq. km) experiencing negative temperature anomalies were observed over the oceans. Data over the oceans are surface temperature anomalies from ship observations. **Figure 61** shows the regions experiencing warmer and colder than normal temperatures in the Northern Hemisphere for the each season during December 1980 through November 1990 period. Especially interesting is the number of occurrences of large colder than normal areas in the Atlantic Ocean between 1983 and 1986. Large areas of negative temperature anomalies were rare over the continents, although the winter season (**Fig. 61a**) does indicate extensive areas of colder than normal temperatures in 1983 in the United States and during a few winters around Greenland and the North Atlantic.

The majority of areas experiencing warmer than normal temperatures were found in the North Pacific Ocean during all seasons and over Asia during spring and fall. Other regions experiencing positive temperature anomalies were located in the equatorial Pacific (associated with the El Niño/Southern Oscillation) and Southeast Asia during the JJA season. A number of small areas with warmer than normal temperatures were found in the Arctic region during winter. Northern Hemisphere temperature and precipitation percentiles for each winter and summer season during the decade of the 1980's can be found in the appendix.

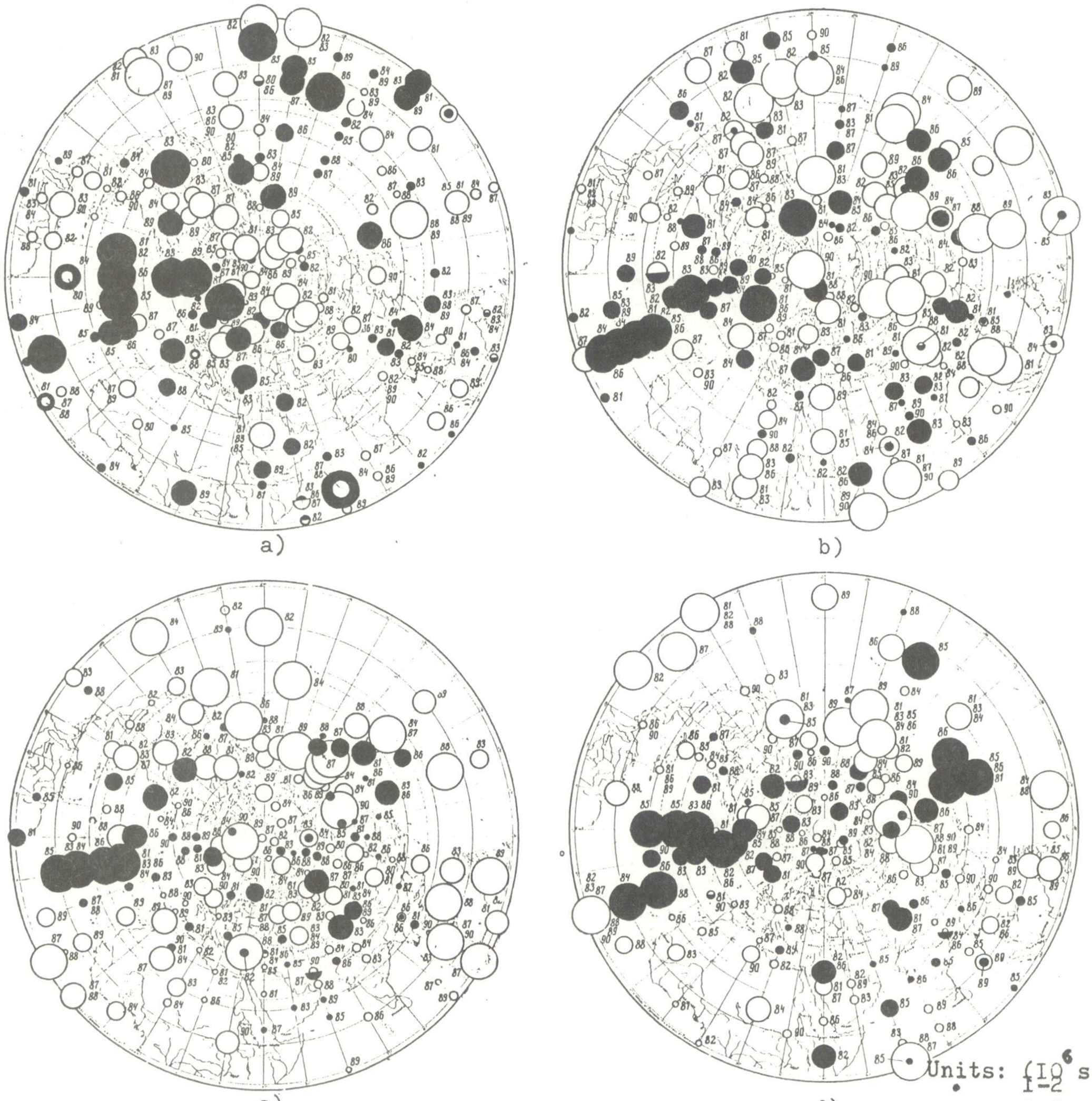

Fig. 61. Locations of regions experiencing warmer and colder than normal temperatures during the decade of the 1980's for a) DJF, b) MAM, c) JJA, and d) SON. Average temperature anomalies are greater than one standard deviation with the extreme anomaly at least two standard deviations. Open circles are for positive anomalies, blackened circles are for negative anomalies. The size of the circle represents the area of the region effected by the anomaly. Smallest circles are for 1 - 2 million km^2., while largest circles are for > 20 million km^2. Figure courtesy of the Institute for Global Climate and Ecology (USSR).

MAJOR CLIMATE ANOMALIES IN THE WORLD: 1981 – 1990

1. *California:*

FIVE CONSECUTIVE DRY WINTERS (1986–1990).

Exceptionally large long–term precipitation deficits have accumulated throughout California since late 1986. California has endured four consecutive dry winters, and a fifth dry winter was well underway. On a long–term basis (since October 1986), precipitation deficits ranged from 164 mm at Bakersfield, CA (73.7% of normal) to 1151 mm at Eureka, CA (74.1% of normal). Less than 60% of the normal precipitation was measured at San Francisco, Los Angeles, and Santa Maria, CA since October 1, 1986, producing deficits of more than 575 mm. Runoff has averaged nearly two–thirds of normal for each of the last four winters, and reservoir levels continued to fall at a time when they would normally rise. In addition, the state's worst freeze (late December 1990) since the 1936–1937 growing season aggravated southern California's high fire potential by killing vegetation already sapped of moisture by years of drought, turning it into highly flammable fuel.

2. *Pacific Ocean Basin:*

EL NIÑO/SOUTHERN OSCILLATION AFFECTS CLIMATE (1982–1983).

If *El Niño*/Southern Oscillation (ENSO) were simply an isolated regional phenomenon, or even confined to the equatorial eastern Pacific, it would be of limited interest; however, it is a major constituent in a vast system of ocean–atmosphere interactions, giving the phenomenon global meteorological implications. The abnormally warm equatorial Pacific waters characteristic of ENSO brought the Intertropical Convergence Zone (ITCZ) unusually far south, generating pronounced upper–level westerly winds. This in turn brought heavy rains that produced massive floods in western Ecuador and coastal northern Peru during November 1982–June 1983. In sharp contrast, rainfall in southern Peru and western Bolivia was only one–third of normal. The high sea surface temperatures were also conducive to tropical cyclone development, making 1983 the "year of the cyclones" in French Polynesia where numerous systems produce extensive damage. Farther west, Australia endured its worst drought since the 1860's as summer (December 1982–February 1983) rainfall was one of the lowest on record across the eastern half of the continent. Major fires raged in January as hot, dry northerly winds prevailed. Major droughts also affected the Philippines and Indonesia as convective activity was suppressed.

3. *United States:*

THE DROUGHT OF 1988.

The United States Drought of 1988 was the most severe in the Midwest since 1936. The driest and/or hottest period in over 90 years was recorded in parts of the Great Plains, Midwest, and lower Mississippi Valley. Low river flow and reservoir storage hindered river navigation, restricted water usage, and reduced irrigation across much of the nation. Over four million acres of forest were consumed by wild fires. In April 1988, long–term moisture deficits existed over the Tennessee Valley, southern Appalachians, northern Plains, and much of the West. During the late Spring and early Summer, large rainfall deficits combined with record high temperatures to produce extreme drought conditions across much of the country. The drought peaked in early July as normal rainfall finally returned to the central United States in the late Summer, easing the dryness. Much of the Far West, however, has since remained in a drought (see #1 above).

4. *Sahel Region:*

SECOND CONSECUTIVE DRY DECADE.

The rainy seasons (typically June–September) across the African Sahel during the 1980's were generally dominated by well below normal rainfall and above normal temperatures, particularly in 1983 and 1984. The 1980's continued a trend of abnormal dryness that has afflicted the region since the late 1960's. The long–term drought and high temperatures caused widespread crop failures, agricultural problems, hydroelectric shortages, navigational difficulties, and large–scale human suffering. Rainfall increased somewhat in 1985–1987, but totals were still subnormal. Finally in 1988, near–normal precipitation moistened much of the region, but severe flooding, especially along the Nile River in Sudan, accompanied the rains in some areas. The following year brought similar conditions, making 1988–1989 the first consecutive years with seasonable rainfall since the mid–1960's. Unfortunately, extremely dry and hot weather returned to the Sahel in 1990.

5. *South America:*

PROLONGED DRYNESS (1988 – 1989).

Unusually dry weather that began in mid–1988 persisted well into 1989. The dry spell commenced in much of central and eastern South America during July, and the normally wet spring months (September–November) showed a pronounced rainfall deficit. Increased late November and December precipitation in the northern sections of the affected area eased dryness there, but southern portions, particularly northern Argentina and Uruguay, remained abnormally dry. Subnormal rainfall continued during the first half of 1989 in the latter two areas, and was aggravated by a heat wave in early January that sent temperatures soaring near 40°C in Argentina. The combination of heat and dryness devastated the country's corn crop, producing a 50% drop from

the previous year's yield and the worst harvest in 26 years. Long term precipitation deficits remained as the 1989 dry season (May–August) got underway. Fortunately, the 1989–1990 rainy season (approximately October–April) brought ample, and occasionally excessive, rainfall to much of the region.

6. *Europe:*

COLD WINTER AND SPRING ACROSS THE CONTINENT (1987).

Severe winter weather plagued Europe in January 1987. Frigid Siberian air became entrenched over the continent by early January, dropping temperatures to –45°C at Leningrad, –25°C at Berlin, and –9°C at London. Coastal and river ice brought a halt to shipping in northern Europe. The cold was accompanied by a major snowstorm in western Europe, and snow fell as far south as the French Riviera. In March and April, unseasonable snow and cold hit the eastern Mediterranean countries. Freezing temperatures devastated Italian citrus crops, and severe cold reduced the almond and citrus crops in Greece by 46% over the previous year. Temperatures were as much as 6°C below normal during March and April, and cool weather occurred again during late June and most of August.

7. *Europe and Northern Africa:*

HEAT WAVES AGGRAVATE PROLONGED DRYNESS (1990).

Prior to 1990, large precipitation deficiencies had accumulated during the normally wet winter months of 1987–88 and 1988–89 across many areas of southern Europe and the northern Middle East. In late 1989, very dry conditions redeveloped across east–central Europe, and the dryness spread into south–central and southeastern Europe during January and early February 1990. Rains in late February and early March provided some relief, but dryness returned by the end of the month. Moderate rains in April brought limited relief; however, another dry spell was under way by early May. During most of July, a dry heat wave enveloped much of southern and central Europe as temperatures soared up to 7°C above normal. The hot weather persisted through most of August, spreading as far north as southern Scandinavia. Cool, moist air swept across the continent in early September, bringing some relief from the mid–summer heat and dryness, but unseasonably hot weather returned to Europe and northern Africa during late September and early October. Weekly temperatures averaged as much as 13°C above normal in the Balkans during late October, but cooler air penetrated southward across the continent around mid–November and ended the second warm spell. Increased precipitation late in the year eased short–term dryness, but long–term moisture deficiencies remained.

8. *Eurasia:*

RECORD WINTER MILDNESS (1988–1989).

The abnormally mild winter weather regime of late 1988 lingered across Siberia into 1989. In January, the largest departures were reported near Lake Baykal. The warmth overspread much of Europe and Soviet Asia by February, with weekly temperatures averaging up to 21°C above normal. The mild weather dominated south–central and extreme eastern Siberia in March, spreading northwestward through central and southern Europe by April. More seasonable conditions were recorded across Europe by late April, but Siberia remained anomalously mild into May.

9. *China:*

SPRING DROUGHT OVERTAKEN BY LATE SUMMER FLOODS (1981).

Millions of people suffered through food and water shortages as abnormally dry weather during the Spring of 1981 aggravated a drought which began late in the previous year. Most of Hebei province measured only 10–30% of normal precipitation during the period. Although substantial rains relieved the drought in June 1981, Beijing's twelve month (July 1980–June 1981) precipitation total was only 40% of normal, demonstrating a need for additional rain to recharge Chinese reservoirs. Torrential rains continued through the rest of the summer and early fall months, ending the drought but causing massive flooding in the central Chinese provinces of Sichuan and Shaanxi. Extensive loss of life and property was reported as the Yangtze River reached its highest level this century.

10. *Australia:*

RECORD RAINS CAUSE FLOODING (1984).

During January 1984, a monsoonal low pressure system covered the interior of Australia and spawned a series of rain–bearing disturbances. Record rains inundated inland districts of New South Wales and extreme northern South Australia. For the first time in recorded history, Lake Eyre (South) filled independently and overflowed into Lake Eyre (North). During a few days in mid–February, a storm system dumped 800 mm of rain near Wollongong, south of Sydney, causing severe flooding. At several locations, the rainfall event had a climatological return period exceeding 100 years.

Anomalies were selected based on human impact, type, years of occurrence, and locations such that a balance would be achieved

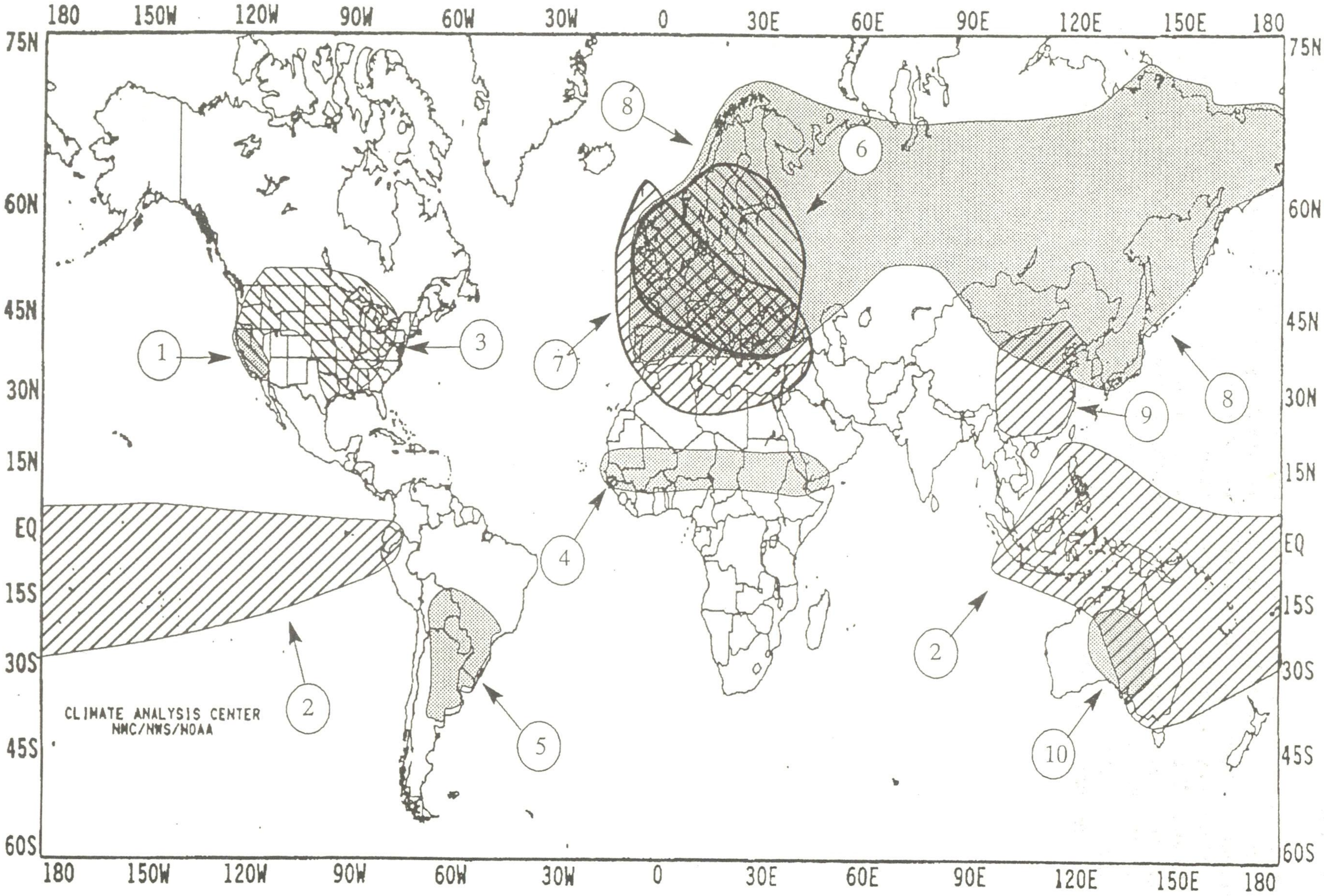

Figure 62. Major global climate anomalies during 1981–1990. Approximate location of each anomaly is depicted for each corresponding anomaly number.

ACKNOWLEDGMENTS

This summary could not have been possible without the cooperation and contributions from several scientists representing a cross-section of the NOAA climate community. We also acknowledge the contributions from several scientists outside of NOAA. Each of the contributors have our sincere thanks for their timely and useful input. Any usefulness of this report is to their credit. We also thank the internal reviewers (D. Rodenhuis, V. Kousky, J. Laver, L. Mannello) for their comments and suggestions. This report is partially supported by the Climate and Global Change sponsored Global Climate Perspectives System (GCPS) Project.

References

Angell, J. K., 1990: Variations in global tropospheric temperature after adjustment for the El Niño influence. Geophys. Res. Lett., 17, 1093-1096.

Barnston, A.G., and R.E. Livezey, 1987: Classification, Seasonality and persistence of low frequency atmospheric circulation patterns. Mon. Wea. Rev., 115, 1083-1126.

Blackmon, M. L., 1976: A climatological spectral study of the 500 mb geopotential height of the Northern Hemisphere. J. Atmos. Sci., 33, 1607-1623.

Blackmon, M. L., Y.-H. Lee and J. M. Wallace, 1984: Horizontal structure of 500 mb height fluctuations with long, intermediate and short time scales. J. Atmos. Sci., 41, 961-979.

Halpert, M. S., and C. F. Ropelewski, 1991: Temperature patterns associated with the Southern Oscillation. Journal of Climate, (Submitted).

Horel, J. D., and J. M. Wallace, 1981: Planetary-scale atmospheric phenonena associated with the Southern Oscillation. J. Atmos. Sci., 109, 813-829.

IPCC, 1990: Climate Change, The IPCC Scientific Assessment, J. T. Houghton, G. J. Jenkins, and J. J. Ephraums, Editors, Cambridge University Press, 365 pp.

Klein, W.H., 1983: Objective specification of monthly mean surface temperature from mean 700mb heights in winter. Mon. Wea. Rev., 111, 674-691.

Lamb P. J., 1982: Persistence of Subsaharan Drought. Nature, 299, 46-49.

Panofsky, H. A., and G. W. Brier, 1968: Some applications of statistics to meteorology. The Pennsylvania State University, University Park, Pennsylvania, 224 pp.

Reynolds, R. W., 1988: A real-time global sea surface temperature analysis. J. Climate, 1, 75-86.

Ropelewski, C. F. and M. S. Halpert, 1987: Global and Regional Scale Precipitation Patterns Associated with the El Niño/Southern Oscillation. Mon. Wea. Rev., 115, 1606-1626.

Ropelewski, C. F. and M. S. Halpert, 1989: Precipitation Patterns Associated with the High Index Phase of the Southern Oscillation. J. Climate, 2, 268-284.

Simmons, A. J., J. M. Wallace and G. W. Branstator, 1983: Barotropic wave propagation and instability, and atmospheric teleconnection patterns. J. Atmos. Sci., 40, 1363-1392.

Spencer R. W., and J. R. Christy, 1990: Precise monitoring of global temperature trends from satellites. Science, 247, 1558-1562.

Spencer, R.W., J.R. Christy, N.C. Grody, 1990: Global atmospheric temperature monitoring with satellite microwave measurements: method and results 1979-84. J. Climate, 3, 1111-1128.

Vinnikov, K. Y., P. Y. Groisman, and K. M. Lugina, 1990: Empirical data on contemporary global climate changes (temperature and precipitation). J. Climate, 3, 662-677.

Wallace, J. M., and D. S. Gutzler, 1981: Teleconnections in the geopotential height field during the Northern Hemisphere winter. Mon. Wea. Rev., 109, 784-812.

APPENDIX

Northern Hemisphere DJF and JJA temperature and precipitation percentiles

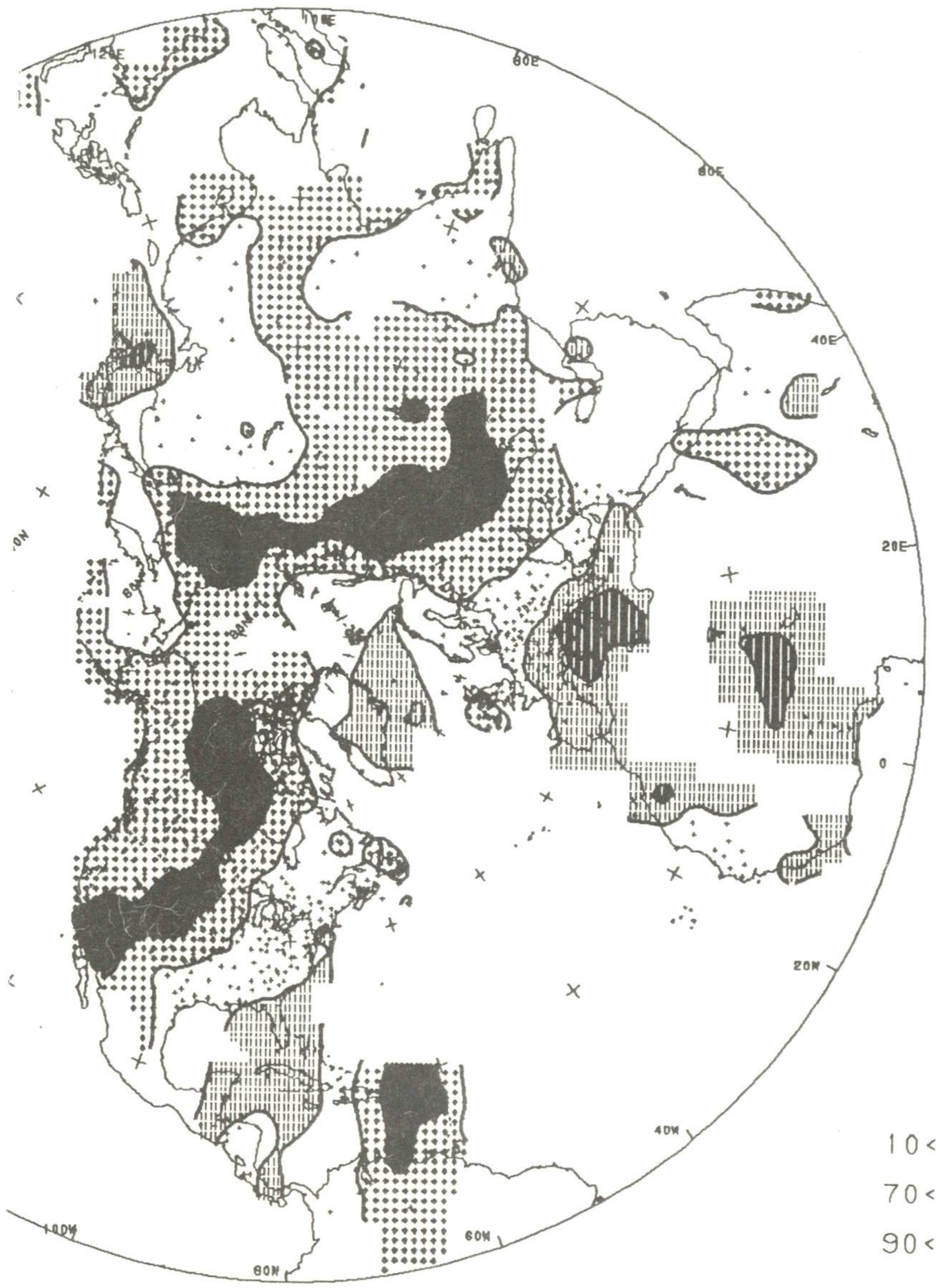

DJF 1980–81 TEMPERATURE PERCENTILES
BASED ON NORMAL DISTRIBUTION

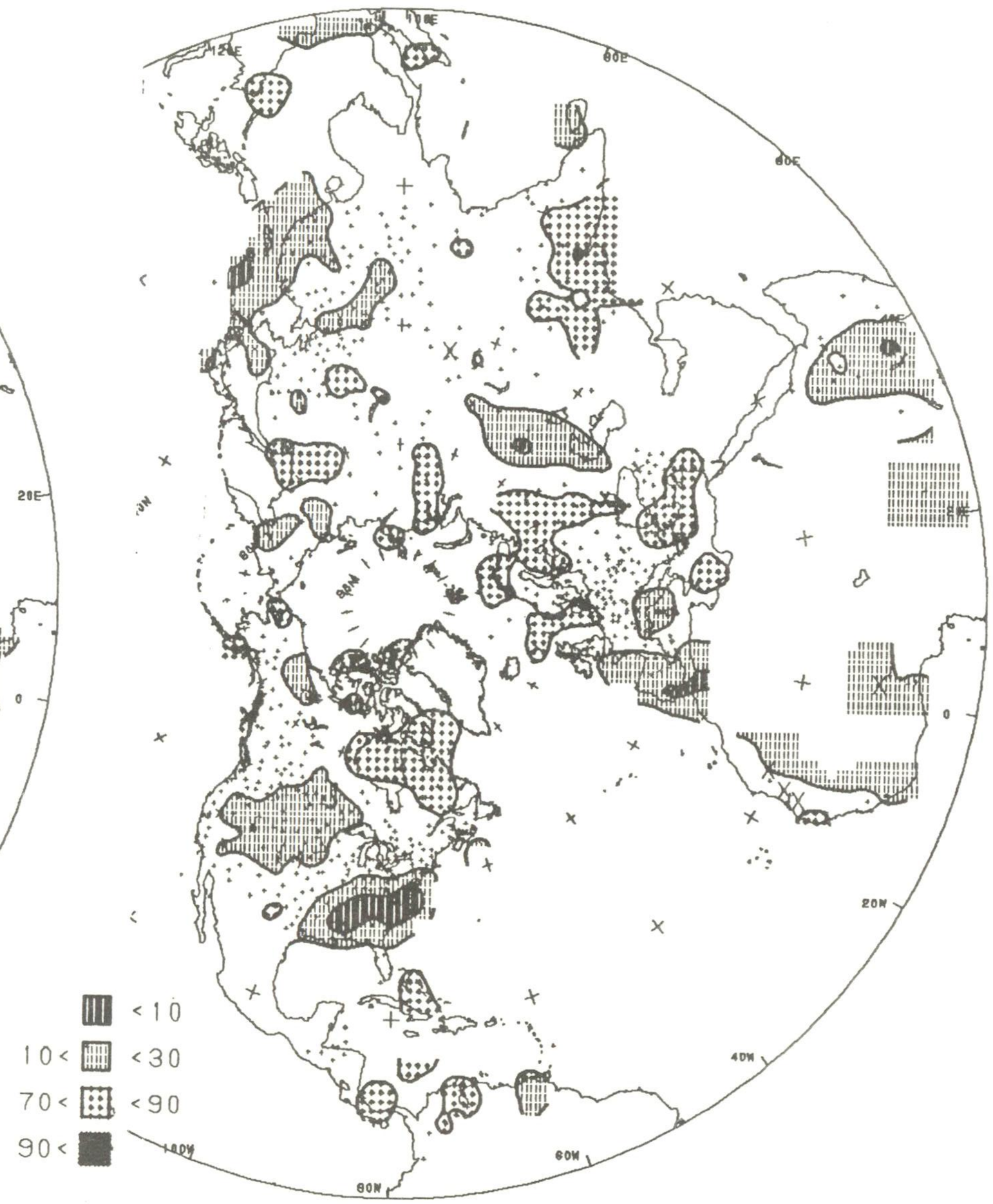

DJF 1980–81 PRECIPITATION PERCENTILES
BASED ON GAMMA DISTRIBUTION

JJA 1981 TEMPERATURE PERCENTILES
BASED ON NORMAL DISTRIBUTION

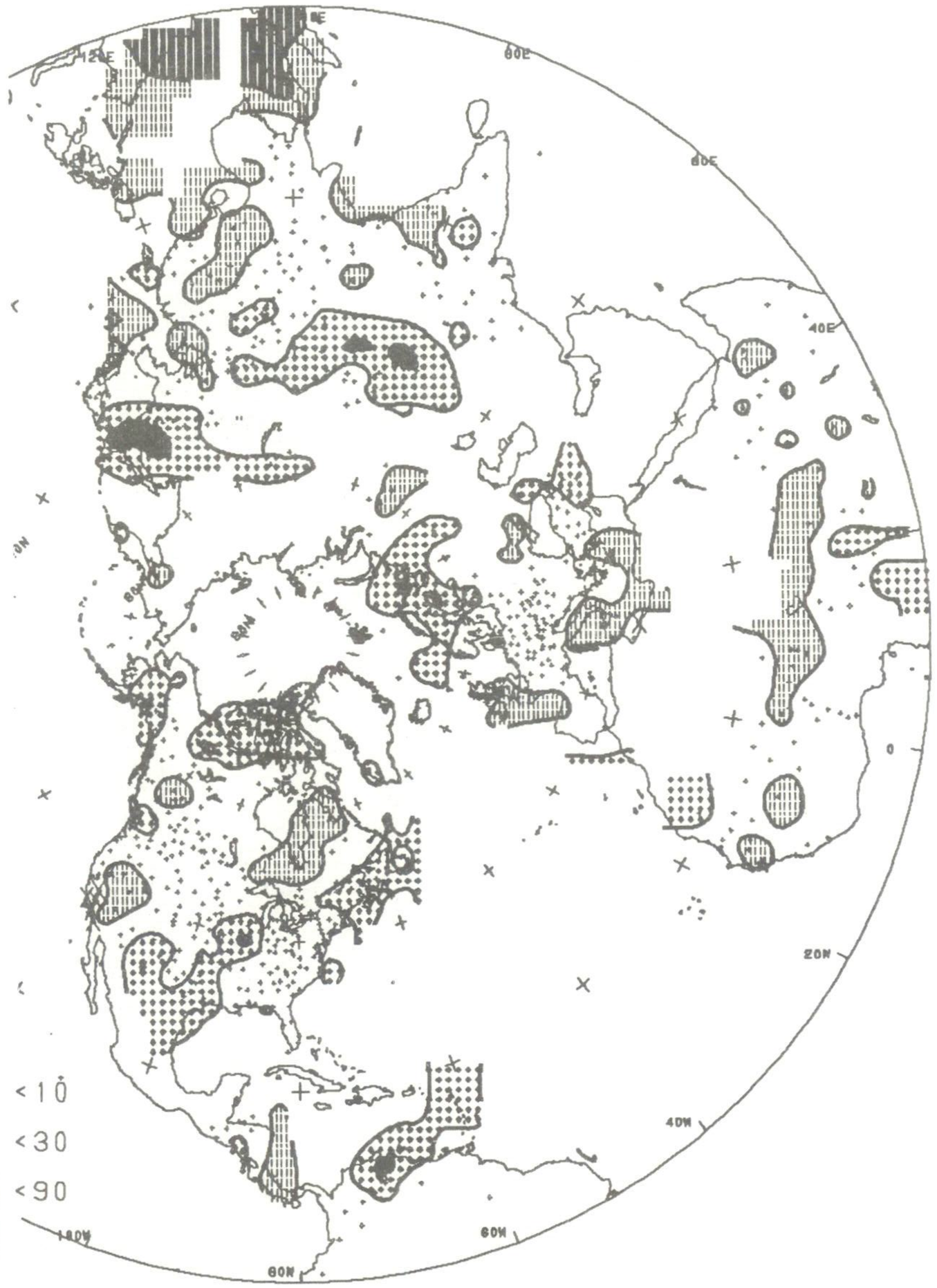

JJA 1981 PRECIPITATION PERCENTILES
BASED ON GAMMA DISTRIBUTION

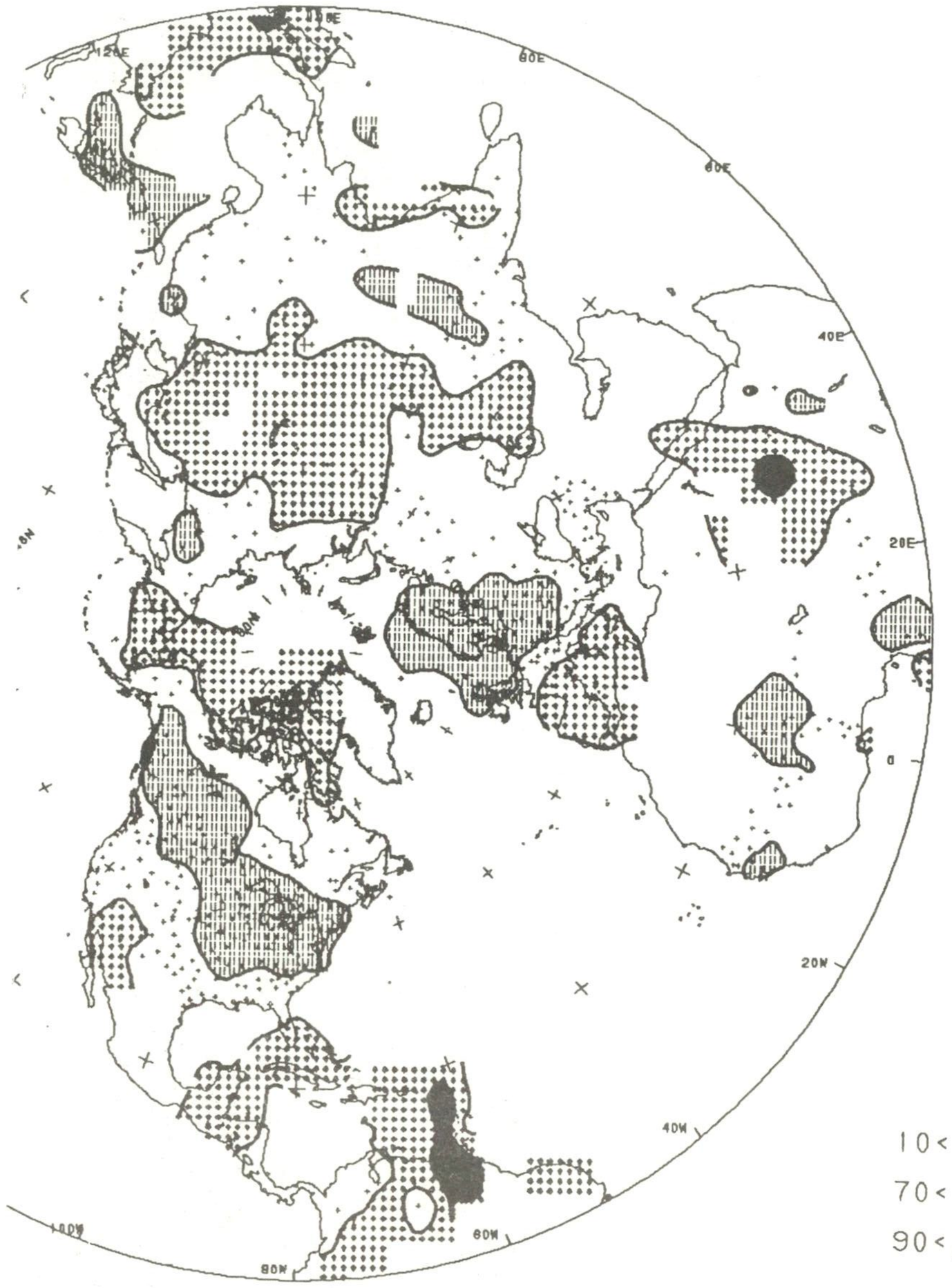

DJF 1981–82 TEMPERATURE PERCENTILES
BASED ON NORMAL DISTRIBUTION

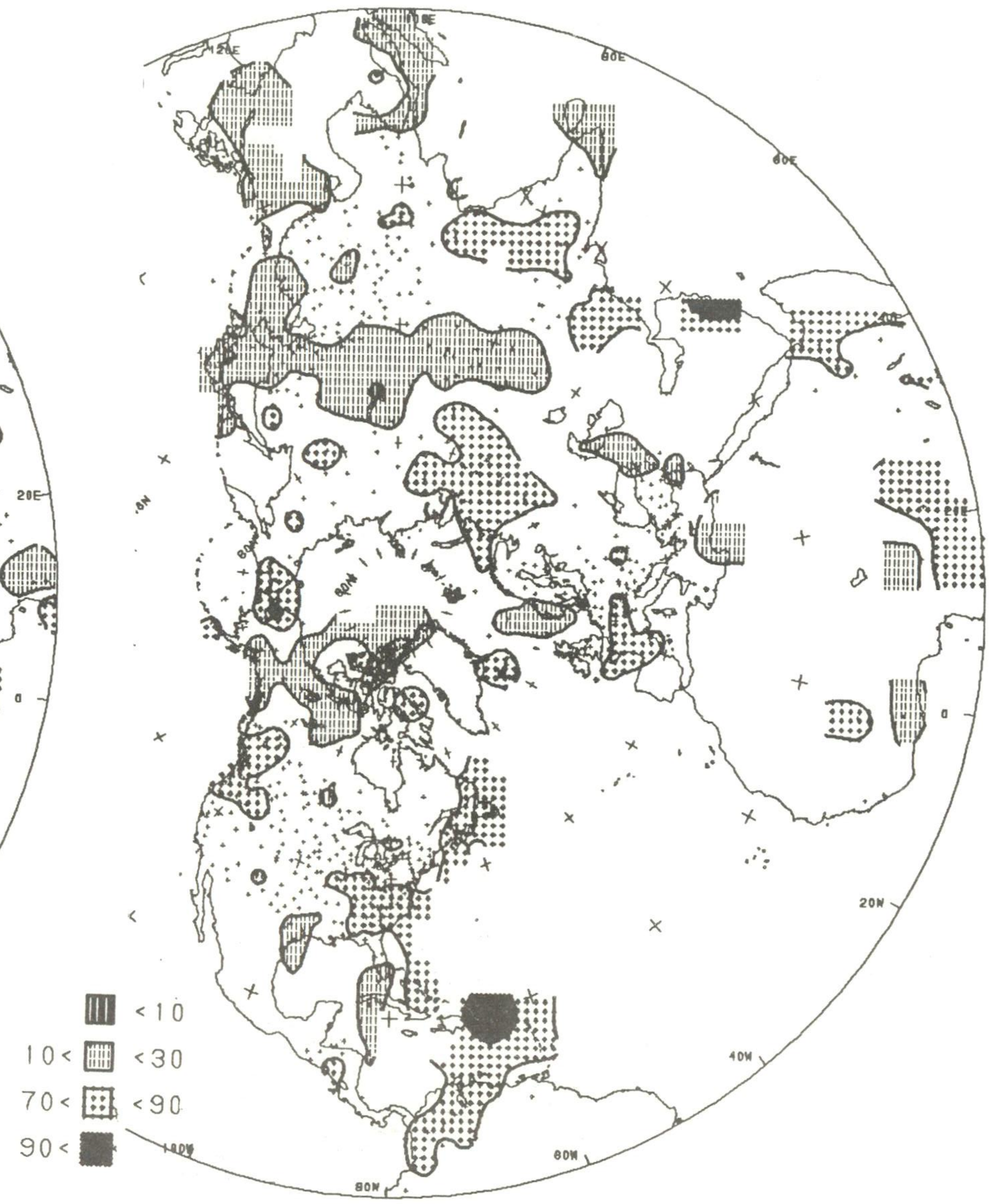

DJF 1981–82 PRECIPITATION PERCENTILES
BASED ON GAMMA DISTRIBUTION

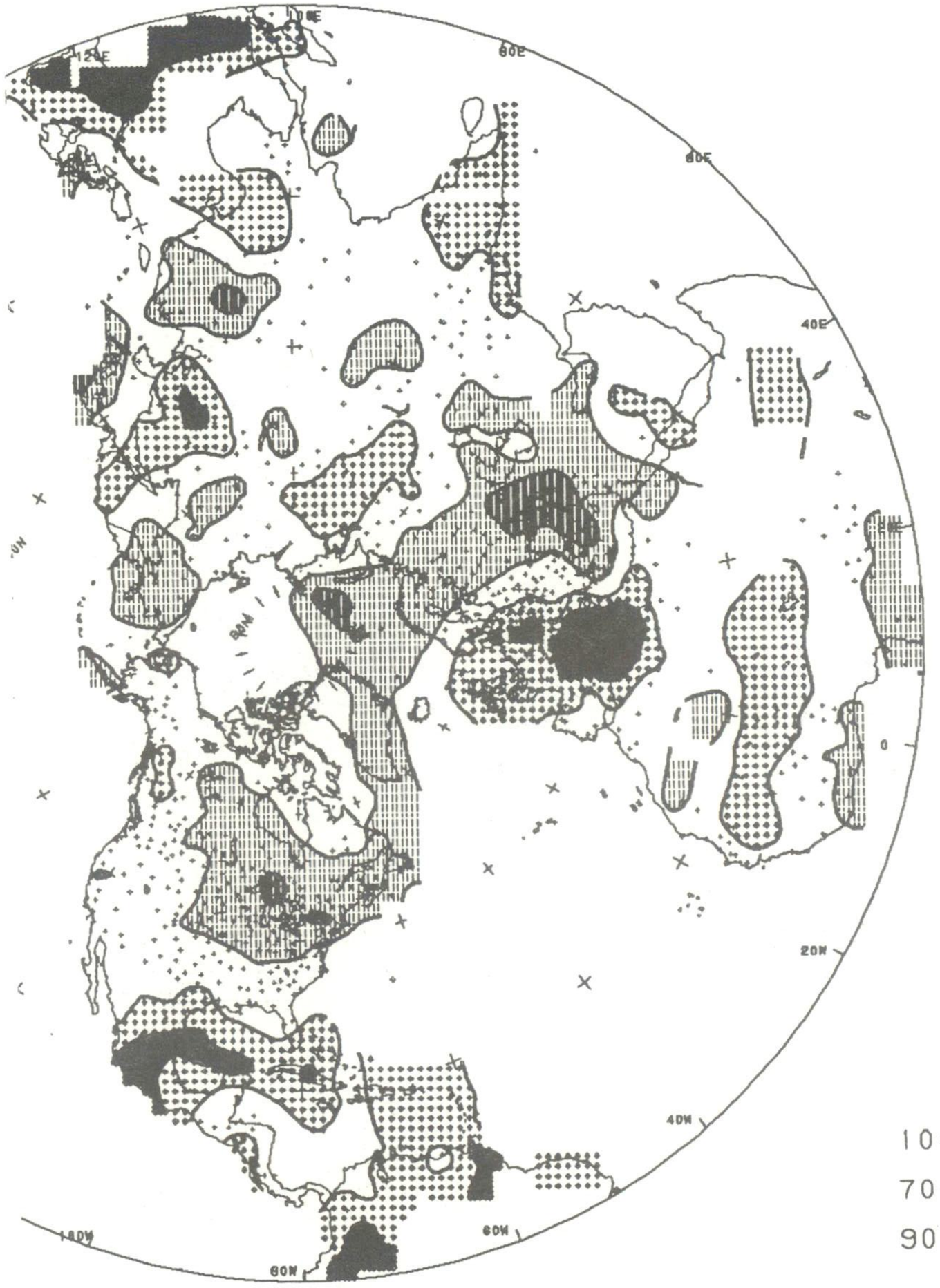

JJA 1982 TEMPERATURE PERCENTILES
BASED ON NORMAL DISTRIBUTION

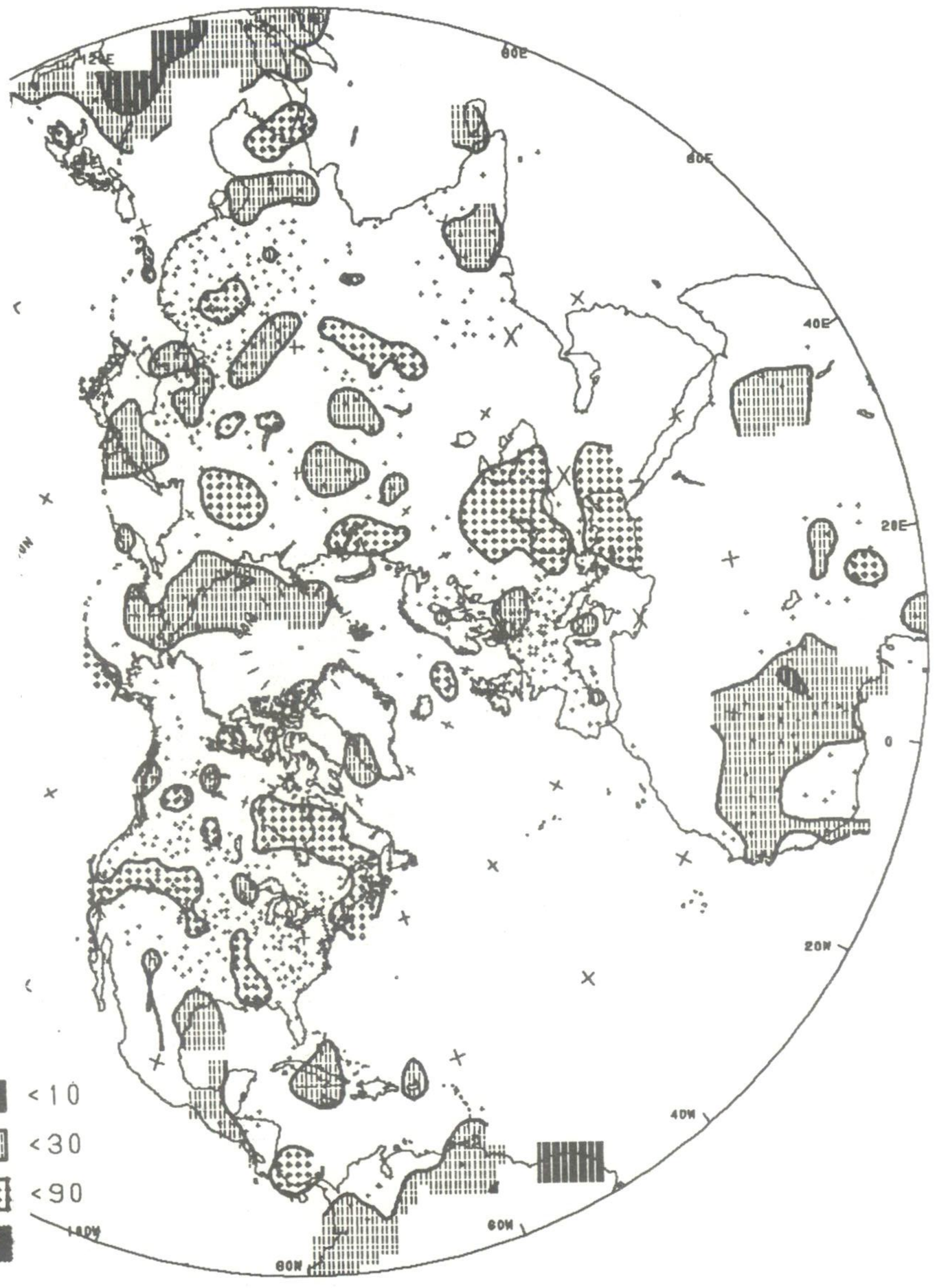

JJA 1982 PRECIPITATION PERCENTILES
BASED ON GAMMA DISTRIBUTION

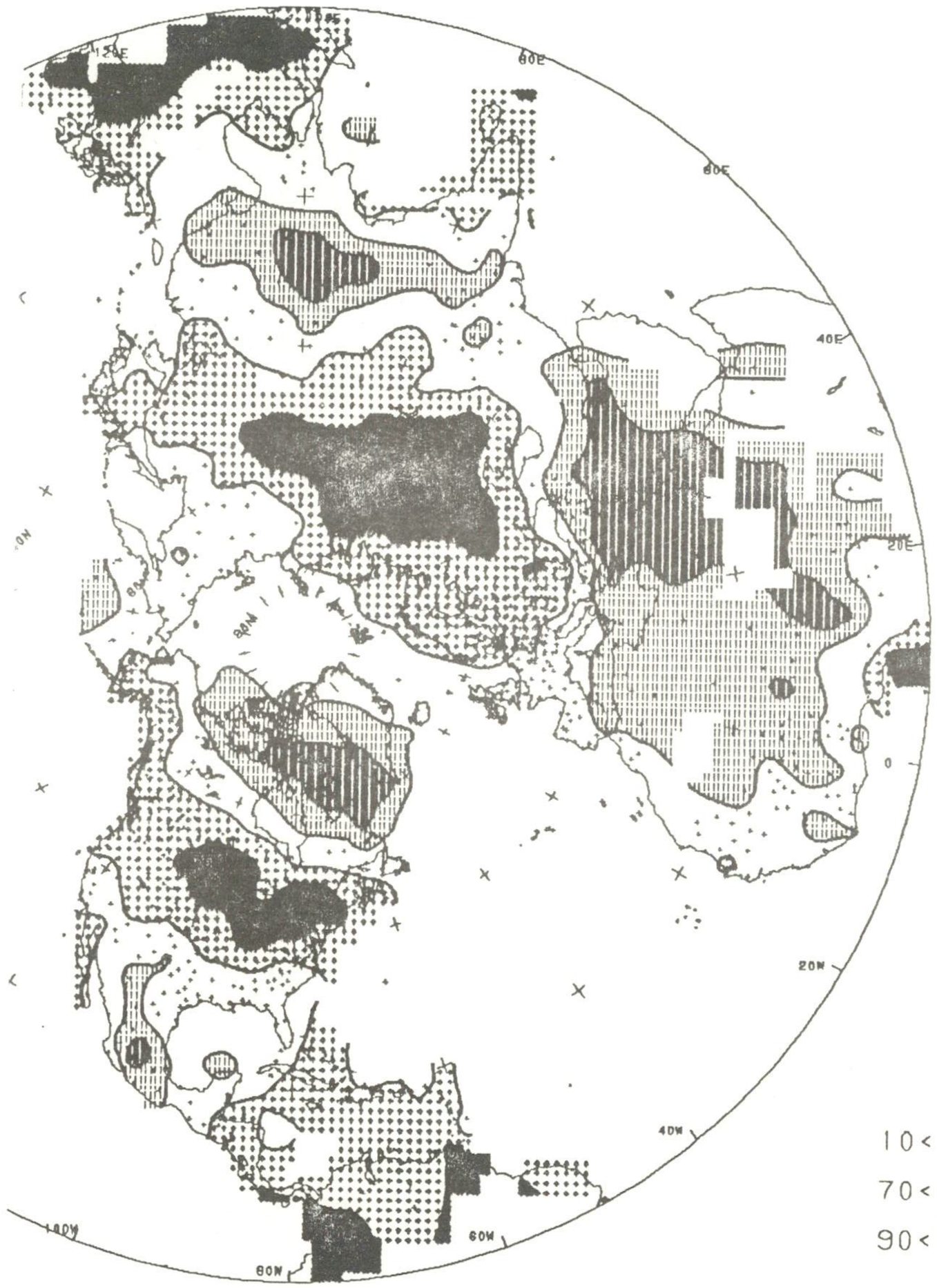

DJF 1982–83 TEMPERATURE PERCENTILES
BASED ON NORMAL DISTRIBUTION

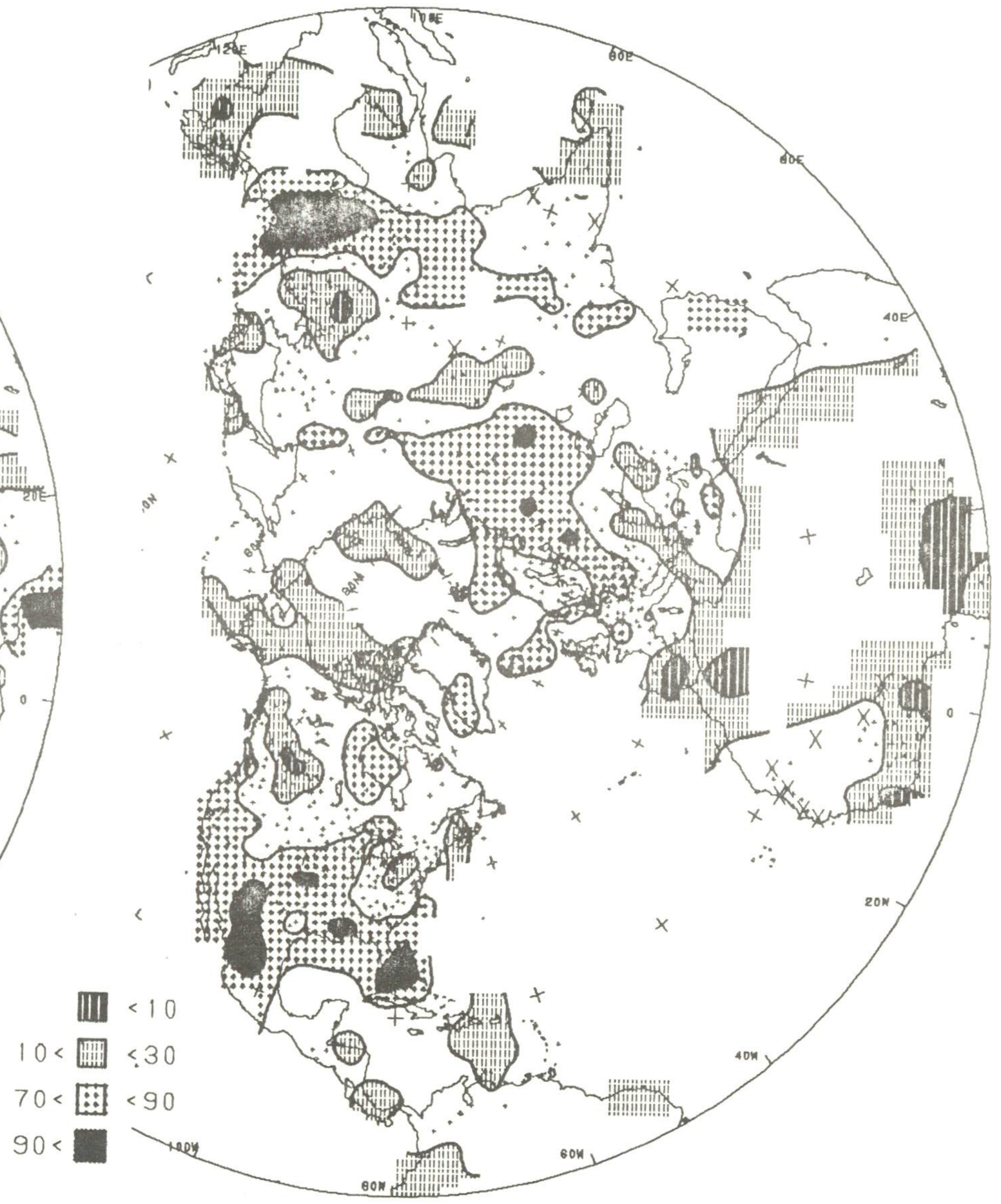

DJF 1982–83 PRECIPITATION PERCENTILES
BASED ON GAMMA DISTRIBUTION

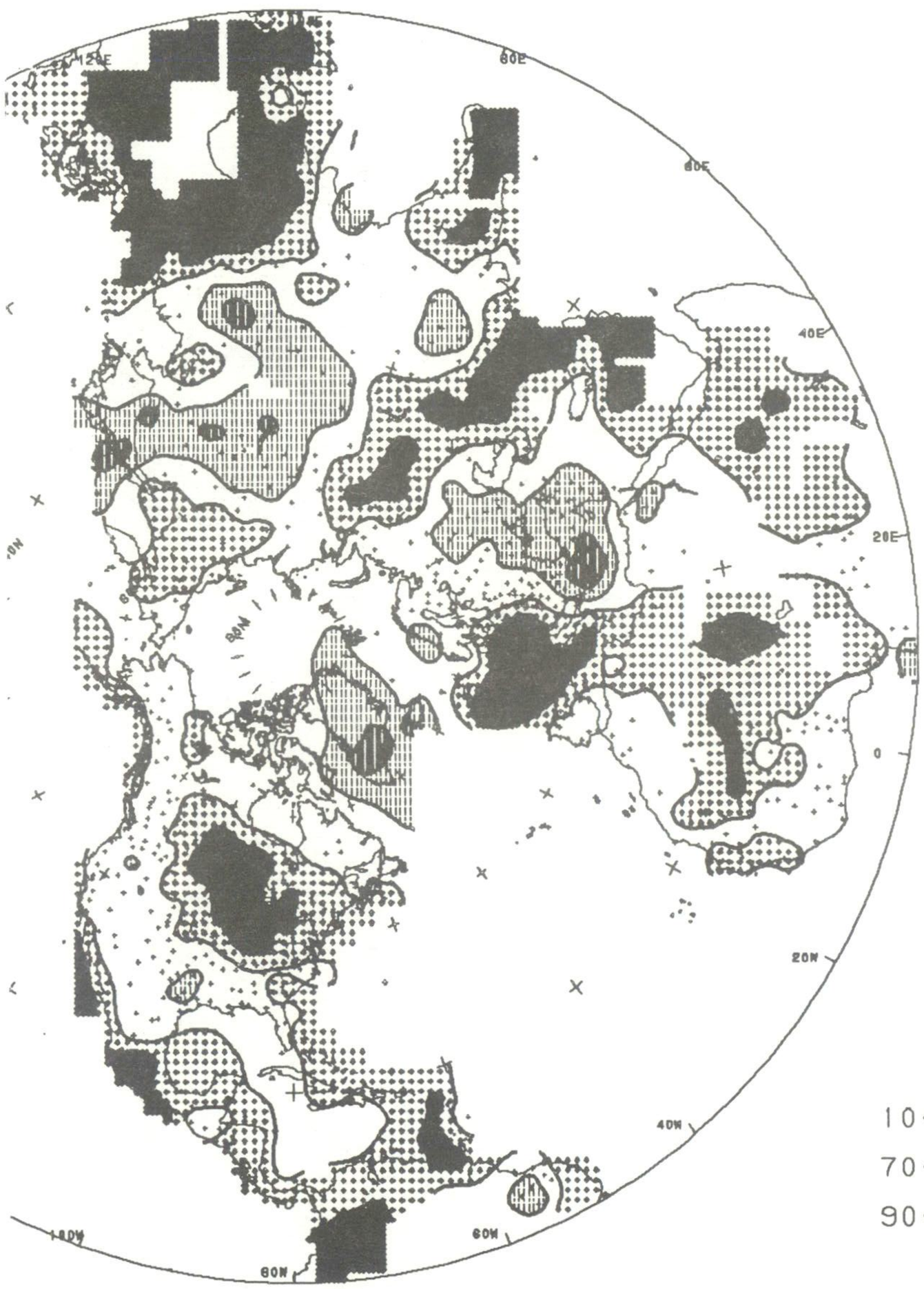

JJA 1983 TEMPERATURE PERCENTILES
BASED ON NORMAL DISTRIBUTION

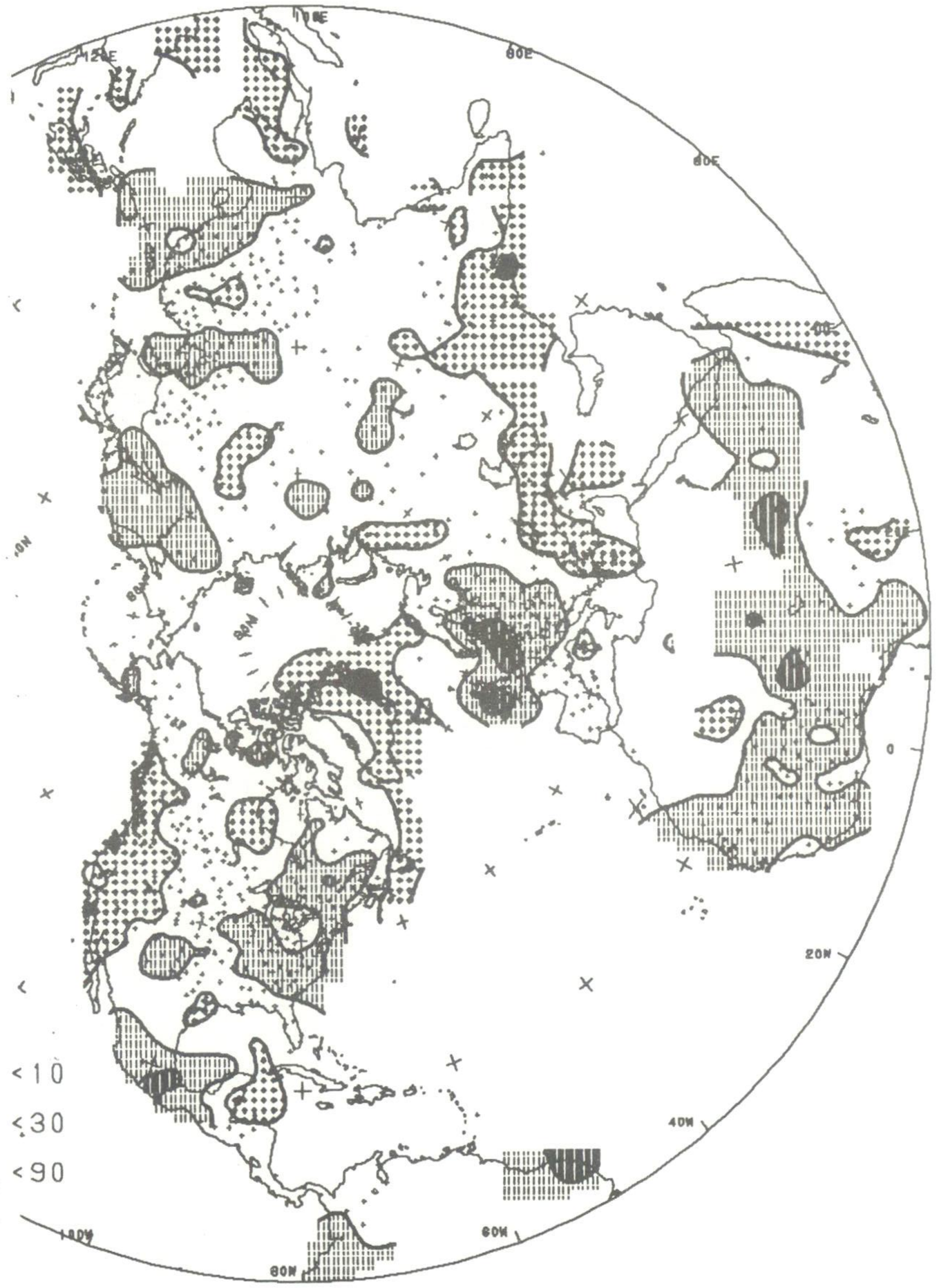

JJA 1983 PRECIPITATION PERCENTILES
BASED ON GAMMA DISTRIBUTION

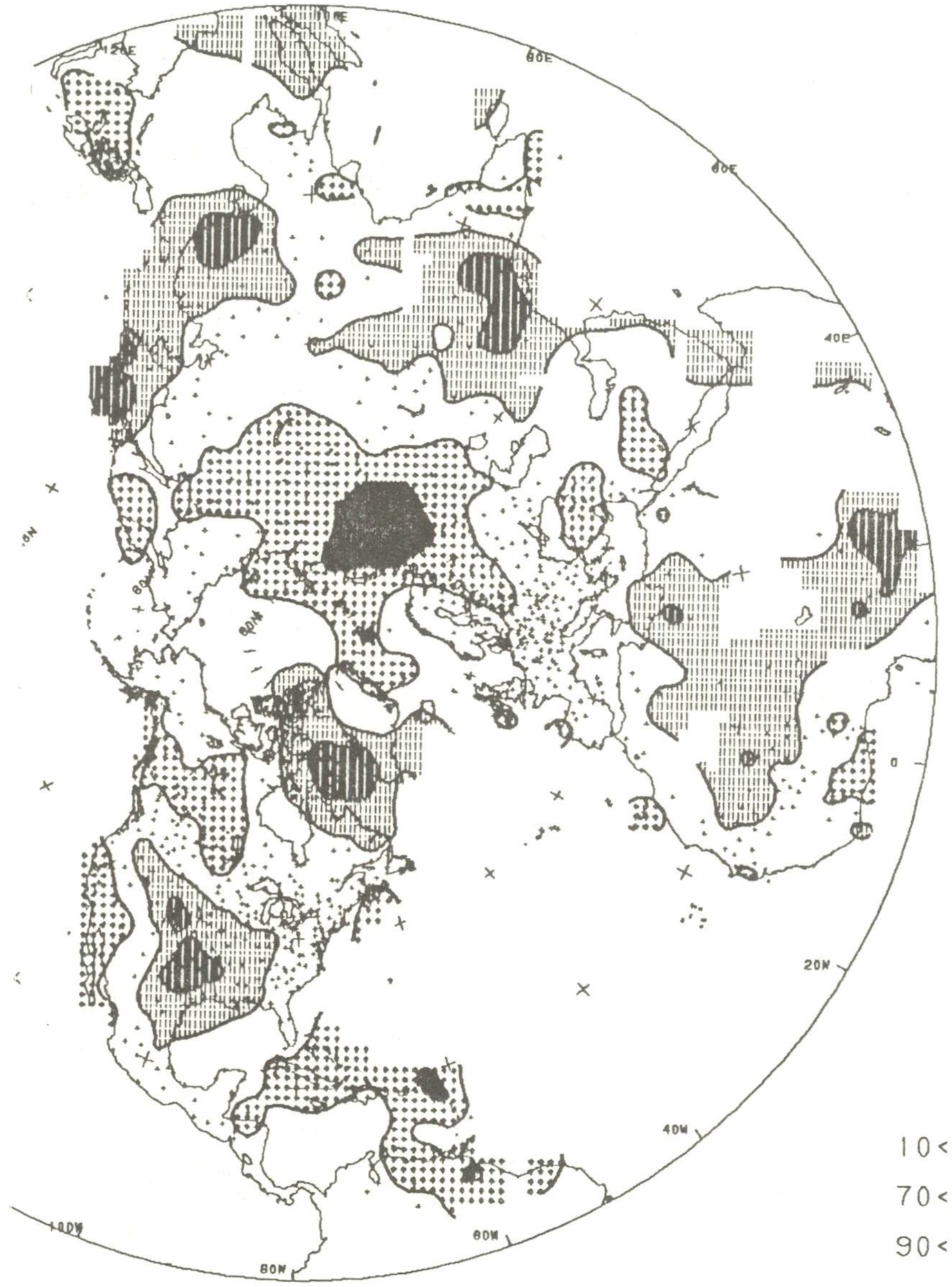

DJF 1983–84 TEMPERATURE PERCENTILES
BASED ON NORMAL DISTRIBUTION

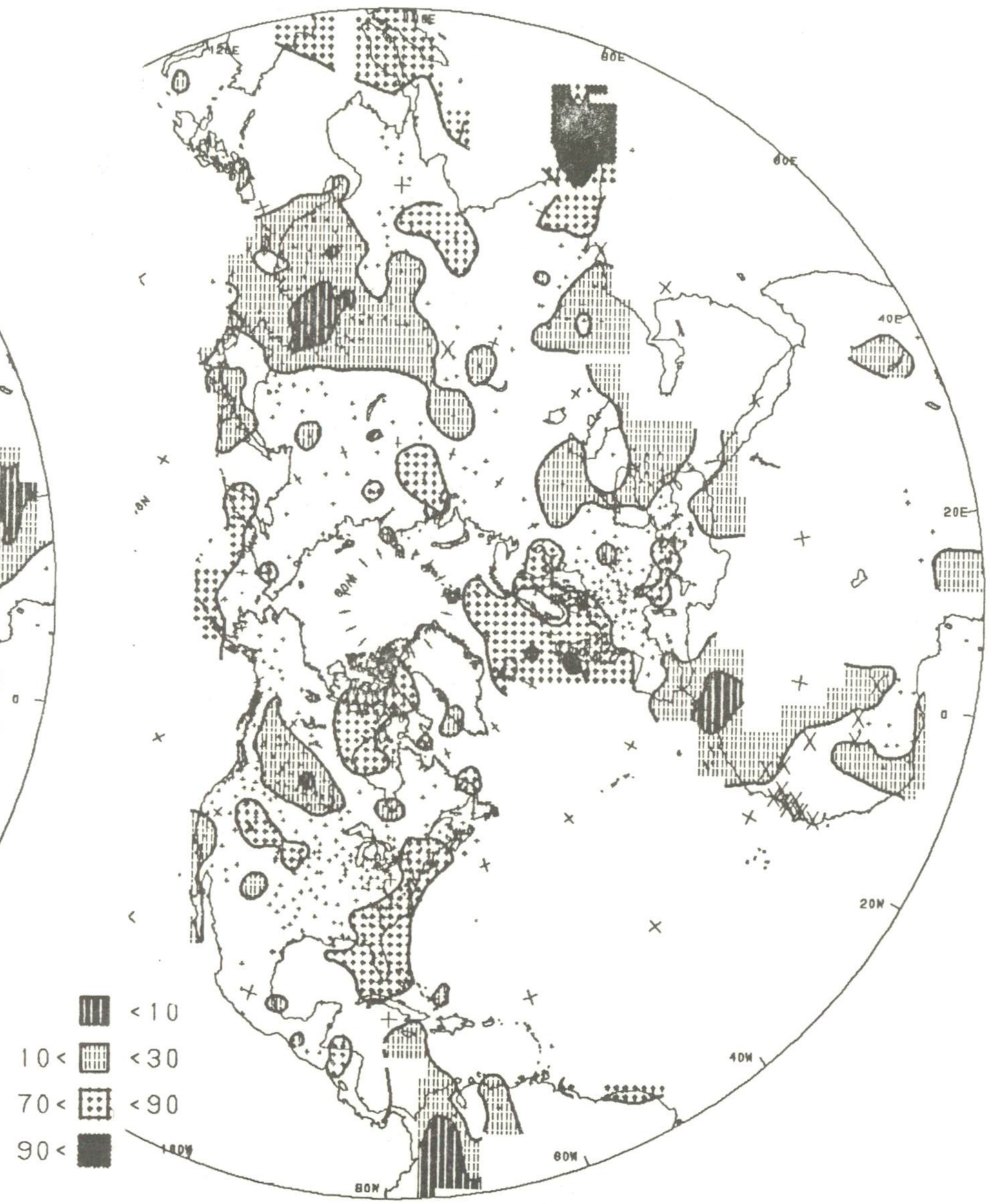

DJF 1983–84 PRECIPITATION PERCENTILES
BASED ON GAMMA DISTRIBUTION

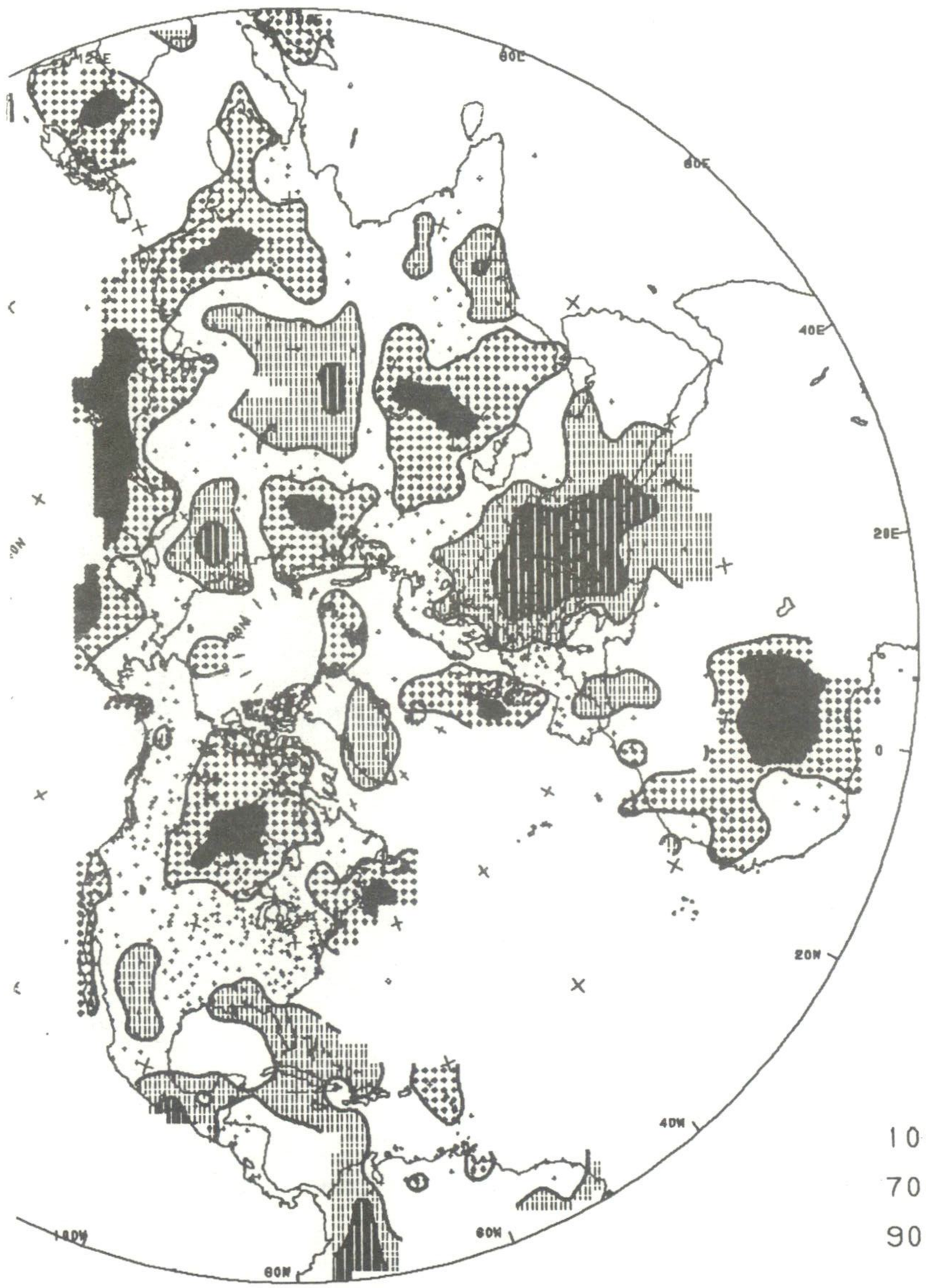

JJA 1984 TEMPERATURE PERCENTILES
BASED ON NORMAL DISTRIBUTION

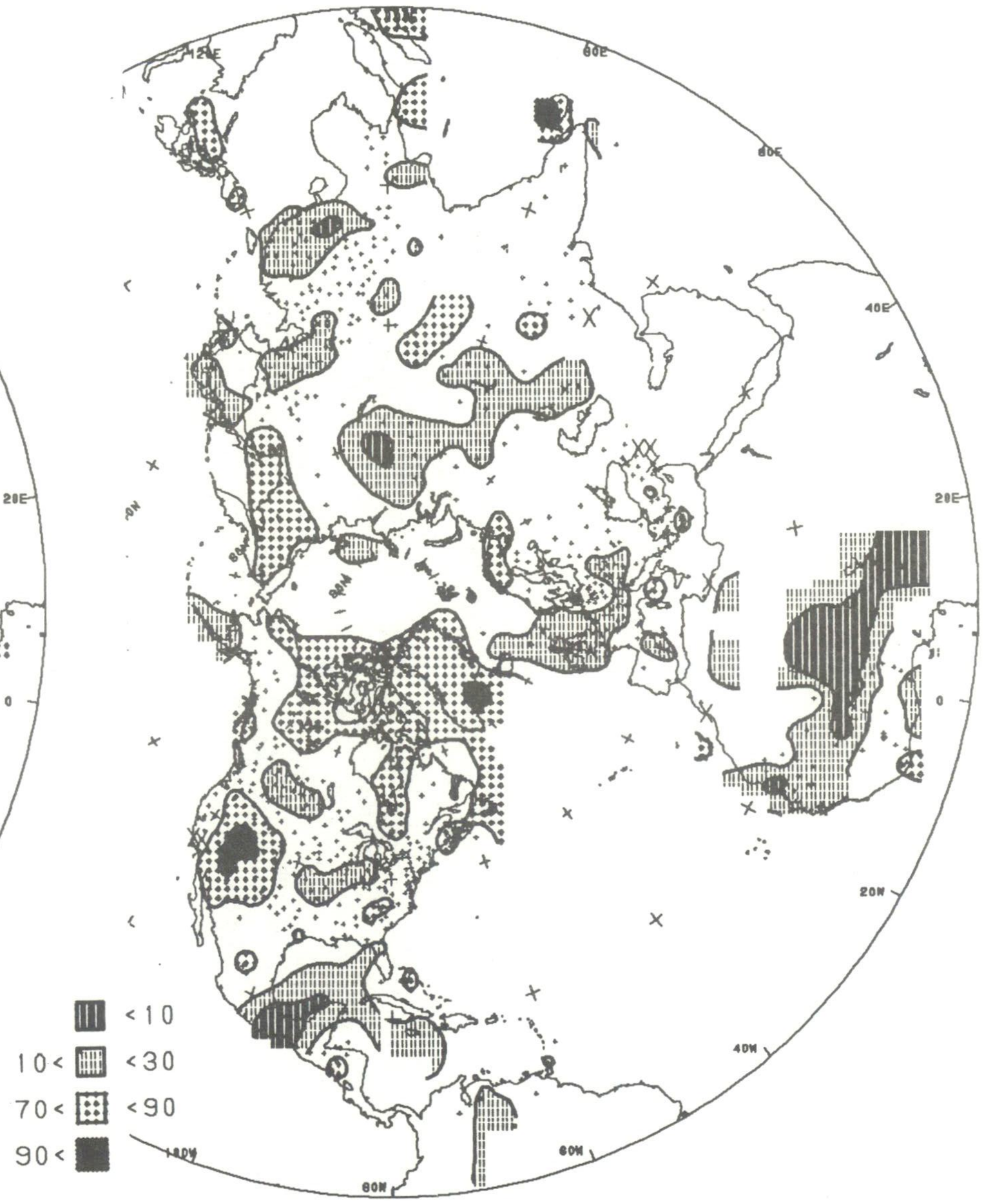

JJA 1984 PRECIPITATION PERCENTILES
BASED ON GAMMA DISTRIBUTION

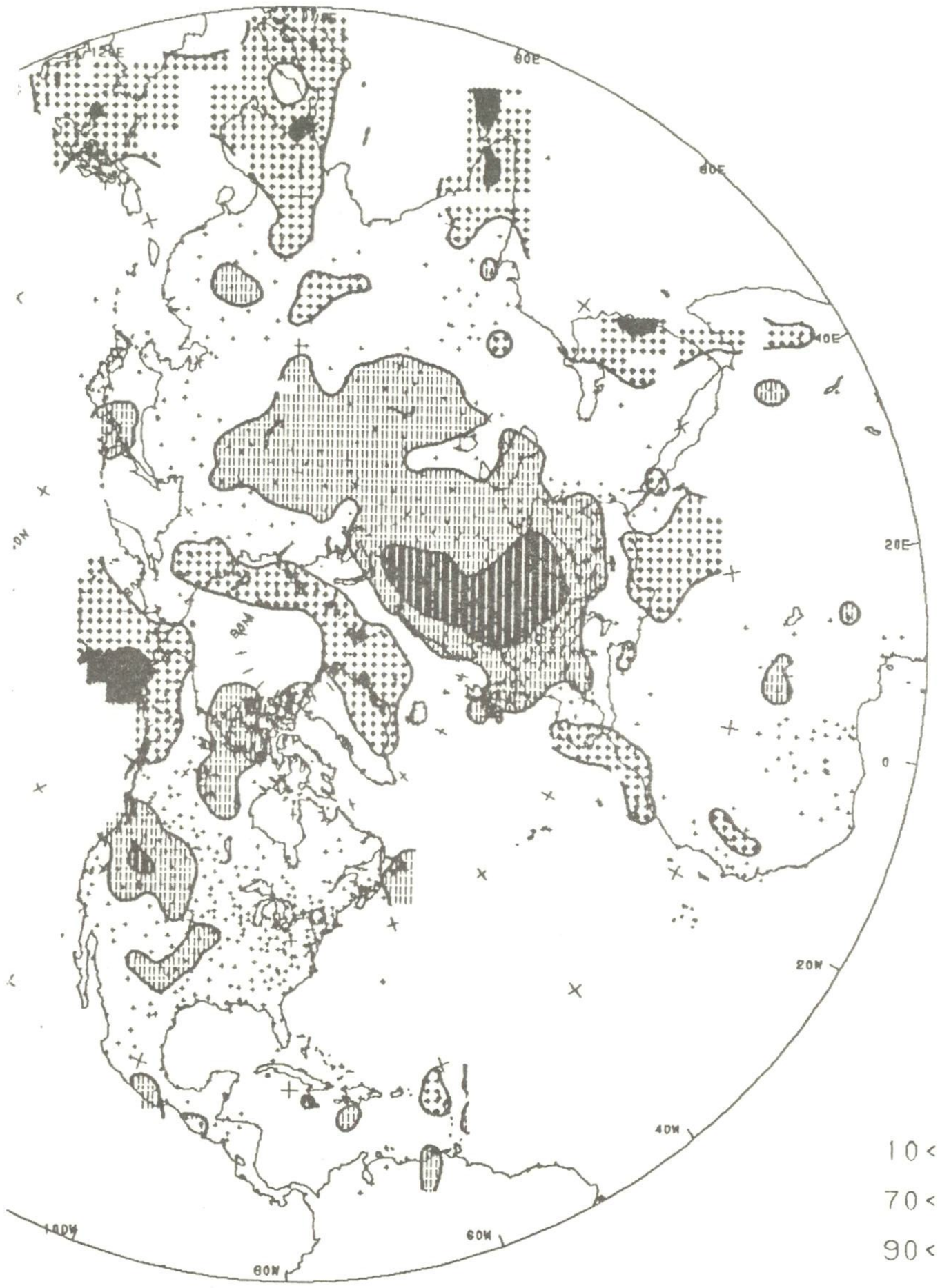

DJF 1984–85 TEMPERATURE PERCENTILES
BASED ON NORMAL DISTRIBUTION

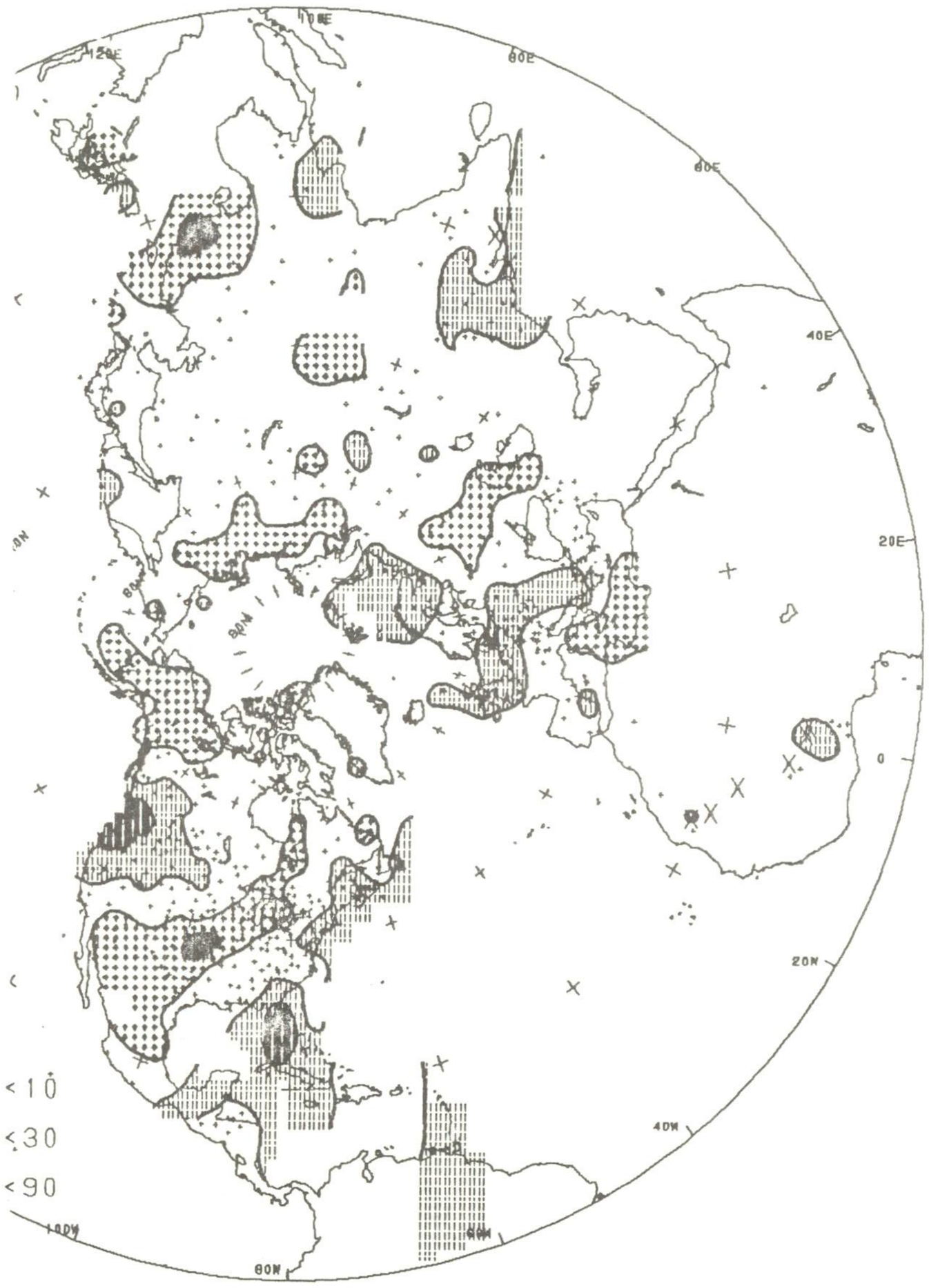

DJF 1984–85 PRECIPITATION PERCENTILES
BASED ON GAMMA DISTRIBUTION

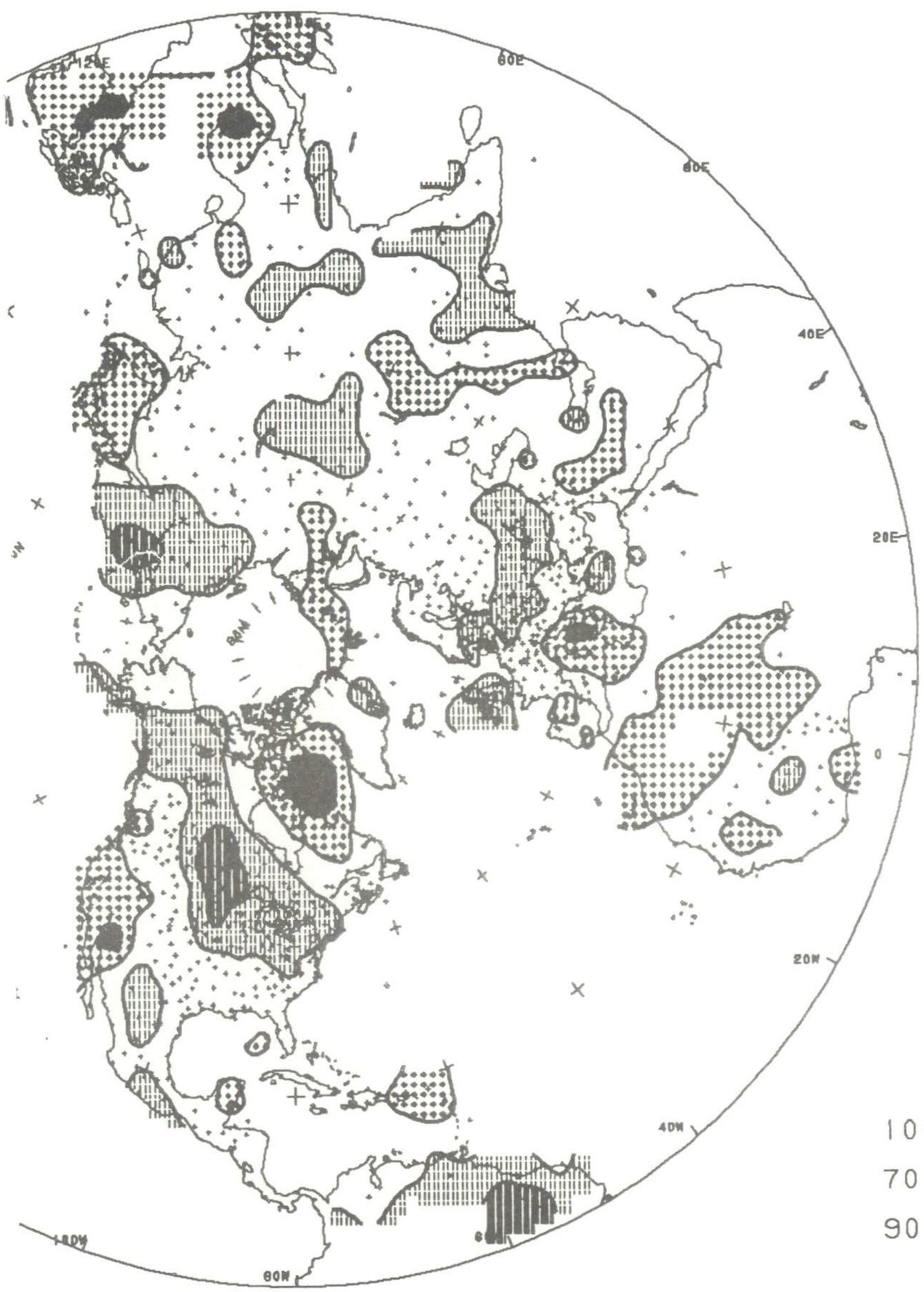

JJA 1985 TEMPERATURE PERCENTILES
BASED ON NORMAL DISTRIBUTION

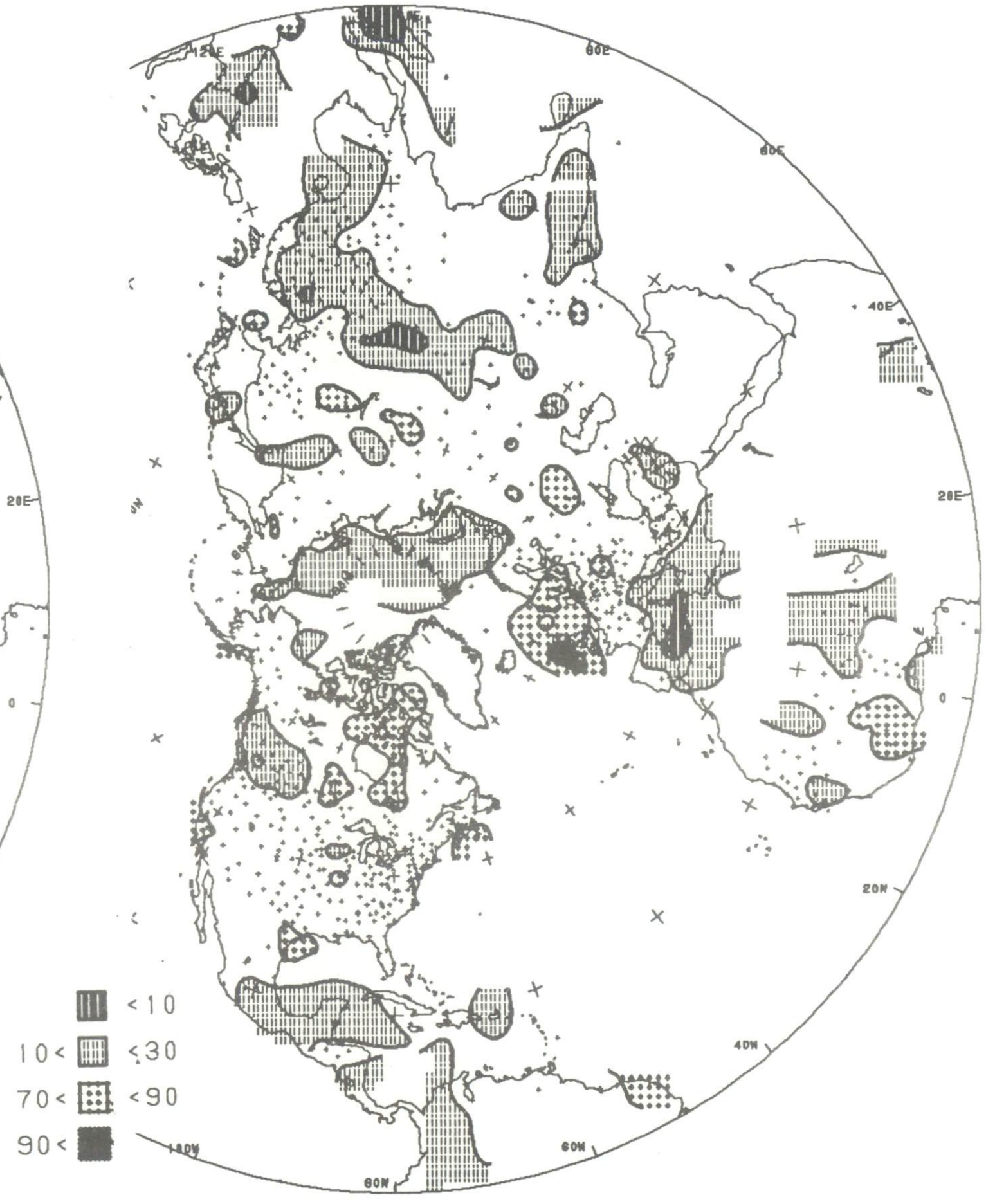

JJA 1985 PRECIPITATION PERCENTILES
BASED ON GAMMA DISTRIBUTION

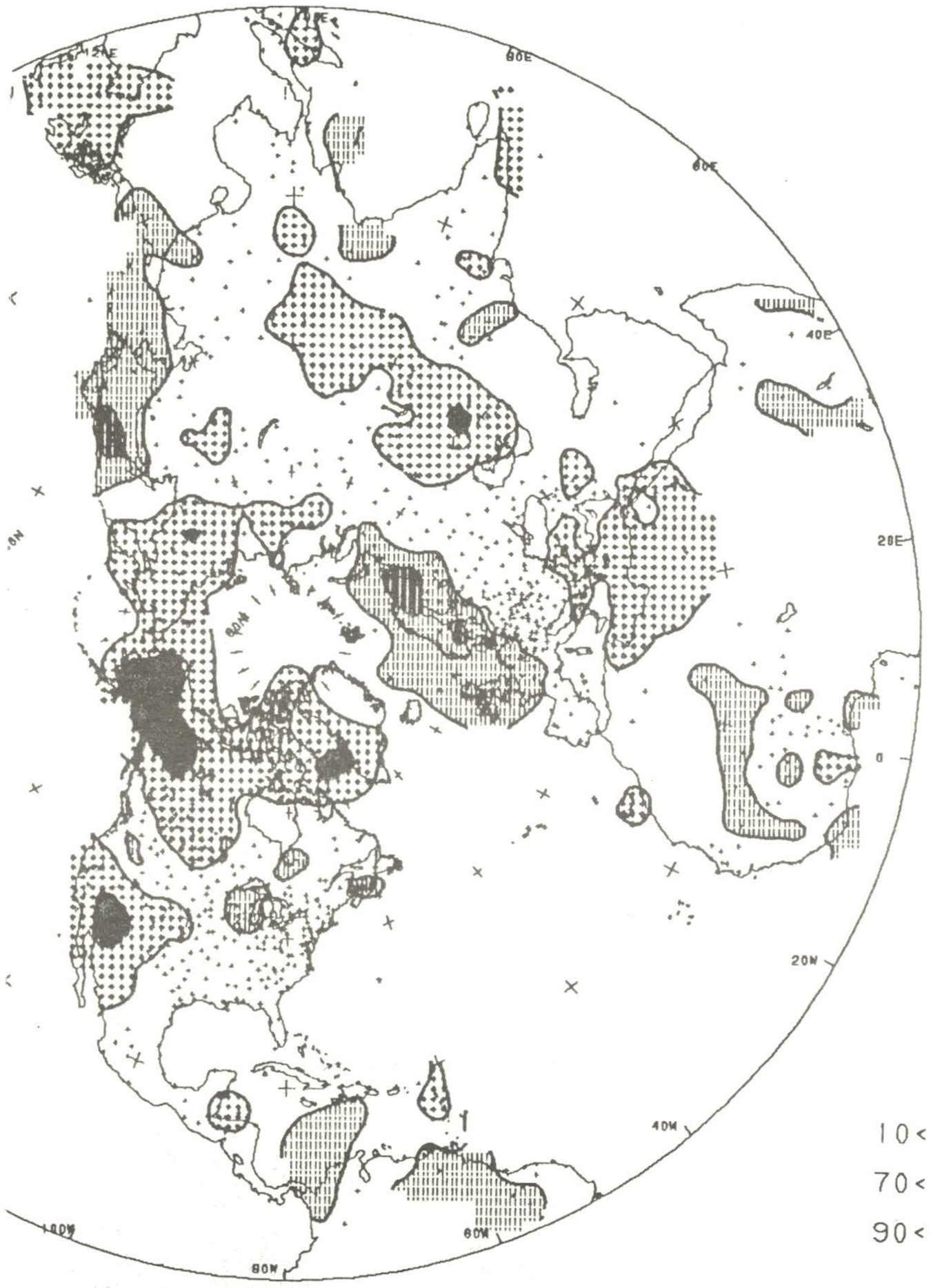

DJF 1985–86 TEMPERATURE PERCENTILES
BASED ON NORMAL DISTRIBUTION

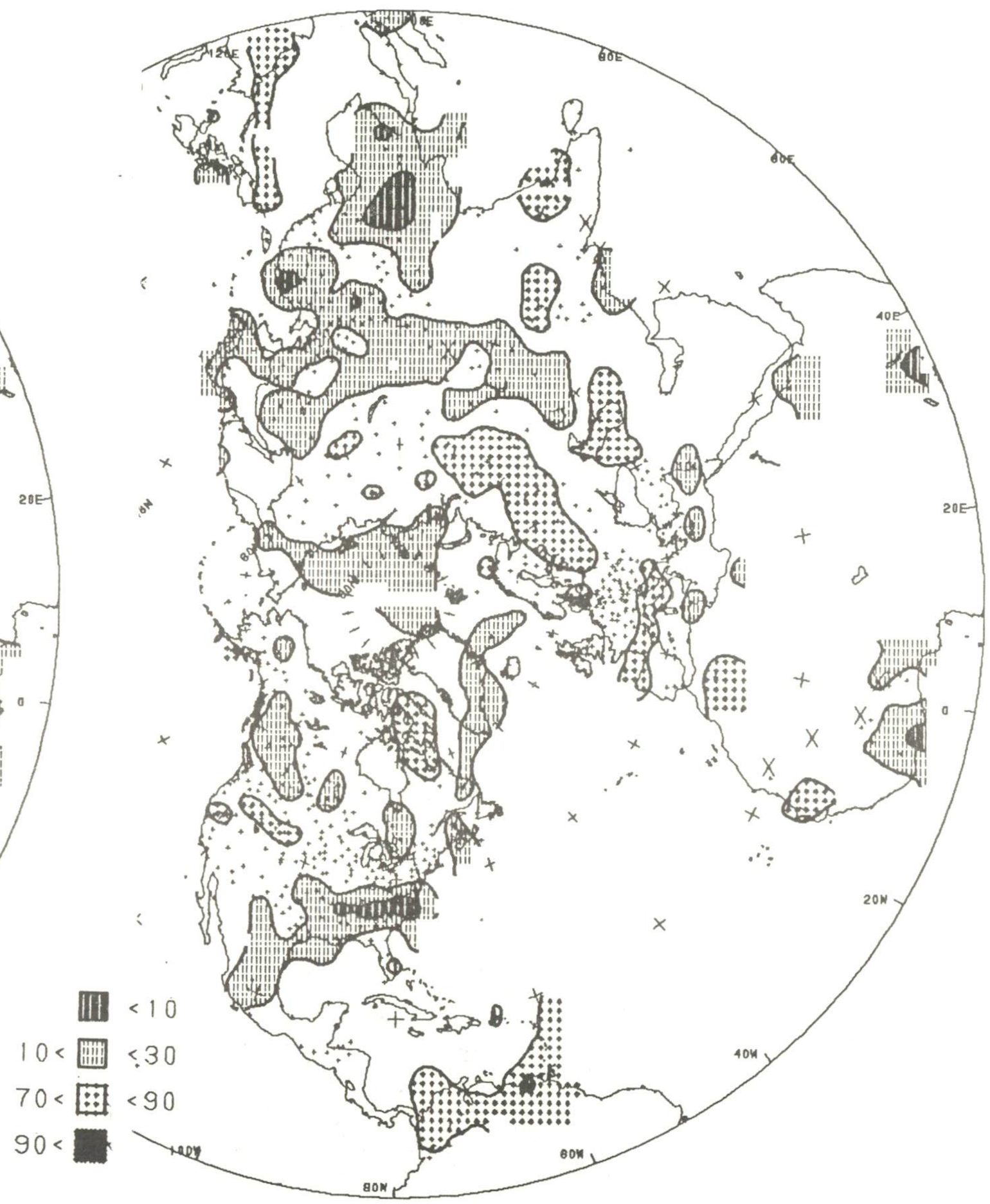

DJF 1985–86 PRECIPITATION PERCENTILES
BASED ON GAMMA DISTRIBUTION

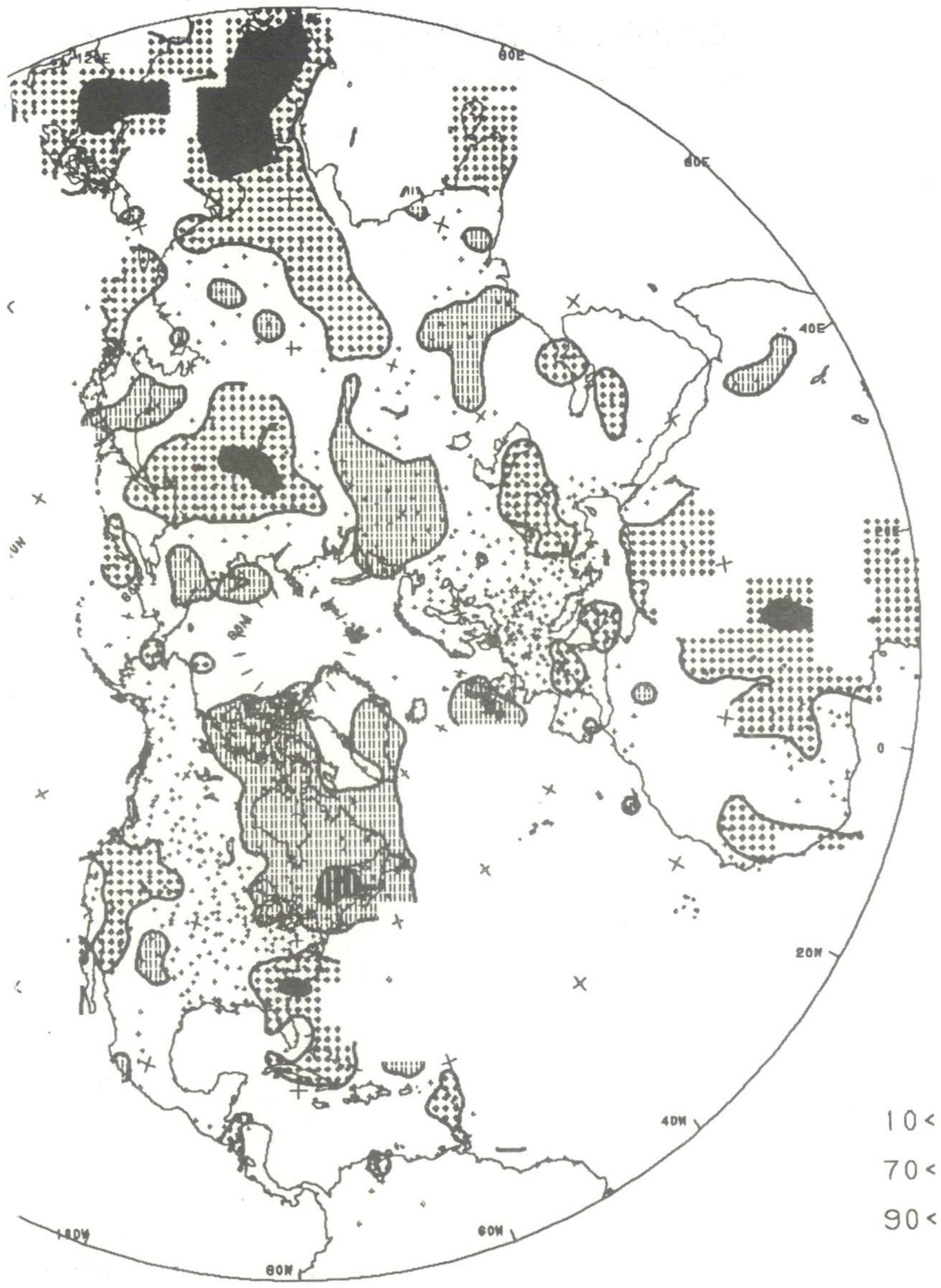

JJA 1986 TEMPERATURE PERCENTILES
BASED ON NORMAL DISTRIBUTION

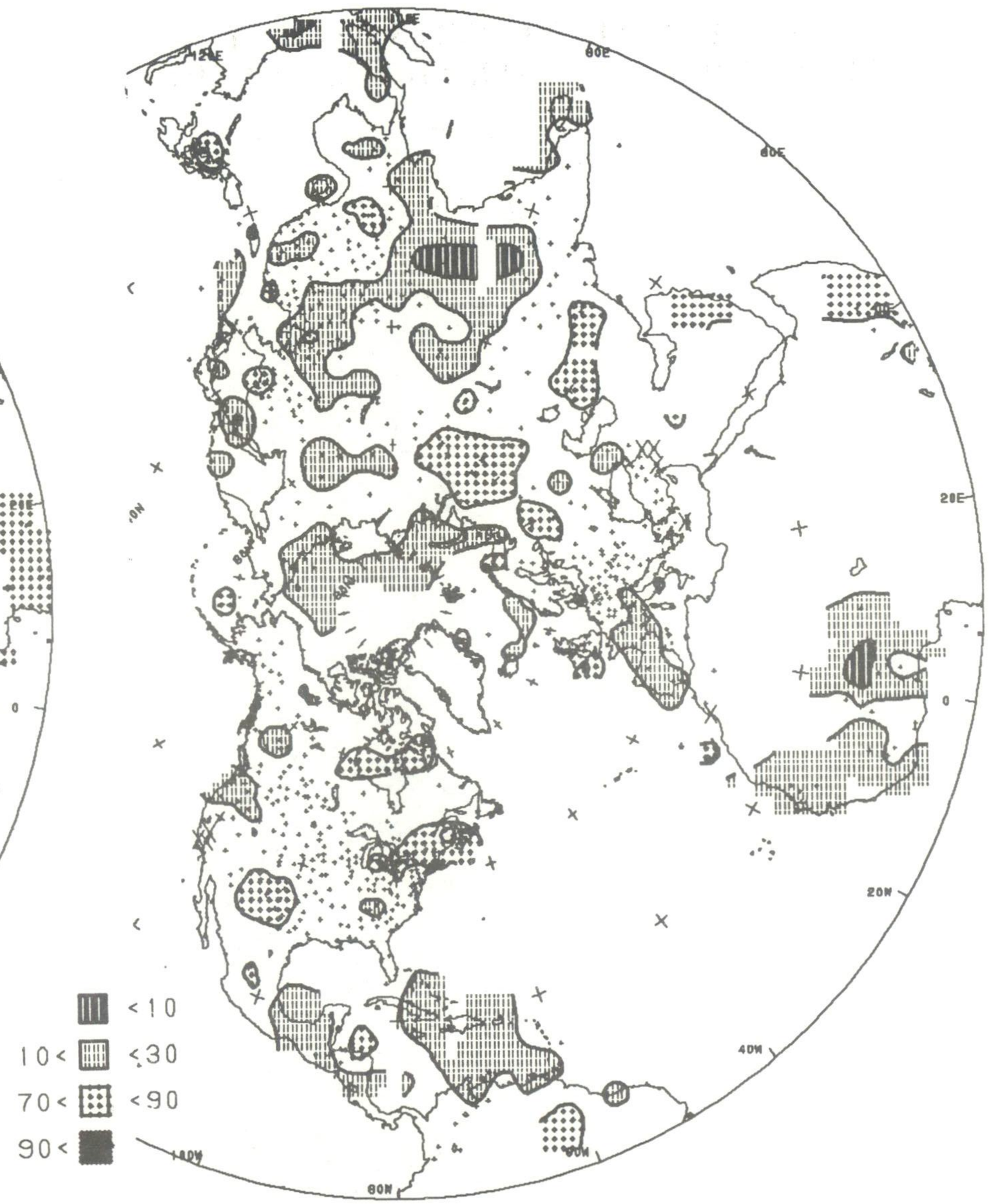

JJA 1986 PRECIPITATION PERCENTILES
BASED ON GAMMA DISTRIBUTION

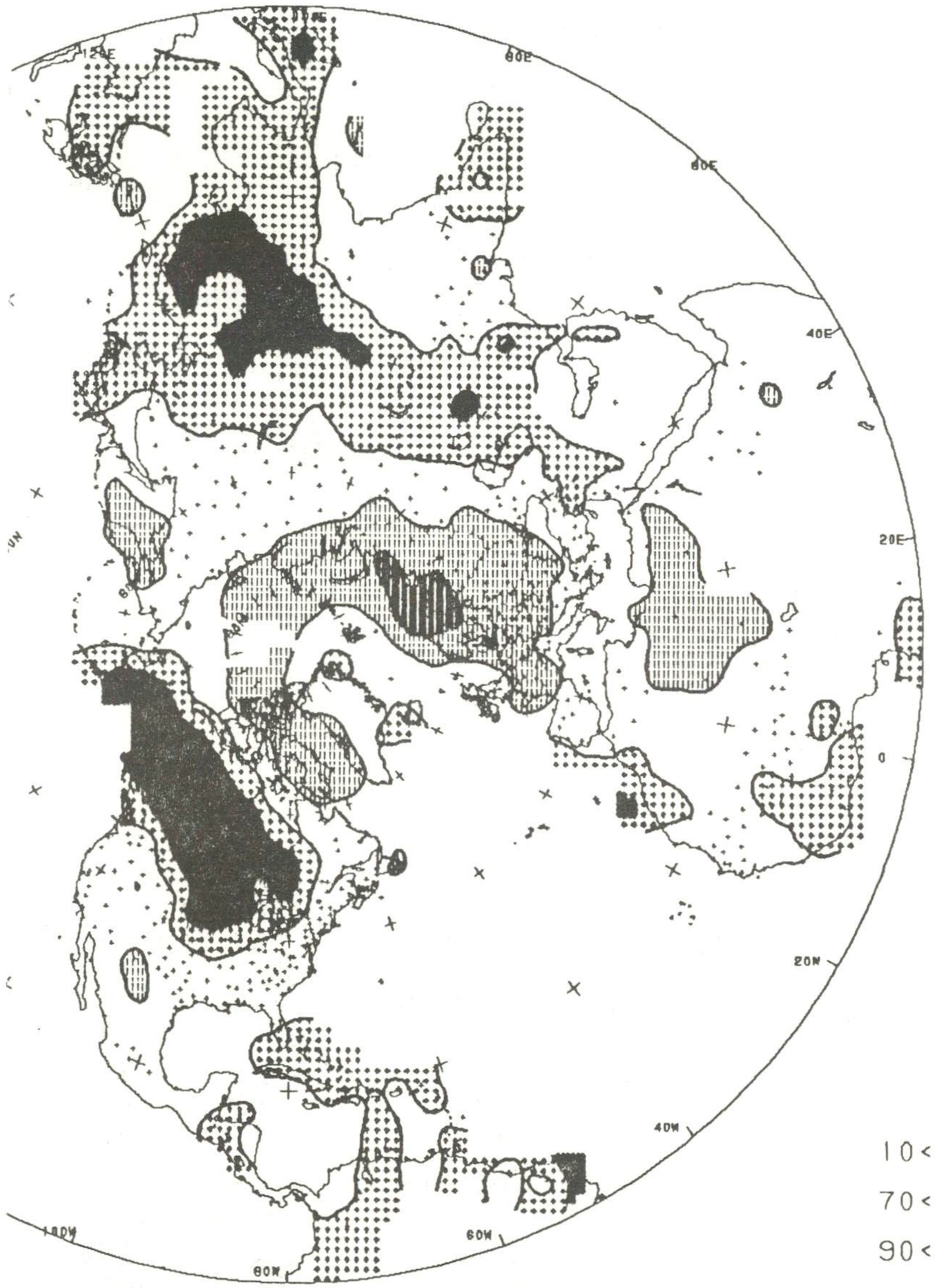

DJF 1986–87 TEMPERATURE PERCENTILES
BASED ON NORMAL DISTRIBUTION

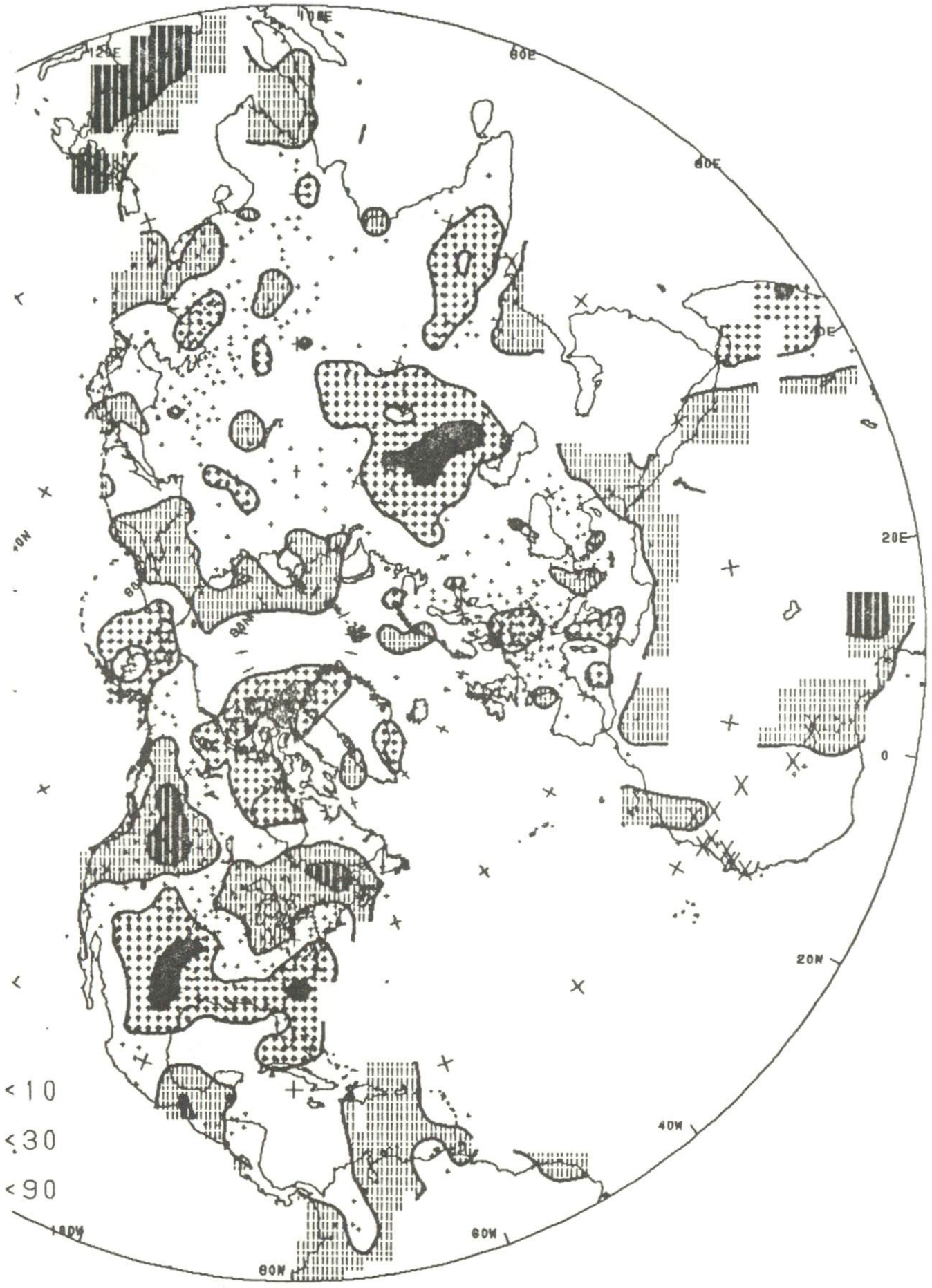

DJF 1986–87 PRECIPITATION PERCENTILES
BASED ON GAMMA DISTRIBUTION

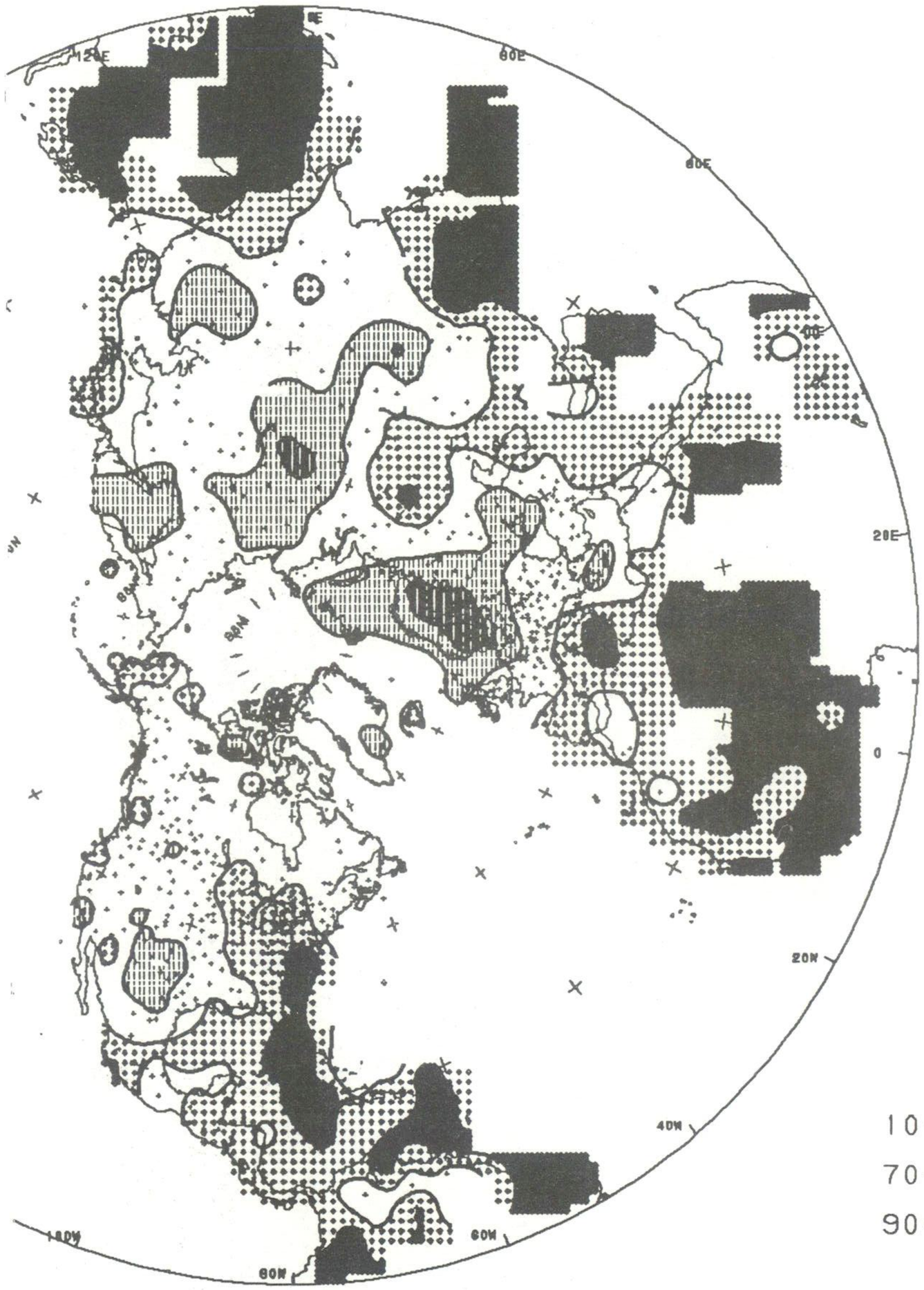

JJA 1987 TEMPERATURE PERCENTILES
BASED ON NORMAL DISTRIBUTION

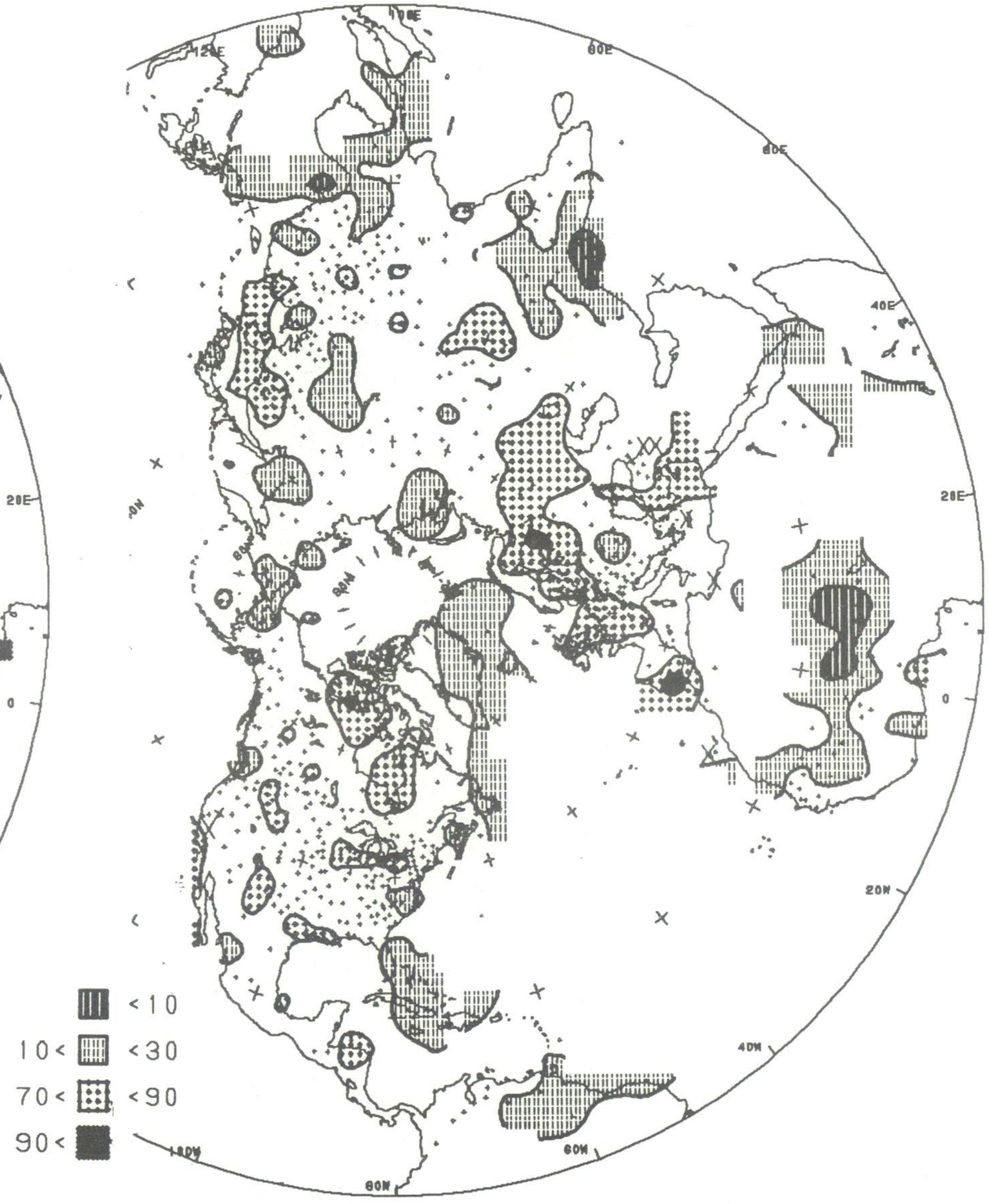

JJA 1987 PRECIPITATION PERCENTILES
BASED ON GAMMA DISTRIBUTION

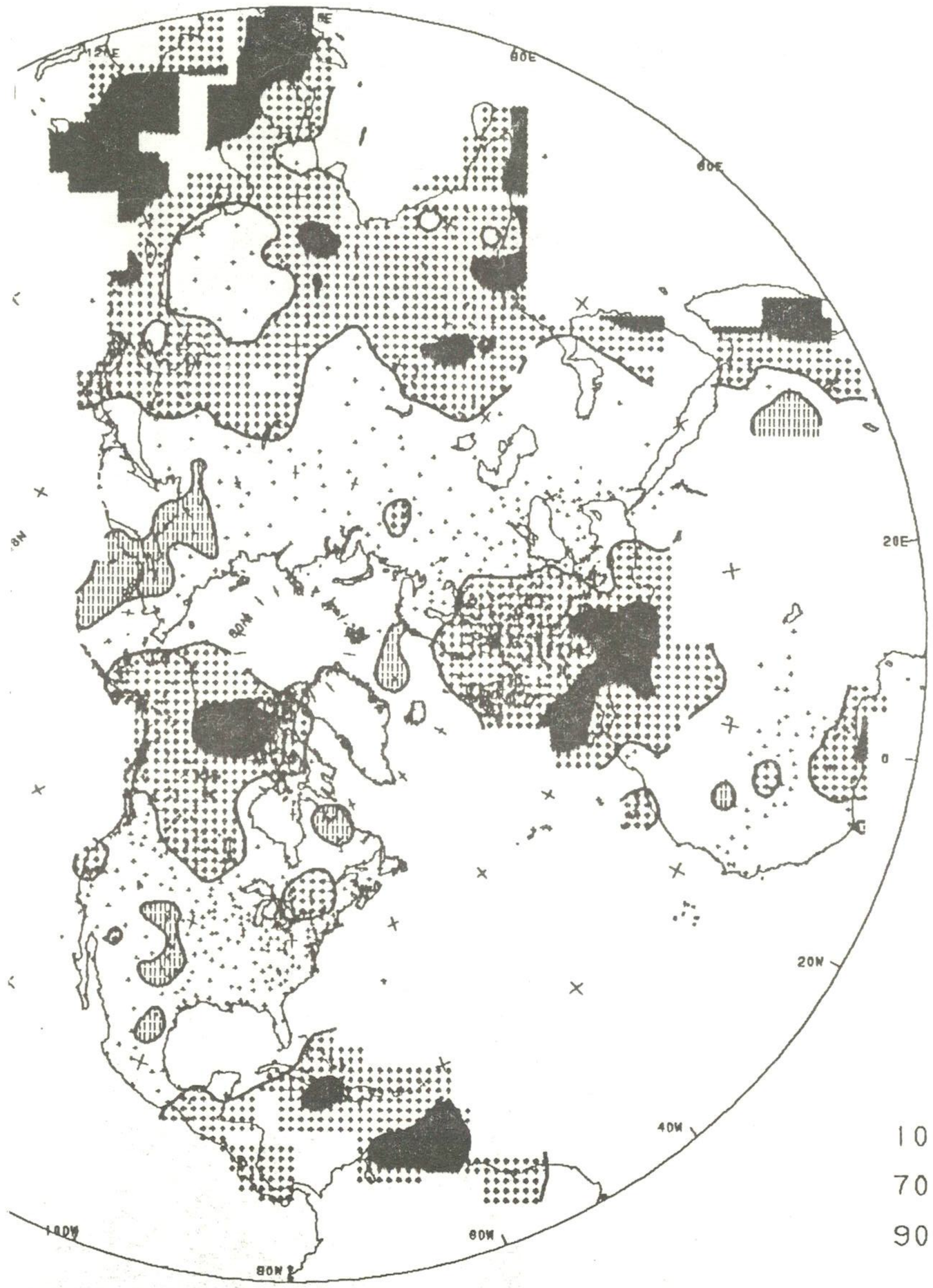

DJF 1987–88 TEMPERATURE PERCENTILES
BASED ON NORMAL DISTRIBUTION

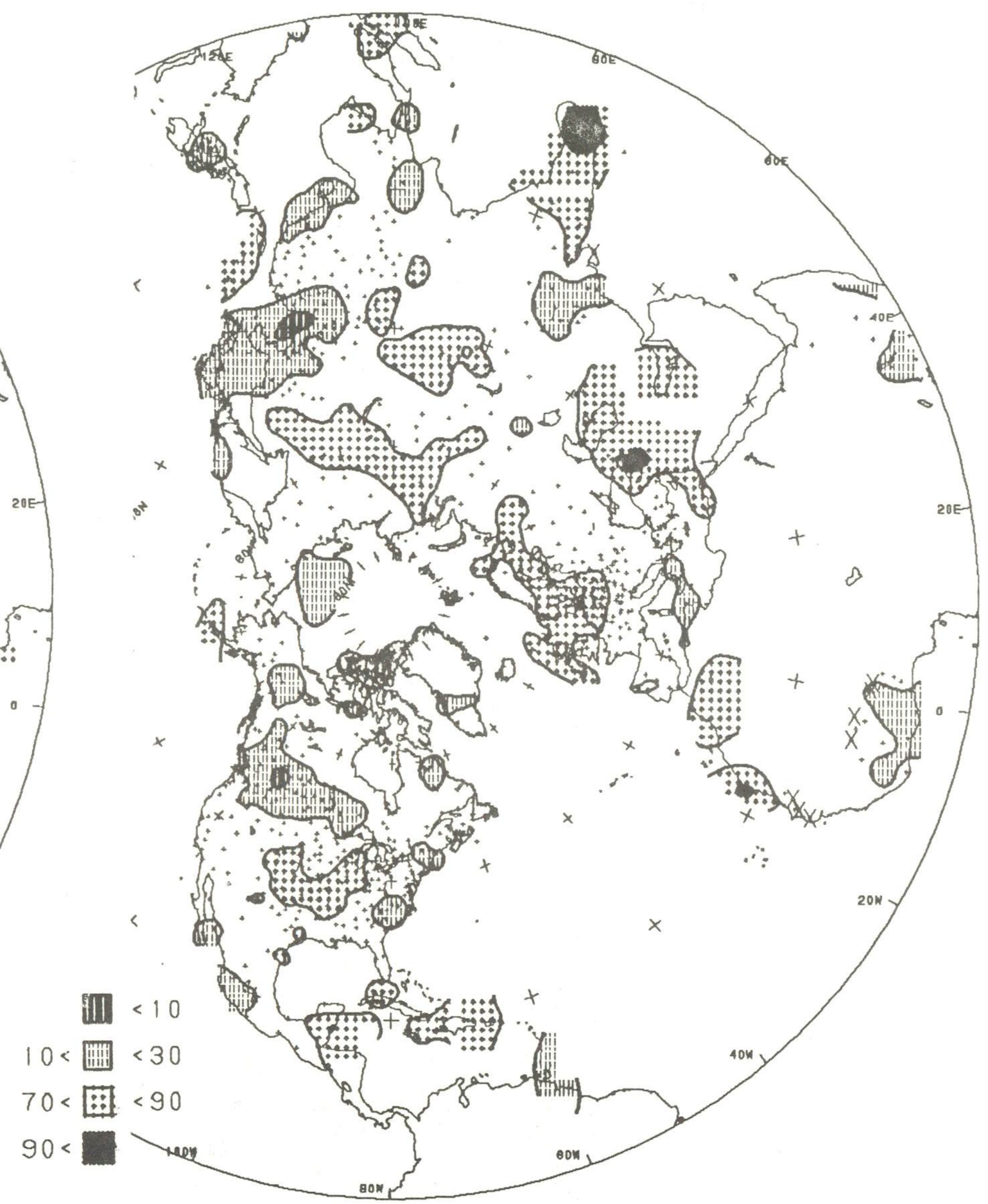

DJF 1987–88 PRECIPITATION PERCENTILES
BASED ON GAMMA DISTRIBUTION

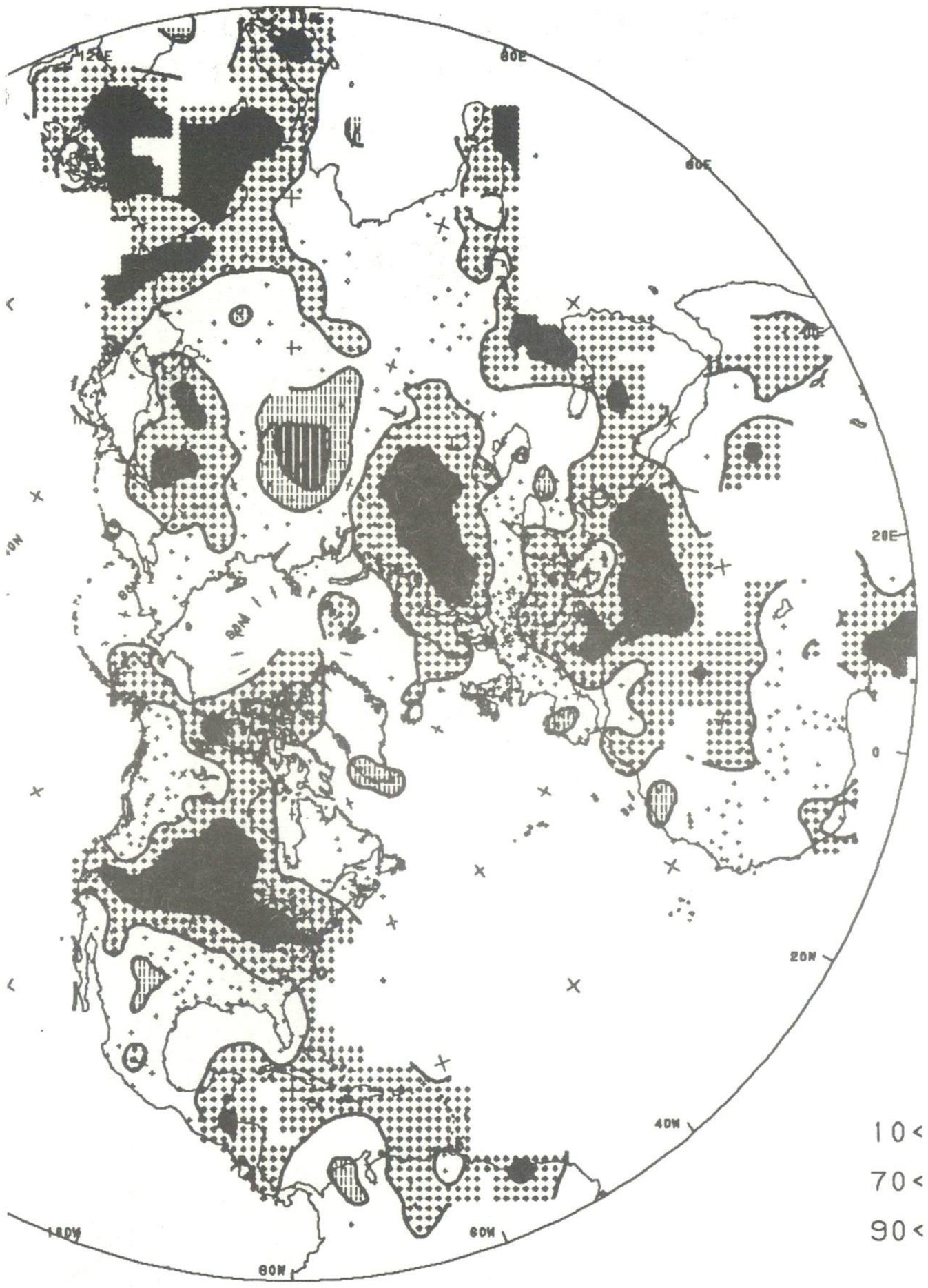

JJA 1988 TEMPERATURE PERCENTILES
BASED ON NORMAL DISTRIBUTION

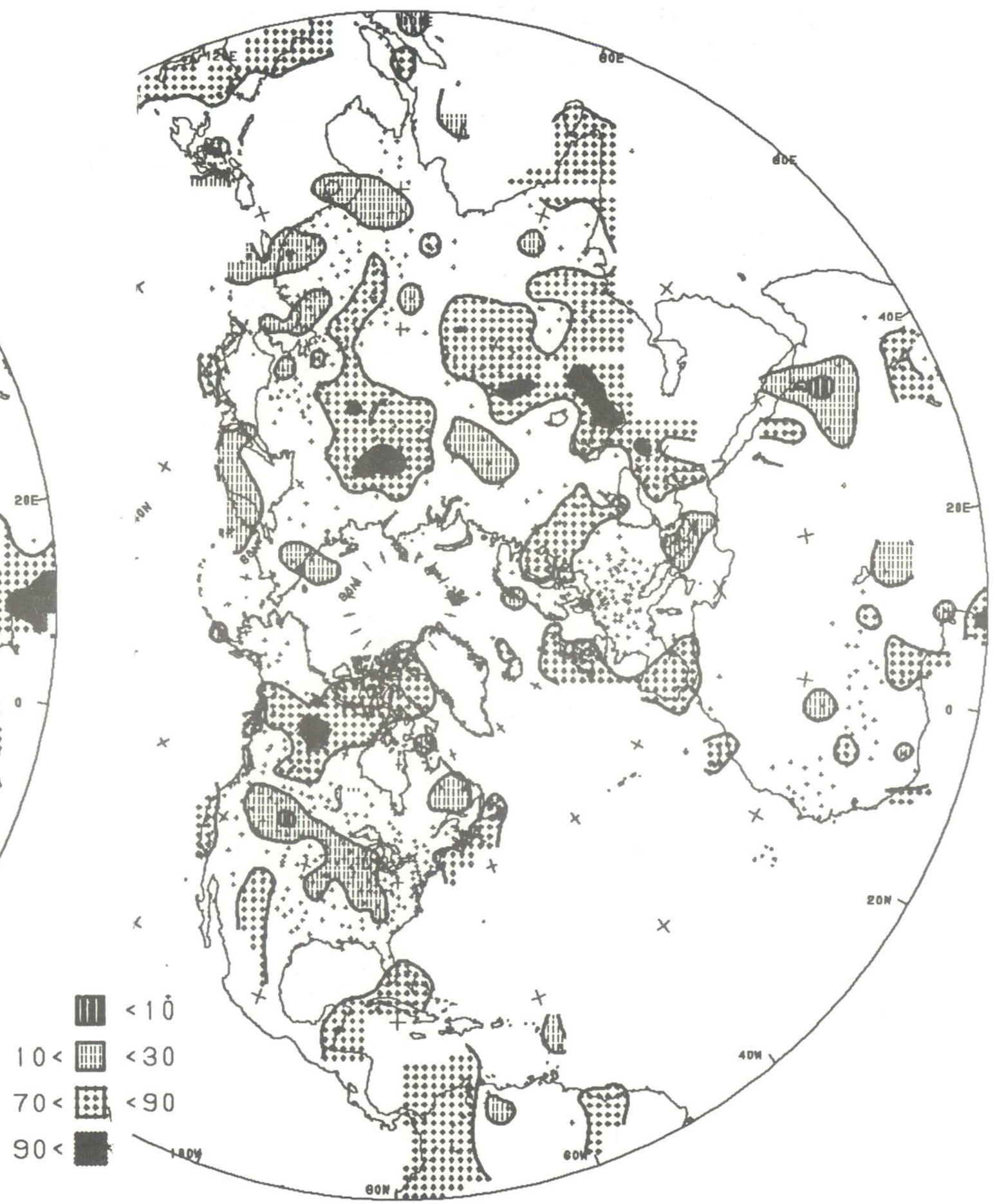

JJA 1988 PRECIPITATION PERCENTILES
BASED ON GAMMA DISTRIBUTION

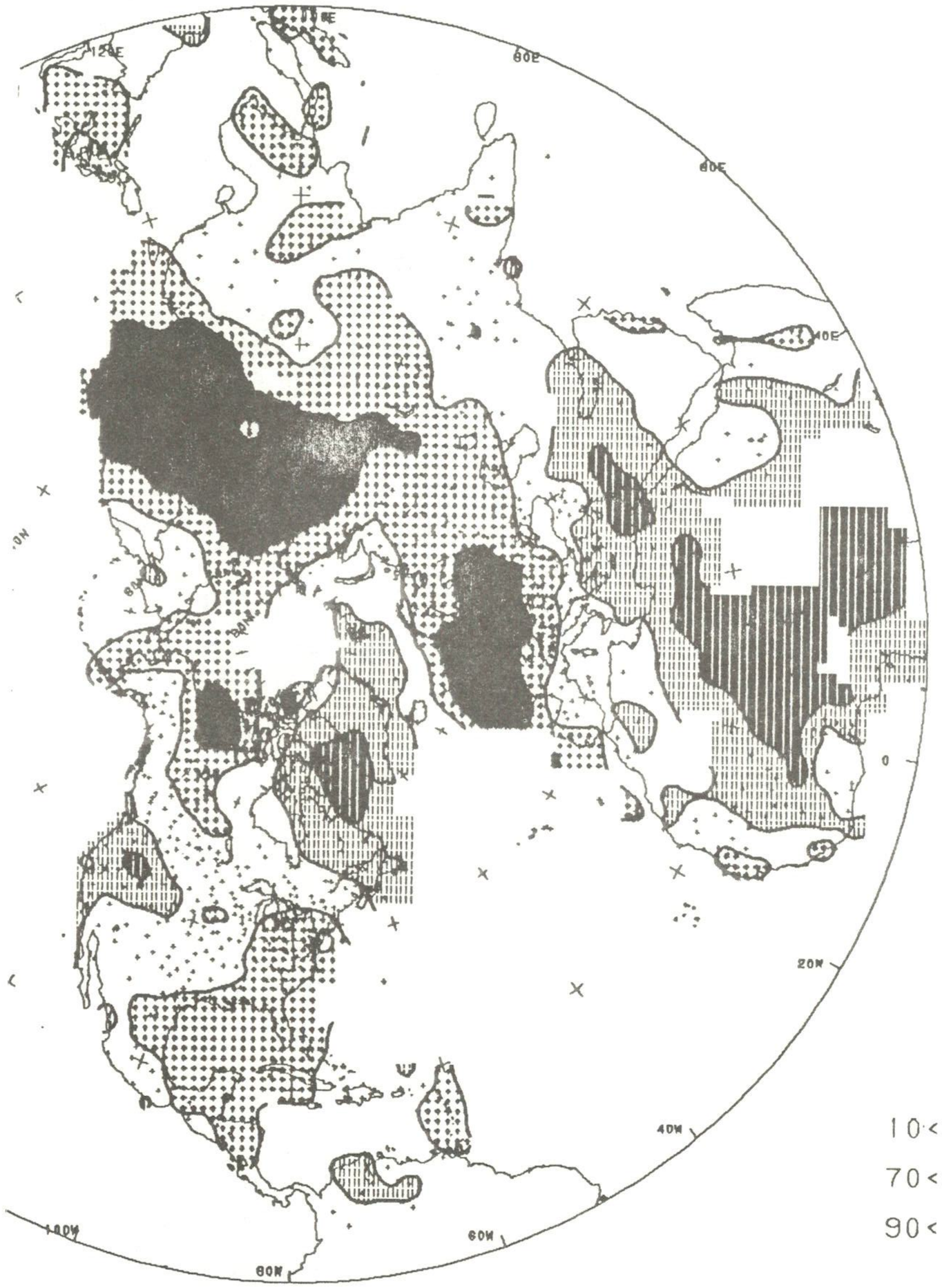

DJF 1988–89 TEMPERATURE PERCENTILES
BASED ON NORMAL DISTRIBUTION

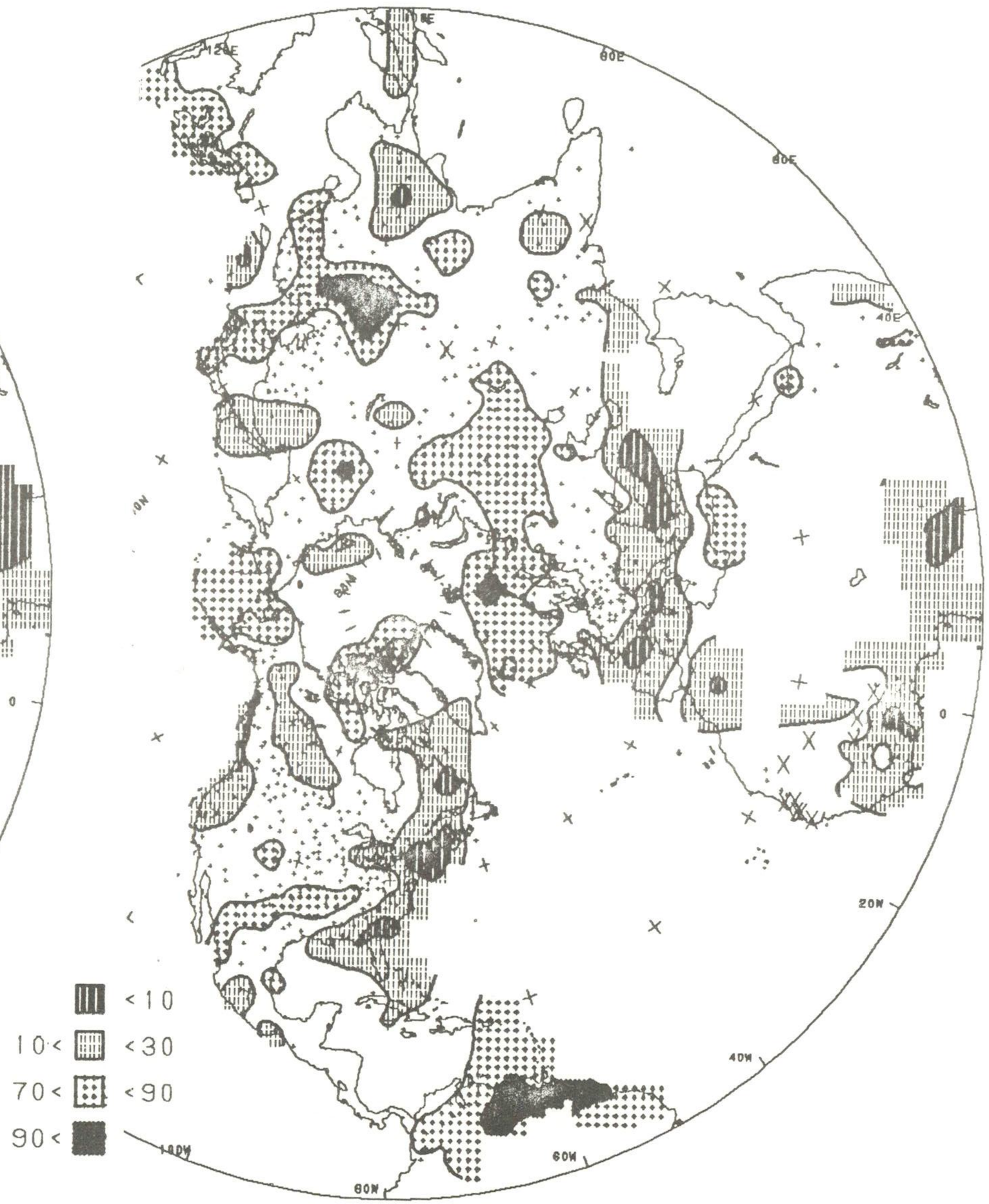

DJF 1988–89 PRECIPITATION PERCENTILES
BASED ON GAMMA DISTRIBUTION

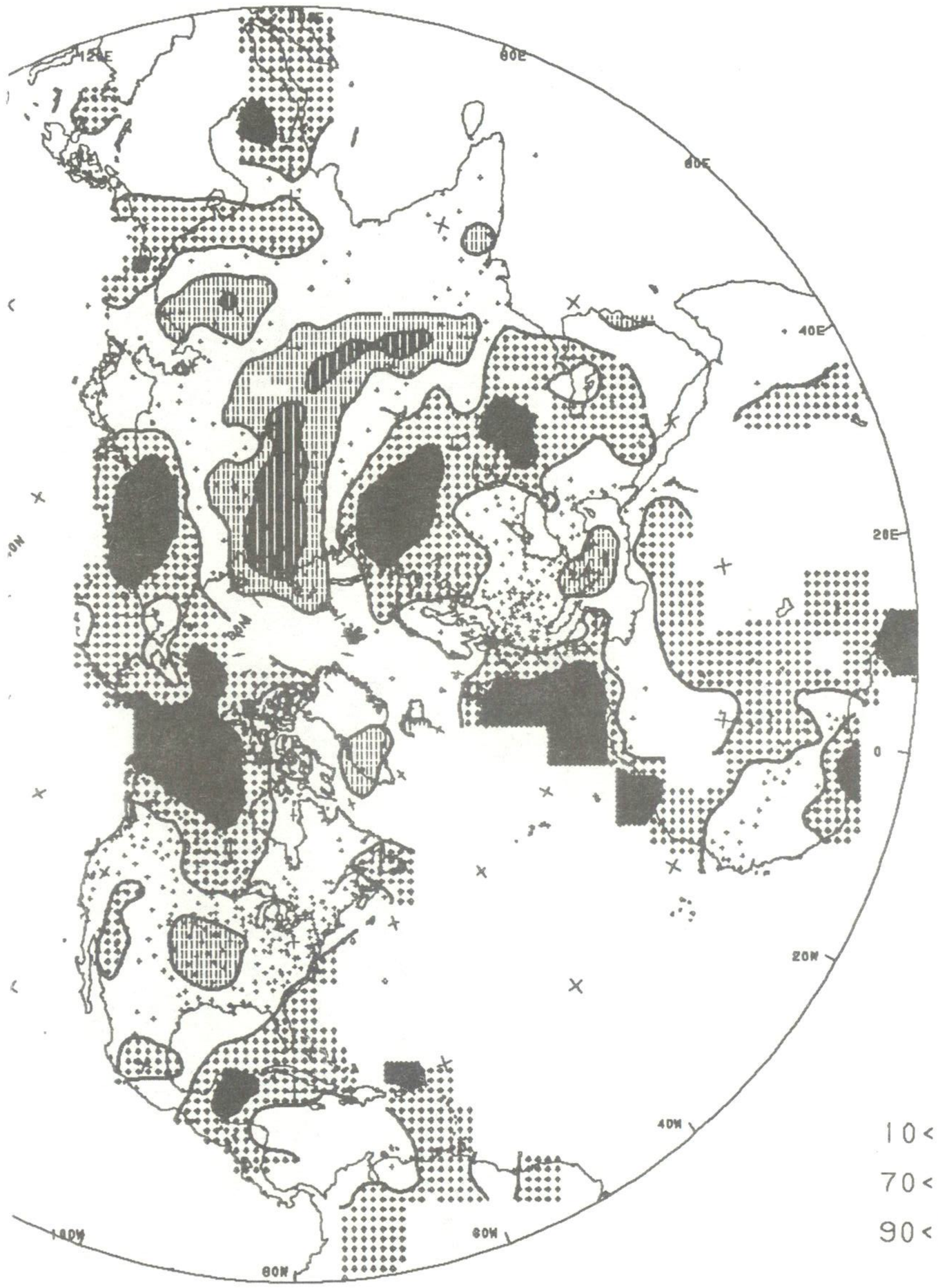

JJA 1989 TEMPERATURE PERCENTILES
BASED ON NORMAL DISTRIBUTION

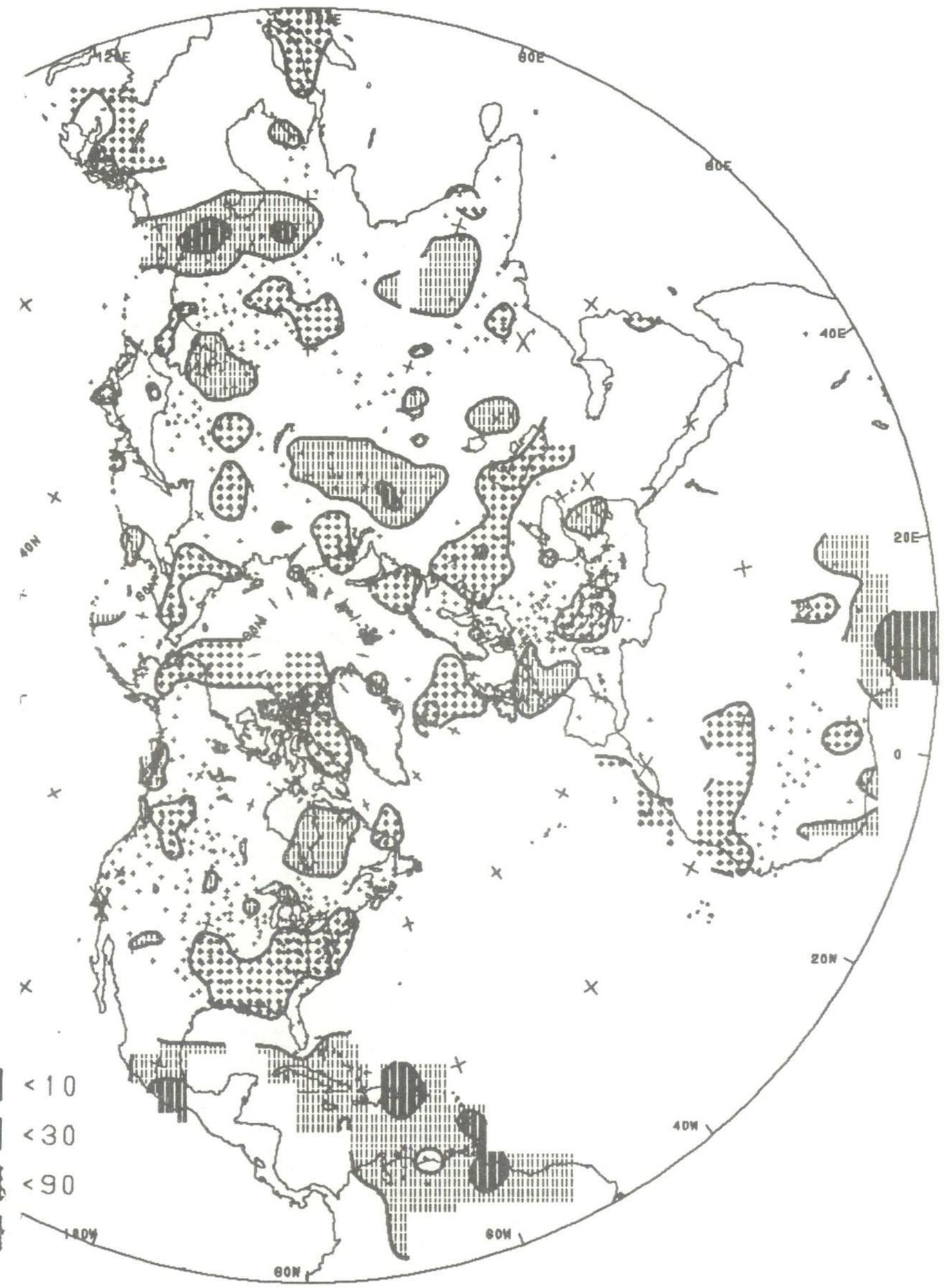

JJA 1989 PRECIPITATION PERCENTILES
BASED ON GAMMA DISTRIBUTION

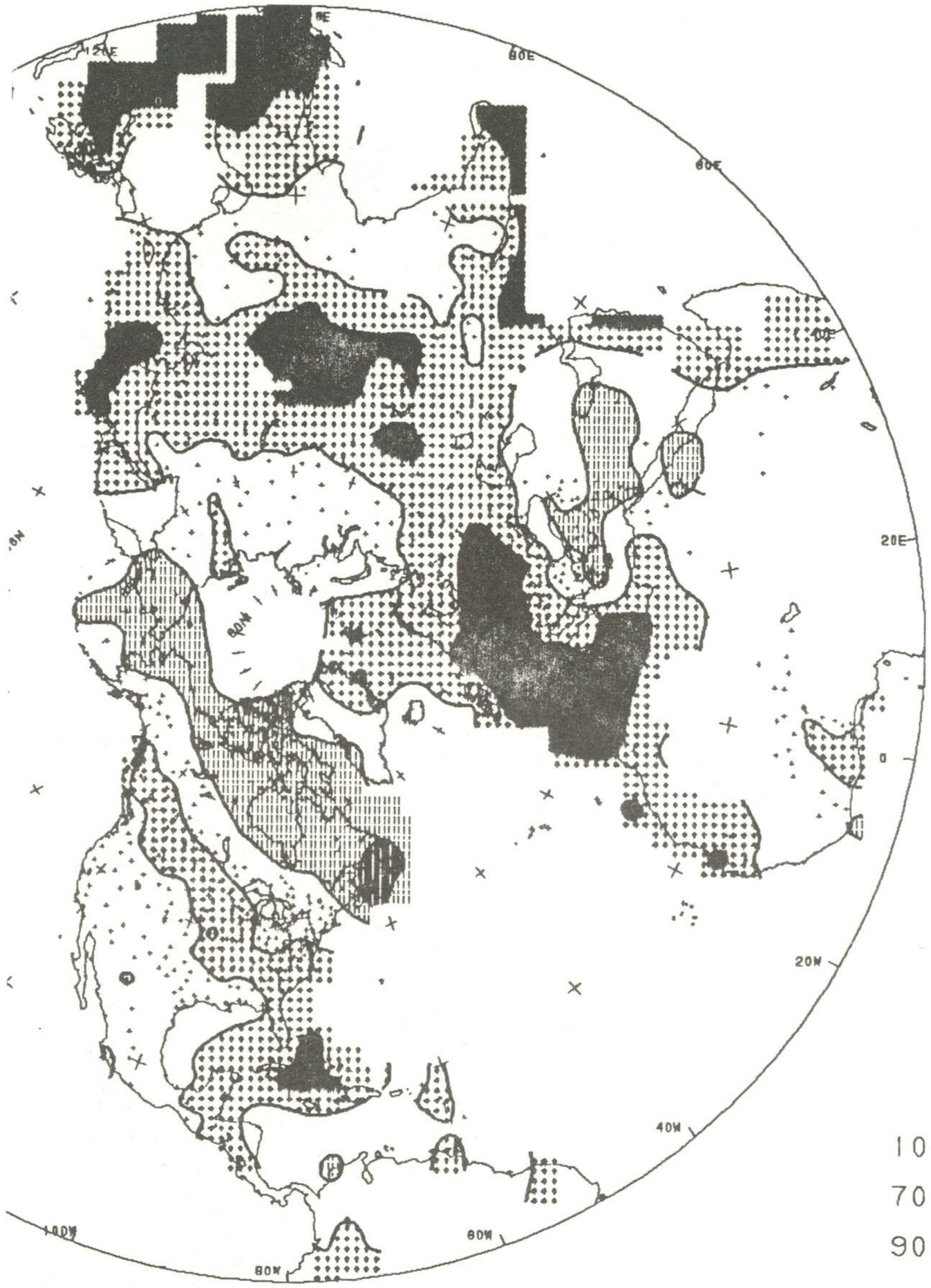

DJF 1989–90 TEMPERATURE PERCENTILES
BASED ON NORMAL DISTRIBUTION

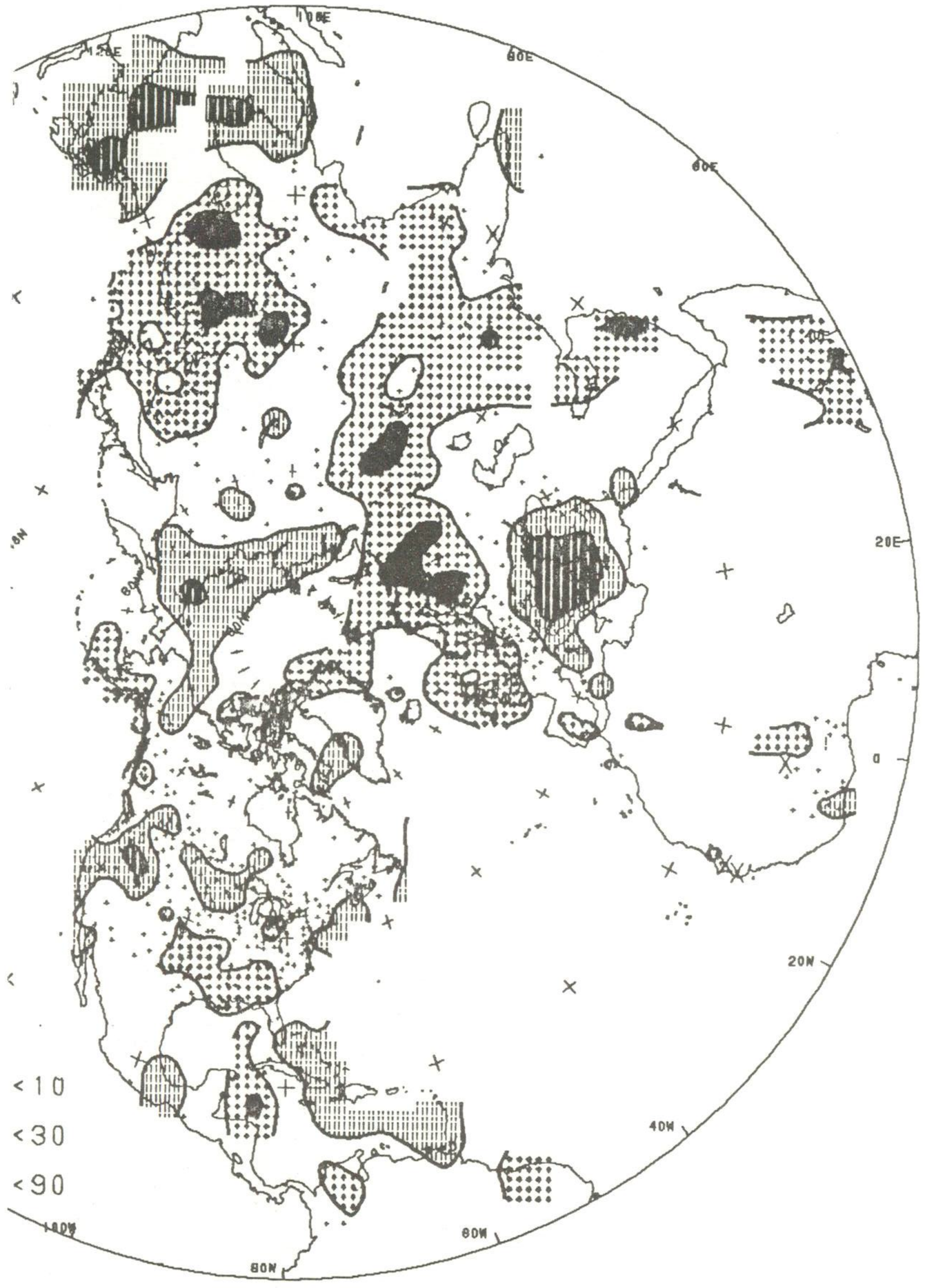

DJF 1989–90 PRECIPITATION PERCENTILES
BASED ON GAMMA DISTRIBUTION

☆ U.S. GOVERNMENT PRINTING OFFICE: 1991 — 281-557/40426

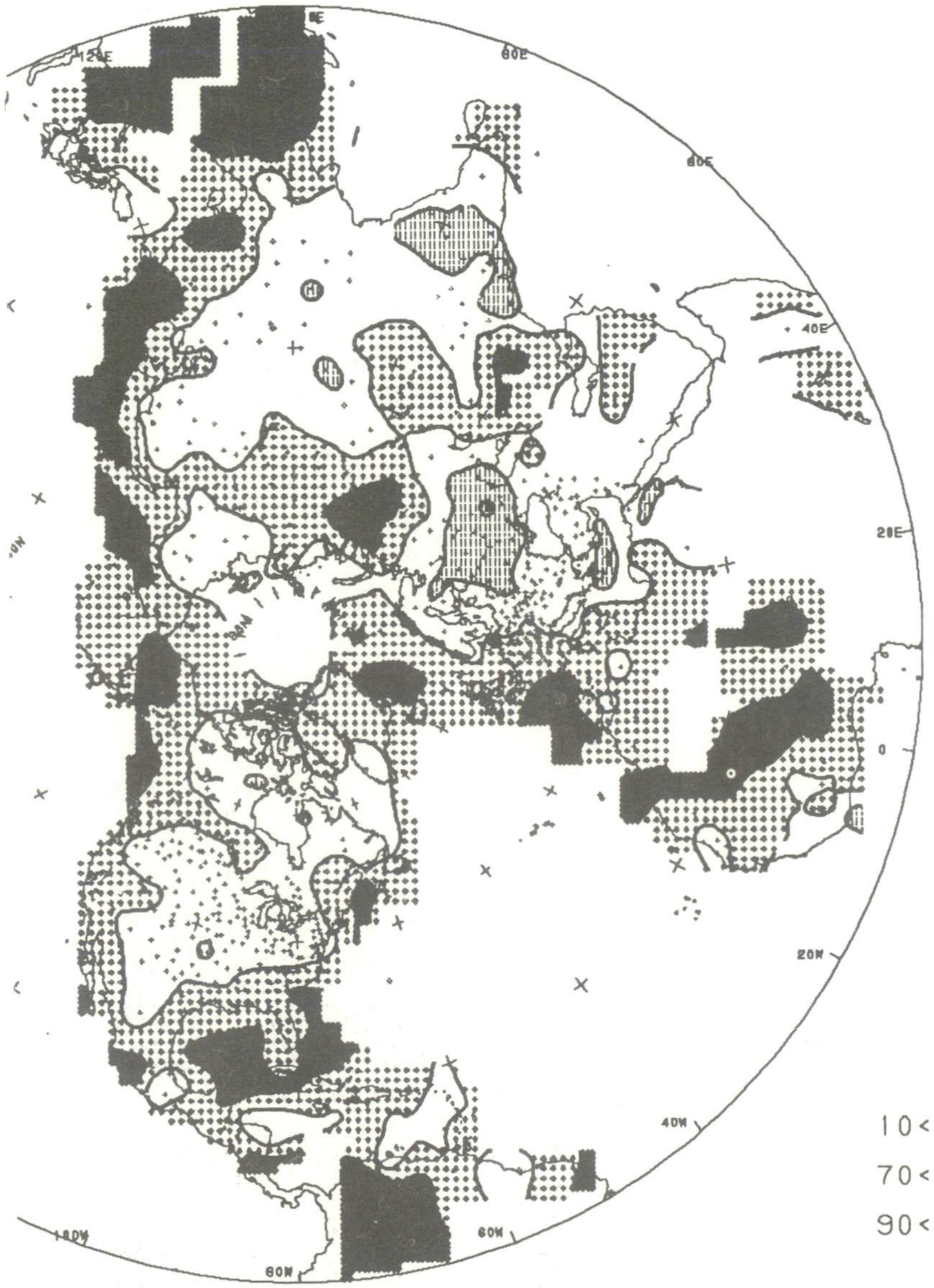

JJA 1990 TEMPERATURE PERCENTILES
BASED ON NORMAL DISTRIBUTION

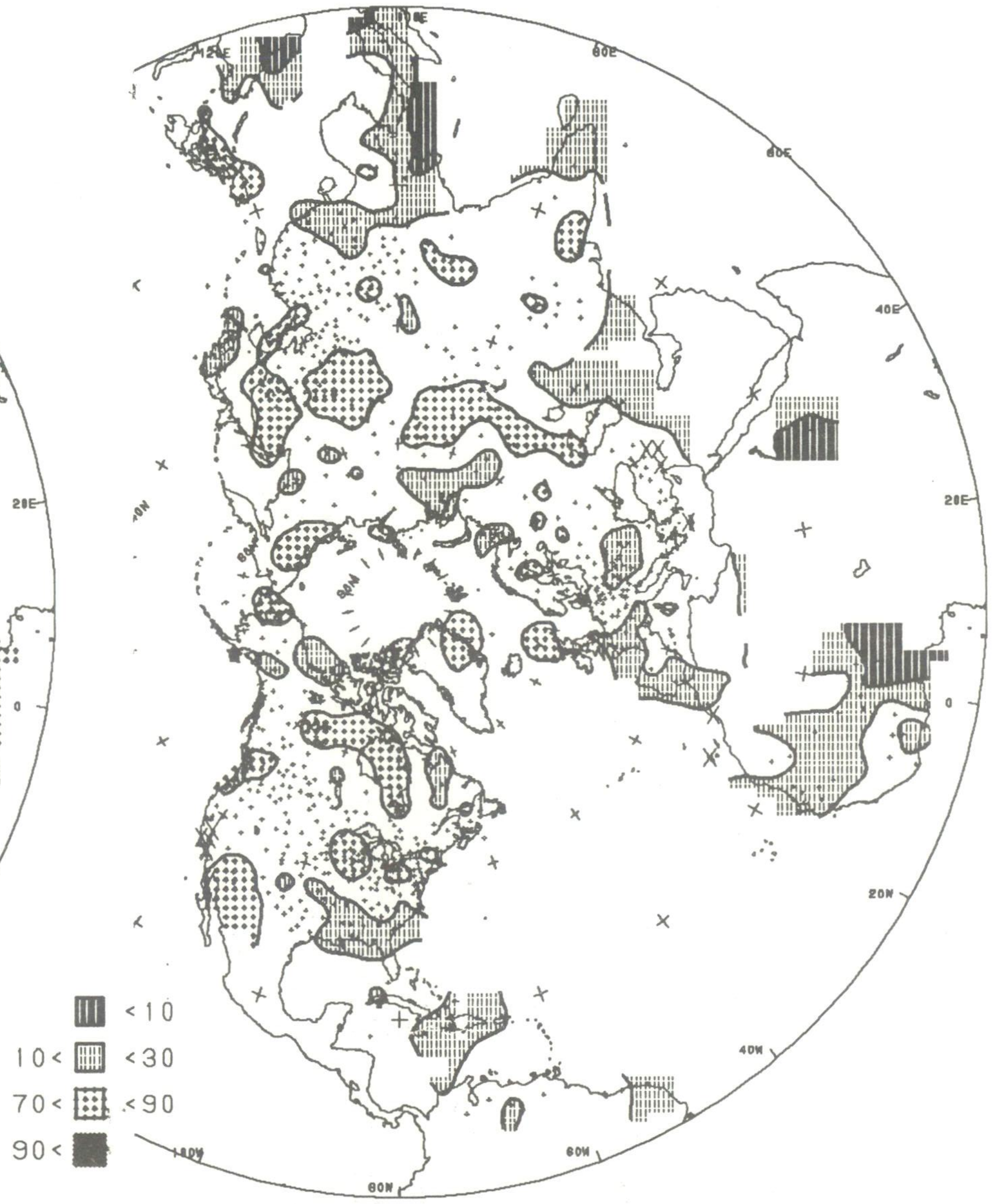

JJA 1990 PRECIPITATION PERCENTILES
BASED ON GAMMA DISTRIBUTION